NUMERICAL STRESS CHARACTERIZATION IN CROSS-BORED THICK WALLED CYLINDERS UNDER INTERNAL PRESSURE.

BY

JOHN MUNIU KIHIU.

"A THESIS SUBMITTED IN FULFILMENT OF THE REQUIREMENTS FOR THE DEGREE OF DOCTOR OF PHILOSOPHY (MECHANICAL ENGINEERING) IN THE UNIVERSITY OF NAIROBI".

2002

DECLARATION

I declare that this is my own original work. I also affirm that to the best of my knowledge, this thesis has not been presented in this or any other university for examination, or for any other purposes.

Signed: _____

John M. Kihiu

We certify that this thesis has been submitted for examination with our approval as University supervisors.

Signed: _____

Dr. George O. Rading

Signed: _____

Prof. Stephen M. Mutuli

ABSTRACT

The aim of this work was to establish and quantify the influence of cross bore entry geometry on the elastic and elastic-plastic stresses and their distributions in thick walled cylinders under internal pressure. The elastic and elastic–plastic stress characteristics in cross-bored thick walled cylinders have been analyzed through computer simulation. The model cylinders had varying thickness ratios, varying cross bore diameters and cross bores with varying cross bore to main bore entry geometry. The plain cross bores, radiused cross bores and chamfered cross bores were considered. The elastic stress profile characteristics, elastic stress concentration factors, elastic-plastic overstrain stress profile characteristics, incipient yield pressures, overstrain pressures, residual stress profile characteristics and minimum residual stresses were determined.

The computer simulations were based on the three dimensional finite element method procedures of elastic and elastic-plastic analysis. The displacement formulation was used together with the Serendipity family of shape functions. Eight noded cubic and four noded tetrahedral isoparametric elements were employed. The incremental theory of plasticity was used for the elastic perfectly plastic pressure vessel elastic-plastic analysis. Computer programs in Fortran source code were developed to carry out the analysis. The Frontal solver solution was adopted to allow reasonable discretization of the structures. By verifying control simulation results for plain cylinders without cross bores, the method and procedures employed were proved to be efficient, accurate and reliable.

The plain cross-bored cylinder results showed that the maximum hoop stress does not always occur at the crotch corner. This was found to be the case for cross bore to main bore radius ratios of 0.2 or less. The exact location was found to be dependent on the cylinder thickness ratio and the cross bore radius. The cross bore to main bore radius ratio of 0.2 was found to be a geometrical constant where cylinders having thickness ratios between 1.75 and 3 have the same stress concentration factor of 2.753. For these thickness ratios, the maximum stress concentration factor was found to occur at a cross bore to main bore radius ratio of 0.05 for a cross bore to main bore radius ratio less than

0.2. The stress concentration factor was also found to increase with increase of thickness ratio. For the 1.25 and 1.50 thickness ratio cylinders, the stress concentration factor curves only have inflexion points and cross at a cross bore to main bore radius ratio of 0.11.

In radiused entry cross-bored cylinders, the maximum hoop stress always occurred around the upper tip of the radius in the meridional plane. Radiusing of the cross bore was found to reduce the stress concentration factor and to result in reduced stress gradients of the cross bore entry. The stress concentration factor was found to decrease with increase of blending radius with the rate of decrease depending on the cylinder thickness ratio and the cross bore radius. The chamfered cross bore analysis showed that chamfering is not always advantageous as a means of reducing the stress concentration factor in a plain cross bore. For most chamfer angles and chamfer lengths, chamfering was found to undermine the structural response of the cylinder. However, for several chamfer angles and chamfer lengths, which have been determined in this work, the stress concentration factor were found to be below those of the equivalent plain cross-bored cylinders. It is these chamfer angles and chamfer lengths that must be used to obtain the minimum stress concentration factors in the design process. It was found that the maximum hoop stress in the chamfered cylinder does not always occur at the crotch corner. The point of maximum hoop stress shifts from the crotch corner to the cross bore chamfer end along the meridional plane as the chamfer angle increases. The exact location is determined by the combination of cylinder thickness, cross bore radius, chamfer length and chamfer angle. Not all the geometric combinations were found to yield a minimum stress concentration factor. Where a minimum stress concentration factor could not be found, the maximum hoop stress was found at the crotch corner for all chamfer angles and chamfer lengths. Where a minimum stress concentration factor could be found, this was greater than the value for a radiused entry cross bore.

In all geometrical configuration cases, the elastic-plastic stress profiles had lower peak stresses and more even distributions that would lead to improved pressure carrying capacity in service. The radiused entry cross bore showed a major structural weakness in

the transverse plane with high probability of gross deformation and reverse yielding. For plain, radiused entry and chamfered cross-bored cylinders, the optimum overstrains were found to be 37, 23 and 27% respectively. The negative residual and service hoop stresses and sharp stress gradients at the cross bore entry have been discussed due to the associated phenomena of stress reversals and plastic strain accumulation.

The results of this work give structural response details (particularly for the plain and chamfered cross bores) which form a good and valid basis for re-evaluating the existing data and collecting further data for design and service procedures. Several recommendations have been made for future work related to this area of research.

ACKNOWLEDGEMENTS

This 6.2MB Ph.D. thesis could not have been written without the consultation, reference, assistance, help and cooperation of various people, journals, bodies and institutions. While it is impractical to list all those whose work has made this thesis possible, at least an attempt will be made here to acknowledge those whose contributions have been especially significant. I am indebted to all the persons, journals, etc., whose help in no small measure enriched my professional knowledge for useful application towards societal ends. Examples of this abound. I am also indebted to many researchers all over the world who, sharing my enthusiasm have contributed through their researches to many of the ideas, methods and techniques here used and reported.

Special thanks and mention is to my first project supervisor, Dr. G. O. Rading (Department of Mechanical Engineering, University of Nairobi), a true professional of his craft who directed the whole lengthy process by which the manuscript was transformed into a published thesis. A thorough critique of the manuscript, which led to improvements based on his suggestions, is recognized. His helpful and valuable comments on both organisation and content are acknowledged.

I am grateful to my second project supervisor, Prof. S. M. Mutuli (Chief Academic Officer, Kigali Institute of Science, Technology and Management, Kigali, Rwanda) for his constant interest and unfailing encouragement in the course of this work, and for many stimulating discussions and suggestions. I can not forget to pay tribute to Prof. L. M. Masu (University of Durban, South Africa) who introduced me to the exciting worlds of pressure vessels, finite elements and computer programming in my early stages of scholarship. I am enjoying each and every bit of this knowledge, as each of the worlds has become a passion.

I am indeed very indebted to the management of the Jomo Kenyatta University of Agriculture and Technology for granting me study leave and support for the entire period of this work. Prof. R. M. Michieka (Vice Chancellor), Prof. H. Thairu (Deputy Vice

Chancellor, Academic) and Prof. G. Agong (Deputy Vice Chancellor, Administration) deserve special mention for their unswerving support of scholarship. I express my deeply felt appreciation to Dr. P. N. Kioni (Dean, Faculty of Engineering) and Dr. S. P. Ng'ang'a (Chairman, Department of Mechanical Engineering) for their unstinting aid and support in every phase of this arduous task.

I highly and deeply appreciate the role played by both KAAD and DAAD in financially supporting this work. Not much progress could have been achieved without their support. Dr. T. Scheidtweiller and Fr. Dr. T. McDonald (KAAD) and Mr. R. Jacob (ex-Director, DAAD) receive my humble thanks. I can not forget to recognise the assistance and cooperation of Mr. E. Kibiro (Chief Technician, Department of Mechanical Engineering) and Mr. C. Maloba (Institute of Computer Science). To all those who knowingly and/or unknowingly influenced, counseled, assisted or contributed their time and effort towards this work, wherever they are and whatever their station in life, I am very grateful.

Special appreciation to my children: Wambui, Ruguru, Wanjiku and Kihiu. I thank them unreservedly for their patience during my long periods of unavailability. Completion of this thesis could not have been realised without the full cooperation, support and understanding of my wife Wambui. Her help and forbearance with numerous occasions when the task of research, writing and indeed the involvement with finite elements, became a full-time preoccupation for me deserves unique mention and unquestionable appreciation. Hopefully, the academic 'widow' syndrome is now over for her.

DEDICATION

This work is dedicated to my mother, Jecinta Ruguru, for her role of fueling, supporting, and persistently encouraging me into the world of learning and education since my childhood days. I deeply appreciate her love, devotion, selflessness and foresight.

NOMENCLATURE

[B]	Displacement-strain matrix.
C	Material constant.
ca	Chamfer angle [^{0}].
clr	Chamfer length ratio [mm].
D_m	Cylinder mean diameter [mm].
[D]	Stress-strain constitutive matrix.
d	Cross bore to main bore radius ratio.
d_n	Nozzle mean diameter [mm].
dV	Elemental volume.
dΓ	Elemental surface area.
E	Young's modulus [N/mm^2].
[f^e]	Surface element force vector.
G	Modulus of rigidity [N/mm^2].
[J]	Matrix of Jacobian transformation.
[K^e]	Element stiffness matrix.
k	Thickness ratio.
L_i	Volume or area coordinates.
[N]	Element surface shape function.
n	Strain hardening exponent.
P	Internal pressure [N/mm^2].
P_D	Design pressure [N/mm^2].
p	Primary stress [N/mm^2].
q	Secondary stress [N/mm^2].
P_i	Surface force components [N].
R_i	Inner radius [mm].
R_m	Mean radius of pressure vessel [mm].
R_0	Outer radius [mm].
rd	Entry radius ratio.
r_m	Mean radius of protruding nozzle [mm].
S	Design stress [N/mm^2].

S_m Allowable stress [N/mm^2].

S_{ult} Ultimate tensile stress [N/mm^2].

T_m Thickness of pressure vessel [mm].

t_m Thickness of protruding nozzle [mm].

u,v,w Displacements in the x, y, z, directions [mm].

$\int$ Volume integral.

W^e Work done on element [Nm].

x,y,z Cartesian coordinates.

Y_S Yield stress [N/mm^2].

α Coefficient of linear thermal expansion [mm/mm/ ^{0}C]

$\int$ Surface integral.

Λ^e Element strain energy [Nm].

$[\Psi]$ Element shape function vector.

ε Strain.

$\{\varepsilon\}$ Strain vector.

ν Poisson's ratio.

σ Stress [N/mm^2].

$\{\sigma\}$ Stress vector.

ξ,η,ζ Natural coordinates.

ABBREVIATIONS

ASME	American society of mechanical engineers.
BS	British standard.
FEM	Finite element method.
SAE	Society of automobile engineers.
SCF	Stress concentration factor.

CONTENTS

LIST OF TABLES

LIST OF FIGURES

CHAPTER ONE
INTRODUCTION

1.1 Overview

Thick walled cylinders in the form of high pressure vessels and boilers play a very important role in our daily lives. In the middle of the last millenium, thick walled cylinders were first used in the form of gun barrels after the discovery of gunpowder. At around the same time, in 1698, the steam boiler was for the first time employed for commercial steam production [1]. These early boilers were made of cast iron and had flat surfaces and leaden or even wooden tops. Copper or granite slabs were at times used for parts in contact with fire. In 1857, steel was introduced in the production of British marine boilers. Pressure vessels are now encountered in the domestic cooking gas cylinders, medical and industrial gas cylinders [1]. Pressure vessels are also used in chemical plant for polyethylene manufacture, in metal extrusion processes [2], in heavy earth moving and rock excavation equipment. Other fields of use are the nuclear power plants, steam generation and steam power plants for power generation. High pressure vessels are also used in under sea mining, deep diving submersibles, down well and deep ocean simulation, water jet cutting, cultured crystal production and supercritical extraction [3]. Hence, knowingly or unknowingly, the human life is very much dependent on safe use of pressure vessels.

1.2 Statement of the Problem

The historical development of pressure vessels and boilers has, however, not been uneventful. A few of the major documented events will be enumerated. In London in 1815, a disastrous boiler explosion led to the formation of a parliamentary probe committee. Thereafter, it was recommended that boilers should be made of wrought iron instead of cast iron or copper. Boilers were thereafter to undergo statutory periodic inspection. Until 1830, boilers worked at a pressure of about 7 psi (48 kN/m^2). The use of better materials boosted the working pressure to 40 psi (276 kN/m^2) but without a simultaneous redesign of the boilers. As a result of this, 288 explosions were reported in England from 1865 to 1870 [1]. In the period 1898 to 1903, there were 1600 documented boiler explosions in the United States which killed 1200 people [4]. This was an average of one boiler explosion per day

[5]. This situation was arrested by the publication of the 1914 ASME (American Society of Mechanical Engineers) Boiler code [5]. This Boiler code specified that the pressure vessel primary membrane stresses to be kept below 1/5 of the ultimate tensile strength [5]. Much latter, between 1972 and 1976, 32 cylinder explosions were recorded in the United States high pressure vessel industry and out of these, 14 cylinders had some relief operating mechanism [6-8]. As a contribution to the conservation of material and reduction of production costs, the nominal factor of safety was reduced to 4 as a Second World War emergency measure [4,9]. Very informative details of investigative findings of a boiler explosion whose diameter was 5 feet and had a working pressure of 125 psi (863 kN/m^2) have been published [10]. Figures 1.1 to 1.3 [3,11] show some modes of pressure vessel failures. Other statistics detailing modes and circumstances of pressure vessel failures have been well documented [12,13]. Investigations into the early boiler explosions mainly focused on the maintainability and process failure aspects. Today, more attention is being paid to metallurgical failure aspects [13].

From the foregoing it is clear that in the nineteenth and early twentieth centuries, bursting of boilers was a very common occurrence. These events which involved enormous losses, marked the beginning of research in pressure vessels [14,15].

Pressure vessels are often subjected to extremes of operating conditions. Forged high pressure reactors with thickness ratios of two and above have been used extensively for stirred autoclaves in the manufacture of low density polyethylene where the operating pressures are as high as 250 MPa, and the temperatures close to 300°C [2,16]. Forged high pressure vessels have also been used for isostatic compaction of metallic and ceramic powders at pressures of up to 300 MPa. Current applications may involve pressures as high as 1380 MPa. From the foregoing, the pressure vessels hold immense potential energy exerted by the working fluid [17,18]. It is therefore very important to minimize or even eliminate human and material damage or losses that may result from inadequate understanding leading to poor design of such vessels.

Pressure vessels are inevitably constructed with holes on their sides (cross bores). These openings are normally for the following purposes [17]: Fluid temperature measurement fittings, internal pressure measurement, bursting discs, inspection covers, relief and safety valves, fluid inlets and outlets. These openings introduce geometric discontinuities on the body of the pressure vessel. When the vessel is in service, and normally at high pressures, the intersection of the cross bore and the cylinder bore forms a stress singularity curve having high relative stresses and sharp stress gradients. The resulting stress concentrations are known to reduce the pressure carrying capacity of such vessels below that of a plain cylinder without cross bores [17,19]. The need for thorough, detailed and informed understanding of the effects of cross bores and the actual stress distributions cannot be overemphasized. Failure in service of pressure vessels due to lack of good understanding of the stresses at these discontinuities is known to have cost the users of such vessels immensely in terms of insurance compensations to injured plant operators and also damage to other connected or nearby equipment as earlier discussed [5].

A proper understanding of the stress severity in these regions of high stress fields would lead to usage of low safety factors in the design of such vessels and hence the economic use of pressure vessel material, enhanced pressure vessel operating life, lower operating costs and a reduction of losses (human and material) due to catastrophic or disruptive failures.

It is an established fact that high stress levels are present at the intersection of the cross bore and the main cylinder [18]. In practice, this problem of high localized stresses has been overcome by introducing a carefully polished radius or a chamfer at this intersection [2]. However, the radius size data has not been provided in any literature. The choice of the radius has been based on experience rather than analysis and hence there is a need of determining the actual state of stress in this region by actual analysis. The choice of the radius should also be a proven optimum. In normal operations, the cross bore to cylinder intersection is rounded off using a grinder, which leaves behind a relatively rough surface finish. Due to this operation, it is difficult to document the level of surface finish. Design of equipment to accurately introduce the radius is therefore necessary.

For high pressure applications, a realistic picture of the state of stress in a vessel with side bores is needed because fatigue life is very critical and present day limitations of strength and ductility in commercial pressure vessel materials prevent high factors of safety [20]. It is clear that Section I and Division 1 of Section VIII of the ASME Boiler and Pressure Vessel code do not call for a detailed stress analysis but merely set the wall thickness necessary to keep the basic hoop stress below the tabulated allowable stress. The higher localized stresses are taken care of by the safety factor and a set of design rules [21]. Though this code provides a quick design procedure, it is certainly inadequate for pressure vessels with cross bores since stress concentration factors have not been considered.

It is also known that from the manufacturing plant or the fabrication workshop, the materials for cylinder manufacture or the finished cylinders are never homogeneous. These inhomogeniuities are in the form of inclusions, scaling, cracking arising from uneven heat treatments, rough surfaces arising from the finishing operations, and so on. These features are important stress raisers when the cylinders are loaded in operation, since they act as possible sources of fatigue crack initiation, propagation and ultimate failure. They are even of further importance when they occur in the region of cross bores since they compound the stress raising effect. Other phenomena that tend to undermine the structural integrity of cylinders particularly in the region of the cross bores are hydrogen embrittlement and stress corrosion cracking [3,22-24]. These are normally overcome by using austenitic steels, which have carbide stabilizing elements (Mn, Mo, Cr, V, W, Ti). Thorough non-destructive testing of pressure vessels especially around the cross bores and the main bore is therefore necessary to ensure absence of cracks or even inclusions [3,25].

As a matter of practice, pressure vessels and pipes are normally subjected to pressures of 1.25-1.5 times the design pressure at the end of the fabrication process [26,27]. This overstrain pressure is designed to cause yielding of the most highly stressed parts of the structure. After the release of the pressure, residual stresses are left in the structure. The nature of these residual stresses is such that the inner surface has negative stresses while the middle and outer regions have positive stresses. Upon actual loading in service, the

vessels are able to carry a much higher load before yielding than would be the case without overloading during testing. For cylinders with complex cross bore entry geometry it is important to establish the exact relationship between the overstrain pressure and the subsequent re-yield pressure. The nature of the resultant stress distributions is also important.

In some cases, the pressure overstraining is deliberately done during manufacture. In this case, the manufacturer chooses the extent of plastic deformation, which would result in a desired level of residual stresses. This process results in a much stronger cylinder with service stresses being more uniformly distributed across the thickness. This technique of inducing additional strength out of the cylinder is called autofrettage or self hooping [28]. This technique has the same advantage as obtained by making a compound cylinder or wire winding the cylinder without incurring any additional costs in terms of materials.

Thick walled tubes carrying fluids at high pressures are now of great importance in many industries and their economic use often depends upon small controlled permanent deformations to occur. The earliest application of autofrettage was in gun barrels but with the advent of high pressure chemical processes, reactive vessels, tubular heat exchangers, pipe work and valves, the design based on the classical safety factors would be more expensive and inconvenient. The pioneering work by Manning in this area envisaged small controlled plastic deformation [29]. Despite the importance of autofrettage in improving the pressure carrying capacity of cylinders, not much has been done to study its effects in cross-bored cylinders.

1.3 Outline of the Work Done

The first aim of this research work was to investigate in detail the structural behaviour or response of thick walled cylinders with varying entry geometry cross bores under internal pressure. The modeling method employed was to transform the cross bore entry geometry to a radiused entry or a chamfered entry into the main bore. This was believed to reduce the stress concentration factors in the resultant configurations. Reduced stress concentration factors were also believed to cause a favourable and more even distribution

of stresses which would result in more economical use of the cylinder material and the associated benefits in servicing and enhancement of the cylinder service life.

In this work, thick walled cylinders with flush and non-protruding cross bores of varying entry geometry were analyzed using the finite element method (due to the unavailability of any analytical solution) to determine elastic stress levels, their distributions and stress concentration factors. Cylinders with thickness ratios between 1.25 and 3 were considered. Cross bore to main bore radius ratios less than 0.5 were analyzed as recommended by ASME Section VIII, Division 2 [30]. The results from the plain cross-bored cylinders were compared with those of radiused entry and the chamfered entry cross-bored cylinders. Various thickness ratios and cross bore to main bore geometrical configurations were considered.

The second aim of the research work was to consider the transformed cross bore entry configuration and carry out the process of autofrettage. The autofrettage was performed for varying degrees of overstrain. Autofrettage was believed to create a favourable system of residual stresses which when superimposed on the service stresses, would result in much lower stress levels and more favourably distributed stresses in the cylinder material. The cylinder may then be able to resist much higher operating pressure without the risk of the highest stressed regions yielding or if yielded, undergoing gross deformation.

The elastic-plastic stress levels and their distributions were determined and the results compared to those of plain cross-bored cylinders. The elastic service stresses were also analyzed and presented. The incremental theory of plasticity was used in the overstrain process. The pressure vessel material was assumed to have an elastic perfectly plastic stress-strain response while the von Mises yield criterion was used. Reverse yielding of the elements was avoided. The advantages of using any of the entry geometry was quantified and compared. The arising limitations of the various entry geometry were discussed. The results of the above work were compared to the results of previous researches where applicable.

In the finite element method, eight noded brick and four noded tetrahedral isoparametric elements were used. The displacement formulation and the Serendipity family of shape functions were employed. Computer programs in FORTRAN language source code were developed for this analysis. While the programs could cater for reverse yielding, the Bauschinger effect was ignored.

Many authors have in the past shown a lot of interest and done intensive research in the area of pressure vessels. However, cross-bored cylinders and the full range of geometrical configurations have not received adequate attention and interpretation of the results. Results from a few tests in the past have erroneously been assumed to represent the gamut of geometrical combinations. It is the principal aim of this research work to fully investigate the effect of cross bore geometry on the structural response of thick walled cylinders and make recommendations for the resultant optimum configurations. Some of the past research findings will be reviewed in the next chapter.

(Source: [11])

FIG. 1.1 Thermal fatigue or alligator pattern on the outside surface of a spherical component.

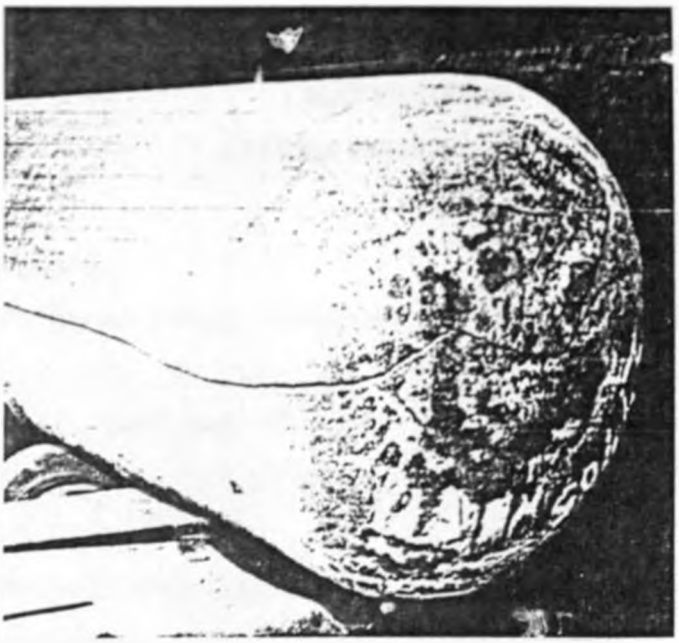

(Source: [3,11])

FIG. 1.2 Brittle fracture in pressure vessel with torispherical head (running along the cylinder and branching across the head).

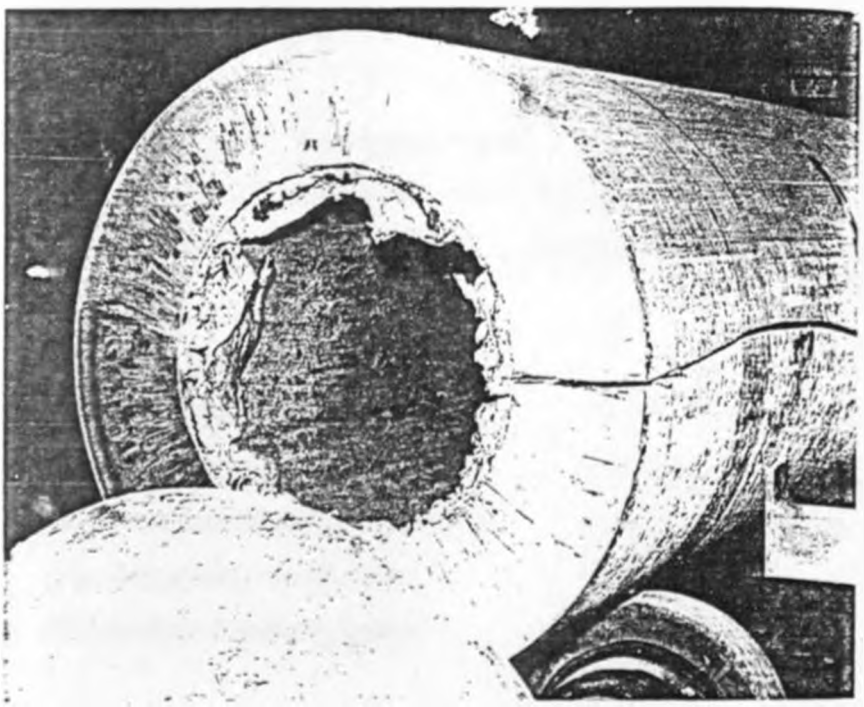

(Source: [3,11])

FIG. 1.3 Brittle fracture in pressure vessel (cut through section).

CHAPTER TWO

LITERATURE REVIEW

2.1 Introduction

The study of pressure vessels, whether plain or cross-bored, has interested a lot of researchers in the past. The aim of the research has been to improve pressure vessel operational safety, enhancement of service life and improvement of pressure carrying capacity of the pressure vessel. The main areas of research have included:

(a) Elastic stress analysis.

(b) Elastic-plastic stress analysis.

(c) Residual stresses.

(d) Service stresses.

(e) Materials.

(f) Design codes and practice.

(g) Constitutive equations.

In the studies of any of the above areas, several solution approaches have been used. These include but may have not been limited to the following:

(a) Experimental methods (strain gauge, photoelasticity, Lueders' line, Moire's method, and so on).

(b) Finite element method.

(c) Boundary integral equation method.

(d) Empirical/approximation methods.

(e) Non contact computer vision [31-33].

(f) Theoretical/analytical models.

(g) Statistical/probabilistic models.

A review of some of the past research findings is presented below.

2.2 Review

2.2.1 Elastic Stress Analysis

In an attempt to understand the state of stress around cross bores, one of the earliest researches involved the evaluation of stress concentration factors around a circular hole in an infinite plate under tension [34]. For plate width to hole diameter ratios between 5 and 8, stress concentration factors of 3.067 were obtained. The results were almost identical to those obtained through the mathematical theory of elasticity developed by Timoshenko [34]. The stress concentration factors were considerably reduced by the introduction of beads around the holes. Elliptical holes were also considered using analytical, photoelastic, Lueders' line and fine extensometer measurements. Several geometrical configurations in tension specimens were also studied using photoelastic methods [35] while the weakening effect of cross bore openings in pressure vessels was demonstrated by making strain measurements around the reinforced and unreinforced nozzles [36]. This weakening effect was only demonstrated through strains and no stress concentration factors or stress levels were presented.

The sensitivity of SR-4 gauges to moisture was overcome by using transformer oil as the pressurizing medium in high pressure stress measurements [37] while accounting for the hydraulic pressure on the gages. Early cross bore stress concentration factor measurements were experimental. The frozen stress photoelastic technique and the strain gauge methods have been used and the results compared with previous theoretical predictions [20,38,39].

A universal stress concentration factor value of 2.5 was predicted for all closed-end cylinders with small cross bores [20]. For large cross bore to main bore radius ratios, shear and bending effects were not accounted for. Stress concentration factors in protruding nozzles have also been studied [40] and results compared with predictions of a thin shell finite element analysis. Radial and offset cross bores have also been studied [41]. Off set cross bores were found to result in lower stress concentration factors and also to increase fatigue life.

The time consuming nature of three dimensional finite element method analysis has led to modeling a cross bore as a cylinder-sphere intersection [42], providing approximate results. The membrane stress distribution was incorporated. The three independent geometric ratios

of radius and thickness were considered and methods based on one or two parameters were found to be subject to error. Calculated results for the ratios R_m/T_m, r_m/t_m, r_m/R_m were tabulated for design purposes. Here, R_m is the mean radius of vessel, T_m is the thickness of vessel, r_m is mean radius of nozzle, t_m is thickness of nozzle. The description of the method and results were confined to flush nozzles and was also limited to cases where the shell could be treated as thin. The design data and the experimental results showed no agreement when thick cylinders were tested [42].

Three dimensional finite element models (using the PATRAN-G interactive graphics program) have been used to evaluate the stress distribution of the elastic stress concentration factors around the periphery of crack-like flaws, which were postulated to exist at the corners of nozzles intersecting cylindrical shells [43]. The models explicitly included the corner flaw with a specified size and shape to make a quantitative evaluation of the flaw shape effect. For this study, a 180 degree section of a cylinder shell intersected by a nozzle was modeled with 1668 elements and 8660 nodes. Circular (with corner radius) and saw-cut (chamfer) flaw shapes were evaluated. The results were compared with:

(a) The simplified solutions using the flaw evaluation procedure of section XI of the ASME Boiler and Pressure Vessel code [44].

(b) The Welding Research Council (WRC) bulletin No. 175 [44].

(c) Previously published empirical formulae.

It was concluded that the results were in good agreement with the average values obtained by the methods above. Detailed analysis was not provided since the study was mainly concerned with fracture around nozzles.

A three dimensional finite element approach has been used to study the stress distribution and stress concentration factors in thick walled closed ended cylinders with cross bores of various blending geometries [17,18,45]. A maximum of 360, 20 noded brick type isoparametric elements were used. A cross bore to main bore radius ratio of 0.12 was investigated. A 3 mm chamfered entry cross bore at 45° and a 3 mm radiused entry cross bore were considered. Two thickness ratios of 1.4 and 2 were considered. The stress concentration factor for a thickness ratio of 1.4 for cylinders having plain, radiused and

chamfered cross bores were found to be 2.84, 1.43 and 2.11 respectively. For a thickness ratio of 2, the corresponding stress concentration factors were 3.30, 1.48 and 1.86. It was concluded that the introduction of cross bores into a cylinder wall greatly increases the hoop stress that would otherwise be present in a plain cylinder. A surprising conclusion was that the introduction of chamfers and radiused entries to cross bore increases the stress concentration factor compared to that of a plain cross bore. For the plain cross-bored cylinder, the maximum hoop stress was found to be away from the crotch corner. The results of this research can not be considered to be conclusive. Several cross bore to main bore radius ratios, chamfer angles and lengths, radiused entry values and thickness ratios should have been considered in order to have justified conclusions.

Determination of the stress distribution along a free boundary reveals a weakness in the conventional finite element method procedures since in general, the chosen element displacement functions do not implicitly satisfy the conditions which prevail at a free boundary [46-48]. A modified finite element method procedure was proposed to obtain boundary stresses with improved accuracy. Improved results were verified using photoelastic and conventional finite element method analysis. Specialized shell intersection finite elements compatible with adjoining shell elements have been developed [49]. The element has the capability of physically representing the complex three dimensional geometry and stress state at the shell intersections. The results compared well with those of a closed form theory of elasticity solution when used to compute the stress state and strain energy in the elements. Fillets are often used to connect the flat heads and the cylindrical shells in pressure vessels. Localized high stress intensity occurs at the round corner when the pressure vessel is subjected to internal pressure. Finite element method analyses have been conducted on various shell/head configurations [50] and the results found valuable when the overall design of the cylinder is considered.

The boundary integral equation method of numerical stress analysis to compute stress concentration factors at intersections between side branches and thick walled pressure vessels was carried out [51]. A three dimensional analysis of circular and elliptical holes led to the conclusion that the use of an elliptical small side hole in a cylinder, with its minor

axis parallel to the axis of the cylinder, can substantially reduce the maximum stresses. For typical geometries considered, reductions of more than 20% of the stress concentration factor were recorded by using elliptical holes. For a cylinder having a thickness ratio of 1.5 and cross bore to main bore radius ratio of 0.5, a stress concentration factor of 3.7 was obtained. This value was quite comparable to the stress concentration factor of 3.08 earlier obtained ([39]). The relatively large cross bore was found to cause some increase in stress concentration factor values. Evaluation of the stresses in an attachment/spherical shell structure has also been done using this method [52] and the results compared with the finite element method and analytical solutions. The boundary integral method was found to be computationally more efficient than the finite element method.

Approximate empirical and variational methods have been used to predict the stress concentration factors in various shell-branch configurations where the cross bore to main bore radius ratio is around one [53-56]. In one study [53], this empirical equation was cast in the form of a polynomial obtained by the least squares method. 120 sets of experimental data from literature were used to fit the polynomial while another 64 sets of experimental data generated was used to verify the empirical equation. The results obtained showed good agreement with those obtained from previous experimental work. Adams [54] analyzed shallow shells with a cut out using a variational method. For a cross bore to main bore radius ratio of 0.2 and a thickness ratio of 1.1, a stress concentration factor of 4.14 was obtained. This compared well with the theoretical value of 4.24.

Approximate solutions based on the theoretical solution for a hole in an infinite plate under uniform tension have also been proposed [39]. For a cylinder with a thickness ratio of 3, a hoop stress concentration factor of 3.7, which was 32% higher than the measured value was obtained. The results thus obtained provided the equations to calculate asymptotic stress concentration factors for cylinders with cross bores sufficiently small compared with the main cylinder bore. An approximate equation was derived to predict the stress concentration factors. This equation is given by:

$$stress\,concentration\,factor\,(SCF) = \frac{4k^2+1}{k^2+1} = \frac{\sigma_{hoop\ (max)}}{\sigma_{hoop\ (no\ min\ al)}} \qquad (2.1)$$

where k is cylinder thickness ratio defined as the ratio of outer diameter to inner diameter,

$\sigma_{hoop\ (max)}$ is the maximum hoop stress,

$\sigma_{hoop\ (nominal)} = [P\ (\ k^2+1)/(k^2-1)]$= nominal hoop stress at the main cylinder bore [1],

P is the applied internal pressure.

Despite providing quick and rough solutions, the equation does not consider the presence of cross bores and the error margin of 32% is really unacceptable.

Analytical and stress function equations to solve for the stress and displacements at thin shell intersections have been developed [57,58]. Diameter ratios of 1:2 were used and the results compared well with finite element analysis results and previous experimental work. Large deflections in strain hardening materials were considered [58].

Empirical stress concentration and effective stress factors for various pipe/junction geometries have been proposed [26]. The stress concentration factors are:

$$SCF = \frac{2+2\,d_n/D_m\sqrt{d_n/D_m\ t_m/T_m}+1.25\,d_n/D_m\sqrt{D_m/T_m}}{1+t_m/T_m\sqrt{d_n/D_m\ t_m/T_m}} \qquad (2.2)$$

or by use of the Money relationship,

$$ESF = 2.5\left\{\left(r_m/t_m\right)^2 T_m/R_m\right\}^{0.2042} \quad 0 < d_n/D_m \le 0.7 \qquad (2.3)$$

$$ESF = 2.5\left\{\left(r_m/t_m\right)^2 T_m/R_m\right\}^{0.241} \quad 0.7 < d_n/D_m \leq 1.0 \qquad (2.4)$$

where, D_m is the cylinder mean diameter, d_n is the nozzle mean diameter, t_m is the nozzle thickness, T_m is the cylinder thickness, r_m is the nozzle mean radius and R_m is the cylinder mean radius.

The long user input time and CPU time for calculations have led several researchers to look for other cheaper but approximate methods of modeling cross bores in thick walled cylinders [59]. Reinforced nozzles have been modeled as sphere shell intersections with a resultant CPU time of only one minute. A combination of Fourier series solutions and simple asymptotic (boundary layer) solutions have also been used for the general intersection curve on a cylindrical vessel.

2.2.2 Elastic-Plastic Stress Analysis

Overstrain and ultimate bursting pressure experimental studies of thick walled cylinders made of four different steel materials have been conducted [60]. A theoretical method was then proposed for computing expansion and bursting strengths based on both tension and torsion data. These results would be only applicable to the main cylinder body away from the cross bores.

Three dimensional finite element method elastic-plastic analysis for cylinders with thickness ratios of 2 and 1.4 have been conducted [17,61]. The PAFEC 75 finite element software was used. Due to limitations of storage and memory of the computer, it was not possible to test all the elements for plasticity and therefore a few elements in the vicinity of the points of peak stresses (determined from an elastic solution) and adjacent to the boundary were allowed to yield. This was done for a plain cross bore, radiused cross bore and a chamfered cross bore. The von Mises yield criterion was assumed. The elastic and plastic strain components in the critical region of the cross bore were determined. The author was mainly interested in fatigue life and therefore overstrain stresses were not presented or discussed.

The deformation behaviour of long elastic-plastic tubes under internal pressure and axial loading has been studied [62] using the finite element analysis with eight noded isoparametric elements. The authors used the constitutive equation derived from the J_2 corner theory of Christofferson and Hutchinson [62] which allows corner formation on the yield surface and also accounts for the Bauschinger effect. Both plane and generalized plane strain conditions were considered. Although the effect of the axial load on the maximum pressure is significant, it was found to diminish as deformation proceeded. Generally, positive axial loads were shown to lower the maximum pressure substantially.

The incremental theory of plasticity was used to study the pipe bore expanding process [63]. The numerical finite element method work also addressed the effect of the yield stress and the strain hardening exponent of the material on the stress and strain levels. By considering that the effective stress is given by the equation:

$$\bar{\sigma} = Y_s + C\bar{\varepsilon}^n \tag{2.5}$$

and that:

$$\bar{\sigma} \approx C\bar{\varepsilon}^n \tag{2.6}$$

where $\bar{\sigma}$ is the effective stress, $\bar{\varepsilon}$ is the effective strain, n is the strain hardening exponent and C is a material constant, the indeterminacy of the initial conditions were eliminated by the use of the approximation that the yield stress is zero.

The bifurcation and post bifurcation behaviour in the axisymmetric deformation of circular elastic-plastic tubes under axial tension and internal pressure has been considered using the finite element method [64]. Elastic-plastic strain hardening material with smooth yield surface was assumed. Shear stress at both ends of the tube arising from deformation was ignored. Two bifurcation modes were identified: cylinder length elongates (necking) and cylinder length contracts (bulging). These observations were attributed to the frequent change of the determinant of the stiffness matrix from positive to negative. During these changes, the determinant vanishes and these are the practical collapse points or bifurcation points. The finite element method has also been used in metal forming elastic-plastic problems. The finite size deformations involved were found

to introduce some instability which was taken care of by modifying the stiffness formulation by means of the mean normal technique [65] in the matrix iteration process.

The plastic stress-strain matrix derivable by inverting the Pradtl-Reuss equations in the plasticity theory was proposed in the solution of continuum elastic-plastic problems using the finite element method [66]. The method uses the small and varying increments of load sufficient to just cause yield in the successive elements. Triangular elements in sample solutions of notched tension specimens were used. In this work, the plastic stress-strain constitutive equation was explicitly developed for the first time. The explicit form of the constitutive equation has now greatly reduced the programming effort in the incremental theory of plasticity. Other numerical finite element method solutions to three dimensional elastic-plastic problems, illustrating the applicability of the isoparametric elements and the order of computation times involved have been presented [67]

Elastic-plastic analysis of thick walled pressure vessels with sharp discontinuities in the form of cylinder head radial circumferential cracks has been carried out using the finite element method [68]. For a shell thickness of 50.8 mm and a crack length of 25.4 mm, it was concluded that as long as the material is sufficiently ductile to prevent local fracture, the effect of local imperfections maybe ignored.

Three dimensional elastostatic analysis of pressurized cross-bored thick walled cylinder in partial autofrettage was carried out using the numerical boundary integration method [69]. Thickness ratios of 2 and 2.25 and a cross bore to main bore radius ratio of 0.25 were considered. Stress concentration factors of 3 and 3.32 were obtained respectively. These results compared well with the results of other researchers ([38]). In both cases, the autofrettage was performed after the introduction of the cross bore. The maximum percentage overstrain that can be induced in the cylinder was found to be 35% and 27.5% for the 2 and 2.25 thickness ratios respectively. The percentage overstrain was taken as that percentage of the cylinder wall thickness which has undergone plastic deformation during the application of the autofrettage pressure. Cases of plain cross bores without autofrettage were also considered in order to confirm the results. A maximum stress concentration factor

to introduce some instability which was taken care of by modifying the stiffness formulation by means of the mean normal technique [65] in the matrix iteration process.

The plastic stress-strain matrix derivable by inverting the Pradtl-Reuss equations in the plasticity theory was proposed in the solution of continuum elastic-plastic problems using the finite element method [66]. The method uses the small and varying increments of load sufficient to just cause yield in the successive elements. Triangular elements in sample solutions of notched tension specimens were used. In this work, the plastic stress-strain constitutive equation was explicitly developed for the first time. The explicit form of the constitutive equation has now greatly reduced the programming effort in the incremental theory of plasticity. Other numerical finite element method solutions to three dimensional elastic-plastic problems, illustrating the applicability of the isoparametric elements and the order of computation times involved have been presented [67]

Elastic-plastic analysis of thick walled pressure vessels with sharp discontinuities in the form of cylinder head radial circumferential cracks has been carried out using the finite element method [68]. For a shell thickness of 50.8 mm and a crack length of 25.4 mm, it was concluded that as long as the material is sufficiently ductile to prevent local fracture, the effect of local imperfections maybe ignored.

Three dimensional elastostatic analysis of pressurized cross-bored thick walled cylinder in partial autofrettage was carried out using the numerical boundary integration method [69]. Thickness ratios of 2 and 2.25 and a cross bore to main bore radius ratio of 0.25 were considered. Stress concentration factors of 3 and 3.32 were obtained respectively. These results compared well with the results of other researchers ([38]). In both cases, the autofrettage was performed after the introduction of the cross bore. The maximum percentage overstrain that can be induced in the cylinder was found to be 35% and 27.5% for the 2 and 2.25 thickness ratios respectively. The percentage overstrain was taken as that percentage of the cylinder wall thickness which has undergone plastic deformation during the application of the autofrettage pressure. Cases of plain cross bores without autofrettage were also considered in order to confirm the results. A maximum stress concentration factor

of 3 at the intersection point was obtained for the case where the thickness ratio was 2. In this work, only one cross bore radius and two thickness ratios were considered. Therefore the results may not be extended to other combinations of cylinder to cross bore geometry.

Approximate equations suitable for a numerical solution of an axisymmetric shell under axisymmetric loadings have been developed [70]. An incremental approach under the consideration of the first order approximation in determining the tangent stiffness characteristics of the finite element was used. The effects of strain hardening, both isotropic and kinematic, were included. Initial stresses were included to account for instability and large accumulated deformations during the loading of the structure.

One of the most comprehensive theoretical studies in this area proposed a stiffness method for the solution of elastic-plastic problems [71]. The stiffness concept enabled the equilibrium equations to be expressed in terms of displacements. The use of the stiffness coefficients removed the need to trace the expansion of the elastic-plastic boundary during the actual solution of the differential equations. The method was found to work for a closed ended tube under internal pressure. It was noted that the change of the slope of the stress-strain diagram at yield usually prevents elastic-plastic problems from being solved by a closed form analysis due to the presence of singularities. The following difficulties were identified in a numerical solution of the elastic plastic problems:

(a) The problem is non-linear. Therefore the use of the von Mises criterion of yielding introduces a further degree of non-linearity.

(b) At yield, there is a sharp drop in the value of the tangent modulus. This decrease is modified to a certain extent by the work hardening of the material.

(c) At any stage of the loading, the boundary between the elastic and plastic material is not fixed but changes with the loading and forms one of the unknowns to be solved with the problem.

Consequently, special complications arise when the elastic part of the structure with stresses near yield become plastic in the next load increment. This is the transition region. A technique was proposed for dealing with this transition region based on an estimate of

the strains that would be caused by the next increment of load. The perfectly plastic material or very small degrees of hardening were found to be special cases in the stiffness method, forming the severest test for the method. Other theories of elastic-plastic stress coining techniques as an effective cold working process to improve fatigue strength of structures particularly plates for riveting in the aircraft industry have been presented [72].

Von Mises and Tresca's yield theories have been compared in conditions of compressibility and incompressibility for elastic-plastic analysis of thick walled cylinders [73]. Large differences in stresses were observed from these two yield criteria. A closed form theory to include the Hencky stress-strain relations, incompressibility and Ludwik strain hardening function was proposed. However, the work does not discuss which of the two yield theories is more accurate.

2.2.3 Residual Stresses

Autofrettage is one practice that has proved useful in the chemical industry and gun barrels (in increasing the fatigue life of high pressure piping, compressor chambers and similar thick walled components) [74,75]. Determination of residual stresses arising from forming, cold working or overstrain procedures is very important, particularly where cross bores may exist. For plain cylinders under partial autofrettage, the analytical residual stresses may be obtained directly by applying an equivalent thermal load [76]. If the temperature gradient of the thermal load and the yield stress of the material satisfies the equation,

$$\frac{E\alpha(T_a - T_\rho)}{2(1-\upsilon)Ln\left(\rho/a\right)} = \frac{Y_S}{\sqrt{3}} \qquad (2.7)$$

where, ν is the Poisson's ratio, a is the inner radius, ρ is the plastic interface radius, T_a and T_ρ are the inside wall and outside wall temperatures and α is the coefficient of linear expansion,

then the autofrettage residual stresses and thermal stresses are equivalent. Using the temperature distributions as the temperature input, thermal stresses are then evaluated [77] and found to be equivalent to residual stresses. The redistributions of thermal stresses due to the presence of geometrical discontinuities are now known to simulate the redistribution of residual stresses caused by the same geometrical changes. The stress intensity factors due to residual stresses for the commonly occurring short radial cracks in autofrettaged vessels may then be determined [76]. The above process refers to a thick cylinder of monoblock construction. Residual stress systems may be established in cylinders when shrink fitting two or more thinner cylinders is the method of construction. This method has advantages and limitations as discussed in section 2.3.8 of this chapter.

Simple methods using two main approaches for measuring residual stresses using a fracture mechanics approach have been developed [78-81]. These methods are:

Destructive: These measure the relaxed strains (displacements) arising from a material on removing its surrounding restrictions partially or wholly.

Non destructive: Some of these are; X-ray diffraction and ultrasonic wave method. These are restricted to surface measurements.

However, the above methods are not satisfactory for measuring the residual stress distributions where stress gradients are high. Destructive procedures employing incremental strain gauge data in a finite element algorithm to construct the initial residual stress distribution are currently in use and include [82];

Sequential (for example, Sach's method): Involves total destruction of the specimen, measuring strain changes throughout the procedure.

Selective (for example, slitting of the bore): Requires localised removal of material, enabling local residual stresses to be estimated.

Any of the above methods for evaluating residual stresses are not adequate for use in cross-bored cylinders. A numerical method such as the finite element method is more suited since

no destructive procedures are involved and the state of residual stress at any location can be determined.

Tensile hoop residual stresses are introduced into seamless gas cylinder necks at the bore during the heat treatment stage of the manufacturing processes. At the neck, the plastically deformed outer surface material experiences compressive hoop stresses and the bore experiences tensile hoop stresses. Material removal corrective procedures to remove the bore residual stresses have been established [83].

The SAE 3320, SAE 4340, SAE 1045 and Cr-Ni-Mo-V steels were used in studying the dilation characteristics of thick walled cylinders in the presence of overstrain, residual stresses and heat treatments [84]. It was concluded that residual stresses due to heat treatments have no effect on the overstrain or bursting pressures. A method was proposed in pressure treatment combined with a thermal treatment to produce a compressive residual stress in the inner and outer parts of tubes. This is applicable particularly in the bend regions where stress corrosion cracking is a problem [85]. As a means of measuring autofrettage in thick walled cylinders, an experimental method based on measuring the hoop strain while axisymmetrically releasing the residual stress field by introduction of radial cuts in the cylinder has also been proposed [86-88]. This is from the fact that access to the cylinder inside surface for purposes of placing strain gauges is usually denied. The practical behaviour of pressure vessel materials shows hardening properties. The degree of hardening has been investigated to determine how it may improve the pressure vessel response in service [89,90].

Strain hardening pressure vessels were loaded using a temperature gradient and an internal pressure [91]. Overstrain plastic stresses and strains were evaluated using the numerical incremental theory of plasticity and the method of successive elastic solutions [92] with reverse yielding and the Bauschinger effect being ignored. Residual stresses were evaluated for 25 and 50% overstrains. It was noted that thermoelasto-plastic and residual stress analysis are important in two major aspects of pressure vessel design: design for strength and design for fracture. For partially overstrained plain thick walled

cylinders, an optimum overstrain radius has been proposed [93] as being equal to $(R_iR_o)^{1/2}$ for medium strength steels, and slightly less for high strength steels.

A destructive technique to determine residual stresses in thick walled pressure vessels coupled with incremental strain gauge data in a finite element algorithm to construct the initial residual stress distribution has been proposed [82]. It was concluded that the method could be applied to thick walled pressure vessels of geometries more complex than plain cylinders. Residual stresses arising from the forming processes or deliberately induced are known to affect greatly the way structures respond under service loads and they are therefore a focus of many researchers [94,95].

Determination of the effects of two outer diameter notch configurations in a cylinder subjected to internal pressure or containing autofrettage residual stresses was performed using finite element analysis [96]. Equivalent temperature loads were used for 60 and 100% overstrain cases. A simple method for residual stress estimation and shakedown evaluation using the GLOSS analysis has also been proposed.

A closed form solution of residual stresses in autofrettaged tubes was obtained from a proposed theoretical model for a high strength steel ($Y_s \approx 1173$MPa) [97]. For this steel, tensile tests exhibit very little strain hardening. Models neglecting both strain hardening and Bauschinger effects were found to overestimate the bore residual hoop stress by 46% while models including the Bauschinger effect only underestimated this value by 25%.

Analytical residual stresses for hardening and non hardening materials considering Tresca's and von Mises yield criteria have been obtained [98]. Closed and open-ended cylinders were considered. The optimum overstrain to prevent re-yielding was proposed. It was noted that overstrain prevents a reduction in fatigue life for cylinders having a thickness ratio greater than 2.96. The Tresca's yield criterion results were admissible for thickness ratios less than 2 but the von Mises citerion was found more practical for thickness ratios greater than 2. The Influence of strain hardening on open thick walled cylinders was found important when the thickness ratio is greater than or equal to 3. Fatigue life under a crack

and residual stress was estimated.

Linear elastic solutions of an axisymmetric boundary value problem can be used as a basis to generate its inelastic solution. This solution may then be used to predict the residual stress fields [99]. The dependency of Bauschinger effect on plastic strains makes significant changes to residual hoop stress near the bore for low level autofrettage but this dependency was found to be insignificant for high level autofrettage.

The evaluation of residual stresses, particularly inside the material, is difficult and various methods have been proposed as presented in this section. However, no relevant work has been dedicated to the evaluation of residual stresses in thick walled cylinders having cross bores. This is despite the fact that residual stresses are induced by forming or fabrication processes of thick walled cylinders.

2.2.4 Statistical and Probabilistic Models

The variations in geometry, loads and material properties using probability methods have been evaluated [100]. Pressure vessels exposed to high static internal pressure may experience both elastic and plastic deformations due to the design variations. The design variation simulation was done using Monte Carlo simulation and available statistical information. The results reinforced the importance of using pressure vessels at or under the design pressure. The work also considered autofrettage as a way of optimizing design by the introduction of a favourable stress system well below that produced by the design pressure. This work involved plain cylinders only.

2.3 Pressure Vessel Design Considerations

While a lot of research has been done on the various aspects of pressure vessels, the design of pressure vessels is normally guided by the use of design codes of practice. A lot of research has also been carried out in order to make the design codes more relevant. Some of the important design aspects will be presented here.

2.3.1 Factor of Safety

A single parameter to describe pressure vessel design progress is best measured by the total advancement in knowledge of the three basic elements; namely, engineering, materials and fabrication that establish safety and costs. Such a single parameter is usually called a factor of safety and is used to indicate proximity to failure or economic survival. This factor is usually assigned to a physical property of a structure such as ultimate strength, yield stress and toughness.

Designs of most structures are based on formulae that are known to be approximate and use materials whose mechanical properties cover a relative band with environmental behaviour not thoroughly known. The missing knowledge is accounted for by use of design stresses that are admittedly below those at which the member will fail. The potential properties of a material can be more fully utilized with confidence with the discovery or recognition of more of the factors affecting behaviour and proper account taken in the design analysis. Factors of safety are therefore a trade off means of establishing equal reliability and safety by assigning a single parameter varying degrees of quality assurance (design analysis, fabrication control, in-service inspection). This is the basis upon which many codes and standards are based. Table 2.1 [3] shows some factors of safety from different ASME codes while figure 2.1 [3] shows the effects of factors of safety on the pressure vessel costs. The factor of safety has been considerably reduced by use of the bursting pressure as the basis for cylinder design [101] while considerations of creep and high temperature influence the choice [102].

It has been a popular concern amongst several researchers that the design requirements specified by certain authorities may, by demanding excessively high factors of safety, precipitate failure which they legislate against. If the factor of safety is too high, the designer may be forced to use higher strength steels which have inadequate resistance to fast fracture [2].

2.3.2 Shakedown Theory

Shakedown analysis is of special importance in the case of pressure vessels and other

2.3.1 Factor of Safety

A single parameter to describe pressure vessel design progress is best measured by the total advancement in knowledge of the three basic elements; namely, engineering, materials and fabrication that establish safety and costs. Such a single parameter is usually called a factor of safety and is used to indicate proximity to failure or economic survival. This factor is usually assigned to a physical property of a structure such as ultimate strength, yield stress and toughness.

Designs of most structures are based on formulae that are known to be approximate and use materials whose mechanical properties cover a relative band with environmental behaviour not thoroughly known. The missing knowledge is accounted for by use of design stresses that are admittedly below those at which the member will fail. The potential properties of a material can be more fully utilized with confidence with the discovery or recognition of more of the factors affecting behaviour and proper account taken in the design analysis. Factors of safety are therefore a trade off means of establishing equal reliability and safety by assigning a single parameter varying degrees of quality assurance (design analysis, fabrication control, in-service inspection). This is the basis upon which many codes and standards are based. Table 2.1 [3] shows some factors of safety from different ASME codes while figure 2.1 [3] shows the effects of factors of safety on the pressure vessel costs. The factor of safety has been considerably reduced by use of the bursting pressure as the basis for cylinder design [101] while considerations of creep and high temperature influence the choice [102].

It has been a popular concern amongst several researchers that the design requirements specified by certain authorities may, by demanding excessively high factors of safety, precipitate failure which they legislate against. If the factor of safety is too high, the designer may be forced to use higher strength steels which have inadequate resistance to fast fracture [2].

2.3.2 Shakedown Theory

Shakedown analysis is of special importance in the case of pressure vessels and other

structures subjected to variable direct or thermal loads [103]. In the presence of plastic strains, there is no one-to-one stress-strain correspondence and the structural response to the same load can depend on the load history. If a structure made of an elastic-plastic material is exposed to cyclic loads, the following situations may arise:

(a) If the load intensities remain sufficiently low, the structural response is perfectly elastic (with the exception of stress singularities).

(b) If the load intensities become sufficiently high, the instantaneous load carrying capacity of the structure becomes exhausted, plastic unconstrained flow mechanism develops and the structure collapses. Obviously, plastic deformations can develop also for loads below collapse load.

(c) If the plastic strain increments in each load cycle are of the same sign, then, after a sufficient number of cycles, the total strains and displacements become so large that the structure departs from its original form and becomes unserviceable. This is called incremental collapse or ratcheting [104,105]. Even when external loads are small, ratcheting is highly influenced by high temperatures [106].

(d) If the strain increments change sign in every cycle, they tend to cancel each other out and the total deformation remains small. This is called alternating plasticity. However, after a number of cycles, the material at the most stressed points begins to break due to low cycle fatigue.

(e) After some plastic deformation in the initial load cycles, the structural behaviour becomes eventually elastic for lower load amplitudes. Such stabilization of plastic deformations is called shakedown or adaptation.

Once the plastic deformations are accounted for in the design process, it is natural that any possible history of loading acting upon the structure will lead to structural shakedown. It is also possible that incremental collapse and low cycle fatigue may appear simultaneously, for example, if one component of the plastic strain tensor increases with each load cycle whereas another one oscillates. The main problem of shakedown theory is to investigate whether or not a given structure will shakedown under given loads. The phenomenon of shakedown is very relevant particularly because the elements around the cross bore elements have a high probability of yielding even when the service stresses are intended to

be elastic.

2.3.3 Categories of Stress

The accurate and detailed determination of the stresses in a pressure vessel would be of little value if the designer did not know the significance of those stresses in relation to failure [107]. Also, the calculated or even measured value of stress or strain means little until it is associated with its location and distribution in the structure and with the type of loading which produced it [107]. In setting the allowable stresses, the stresses in pressurised pressure vessels are divided into the following categories;

(a) Primary stress: a stress developed by the imposed loading which is necessary to satisfy the laws of equilibrium of external and internal forces and moments. If it exceeds the yield stress of the material, the prevention of failure is entirely dependent on the strain hardening properties. According to ASME Section II NB-3213.8 and Section VIII, Division 2 4-112/g [108], the primary stress is defined as:

The primary stress is any normal stress or a shear stress developed by an imposed loading which is necessary to satisfy the laws of equilibrium between external and internal forces and moments. The basic characteristic is that primary stress is not self limiting.

Primary stresses which considerably exceed the yield strength will result in failure or, at least, in gross distortion. A thermal stress is not classified as a primary stress. The primary membrane stress is divided into general, local and bending stresses. A general primary membrane stress is one which is so distributed in the structure that no redistribution of load occurs as a result of yielding. The code provides classification of stresses for some typical cases. Implicit in this is the method of analysis employed.

(b) Secondary stress: a stress developed by the self constraint of a structure. They may be of great significance in high strength brittle materials and even in ductile material when the material is subject to ratcheting under cyclic loading [3,109].

(c) Local or peak stress: the highest stress in the region under consideration. This causes no significant distortion and is objectionable only as a possible source of fatigue failure, brittle fracture or stress corrossion cracking.

The condition required for the peak stress to be objectionable (in part (c)) is not properly stipulated for pressure vessels. It has been established from failure analysis studies that fatigue failure and brittle fracture in pressure vessels normally start at the points of peak stresses, that is, around the cross bore crotch corner. Stress corrosion cracking is also severest at the points of peak stresses. There is then a need to review or reformulate the emphasis laid on peak stresses.

At the time the stress classification system was introduced, the common method of analysis was the discontinuity (interaction) analysis. Today, an inelastic analysis, as described below, offers the most accurate stress solution possible. The method results in lower factors of safety and may give a clear picture of the state of stress throughout the structure if required.

2.3.4 Inelastic Analysis

This provides an alternative to a direct assessment of the primary stress limit and often results in some increase in the allowable design pressure. The two types of inelastic analysis are:

(a) Limit analysis

The rules of the design by analysis have been in ASME Boiler and Pressure Vessel Code (Section III, and latter in Section VIII Division 2) since 1963. From this approach, a designer calculates the stress intensities in a vessel under all loadings and compares them to code limits. The calculated membrane, shear and bending stresses are classified to facilitate the process of combining them and checking code limits. Code limits are set to preclude identified failure modes. The goal of design by analysis is to permit the use of higher allowable stresses without reduction in safety by making better use of modern methods of stress analysis [108].

Limits on general and local primary membrane stress intensity and primary membrane

plus primary bending stress intensity need not be satisfied at a specified location If it can be shown by limit analysis that the specified loadings do not exceed 2/3 of the lower bound collapse load. The limit analysis is a special case of plastic analysis in which the material is assumed to be ideally plastic.

(b) Plastic analysis.

Plastic analysis is a method of structural analysis by which the structural behaviour under given loads is computed by considering the actual material stress strain relationship.

The purpose of the primary stress limits are:

(a) The primary stress limits are provided to prevent plastic deformation and to provide a nominal factor of safety on the ductile burst pressure.

(b) Primary plus secondary stress limits are provided to prevent excessive plastic deformation leading to incremental collapse and to validate the application of elastic analysis when performing the fatigue evaluation.

Today, elastic finite element analysis has replaced the interaction analysis as the tool of choice in the pressure vessel industry. However, one drawback of the method is the difficulty in classifying the primary and secondary membrane stresses when a single elastic analysis is performed. This can be solved by:

(a) Elastic compensation method [110]; In this method, iterative elastic finite element analysis is performed.

(b) GLOSS R-node method [111]; This is the generalised local stress strain method.

The ASME Boiler and Pressure Vessel code empirical design formula has been found to lack a thorough elastic-plastic analysis to justify itself [112]. For example, the maximum elastic stresses predicted by the code are underestimated and the considerable redistribution of stresses during the water pressure test are not explicitly recognized [112].

2.3.5 Design Codes and Proposed Modifications

The main purpose of any industrial code is safety though it is additionally viewed as a product standard in today's competitive world. Though most industrialized countries have their own design codes, most designs of pressure vessels are done using either of the two major design codes;

(a) The ASME Boiler and Pressure Vessel Code.

The first legal code of rules for the construction of steam boilers was enacted in 1907, in the United States. The first ASME Boiler and Pressure Vessel Code (Section I, Power Boilers) was prepared in 1914. Other sections of this code were developed as shown in table 2.2 [113]. The current code was adopted in 1992.

Section VIII Division 2 formulae for wall thickness are given as [114]:

$$T_m = \frac{P_D R_i}{S - 0.5 P_D} \tag{2.8}$$

or

$$Ln\left(\frac{R_i + T_m}{R_i}\right) = \frac{P_D}{S} \tag{2.9}$$

Where, P_D is design pressure and $P_D \succ 0.4S$, R_i is internal radius and T_m is wall thickness. S is design stress equal to $S_{ult}/3$ or $2Y_S/3$. It is noted that Division 2 does not set any upper limit on pressure and materials with $Y_S \geq 932$ MPa are not listed. In fatigue analysis, shrink fitting and autofrettage effects are not accounted for. A maximum pressure of 1400 MPa so as to take advantage of high strength materials has been proposed. It is mandatory for manufacturers to observe this code.

(b) Unfired Fussion Welded Pressure Vessels [115].

This is a British Standard (BS) Institution code. BS 5500: 1997, which was first effected in 1976 and is reviewed on a regular basis [116]. This standard is based on the concept of achieving shakedown to elastic behaviour when pressure cycling to the design conditions. The achievement of shakedown at all locations avoids incremental straining and, by inference, the avoidance of a ratcheting behaviour

towards incremental collapse in service. The standard test [117] (usually hydraulic) is done at 1.25 times the design pressure. A further margin is allowed for pressure testing being made at normal ambient temperature with materials of construction stronger than they are likely to be at the vessel design temperature and also not corroded at the end of the expected service life. If the pressure vessel has parts for which the strength can not be satisfactorily calculated, the use of the proof hydraulic test is required using strain measuring equipment in a local search for inelastic behaviour. Strain indicating coatings or electric resistance strain gauges are used. Strain indicating coatings are allowed on carbon or carbon-manganese steel pressure vessels. Here, a test pressure of 1.5 times the design pressure is used. The materials exhibit a sharp yield in uniaxial testing. Brittle lacquer is not to be used. Real materials are not perfectly elastic-perfectly plastic [117] and also exhibit some hysteresis. In practice, this leads to a poor definition of shakedown. Therefore, BS 5500 allows for up to six successive applications of the desired test pressure in attempts to obtain two successive cycles of strain and pressure readings which when plotted tend to substantially coincide [117].

The BS 5500 deals purely with the specification and the requirements of pressure vessel design, construction, inspection and testing. The code is divided into sections as shown in table 2.3 [115]. The wall thickness design formula is given as [118];

$$T_m = \frac{2P_D R_i}{2S - P_D} \tag{2.10}$$

where P is the design pressure and f is the design stress. For this code it has been proved that proof testing tends to inhibit all strain accumulation during subsequent operation of the vessel at the design pressure.

Pressure vessel design by analysis in BS 5500 has been under constant development. The primary stress is limited to prevent bursting under static loading while the secondary stress is limited to ensure shakedown under cyclic operation.

The peak stress arises from local structural discontinuities and is limited to prevent fatigue under cyclic operation [119]. Neglecting peak stresses,

$$\sigma_e = p_{\text{prim stress}} + q_{\text{secondary stress}} \tag{2.11}$$

while the elastic stress field is uniquely defined by an elastic analysis, its primary and secondary stress constituents are not uniquely defined. From the code,

$$p + q = 3\,S_m \tag{2.12}$$

where S_m is the code allowable stress value. The guidelines are given in the code but only for shell-type stress distributions. This design code is not mandatory and only serves as a guide.

Solid finite element analysis in two or three dimensional form is based on elasticity theory, making it difficult to interpret and apply code limits. The problem has been addressed by using stress linearization procedures to extract constant (membrane) and linear (bending) stress distributions which give the same net section forces and moments as the actual finite element stress along class lines. However, this is not applicable to all pressure vessel geometries [120, 121].

Various National design codes incorporate rules for determination of the shell and nozzle sizes. Some are based upon the idea of replacing in the nozzle the cross sectional area from the shell [26], while others are based on rules aimed at limiting the highest stress to a prescribed value [42]. Figure 2.2 [5] shows a striking comparison between the wall thicknesses which were required in 1960 in various countries for essentially the same service and material. Figure 2.3 [122] also shows the different wall thicknesses that are prescribed by two different divisions of the ASME. Several approaches based on reliability analysis have been adopted for determining the safety factors in pressure vessel design [123].

Simplified design formulae have been proposed for thick walled cylinders and spherical pressure vessels manufactured from work hardening materials [124]. Rational design of pressure vessels under internal pressure requires the study of two modes of failure:

1. when the deformation becomes excessive and there is a possibility of permanent deformation.
2. Failure occurs at a higher pressure and takes the form of bursting of the vessel.

Design formulae for high temperature service has tended to be over conservative leading an economic burden. A wall that is too heavy can adversely affect reliable operation due to thermal stresses set up by temperature differences between inner and outer surfaces during temperature transients. The following formula has been proposed [26];

$$T_m = \frac{2PR_o}{2S - 2yP} \tag{2.13}$$

where, P is the internal pressure, y is a temperature dependent parameter and S is the code allowable stress value.

ASME Section VIII, Division 1 is inadequate in certain d/D and D/T ranges as has been proved by vessel leakage. A proposed empirical design method allows a designer to predict the maximum allowable working pressure of an opening reinforcement using an allowable stress basis for large openings [30,125]. The method produces nozzle reinforcements that should remain in the elastic stress range for internal pressure up to the code allowed hydraulic test of 1.5 times maximum allowable working pressure. ASME Boiler and Pressure Vessel code Section VIII Division 2 limits the size of openings to 0.5 times the vessel inside diameter unless a detailed stress analysis is made. Statistical analysis based design formulae have been proposed for elastic breakdown pressure and bursting pressure for temperatures ranging from of 24 to 350^0 C and also considering mild, hardened and tempered steels [21].

The marked drop in the rate of pressure vessel and boiler explosions (in 1950's) caused a reconsideration of most code design criteria. Three aspects were considered as discussed below [4]:

(a) Economics.

(i) Because so few vessels were failing, was the safety factor still too high?

(ii) Because a few vessels in severe service were failing, should more detailed criteria be adopted?

(b) Technology.

Because of the rapid development in stress analysis techniques and in knowledge of material properties, which greatly improved the ability to predict structural response to service loads.

(c) Nuclear power.

This was a potentially significant source of energy, but one that would be more sensitive to failures because of considerations of public health, cost and difficulty of repair. This prompted the inclusion of Section III, into the ASME Boiler and Pressure Vessel Code in 1963.

Developments in large chemical vessels and rocket engines necessitated urgent need for accurate and reliable solutions for pressure vessel designs in order to avoid the repetitions of past catastrophes.

2.3.6 Design Options

The quality of a pressure vessel or piping system depends not only on proper design but also on other facets of the pressure vessel and piping technology. These are materials, fabrication, operation and testing. Present technology demands use of high pressures and hence the importance of these other facets. The potential or stored energy in the system increases with pressure and volume and hence the safety aspects of storing large sources of energy must be seriously considered [17]. The range of uses and types of pressure vessels is depicted in table 2.4 [126].

Two design approaches are used concurrently in the pressure vessel design:

(a) Design by rule.

This approach was exclusively used before the onset of computers by designers such as Manning [2] who dominated the pressure vessel design industry in the early part of the last century. Generous safety margins were employed due to ignorance or lack of knowledge of the stress levels. Typically, a safety factor of 5 was used during the period before the Second World War [4]. In addition to requiring consideration of pressure and superimposed internal and external loads, requirements that follow design by rule method require consideration of impact loads, earthquake loads and effects of temperature gradients on maximum stresses [4].

In service, a vessel deforms first elastically and then plastically. This is a complicated process. The theory of limit analysis, an idealized theory, enables the limit load (plastic collapse load) to be found considering only the limit state and by neglecting any previous deformation. This theory has been used in determining the design parameters of pressure vessels using the design by rule method [4].

(b) Design by analysis

The computer has been the single most powerful catalyst by far in the advancement of the concept of design by analysis [33]. In the design by analysis approach, the design by rule steps of ASME are retained in Section III to assure that maximum advantage is taken of past experience with the method, although the nominal factor of safety has been reduced from 4 to 3. The design by analysis procedure was intended to assure that the nominal safety factor is achieved or exceeded through the explicit consideration of additional modes of failure. This was as a result of work done in the 1950's [4] which showed that low cycle fatigue is characterized by the strain range, and not by the stress range of the cycle as believed earlier. This paved the way for the application of quantitative fatigue analysis in vessel design [4]. The effort of design by analysis is to reduce material and labour costs by the application of advanced technology. Significant savings in materials may of course be obtained by adopting design codes based on analysis rather than on large safety factors. This is illustrated by figure 2.4 [127] which compares the weight and Table 2.5 [127]

which shows the price breakdown for a typical nuclear vessel designed for the same performance according to Section III and Section VIII, Division I, respectively, of the ASME Boiler and Pressure Vessel code. Design by analysis according to Section III is seen to result in weight savings of between 15 and 30% [127].

2.3.7 Pressure Vessel Materials

Pressure vessels operating under severe conditions have been in existence since 1939 [2], when two vessels of 50 litre capacity and operating at 150 MPa were built. In 1946, a vessel of 250 litre capacity with a thickness ratio of 1.67 was introduced using the EN25 steel [2]. This material had a proof stress of 570 MPa and an ultimate tensile strength of 805-930 MPa. As late as 1970, vessels of nominal capacity over 1000 litres were introduced. These later vessels were made from Ni-Cr-Mo-V alloy steel which exhibits higher impact strength and fracture toughness for a given tensile strength than the EN25 steel [113]. The modes of failure of a pressure vessel which are influenced by the choice of material and wall thickness are:

(a) Bursting due to general yielding and rupture of the shell wall.

(b) Ductile tearing at a discontinuity such as a nozzle or head to shell junction.

(c) Brittle fracture at a defect.

(d) Creep rupture at elevated temperature [5].

Thus, the choice of material used in a pressure vessel is very important in its design. In modern technologies, pressure vessels are being operated over a wide range of loading conditions. Temperatures may be as low as -163^{0}C in hydrogen service or as high as 1000^{0}C in cracking processes [2]. At temperatures of 325-575^{0}C, Cr-Mo vessels experience toughness degradation during long term operations. At these temperatures, creep effects are at play. There may be extremely severe electrolytic corrosion conditions combined with high operating pressures, for example, 700 bar in the acetic acid synthesis, or there may be chemical corrosion as in the coal gasification process, or heavy wear conditions, neutron irradiation, embrittlement and many other aggravating conjoint working environments [126,128]. Table 2.6 [126] gives a summary of these exacting conditions. Table 2.7 [129] shows some design conditions for a coal liquefaction plant while table 2.8 [122] shows the

typical chemical composition of most pressure vessels made of the carbon-manganese steel alloys. However, a wide range of steels is available for the manufacture of the pressure vessels, the choice depending on operating temperature and other service conditions [122]. In alloying the steel for pressure vessel application, the factors normally considered are: Mechanical properties, weldability, deoxidation process and impurity elements.

Steels included in Section III and VIII of the ASME Boiler and Pressure Vessel Code severely limit the code's application for high pressure design [130]. Gun steels (AISI 4300 series) have been widely used for pressure vessel applications. The ASTM specification A-723 was developed to cover these Ni-Cr-Mo alloys for pressure vessel use and is being adopted by Section II of the ASME Boiler and Pressure Vessel Code for use in section VIII, Division 2 and in Section III, part NF for component supports.

The trend towards rising temperatures and pressures in steam power plants during the 1930's resulted in the inclusion of creep resistance and rupture strength as criteria for setting ASME Boiler and Pressure Vessel code allowable stresses [131]. Operating conditions continued to become more severe until the early 1960's when the utility industry reached a plateau with respect to steam temperatures and pressures. At temperatures below 540°C, the Cr-1/2Mo steel is frequently more economically attractive than other higher alloy Cr-Mo steels.

Because of the extensive application of 2.25Cr-Mo steel in steam power and petrochemical applications, extensive documentation of its behaviour has been done. However, Cr-1/2 Mo steel has not been nearly as widely used and the data base on its mechanical properties is scarce. The tensile, creep, rupture and fatigue properties of Cr-1/2 Mo steel in the normalized and tempered condition has been characterized and found competitive [132]. Superior performance of 5Ni-Cr-Mo-V compared to existing high yield strength pressure vessel steels has been observed [132]. The 2.5Ni-Cr-Mo austenitic steel has been extensively tested in cyclic loading [133]. The choice of the right proportions of the carbide stabilizing elements is very important in preventing hydrogen

embrittlement and stress corrosion cracking. It also influences the strength and fracture toughness properties.

The increasing use of high yield strength materials in the manufacture of pressure vessels has created the need for stress analysis techniques not restricted to linear elastic theory. Increased use of high strength steels brings a tendency to use thinner sections which in turn leads to larger deflections (non linear theory). Also, due to the limited capacity of such materials to absorb the plastic strains that exist at severe stress raisers, such as nozzles and cross bores, failure due to brittle fracture or fatigue are more likely to occur and an accurate analysis of the plastic deformation is needed [60].

Glass reinforced plastic (GRP) pressure vessels with radial branch connections are now used throughout the chemical industry and the design of their critical components, such as nozzles and end closures, has received a lot of attention [134,135]. BS 4994 [136] gives guidance on the design of GRP pressure vessels. In GRP nozzles and branches, the brittle nature of the material does not allow redistribution of high local stresses by yielding [137]. Light weight Titanium 318 pressure vessels operating at about 69 MPa are now also being used [138].

2.3.8 Pressure Vessel Construction

In the design of pressure vessels, consistent nomenclature is used in order for specifiers, designers, manufacturers and users to communicate effectively. These definations are used also by regulatory agencies, codes and standards. Some of these are [3]:

(a) Design Pressure.

The highest pressure specified and permitted in a vessel at a given temperature when the vessel is new and just being manufactured. This value may be modified for an existing vessel being derated after repairs or the required number of years in service.

(b) Operating Pressure.

The maximum pressure in a vessel at normal operating or working conditions. This should always be lower than the design pressure by about 10%. The difference may be modified depending on the stability of the process to be contained in the vessel.

(c) Design temperature.

The highest mean material temperature permitted in a given part of a vessel at either the design or operating pressures. It is the basis for the allowable stresses to be used for establishing the minimum required thickness of the vessel part.

(d) Overpressure Protection (Relief) device.

A mechanical device intended to release a portion of the contents of a vessel if there should be an unintended source of energy causing the vessel pressure to exceed the set pressure of the device.

(e) Set Pressure.

The inlet pressure at which the vessel overpressure protection device is set to function. The set pressure may not exceed the vessel design pressure.

Due to current demands on the performance of the pressure vessel and the limitations on available forging capacity, different construction techniques have been devised. These are [126]:

(a) Multilayer.

This is the most widely used and consists of an inner shell on which formed concentric layers, approximately 6 mm thick are wrapped and welded to obtain the required thickness. It has the advantage of low costs, brittle fracture resistance and crack propagation resistance [11]. However, it is limited by; high local discontinuity stresses, restricted thermal gradients and limited external pressure or vacuum service. The theory of multilayer pressure vessel design is now well understood [139].

(b) Modular construction

This is an exception to the economic trend from multiple small vessels to single large ones. It consists of utilizing a single standardized mass produced module or building block and changing the total size of vessel required in constant increments by addition or subtraction of a module.

Other construction methods are: banded, wire wrapped and link belt construction. Prestressed concrete/cast iron pressure vessels are also widely used in the nuclear power

industry [11]. Composite compound cylinders composed of an isotropic liner and an orthotropic jacket have been investigated and details of the amount of composite necessary to replace the material machined away from the outer diameter are now available [140]. For an equivalent compound cylinder with the same bore radial displacement per unit of internal pressure, significant weight savings (34%) have been achieved with only 7.55% increment in outer radius. This is applicable to long cannons with higher muzzle velocity. Reinforced composite materials in pressure vessels are becoming increasingly popular due to the controlled directional properties which inherently result in low weight to strength and stiffness properties [141].

It is known that work hardening or cold stretching of steels increases their yield strength. It may also increase the ultimate strength of some steels, especially austenitic stainless steels and is the primary way their physical properties are controlled. If cold working is done at extremely low or cryogenic temperatures, the room temperature strength is even further increased. This is the basis of a fabrication procedure for high strength stainless steel pressure vessels called cryogenic stretch forming. It consists of soaking a pressure vessel prefabricated by conventional welding practice in a liquid nitrogen bath. After the vessel has reached the -160^0C of the nitrogen bath, it is internally pressurized with nitrogen gas to force it against the walls of a forming die so sized as to control stretching to 11-15%. With a stretch of 13%, strength improvements of 2.5 times have been achieved [11]. Figures 2.5 to 2.8 [3,11] show some past and present construction methods and layouts of typical pressure vessels.

Pressure vessels are mainly manufactured by the forging process. Heavy components are used in many industries, see figure 2.9 [126]. Among the heaviest sections are the nuclear rings and hydrocracker components with raw ingot gross weights between 300 and 400 tons.

2.3.9 Pressure Vessel Costs

The layout of a typical pressure vessel would be as shown in figure 2.10 [142] and the percentage cost breakdown would be like that in table 2.5 [127]. This size of vessels makes

up 80% of the current turnover of pressure vessel shops in the industrialized countries. The market for pressure vessels consists of the chemical industry, mineral oil production and processing, electricity generation and the gas industry. On average, the chemical industry accounts for 70% of the pressure vessel usage [142].

A simple and systematic procedure based on redistribution nodes (R–node) concept for minimizing the weight and hence the cost of mechanical components and structures has been proposed [143].

2.3.10 Pressure Vessel Inspection and Testing

Preventing failure is within the realm of technology and can be achieved by conducting responsible and regular in-service inspections. It involves creating a rational inspection frequency and appropriate inspection instructions. The inspection objective is based on recognizing that flaws and/or cracks will grow as a function of cyclic stress and must be found before they reach critical size.

Before a pressure vessel can be employed in service, it is mandatory in the majority of the pressure vessel codes, for it to undergo a non-destructive test and inspection procedure. Some of the non-destructive inspection tests done on pressure vessels are:

(a) Radiography.

Gamma rays are used to produce images of defects, flaws and inclusions. In industry, Iridium-192 or Cobalt-60 are used for the Gamma ray production. This method is used where effective use of other techniques may prove difficult.

(b) Ultrasonic testing.

This test is particularly useful for subsurface indications in thick vessels which have flaws which cannot be detected by the radiography test [25].

The driving force for development in non-destructive testing is the continually increasing need to demonstrate the integrity and reliability of engineering plant. Assurances of plant integrity are necessary for reliability, safety and economic reasons [25]. Another test done on a vessel before delivery of the order is the leak/pressure test. This is either hydrostatic or

pneumatic. The vessel is subjected to a pressure 50% [25] above the design operating pressure. A wet soap film is used to detect leakage in case of a pneumatic test. A hydrostatic test is preferred because a pneumatic failure is much more hazardous than a hydrostatic failure [25]. Leak proof pressure vessels have received a lot of attention from the early days of the pressure vessel industry [144]. The leak/pressure test may at times lead to detection and elimination of weak pressure vessels when failure occurs. Figures 2.11 to 2.13 [11] are evidence of the importance of this test.

Other in-service checks include: dimensional measurements, fluorescent dye penetrant and fluorescent magnetic particle. Visual checks are also carried out at critical regions for scratches, gouging and unusual wear [3].

Analysis procedures that allow the benefits of periodic in-service inspection and proof testing applied to a cyclically loaded structure to be assessed in a quantitative manner are now available [145]. The increasing costs and consequences of structural failures have resulted in the increased need for assuring structural reliability. Pre-service and in-service non-destructive inspection and proof testing have been used to decrease the possibility of structural failures in service.

2.3.11 Other Pressure Vessel Loads

The influence of external loads on pressure carrying capacity of outlet connections must also be considered. Often, the loadings which act upon a pressure vessel and which may cause its failure are not all due to internal pressure. In practice, pressure vessels are a part of a complex system and therefore are subjected to loadings at attachments such as outlets and supporting lags. External loadings may also arise from unequal expansion, unequal foundation settlement and earthquakes [146]. The presence of external loads have been found to cause a reduction in the limit pressure capacity of pressure vessels and therefore the connections that are likely to be subjected to external loads must be adequately designed [146].

2.4 Summary

From the foregoing, it is clear that the pressure vessel codes do not adequately establish the real state of stress which exists in pressure vessels with nozzles or where stress concentrations occur. Even the design by analysis method which uses some analytical supplemented by numerical approaches, still incorporates and emphasizes on some design by rule aspects. Hence the design criteria used by the ASME and BS 5500 are not adequate to fully maximize on the mechanical properties of the pressure vessel material. More analysis data needs to be provided with the aim of improving the design codes. From the above literature review, previous research was mainly concerned with evaluation of cylinder strength. A few cases have considered stress concentration factors in plain cross bores while little has been done to clearly present the overstrain stress state around cross bores. Experimental methods, and lately, the numerical methods have been used.

Due to the large number of elements required to model a thick walled cylinder, most researchers have treated the cylinder as a shallow shell. This approach inevitably results in errors. Thick walled cylinder studies require a lot of data input time (unless the discretization process is automated) and long CPU processing time. The computer memory and hard disk space also need to be adequate to handle the large stiffness matrices generated (particularly for three dimensional work). Only a few researchers have attempted to accurately model the cross bore entry geometry and when they have, not enough cases have been analyzed. There is therefore a need to evaluate proper models and collect enough data to show variations in the stress concentration factors, overstrain, residual and service stress profiles.

This work will aim to fill this void of data and highlight details of stresses around the cross bore region. Various cross bore entry geometries will be analyzed. In the elastic-plastic analysis, varying overstrain levels will be considered and the results presented and discussed. Comparison with previous research findings will be done. The finite element method will be used for the analysis since the literature on its implementation procedure is widely available and the parameters of interest may be obtained at any point in the structure.

Table 2.1 Factors of safety for various ASME codes.

(Source: [3])

ASME Code Section	Factor of Safety	Basis	
		Theory of Failure	Material Property
Section VIII Div. 3, Pressure Vessels	2	Distortion Energy	Material yield strength first reached throughout wall thickness
Section III, Nuclear Components, and Section VIII Div. 2, Pressure Vessels	3	Maximum Shear	Average shear stress in wall thickness reaches material ultimate shear stress
Section I, Power Boilers and Section VIII Div. 1, Pressure Vessels	4	Maximum Stress	Average tensile stress in wall thickness reaches material ultimate tensile strength
Section IV, Heating Boilers	5	Maximum Stress	Average tensile stress in wall thickness reaches material ultimate tensile strength

ENGINEERING	Structural Integrity Evaluation	Creep Distortion	X	X				
		Creep Stress Rupture	X	X				
		Brittle Fracture	X	X				
		Fatigue	X	X				
		Material Damage	X	X				
		Crack Growth	X	X				
		Crack Initiation	X	X				
	Inservice Inspection NDE	Continuous Sub-surface Monitoring	X					
		Periodic Sub-surface Monitoring	X	X	X			
		Continuous Surface Monitoring	X					
		Periodic Surface Monitoring	X	X	X	X		
	DE	Surveillance Samples	X	X				
	Design Stress Analysis	Local Deformity	X					
		Noncircularity	X	X				
		Creep-Rupture	X	X	X			
		Fatigue	X	X	X			
		Thermal	X	X	X			
		Secondary	X	X	X			
		Primary	X	X	X	X	X	X
FABRICATION	Fabricated Component Treatment	Metallurgical Property Enhancement	X	X				
		Residual Stress Relief	X	X	X	X		
	NDE	Volumetric	X	X				
		Surface	X	X	X	X	X	
	NDE	Volumetric	X	X	X			
		Surface	X	X	X	X	X	X
MATERIAL	Base Material and Weldment Properties Destructive Examination	Environment Neutron Flux	X	X				
		Environment Atmosphere	X	X				
		Environment Temperature	X	X				
		Crack Growth	X	X	X			
		Creep-Rupture	X	X	X			
		Fatigue	X	X	X			
		Dynamic Toughness	X	X	X			
		Metallurgical	X	X				
		Chemical	X	X	X	X	X	
		Static, Room Temperature	X	X	X	X	X	X

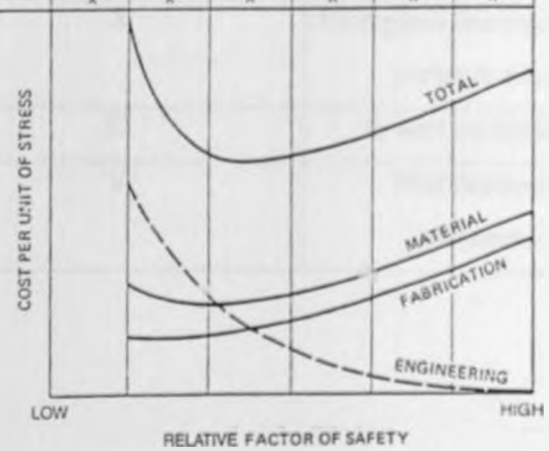

(Source: [3])

FIG. 2.1 Effect of factor of safety on cost of pressure vessel.

Table 2.2 Chronological development of ASME Boiler and Pressure Vessel code (Section I, power boilers).

(Source: [128])

Year	Components	Section
1921	III	Boilers for locomotives
1922	V	Miniature boilers
1923	IV	Low pressure heating boilers
1924	II	Materials
1925	VIII	Unfired pressure vessels (revised in 1968 to be Div. 1)
1926	VII	Care of power boilers
1937	IX	Welding qualifications
1963	III	Nuclear vessels
1968	VII	Pressure vessels Div. 2 (alternate rules)
1970	X	Fibreglass reinforced plastic pressure vessels
1970	XI	In-service inspection
1971	V	Non destructive examination

Table 2.3 Summary of BS 5500: 1997.

(Source: [115])

Section	Components
1	General.
2	Materials.
3	Design.
4	Manufacture and workmanship – Steel.
4a	Manufacture and workmanship – Aluminium.
5	Inspection and testing – Steel.
5a	Inspection and testing – Aluminium.
Appendix A	Design requirements for loading.
Appendix B	Shells under combined loading, including winds and earthquakes.
Appendix C	Vessels under fatigue
Appendix D	Cr-Mn vessels at low temperatures.
Appendix E	Weldings.

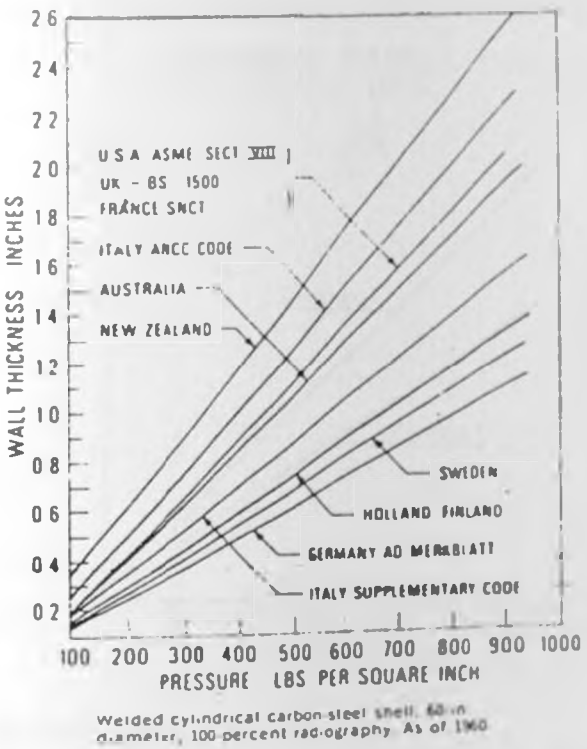

(Source: [5])

FIG. 2.2 Wall thickness required by different codes in 1960.

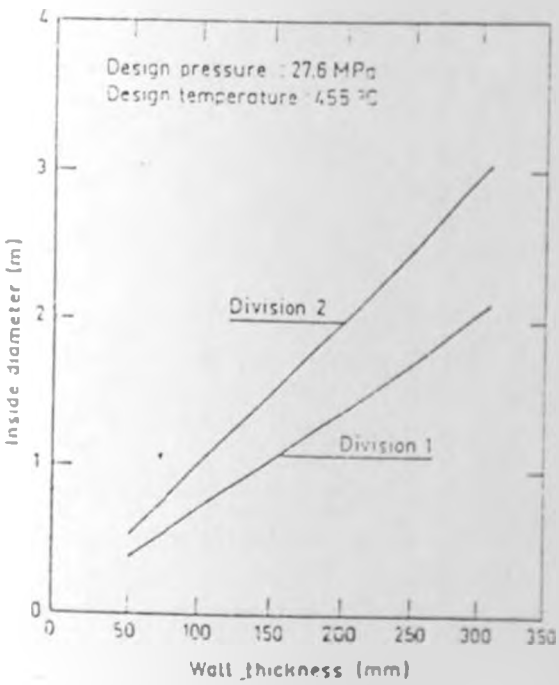

(Source: [122])

FIG. 2.3 Effect of code (ASME Section VIII, Div. 1 vs. Div. 2) on wall thickness of coal liquefaction vessel.

Table 2.4 Fields and types of application for pressure vessels at different loads and temperatures.

(Source: [126])

	Operating temperature		
	Low temperatures (below 253K)	Ambient temperatures (253 to 323K)	High temperatures (above 323K)
Field of application	Vessels for media cooled externally or by evaporation.	Vessels for gaseous or liquid media of ambient temperature.	Vessels for gaseous or liquid of elevated temperature, fired or unfired.
Type	Spherical, cylindrical, or rectangular shape, also double walled with insulation, for storage and/or transport of media.	Predominantly of spherical or cylindrical shape, for storage, transport and treatment of media or as a containment.	Mostly of cylindrical shape, for chemical and thermal treatment.
Examples of application	Vessels for liquefied gaseous (stationary or mobile), evaporators, columns, heat exchangers, condensers.	Vessels for gaseous and liquids (stationary or mobile), bottles, safety vessels, reactors, agitators, pressure chambers.	Preheaters, boilers, drums, generators, manifolds, superheaters, reactors, agitators, columns, gas coolers or heaters, heat exchangers.

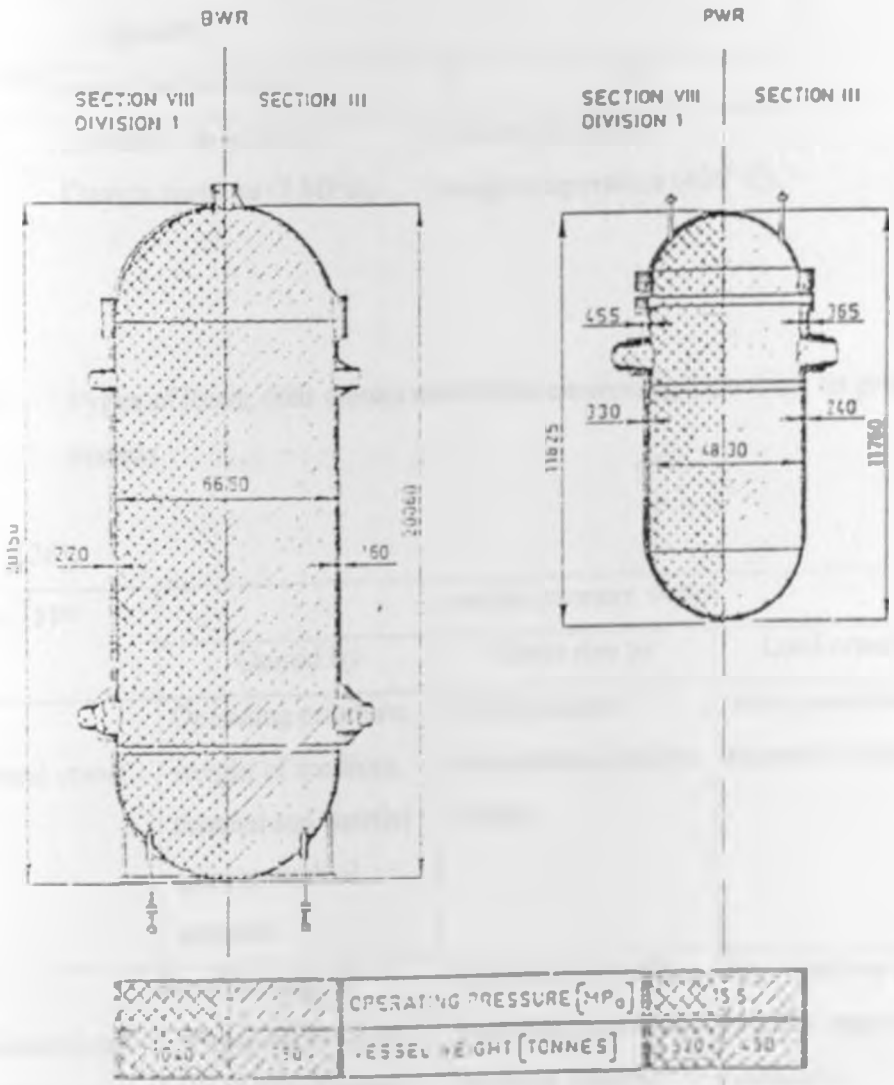

(Source: [127])

FIG. 2.4 Comparison of nuclear vessels designed to different ASME codes.

Table 2.5 Price breakdown for a typical pressure vessel.

(Source: [127])

Item	Percentage cost
Materials (including consumables).	50
Direct labour.	25
Overheads (including engineering and quality).	15
Transport and site wotk.	10

NOTES: Material: mild steel, Profit not included.
Design pressure (7 MPa), Design temperature (400^0 C).

Table 2.6 Types of loads, their causes and effects emanating from them on pressure vessels.

(Source: [126])

Load Type	Load on pressure vessel		
	Caused by	Gives rise to	Load condition
Mechanical stress	Operating pressure, weight of medium, thermal and inertial forces, residual stresses.	Elastic-plastic deformation, cracks, fatigue.	Static, sustained, repeated, impact.
Electro-chemical attack	Inefficiency of protective devices, reactivity of metal.	Reduction of wall thickness, corrosion products, cracks.	Localised or general attack, long or short duration.
Wear of pressure bearing material	Interaction of surface and medium	Reduction of wall thickness, corrosion products, cracks.	Localised or general attack, long or short duration.

Table 2.7 Typical parameters of a pressure vessel.

(Source: [129])

PARAMETER	RANGE OF VALUES
Design pressure	18.4 – 26.5 MPa
Design temperature	440 – 500^{0}C
Material	2.25Cr-Mo or 3Cr-Mo
Design stress	150 – 185 MPa
Inside diameter	3 – 5 m
Total length	20 – 40 m
Wall thickness	200 – 450 mm
Total weight	400 – 2600 tons

Table 2.8 Typical chemical composition of pressure vessel steels.

(Source: [122])

MATERIAL TYPE	TYPICAL CHEMICAL COMPOSTION						TEMP (^{0}C)	COMPONENT	BS SECTION.
	% C	% Mn	% Ni	% Cr	% Mo	%V			
Mild steel	.12	.6	-	-	-	-	450	Furnace, economiser tubes, feed water heaters.	3059/33
Carbon steel	0.15	1.0	-	-	-	-	450	Furnace, economiser, superheater tubes, vessels and receivers.	3059/45 1501, 1503
Carbon steel	0.28	0.8	-	-	-	-	450	Feed water pump, valve body casings.	3592
Carbon manganese steel	0.2	1.25	-	-	-	-	450	Drums, headers, vessels, receivers.	1501, 1503
Cr-Mn-Mo-V	0.15	1.25	-	0.6	0.25	0.1	450	Drums, headers, vessels, receivers.	1501, 1503
1%Cr-Mo	0.12	0.5	-	0.9	0.55	-	550	Superheaters, vessels, pipes, reheater tubes.	3059, 1501
2.25%Cr-Mo	0.12	0.5	-	2.25	1.0	-	580	Superheaters, vessels, pipes, reheater tubes	3059, 1501
0.5%Cr-0.5%Mo-0.25%V	0.12	0.5	-	0.4	0.6	0.3	580	Headers, pipes.	3059, 1501
9%Cr-Mo	0.1	0.5	-	9	1	-	660	Superheater, reheater tubes.	1503, 50604
12%Cr-Mo-V	0.2	0.5	0.5	12	1	0.3	630	Superheater, reheater tubes.	1503, 50604

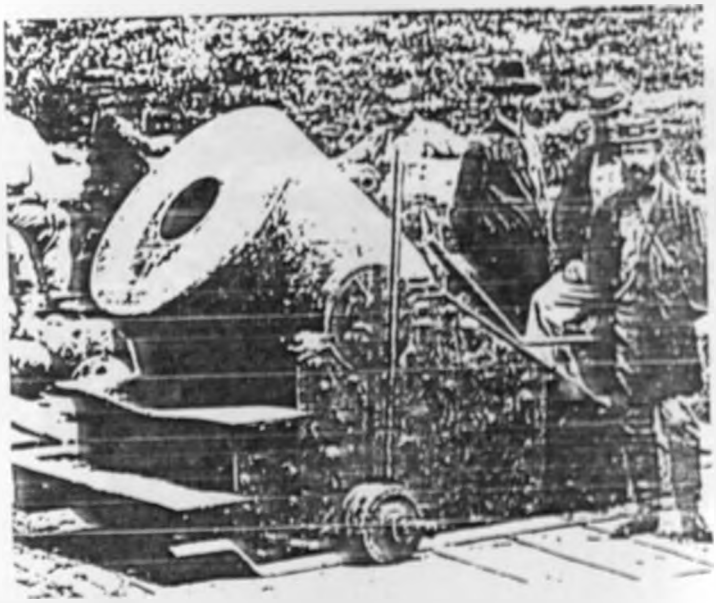

(Source: [3])

FIG. 2.5 Thick walled mortar used in the American civil war.

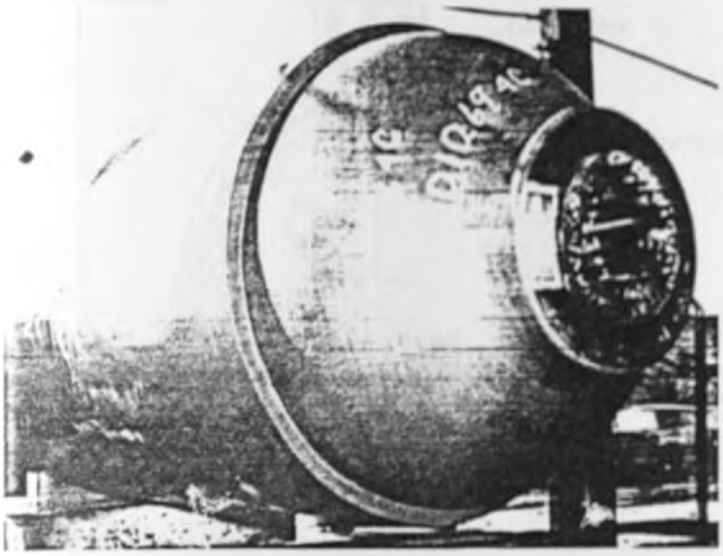

(Source: [3,11])

FIG. 2.6 Banded vessel (spherical head and banded cylinder)).

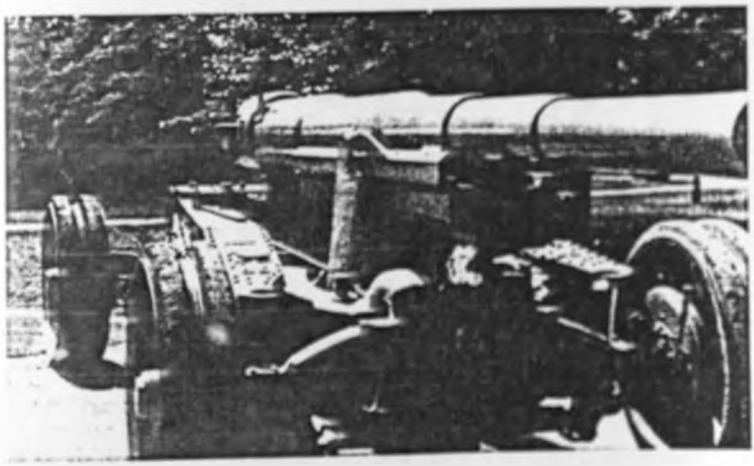

(Source: [3])

FIG. 2.7 Multiple shrink fits in the barrel of a heavy field cannon.

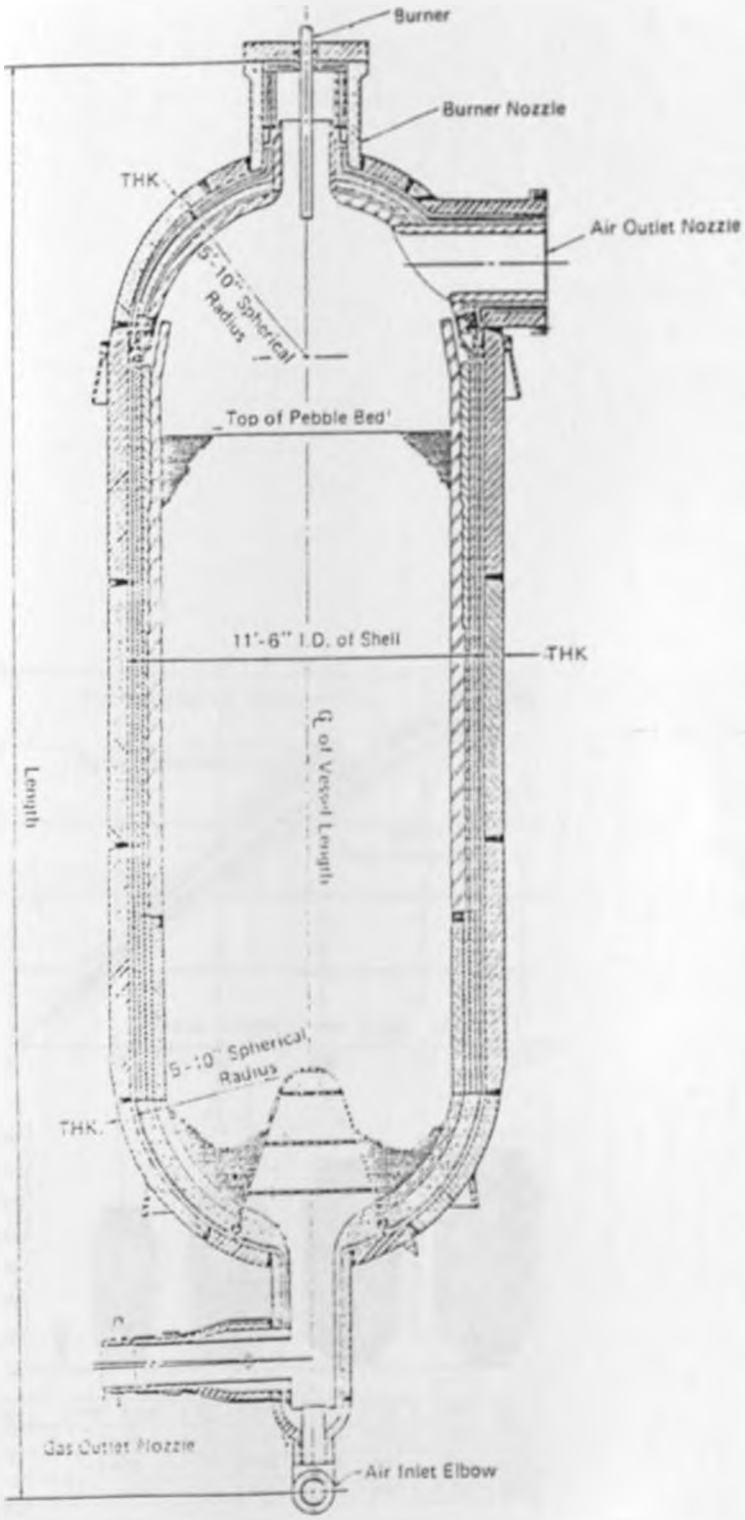

(Source: [11])

FIG. 2.8 Internally insulated and internally cooled pressure vessel.

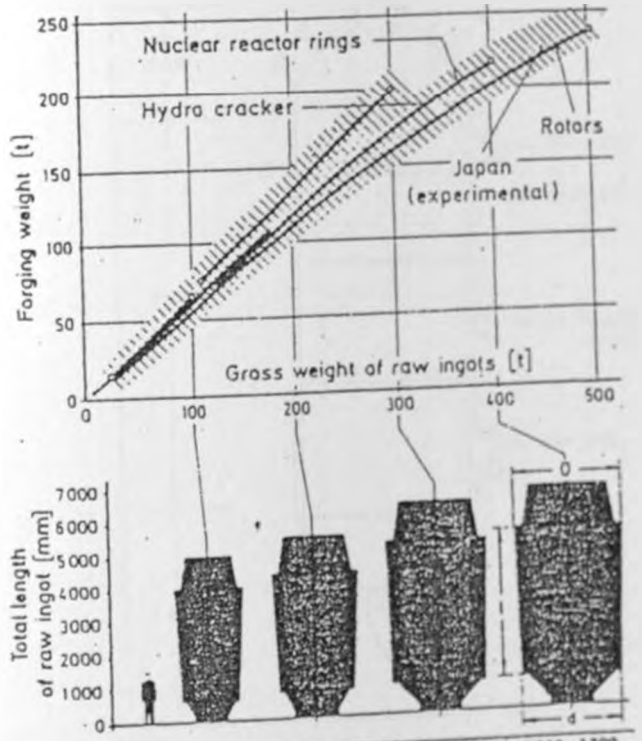

D [mm]	2 100 - 2 200	2 700 - 2 900	3 200 - 3 400	3 500 - 3 700
dm "	- 2 000	2 600 - 2 800	3 100 - 3 300	3 400 - 3 600
d "	- 1 820	2 400 - 2 500	3 000 - 3 100	3 200 - 3 400
l "	3 100 - 3 600	3 500 - 3 800	4 300 - 4 600	4 100 - 4 300
ratio of slenderness l : dm	1.5 - 1.9	1.3 - 1.5	1.2 - 1.4	1.1 - 1.3
conicity [pct]	6 - 12	6 - 10	6 - 8	6 - 8

(Source: [126])

FIG. 2.9 Dimensions and gross weights of raw ingots.

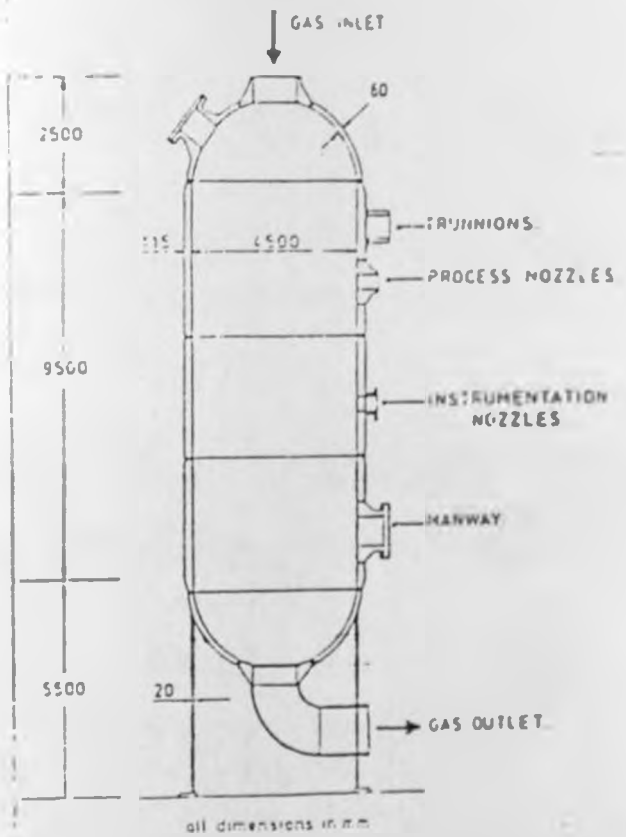

(Source: [142])

FIG. 2.10 Typical pressure vessel arrangement and dimensions.

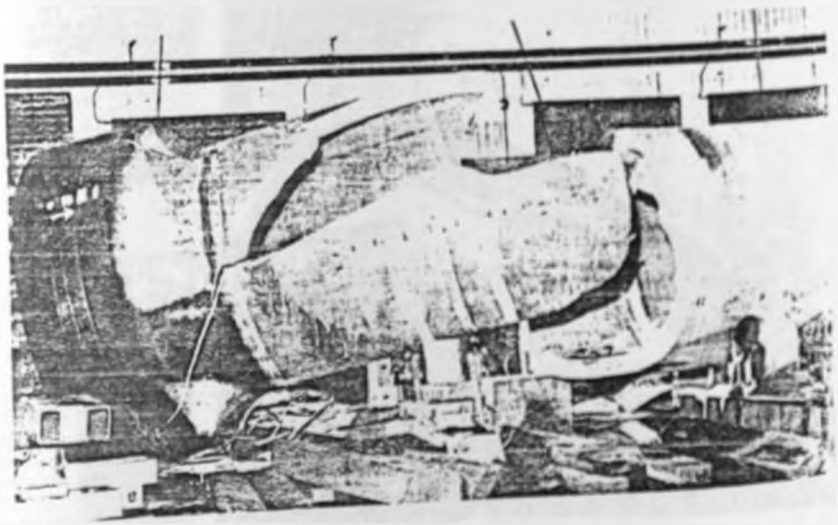

(Source: [11])

Fig. 2.11 Brittle hydrostatic failure of high pressure chemical reactor.

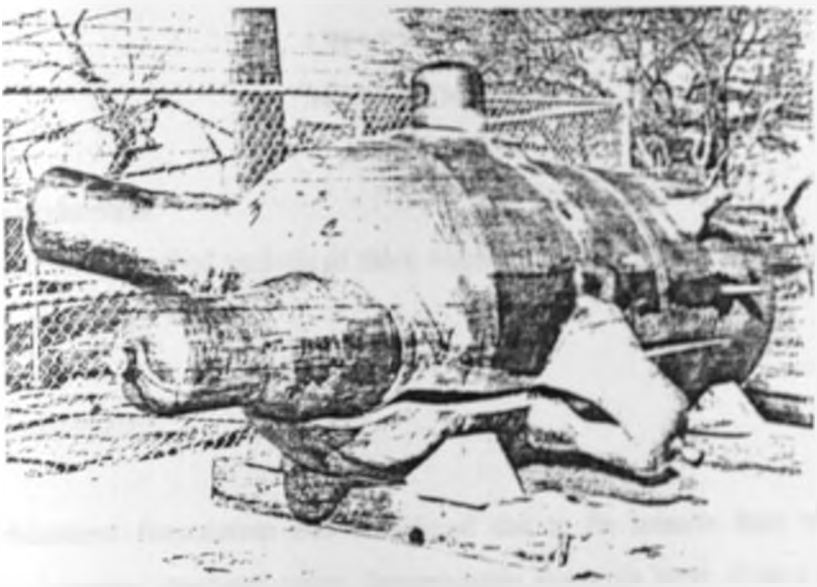

(Source: [11])

FIG. 2.12 Fatigue failure of test pressure vessel (nature of propagation throughout nozzle and vessel).

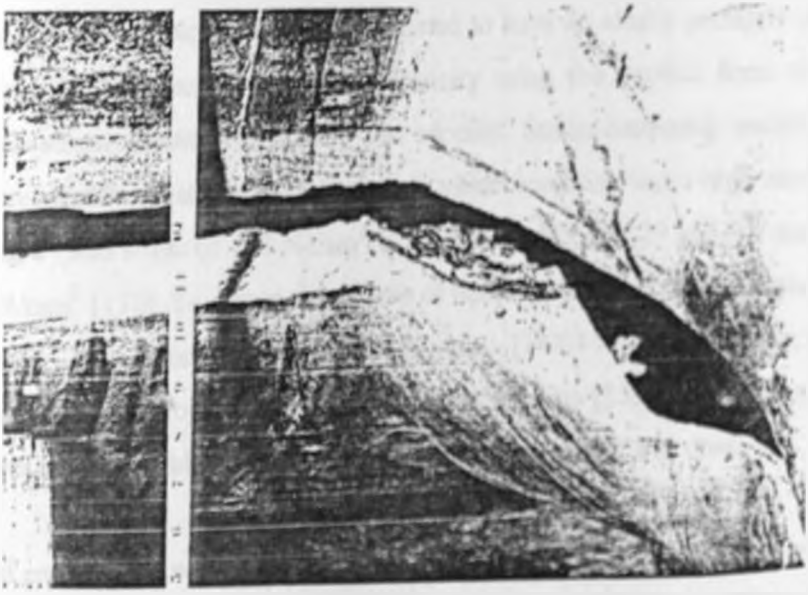

(Source: [11])

FIG. 2.13 Fatigue failure of test pressure vessel (origin of fracture at inside corner of nozzle).

CHAPTER THREE
METHODOLOGY

3.1 Introduction

The finite element method analysis of thick walled cylinders in this work was done for the two stress states:

(a) Elastic

(b) Elastic-Plastic.

The displacement formulation was considered due to its relative ease of writing the associated computer program codes. Isoparametric elements were chosen because they result in simplified numerical integration procedures when generating the stiffness matrices. Serendipity family of element shape functions satisfying the Lagragian interpolation function requirements were chosen. Serendipity shape functions are easily generated. Geometric invariance and completeness requirements were met by the shape functions. Some of the essential basics of the finite element method are shown in appendix I. In the elastic-plastic analysis, the material was assumed to have an elastic perfectly plastic stress-strain curve. The incremental theory of plasticity using the explicit form of the elastic-plastic stress-strain constitutive matrix was adopted. Strain hardening material behaviour was not considered in this work. The pressure vessel material was a high strength SA-372 steel having a yield stress of 450 N/mm^2, a Poisson's ratio of 0.29 and a Young's modulus of 209e3 N/mm^2 [130]. To obtain the degree of freedom displacements, Gauss point strains and stresses, the Frontal solution technique [147-149] was employed. Tensor transformation, stress projection and smoothing techniques [150] were employed to obtain stress curves for the nodal arrays. The von Mises yield criterion was used.

The closed ended thick walled cylinders were represented by only a quarter of the structure due to symmetry. Hence only a quarter of the cylinder was considered. This has far reaching advantages in the finite element method in that computer storage requirements are reduced by 75% and the computer (CPU) run time is also highly minimized. A semi-automatic mesh generation Fortran computer program was developed for use in this work. The program had

both elastic and elastic-plastic capabilities.

3.2 Study Cases

In order to observe the variation of the elastic stress profiles, elastic stress concentration factor values and variations, overstrain elastic-plastic stress profiles, residual stress profiles and service stress profiles, finite element method analysis was carried out for the geometrical configuration cases listed below:

(a) Plain thick walled cylinder.

(b) Plain cross-bored cylinder.

(c) Radiused entry cross-bored cylinder.

(d) Chamfered cross-bored cylinder.

The quarter cylinder geometries for these structures are shown in figures 3.1 to 3.4.

3.3 Element Types

After preliminary pilot investigations, the isoparametric master element types found most appropriate for all the analysis cases were:

(a) Brick element

This has eight corner nodes and eight Gauss points. The variation of the displacements, strains and stresses along any of the element edges is linear. This element is shown in figure 3.5. The natural coordinates, ξ, η and ζ correspond to the x, y and z in the Cartesian coordinate system and have values ranging from –1 to 1. The eight shape (interpolation) functions for this element are given by [151];

$$\Psi_1 = \frac{1}{8}(1-\xi)(1-\eta)(1-\zeta) \qquad (3.1a)$$

$$\Psi_2 = \frac{1}{8}(1+\xi)(1-\eta)(1-\zeta) \qquad (3.1b)$$

$$\Psi_3 = \frac{1}{8}(1+\xi)(1+\eta)(1-\zeta) \qquad (3.1c)$$

$$\Psi_4 = \frac{1}{8}(1-\xi)(1+\eta)(1-\zeta) \qquad (3.1d)$$

$$\Psi_5 = \frac{1}{8}(1-\xi)(1-\eta)(1+\zeta) \qquad (3.1e)$$

$$\Psi_6 = \frac{1}{8}(1+\xi)(1-\eta)(1+\zeta) \qquad (3.1f)$$

$$\Psi_7 = \frac{1}{8}(1+\xi)(1+\eta)(1+\zeta) \qquad (3.1g)$$

$$\Psi_8 = \frac{1}{8}(1-\xi)(1+\eta)(1+\zeta) \qquad (3.1h)$$

The computed stresses refer to the Gauss points having the following sets of coordinates [151]:

Gauss point number:	(ξ, η, ζ) coordinates	
1	(-0.57735, -0.57735, -0.57735)	(3.2)
2	(0.57735, -0.57735, -0.57735)	
3	(0.57735, 0.57735, -0.57735)	
4	(-0.57735, 0.57735, -0.57735)	
5	(-0.57735, -0.57735, 0.57735)	
6	(0.57735, -0.57735, 0.57735)	
7	(0.57735, 0.57735, 0.57735)	
8	(-0.57735, 0.57735, 0.57735)	

The weighting factor for each Gauss point is unity. This element was entirely used in the analysis of plain cylinders and plain cross-bored cylinders. In the radiused entry cross bores, it was used entirely except at the center or origin of the entry radius (points O in figure 3.3). For the chamfered cross bore, it was used entirely except on the surface of the chamfer.

(b) Triangular prism

This element has six corner nodes with the primary and secondary degrees of freedom values varying linearly along any of the element edges. The area coordinates are L_1 and L_2 corresponding to x and y in the Cartesian coordinate

system. The z Cartesian coordinate is represented by the natural coordinate ζ. The element is shown in figure 3.6. The area coordinates have values ranging from 0 to 1 while the natural coordinate has values ranging from –1 to 1. The shape functions are [151]:

$$\Psi_1 = \frac{L_1}{2}(1-\zeta) \tag{3.3a}$$

$$\Psi_2 = \frac{L_2}{2}(1-\zeta) \tag{3.3b}$$

$$\Psi_3 = \frac{(1-L_1-L_2)}{2}(1-\zeta) \tag{3.3c}$$

$$\Psi_4 = \frac{L_1}{2}(1+\zeta) \tag{3.3d}$$

$$\Psi_5 = \frac{L_2}{2}(1+\zeta) \tag{3.3e}$$

$$\Psi_6 = \frac{(1-L_1-L_2)}{2}(1+\zeta) \tag{3.3f}$$

The computed stresses refer to the Gauss points having the following sets of coordinates and weighting factors [151]:

Gauss point number:	(L_1, L_2, ζ) coordinates	$(W_{L1}, W_{L2}, W_\zeta)$	
1	(0.6667, 0.3333, -0.57735)	(0.33, 0.33, 1)	(3.4)
2	(0.3333, 0.6667, -0.57735)	(0.33, 0.33, 1)	
3	(0.3333, 0.3333, -0.57735)	(0.33, 0.33, 1)	
4	(0.6667, 0.3333, 0.57735)	(0.33, 0.33, 1)	
5	(0.3333, 0.6667, 0.57735)	(0.33, 0.33, 1)	
6	(0.3333, 0.3333, 0.57735)	(0.33, 0.33, 1)	

This element was only used at the center or origin of the entry radius (points O in figure 3.3).

(c) Tetrahedron

This is a four noded element as shown in figure 3.7. In the local coordinate system,

the volume coordinates for this element are L_1, L_2, L_3 and L_4. The four nodes in this type of element make it easy to process since the interpolation function in the global coordinate system for displacements (u) are given by;

$$u = a + bx + cy + dz \qquad (3.5)$$

where; a, b, c and d are constants. With the set of constants, (b, c, d) being zero, the constant 'a' satisfies the constant strain state. This is the translation transformation mode.

Equation 3.5 ensures compatibility, completeness and geometric invariance of the polynomial and hence there was no need to use the volume coordinates. The computed stresses refer to the centroid of the tetrahedron. This element was easily generated from the prism and was only used on the chamfered surface of the cross bore.

3.4 Discretization Details

The complex geometrical nature of cross bores in cylinders and in particular cross bores with entry geometry does not allow the nodal coordinates or the connectivity matrices to be obtained in one single step as it may happen in simple structures. It was convenient in this work to carry out a structural subdivision process and obtain the nodal numbers and coordinates, element numbers and element nodes for each geometrical block. The results were combined and assembly of the different parts into one structure by use of identifying flags for the border nodes and elements was carried out. The different subdivisions used in the various configurations are discussed below:

(a) Plain thick walled cylinder

This was the simplest case and subdivisions were not required. The discretization is as shown in figure 3.1. The geometrical inputs for complete description of the geometry were the outer radius, inner radius, length of the cylinder, number of elements along line AB and the geometrical ratio of the node spacing, number of elements along arc AD and the number of elements along line DE. Along line DE

and arc AD, a geometrical ratio was not required since the stresses were not anticipated to have any gradients. The geometrical ratio of 1.15 was found to give the best results with the hoop stress at point D having an error of 1.109% compared to the analytical solution. The number of elements along lines AB, AD and DE were 21, 20 and 8 respectively. The inner radius was 75 mm, the outer radius was 150 mm and the cylinder length was nine times the cylinder thickness. Only one thickness ratio was considered. This resulted in a structure with 4158 nodes, 3360 elements, 12474 degrees of freedom and a frontal width of 1458. The global stiffness matrix coefficients were reduced by 98.6%. This meant that only 1.4% of the potential computer memory requirements was now required, leading to efficient solutions despite the slow read-write computer operations.

(b) Plain cross-bored cylinder

This geometrical configuration was more complex than that of a plain cylinder and required subdivision into the three substructures A1, A2 and A3 as shown in figure 3.2. The overall geometrical inputs were the outer radius, inner radius (75 mm), length of cylinder (nine times the thickness) and radius of cross bore. In part A1, the number of elements was input for lines CD (14), CI (12) and CB (6). A geometrical ratio was also required for line CD (1.5). The geometric ratio on line CB (1.5) and AB (0.95) were also input. The number of elements along lines HG (3) and AB (6) were also input. The geometric ratio of line HG (5) was input. Also input was the length of line HI (10% of the main bore radius). This completely defined the structure. This resulted in a structure with 2580 nodes, 2016 elements, 7740 degrees of freedom and a frontal width of 801. The global stiffness matrix coefficients were reduced by 99%.

(c) Radiused entry cross bore

This configuration required subdivision into five distinct parts A1, A2, A3, A4 and A5 as shown in figure 3.3. The general inputs were the inner radius (75 mm), outer radius, cross bore radius, radius of cross bore entry, length of line JI (nine times the cylinder thickness). In part A1, the number of elements for lines DE (7), EF (6) and EM (10) were input. The geometric ratios of lines DE (1.5) and EF (1.5) were also input. In part A2, the number of elements along arc CD (6) was input. In part A3 the

number of elements along line CB (3) and the angle BUC (5% of angle AUC) were input. In part A4 the number of elements along line JI (3) and the geometric ratio (4) were input. In part A5, the number of elements along arc AB (6) and the corresponding geometric ratio (0.975) were input. This resulted in a structure with 2790 nodes, 2269 elements, 8370 degrees of freedom and a frontal width of 678. The global stiffness matrix coefficients were reduced by 99.3%.

(d) Chamfered cross bore

This configuration required subdivision into five parts A1, A2 A3, A4 and A5 as shown in figure 3.4. The general inputs were the inner radius (75 mm), outer radius, length of line JI (nine times the cylinder length), radius of cross bore, chamfer angle and chamfer length. In part A1, the number of elements was input for lines DE (8), EF (6), and arc EM (12). The geometric ratios for lines DE (1.5) and EF (2.5) were also input. In part A2, the number of elements along chamfer line CD (6) was input. In part A3, the number of elements along line KJ (4) was input as well as the angle BÔC (10% of the angle AÔC). In part A4, the number of elements along line JI (3) were input together with the geometric ratio (4). In part A5, the number of elements (6) and geometric ratio (0.8) along arc AB were also input. This resulted in a structure with 3087 nodes, 2652 elements, 9261 degrees of freedom and a frontal width of 771. The global stiffness matrix coefficients were reduced by 99.3%.

For cross-bored cylinders, the outer radius was determined by the thickness ratio. The thickness ratios varied from 1.25 to 3. The cross bore to main bore radius ratio values varied from 0.005 to 0.4. The above data entered for each configuration completely defined the geometry. The geometric ratios were chosen where stress gradients were anticipated and to ensure that on moving from one part to the other, the element edges have about the same size. The geometrical ratios were also used in controlling the element aspect ratios and volume ratios. The choice of the number of elements and geometric ratios in each division or line edges was based on:

(a) For parts away from the cross bore, to ensure that the far field stresses are close to the exact solution of a plain cylinder.

(b) In the cross bore areas, to ensure that the stress concentration factor reasonably

converges while minimizing the frontal width and processing time.

For example, for a plain cross-bored cylinder having a thickness ratio of 2.25 and a cross bore to main bore radius ratio of 0.1 the hoop stress at point G was 62.51 N/mm^2 while the exact solution was 62.23 N/mm^2. The error involved, 0.5%, was acceptable. By increasing the number of elements along line GH from 14 to 15, the stress concentration factor changed from 2.832524 to 2.832407, showing a decrease of 4.13e-3. This variation is insignificant. Some of the preliminary pilot study results influencing the choice of number of elements are represented and shown in figures 3.8 and 3.9. The small drop, 0.031%, in stress concentration factor between 14 and 16 elements along line GH is brought about by an unfavourable aspect ratio. However, this drop is very insignificant and the input of 14 was adopted. Though other methods of mesh refinement may be implemented [152,153], their need does not arise in this work since the accuracy obtained is sufficient.

3.5 Procedure

The finite element method based computer program used to carry out the simulation for both elastic and elastic-plastic states and any geometrical configuration had the following steps:

(1) Open the program GEOM and input discretization details as per section 3.4. The material properties as well as the stress-strain constitutive matrix coefficients were entered. Choose if cylinder is closed or open. Input the element shape functions and Gauss point coordinates. Input the planes where primary degrees of freedom are prescribed or restrained. In all cases, $u = 0$ and $v = 0$ in the planes given by $x = 0$ and $y = 0$ respectively. For an open plain cross-bored cylinder, $w = 0$ in the plane passing through points G and N as shown in figure 3.2. Input if analysis is elastic or elastic-plastic, Input the yield condition for elastic-plastic cases as well as the desired overstrain. Input the internal pressure, element effective stress yield condition and a yield criterion (Tresca's or von Mises).

(2) Run the program GEOM to generate the following; total number of nodes and their Cartesian coordinates, global element connectivity matrix and element types, loaded elements and the faces loaded, nodal arrays of interest, for example, along line

ABCDE for plain cross bore. Store all the input data and generated data for use by program GAUSS.

(3) Open the program GAUSS and read the stored data.

(4) Set up arrays of elements surrounding each node.

(5) Obtain the nodal and element destination vectors by processing and modifying the global connectivity matrix. This is implemented by the subroutine PRERE.

(6) Generate element nodal forces and their components, in vector form.

(7) Use the shape functions to obtain the stress-strain matrices [B] and the Jacobian of the transformation.

(8) Generate the Gauss point stiffness matrices and assemble on the element stiffness matrix.

(9) Assemble the element stiffness matrix on the active global stiffness matrix. Assemble the element force vector on the active global force vector. This is accomplished by using the element and nodal destination vectors.

(10) By use of the modified connectivity matrix, determine when a node ceases to be active and carry out a Gaussian elimination procedure after applying the boundary conditions. Store in a data file the stiffness matrix and force coefficients associated with the condensed node.

(11) Continue assembly and elimination to the last element.

(12) Carry out a Gaussian back substitution procedure using the stored force and stiffness matrix coefficients to obtain the primary degrees of freedom (displacements).

(12) Generate the Gauss point stresses.

(13) Use the shape functions in a stress projection procedure to obtain element nodal stresses and strains.

(14) Transform the stresses to cylindrical coordinate system using the tensor transformation rules [154] to yield the radial, hoop and axial stresses.

(15) For elastic analysis, obtain the stress concentration factors and carry out a stress smoothing technique to obtain global nodal stresses for nodal arrays of interest. This is the last step for elastic analysis.

(16) For elastic-plastic analysis, obtain the effective stress for the most highly stressed

element. Use the factor $\frac{Y_s}{\sigma_{eff}^{max}}$ to scale up the stresses and strains in all elements. Also scale up the degree of freedom displacements and the pressure. This procedure enforces yielding in that element. Flag the element as having yielded. σ_{eff}^{max} is the effective stress of the most highly stressed element in the elastic analysis [66].

(17) Apply the yield condition $\sigma_{eff}^{e} \geq 0.95 Y_s$ to all the other elements. Any element meeting this condition is considered to have yielded and is flagged. Scale up the stresses and strains in this element by the factor $\frac{Y_s}{\sigma_{eff}^{e}}$, where σ_{eff}^{e} is the effective stress of that element. This yield condition has been shown to reduce the load cycles by a big margin without introducing large errors as shown and discussed in chapter five.

(18) If overstrain value has not been achieved, assign the pressure a small value, say 0.1 N/mm^2. Initialize the force vector, element and active global stiffness matrices. Start loading again.

(19) Record the overstrain pressure at the desired overstrain level. If residual stresses are required, load the structure with a negative pressure equal to the highest overstrain pressure. Initialize the force vector, load again and obtain the resultant residual stresses.

(20) If service stresses are required, choose the service pressure required. Initialize the force vector, go to step 6 and load again.

The above steps are shown in a simplified flow chart in figure 3.10 and are improvements from previous closely related methods [155]. The main computer program and some of the important subroutines are shown in appendix II.

3.6 Summary

The most widely used approach to finite element modelling of solids is based on linear displacement approximation. In this case, the state of stress within the element is constant. In the case of quadratic shape functions, the stress components vary linearly within the

elements. The method adopted here fits into this kind of a model. In the elastic-plastic analysis, the Pradtl-Reuss flow rule (see [66]) was found adequate though Nadai's deformation theory has also been shown to provide rapid iterative convergence [156]. The matching of this later method with the Frontal solution technique was found cumbersome to program. The load increment method [66] adopted in this work, though slower than other iterative schemes [157-159,160], is very suitable when there is a need to have many elements while the computer memory is limited. However, the incremental method using larger load steps has been found to be efficient under certain modified conditions [161]. The finite element method analysis programs in FORTRAN code were developed and run on a computer with the following capabilities: RAM (500MB), speed (1GHz) and hard disk space (20GB). The results obtained will be presented and discussed in the following chapter.

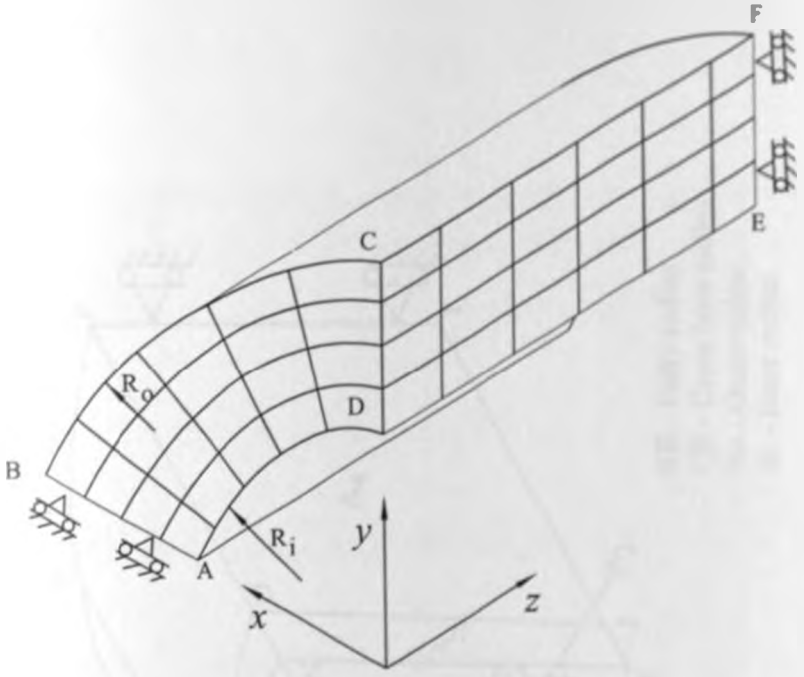

FIG. 3.1 Discretization of plain cylinder

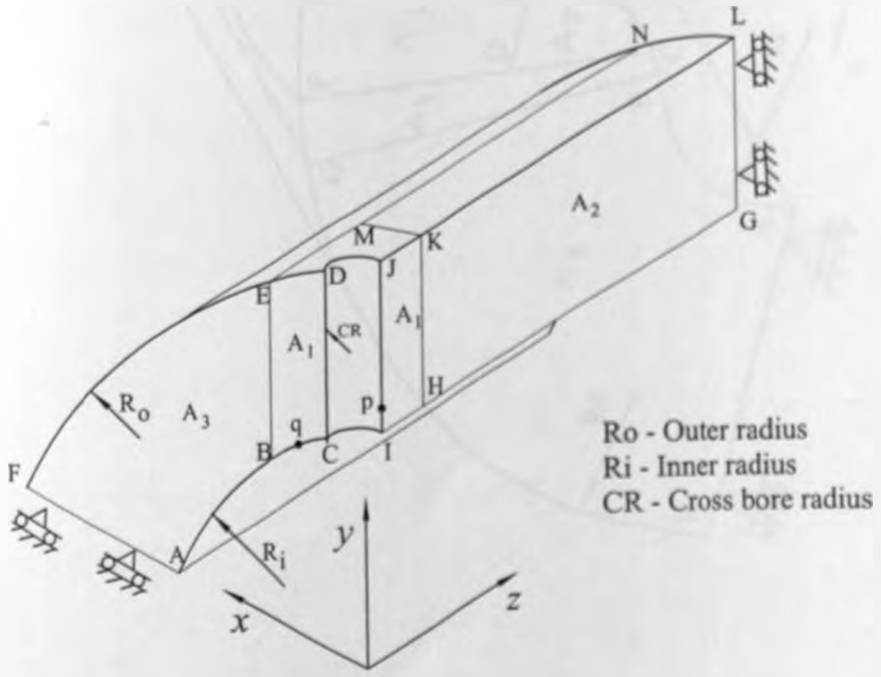

FIG. 3.2 Discretization of plain cross-bored cylinder

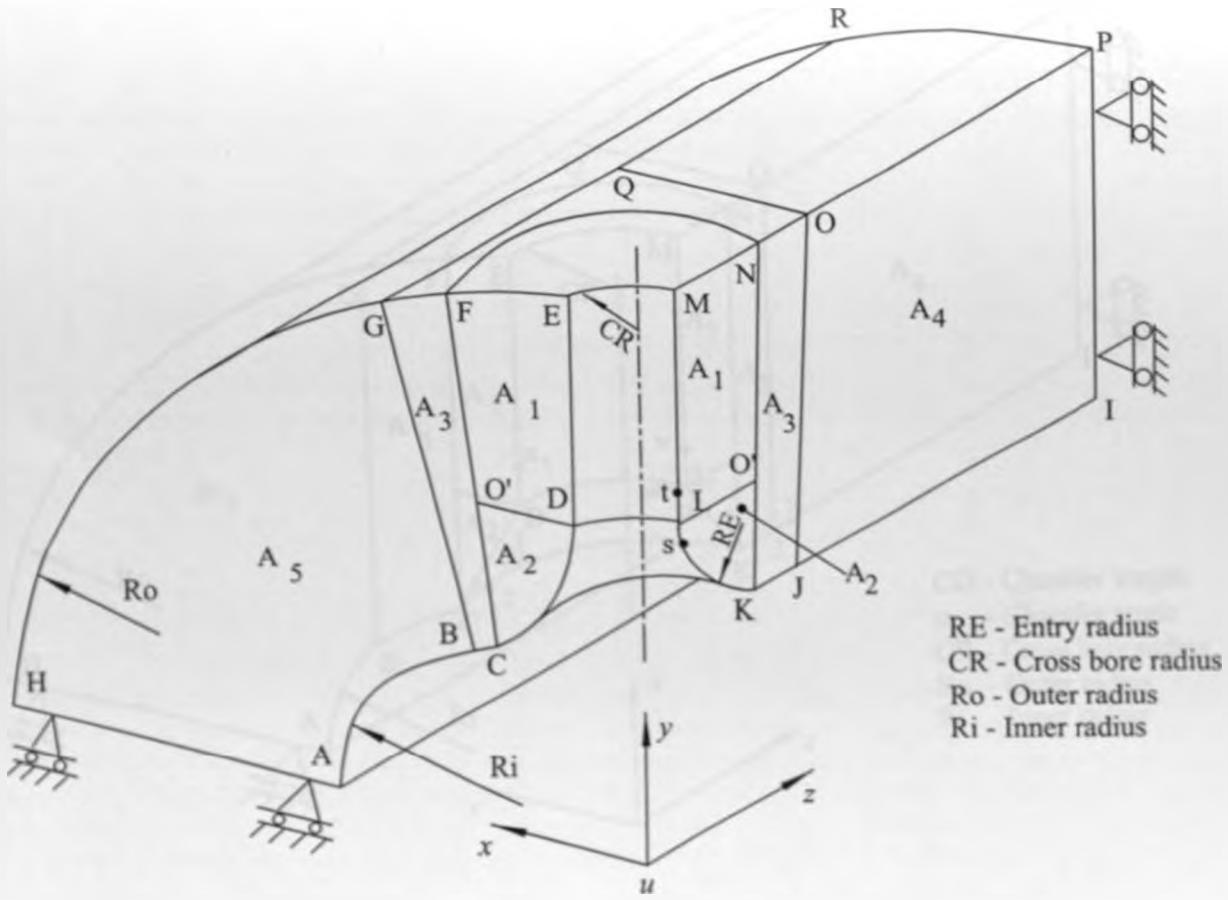

FIG. 3.3 Entry radiused cross-bored cylinder

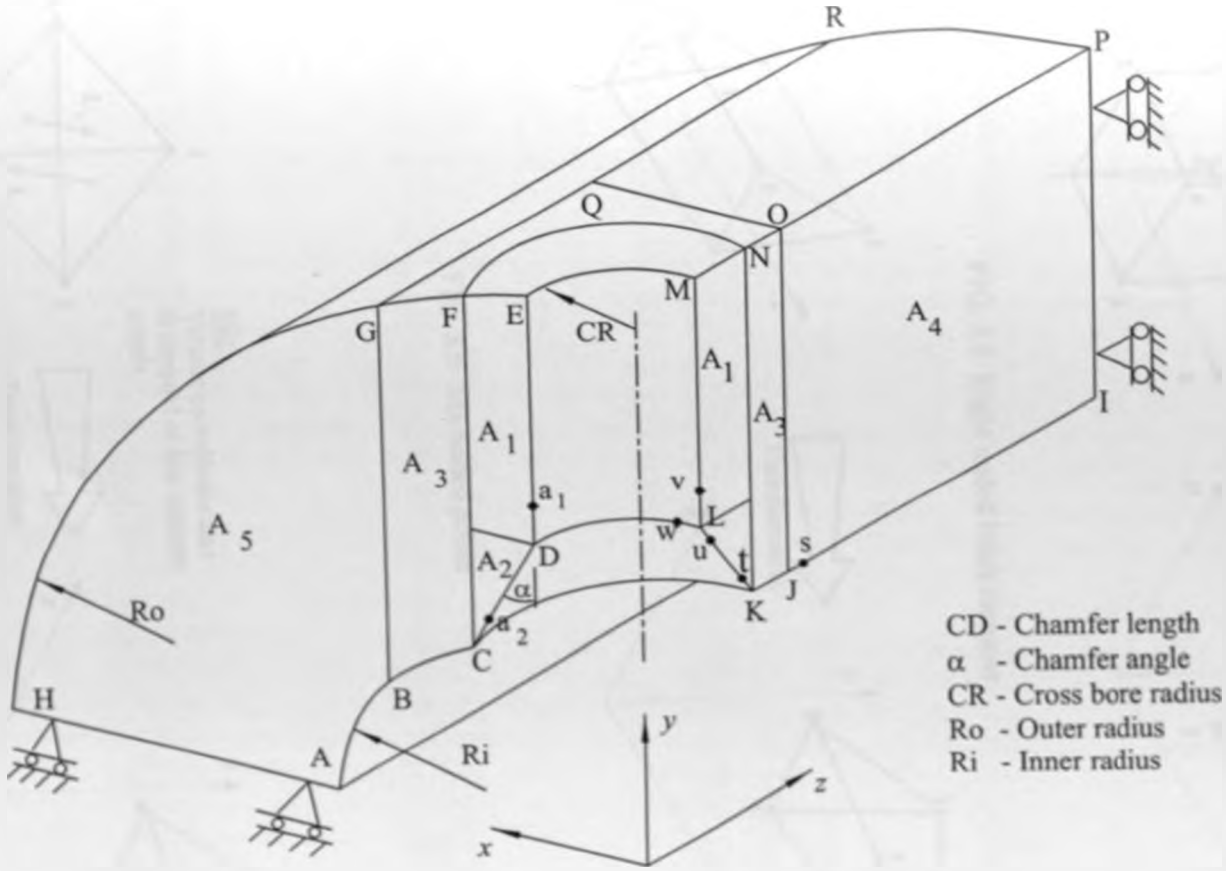

FIG. 3.4 Chamfered cross-bored cylinder

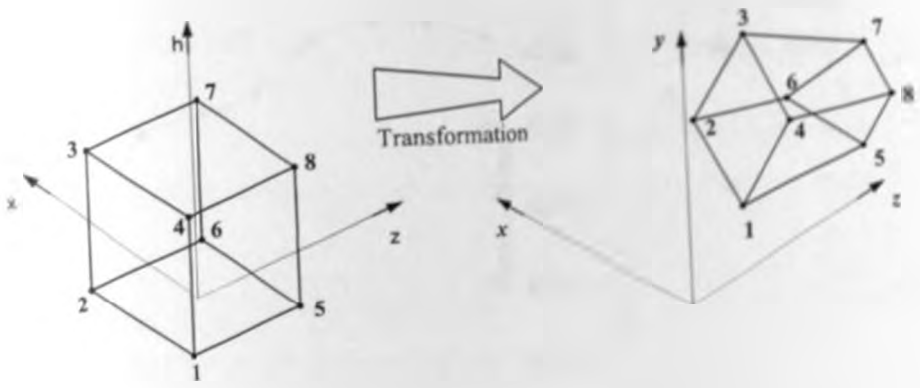

FIG. 3.5 Eight noded brick element

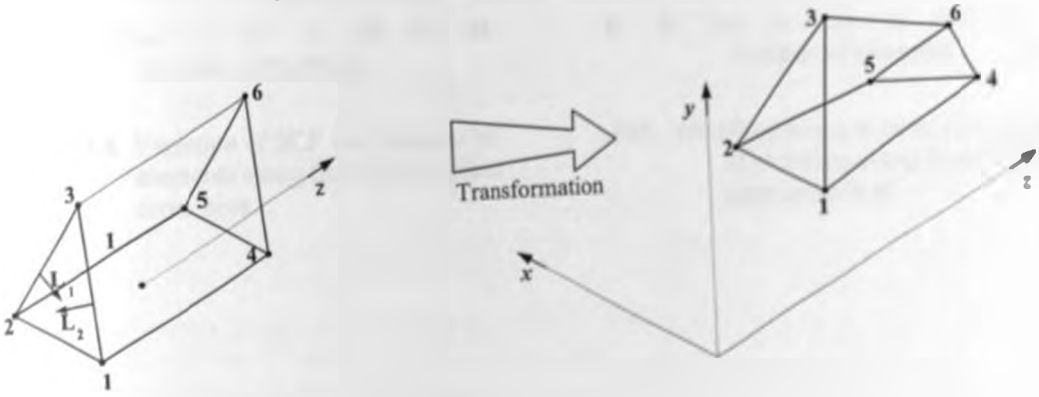

FIG. 3.6 Six noded prism

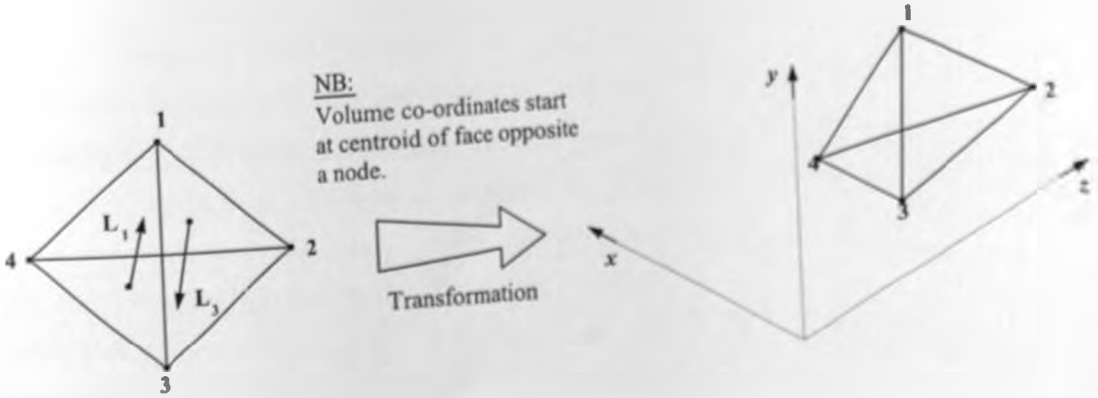

FIG. 3.7 Four noded tetrahedron

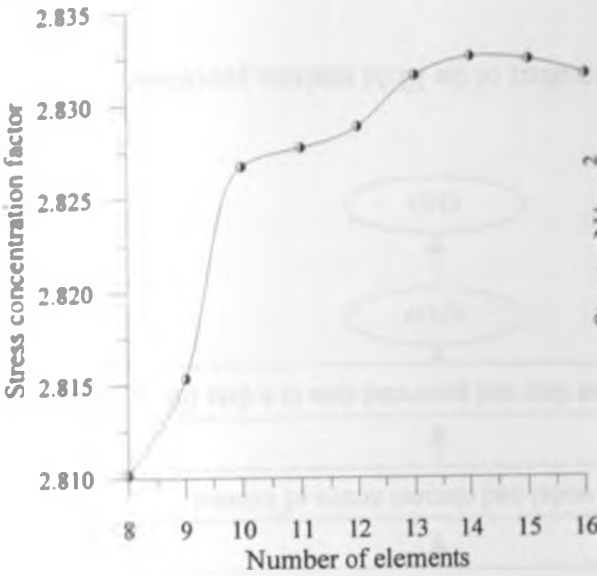

FIG. 3.8 Variation of SCF with number of elements along line CD in a plain cross bore.

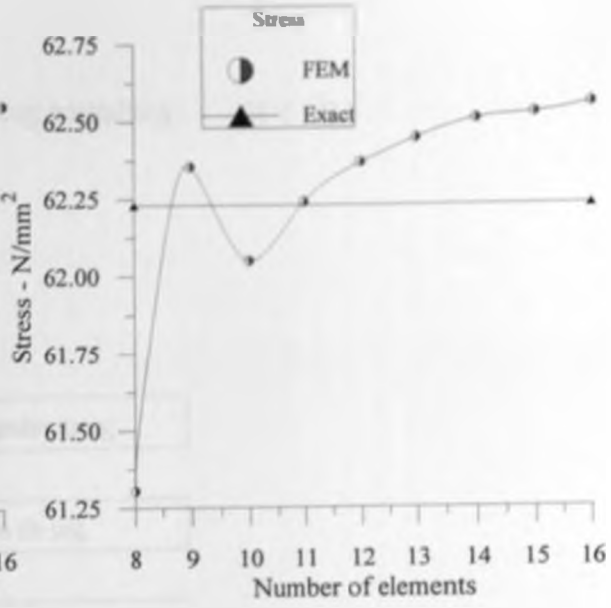

FIG. 3.9 Hoop stress at point G vs. number of elements along line CD in a plain cross bore.

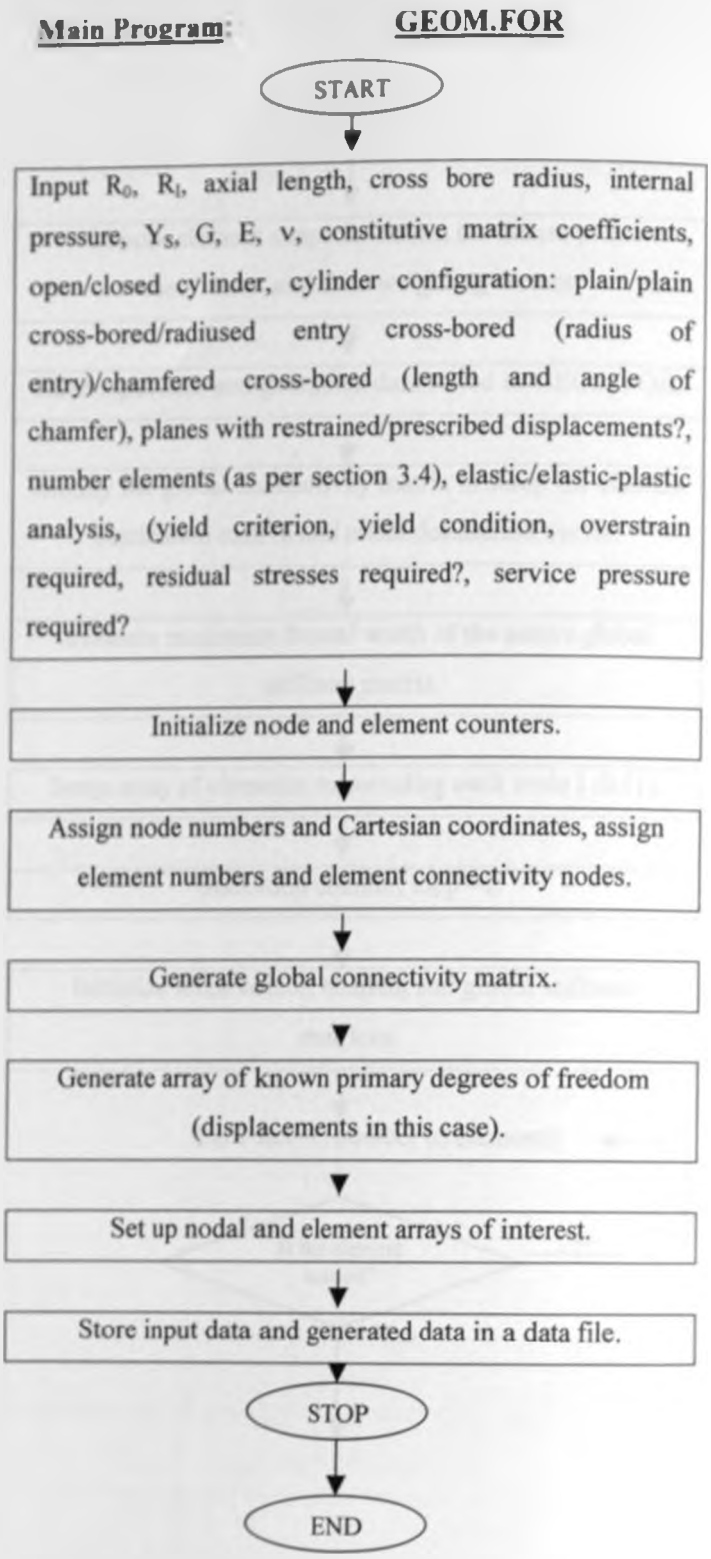

FIG. 3.10 Simplified flowchart of the FEM analysis procedure.

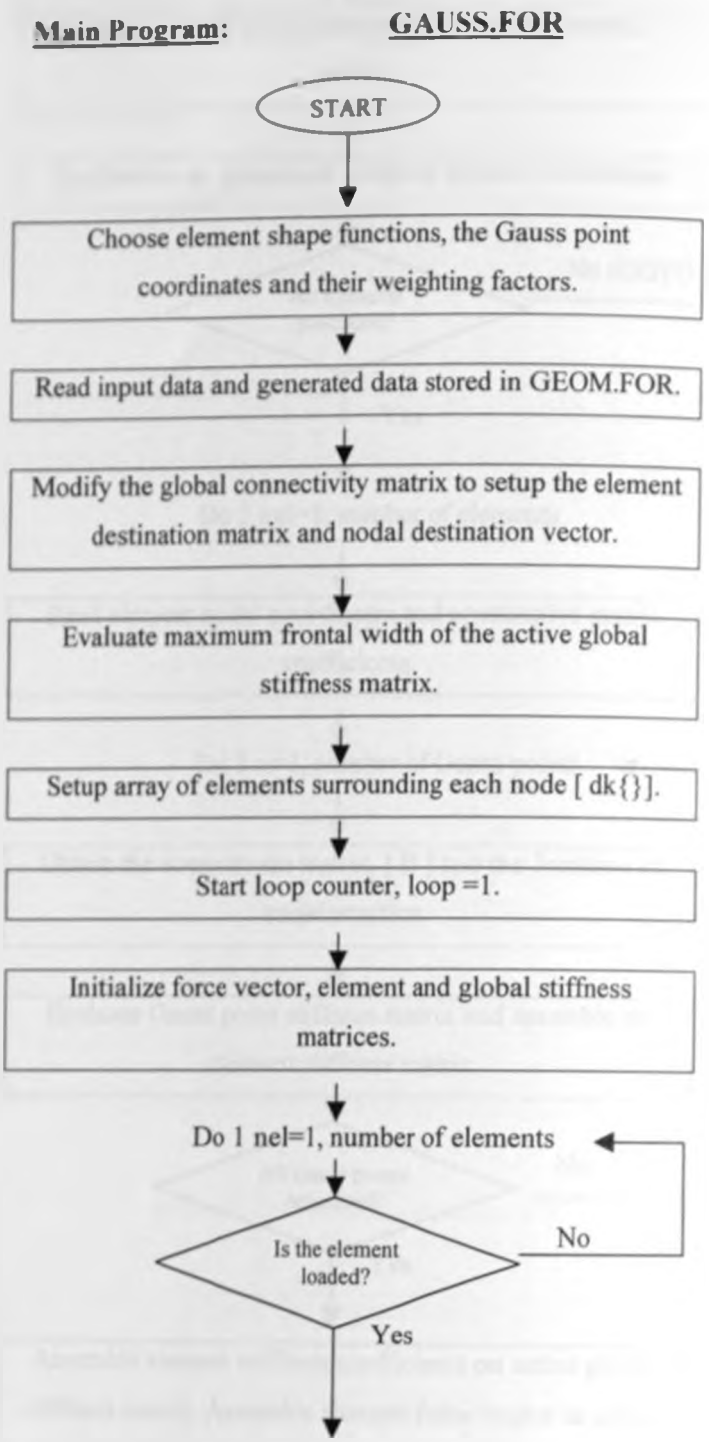

FIG. 3.10 (contd.) Simplified flowchart of the FEM analysis procedure.

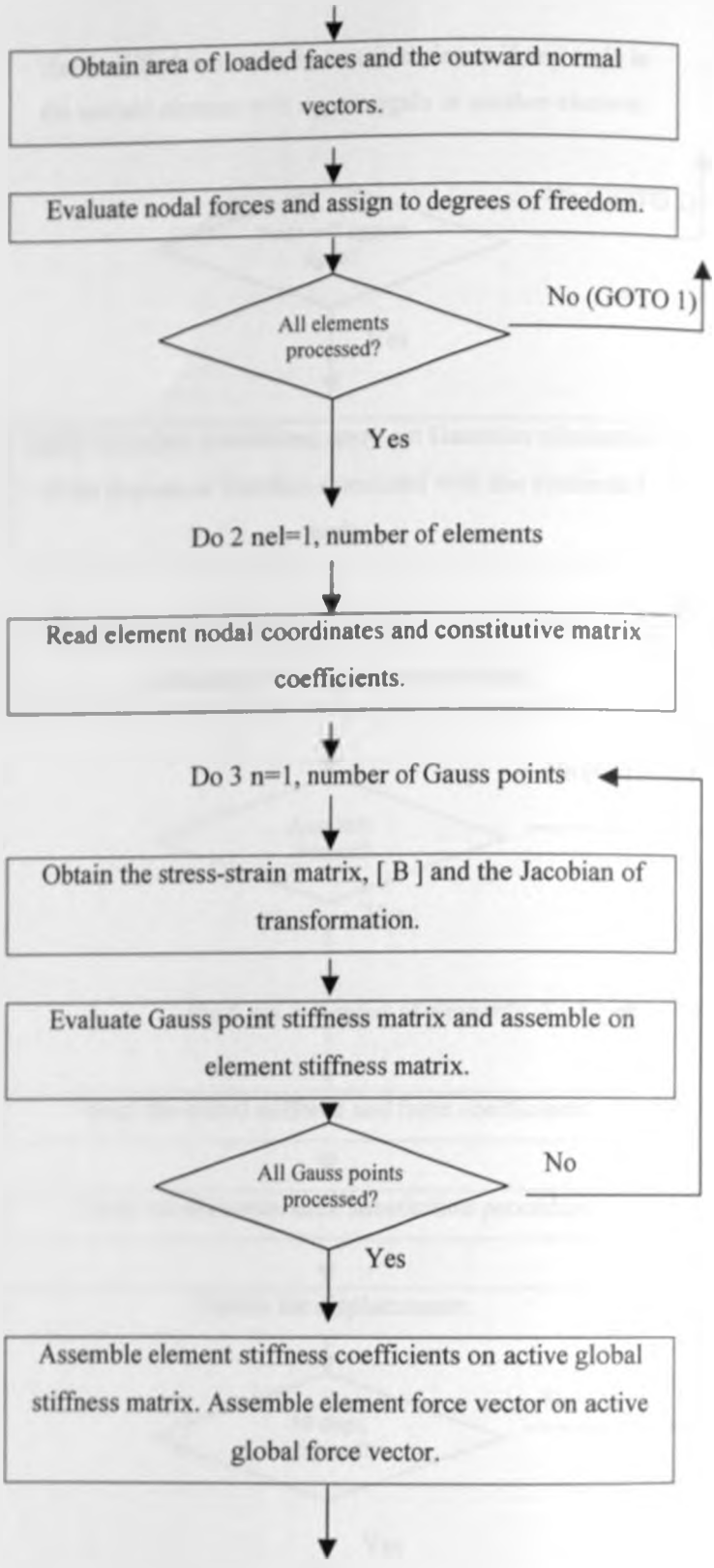

FIG. 3.10 (contd.) Simplified flowchart of the FEM analysis procedure.

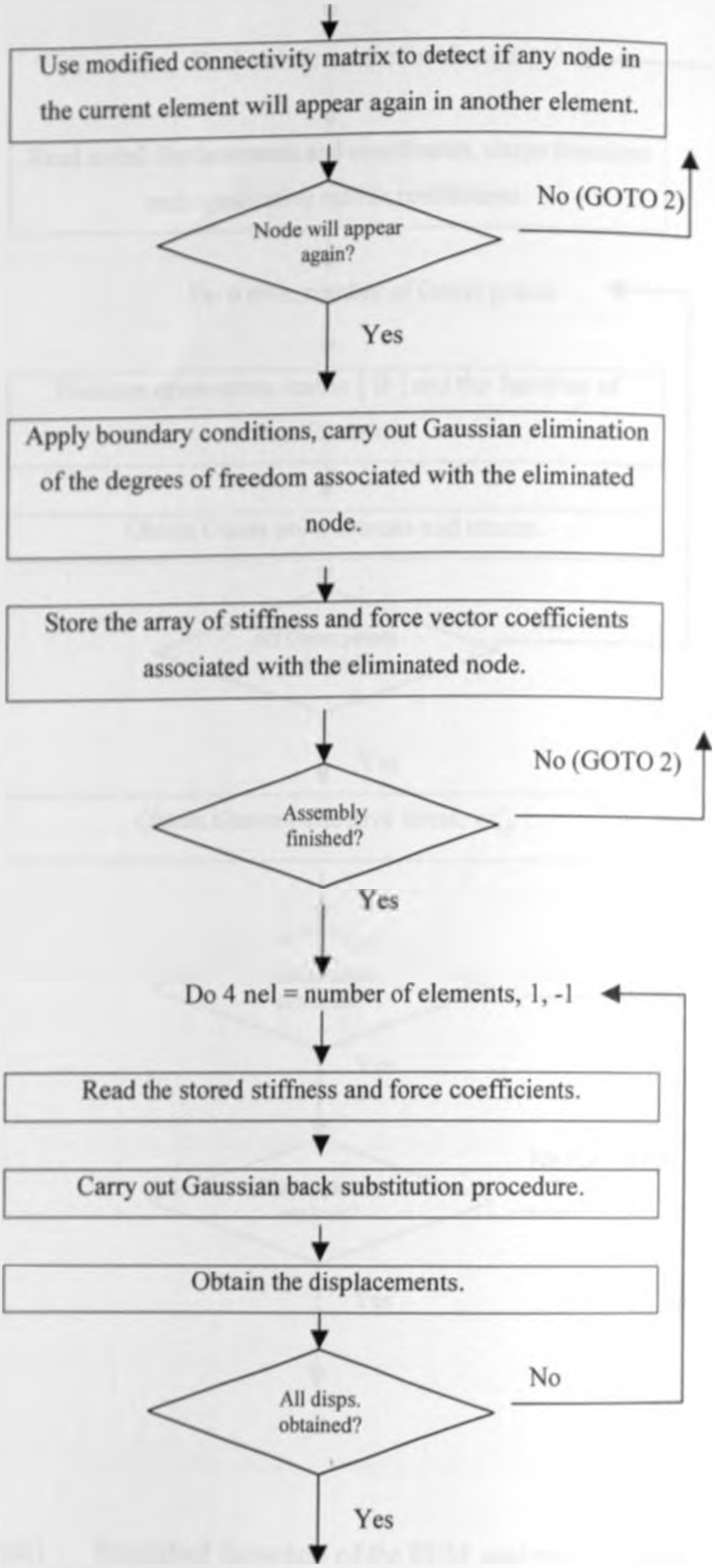

FIG. 3.10 (contd.) Simplified flowchart of the FEM analysis procedure.

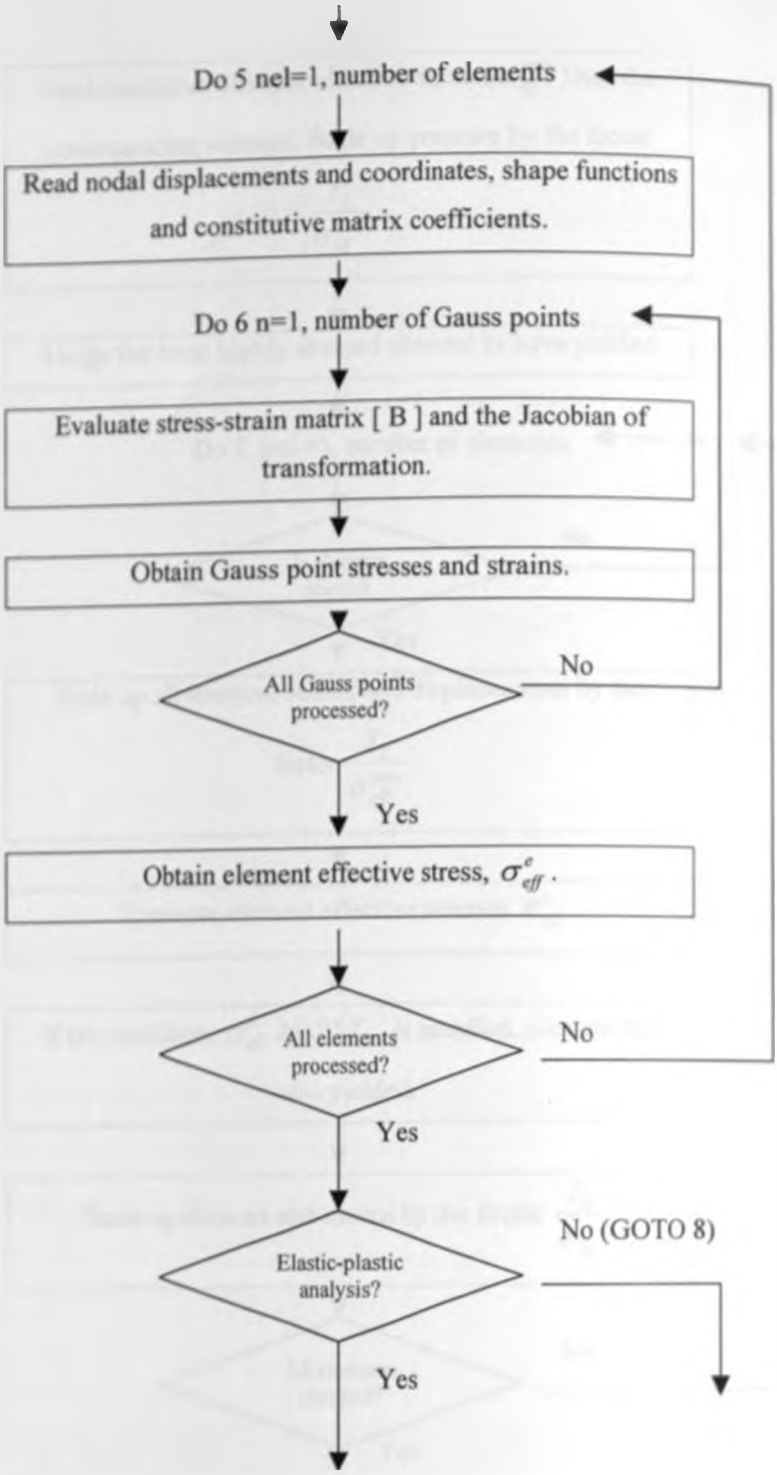

FIG. 3.10 (contd.) Simplified flowchart of the FEM analysis procedure.

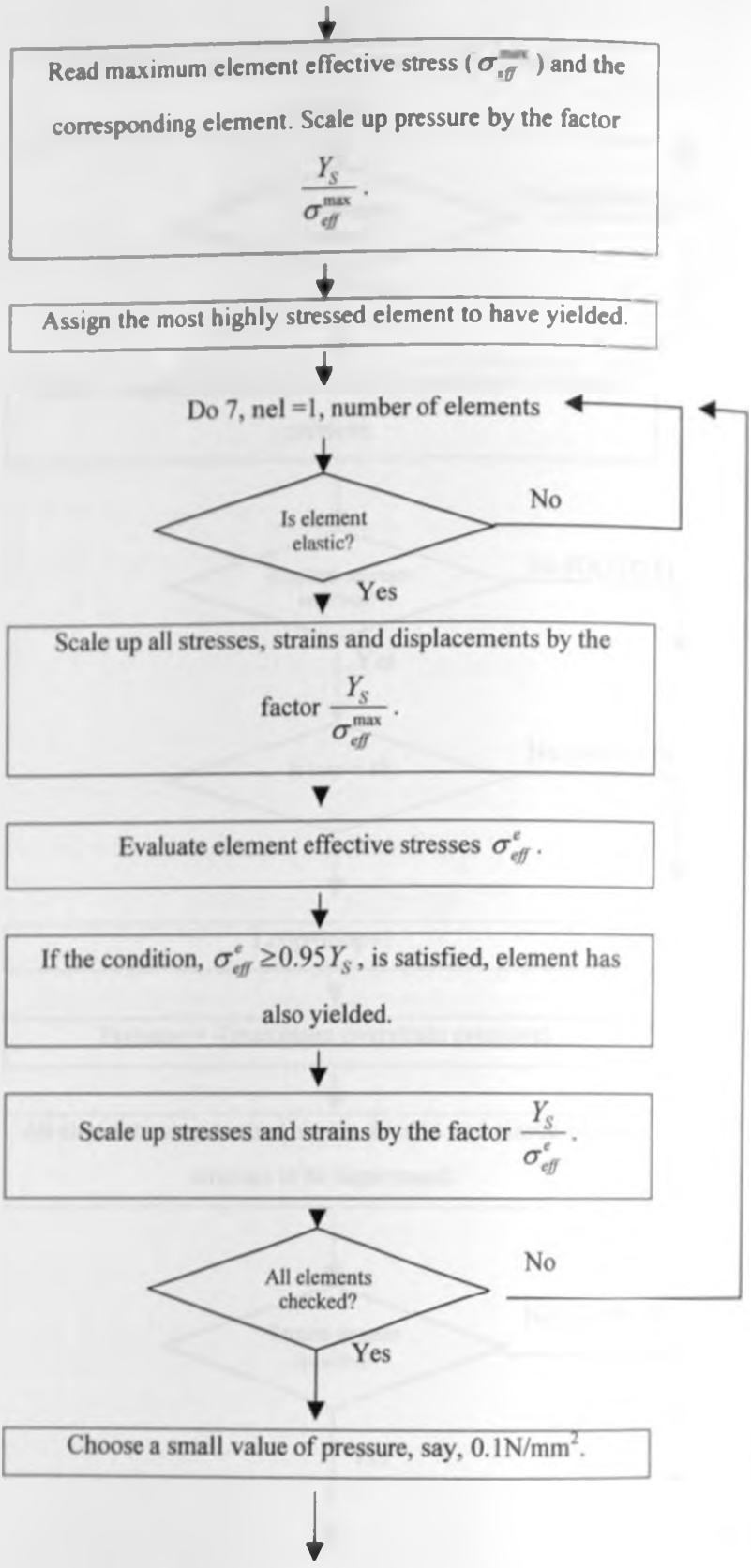

FIG. 3.10 (contd.) Simplified flowchart of the FEM analysis procedure.

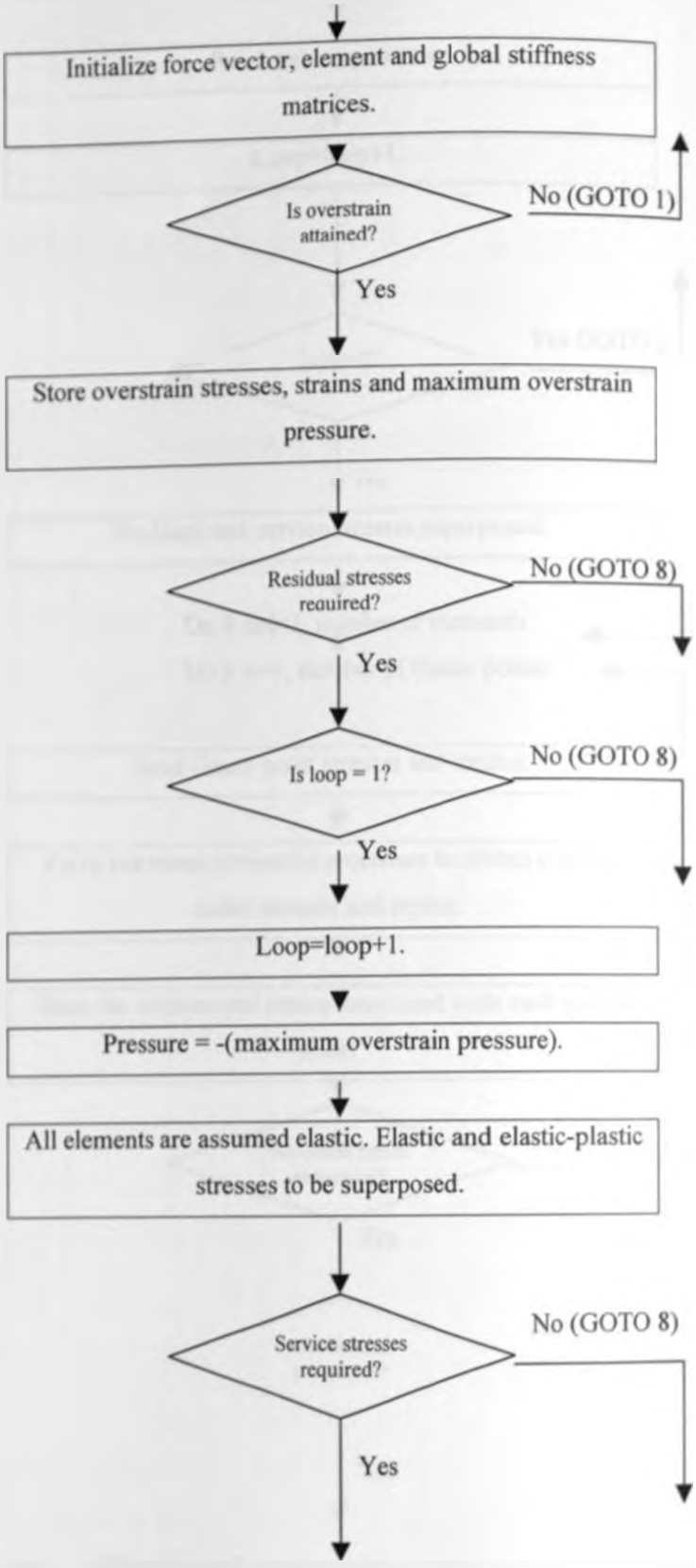

FIG. 3.10 (contd.) Simplified flowchart of the FEM analysis procedure.

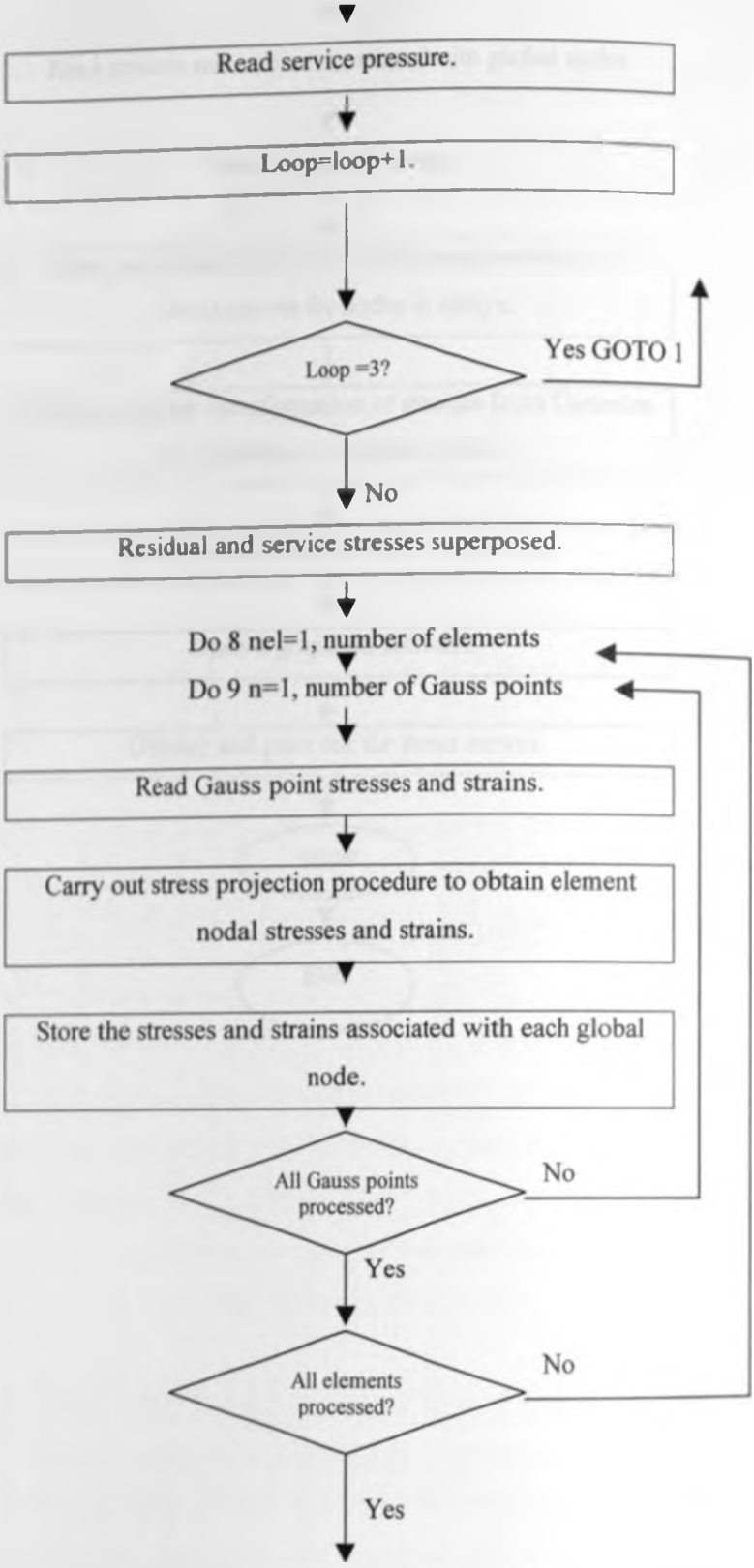

FIG. 3.10 (contd.) Simplified flowchart of the FEM analysis procedure.

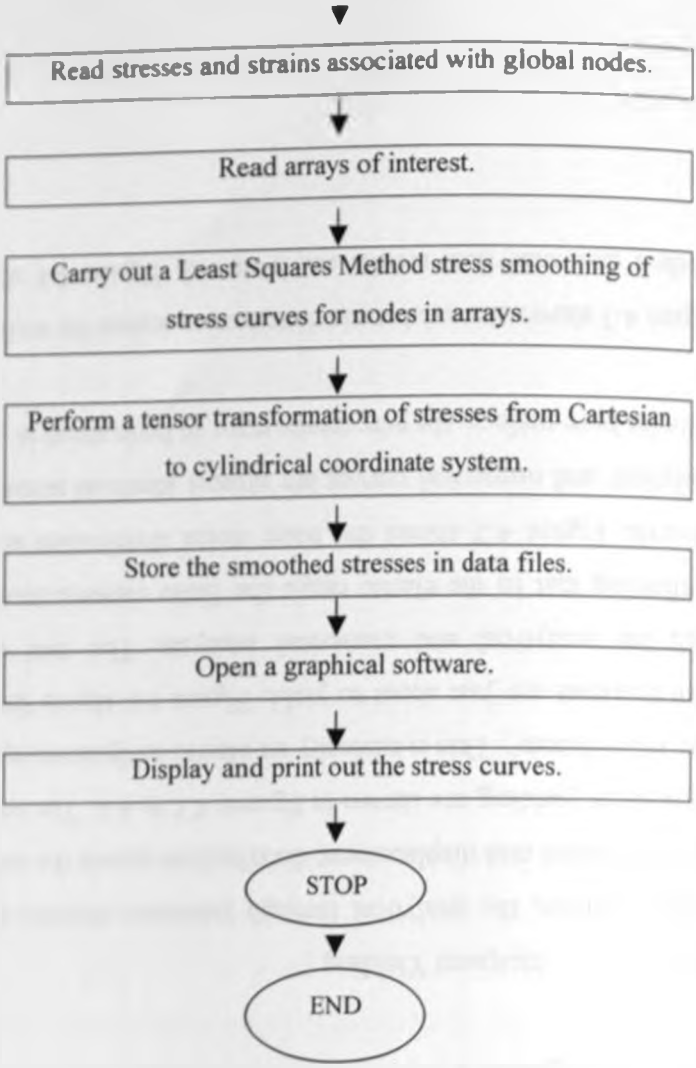

FIG. 3.10 (contd.) Simplified flowchart of the FEM analysis procedure.

CHAPTER FOUR
RESULTS AND DISCUSSION

4.1 General Introduction

In this section, the analytical and numerical stress and displacement results for the various thickness ratios and cross bore to main bore radius ratios are presented and discussed. The elastic and elastic-plastic analysis results will be presented. The three cross bore geometries considered are: plain, radiused entry and chamfered.

4.2 Plain Thick Walled Cylinder

4.2.1 Introduction

This section is presented with the aim of showing the validity, accuracy and hence the reliability of the elastic and elastic-plastic finite element method analysis adopted for this work. The results presented here refer to the case of a plain cylinder without a cross bore as shown in figure 3.1.

4.2.2 Incipient Yielding

In this analysis, the analytical through thickness stresses are easily available [77]. The results of stress and displacement distributions across the wall of the cylinder at the point of incipient yielding are shown in figures 4.1 to 4.4. The incipient yield pressure applied was 162.4 N/mm^2. This is basically an elastic analysis except for the fact that the cylinder bore elements are just about to yield. Figure 4.1 shows the radial stress distribution for both the analytical and numerical analysis. The two curves are almost identical, confirming that in the elastic range the finite element method analysis adopted is very accurate. Figure 4.2 shows the hoop stress distribution across the wall thickness. The analytical and numerical curves are almost identical across the entire thickness. At the cylinder bore surface, the percentage error in hoop stress is 1.109%.

Figure 4.3 shows the axial stress distribution across the wall thickness. The finite element method and analytical results are identical. Figure 4.4 shows the radial displacement

across the cylinder wall thickness. It is notable here that the numerical and analytical results are almost coincident.

From the above results it is clear that there is a slight discrepancy in the finite element method and analytical values of stress at the outside and inside surfaces of the cylinder. Whereas the outer surface elements are larger than the inner elements given a geometrical ratio of 1.15 used in spacing the elements (from the bore), the more important reason for this discrepancy is attributed to the system of stress projection and averaging. The average stresses at the center of the inner and outer elements are not averaged (again) due to the obvious reason that they have neighbours in only one direction. However, this phenomenon does not arise in the axial stress due to lack of stress gradients in that direction. Increasing the geometric ratio gives more accurate results at the cylinder bore due to the fine mesh refinement in areas of high stress gradients but reduces the accuracy on the outside (if a fixed number of elements are used). The geometric ratio of 1.15 was found to give the best results without having to increase the number of elements in the radial direction. The presence of small errors in the stress values on the inside and outside of the cylinder has been a subject of research [58-61]. Inside the material, the finite element method shows very high accuracy compared to the analytic solution. However, this error is not reflected in the displacements.

The above results, carried out at the incipient yield pressure confirm that the finite element method elastic analysis used in this work is reliable and accurate. It may then be reliably used for more complex geometries and load conditions.

4.2.3 Overstrain Stresses

In the elastic-plastic analysis convention, the overstrain is defined as the percentage of the wall thickness that is in the plastic state. The results presented here represent the elastic-plastic stresses across the wall of the cylinder for an overstrain of 51%. This choice of overstrain was made in order to clearly highlight the changes that arise in the stress profiles once the cylinder is in the elastic-plastic range. It is important to highlight

that due to St. Venant's principle, the first element to yield was noticed at the ends of the cylinder. However, this was ignored.

Figure 4.5 shows the incremental loading for this overstrain. 46 loading increments were performed before the overstrain was attained. Six linear reload increments were subsequently performed before re-yield. A staircase pattern is noticeable in the loading increments. This is because concentric elements will yield at around the same pressure. The time to perform this analysis was 96.5 hours. At the overstrain of 51%, the internal pressure applied was 327 N/mm^2. The elastic-plastic interface radius was 113 mm. For less accurate work, the number of load increments could be reduced to the number of stair steps. In this case the load increments would be 25. This would reduce the processing time to 45.5 hours. This demonstrates the expensive nature of the finite element method. By assuming that the elements whose effective stress is within 5% of the material yield stress have also yielded, only 3% of the potential processing time was used. This translates to a saving of 97% in time and expenses and also enhances justification for use of the finite element method in this work.

Figure 4.6 shows the variations of stresses of a typical element adjacent to but not at the cylinder bore in the radial direction with the load increments for the 51% overstrain. Beyond the yield point stress of the element, the hoop and radial stresses decrease as the internal pressure is increased. Upon unloading, negative residual stresses are evident. These stresses become positive upon further loading for the typical element. The radial stress increases numerically as the internal pressure is increased. This figure serves to demonstrate the progression of stresses with increasing internal pressure at the element level. These results also help in the understanding and interpretation of the stress results even for complex cylinder configurations.

Figures 4.7 and 4.8 show a comparison of the finite element method and analytical solutions of the hoop and radial overstrain stresses for the 51% overstrain. The figures show that the finite element method model adopted is accurate and reliable. Figure 4.9 shows the overstrain axial stress distribution across the cylinder wall thickness for the

51% overstrain. This shows a discrepancy of 2% in the stress over the elastic zone. This discrepancy increases significantly as the elastic-plastic interface radius is approached. This error is attributed to the fact that in modeling the analytical solution, a plane stress formulation was used instead of the more appropriate generalized plain strain where $\varepsilon_Z \neq 0$ in the volume constancy condition. This discrepancy has no significant effect on the hoop and radial stresses. The crossing over of the two curves would be expected, recalling that the finite element method analysis gives an upper bound solution to the stiffness matrix and hence a lower bound to the stress solutions.

The axial stress was found to be very sensitive to the discretization in the axial direction. A refined mesh in this direction was found to give more accurate results if the cylinder length was reduced to less than the wall thickness. However, practical analysis requires an infinite cylinder length. The results presented were a compromise of the two requirements. The cylinder length selected was nine times the wall thickness. In most of the previous research work done in this area, the axial stress is seldom discussed, the reason being that it is a median stress and hence not the most critical. However, it could be important to investigate this behaviour more thoroughly. Future work will investigate this phenomenon.

Figure 4.10 shows the variation of the effective overstrain stresses across the wall thickness for the 51% overstrain. In the region of interest, (near the bore and over the elastic-plastic region), the finite element method and analytical solutions are identical and equal to the yield stress of the material. Figure 4.11 shows the nodal radial displacement across the wall thickness for the 51% overstrain. Analysis of this figure yields elemental radial strains of 0.476% for the inner element and 0.068% for the outer element. This gives a strain ratio of 7 compared to a strain ratio of 5 from figure 4.4 (finite element method solution). Failure by gross deformation is therefore more likely to occur at the bore for increased overstrains. Figure 4.12 shows the nodal radial displacements for varying overstrains. At the bore, the increase in displacements is more rapid than anywhere else in the wall thickness. Whereas large overstrains may provide desirable stress distributions, they may also give rise to undesirable effects of gross deformations

during the overstrain process. The overstrain process must also be very gradual for safety reasons. In this work, gross deformation was to be detected by a negative slope of the effective stress-strain curve as the analysis proceeded. The program would terminate if this condition was reached.

Figures 4.13 to 4.15 show the overstrain stresses for varying degrees of overstrain. For the cylinder geometry and material selected, it is then possible to make a fair estimate of the stress levels at intermediate overstrains and internal pressures. Figure 4.16 shows the corresponding variation of effective overstrain stresses for different overstrains and internal pressures.

4.2.4 Residual Stresses

The residual stress results when the 51% overstrained cylinder was unloaded are shown in figures 4.17 to 4.19. The unloading was envisaged as a reversed linear loading by an applied pressure equal to the last overstrain pressure (327 N/mm^2). A number of researchers [66,160] describe the unloading path as being composed of a number of steps while in this work, the unloading was done in one linear step. The results obtained in the formulation of this work are accurate. It is clear that the residual stress distribution is favourable particularly in regard to the tensile hoop stress which is negative at the bore.

Figure 4.20 shows the effective residual stresses for varying overstrains. There is no yielding at the bore or anywhere else in the cylinder due to the residual stresses. The overstrain process should be so designed that reverse yielding due to residual stresses is avoided. For each overstrain, the effective residual stress curves have a minimum but not at the respective overstrain radial position. The residual stress results are similar to those obtained by the thermal load simulation method [77].

4.2.5 Service Stresses

Figures 4.21 to 4.23 show the distribution of the service stresses across the wall thickness. The applied pressure is equal to the initial yield pressure of 162.4 N/mm^2. It is notable here that the stresses at the bore are all negative and the maximum hoop stress

occurs at the overstrain radius. Indeed this is the major advantage of autofrettage. Below certain service pressures, it is then possible to have the bore permanently under compressive stresses. Should any crack have occurred at the bore, then it is always closed in service and its chances of propagation are highly minimized. The maximum hoop stress of 275 N/mm^2 occurs at the overstrain radius. This is comparable to the maximum hoop stress of 275 N/mm^2 occurring during incipient yielding at the bore.

Figure 4.24 shows the variations of effective service stresses at different levels of service internal pressures. It is seen that for any overstrain level, no re-yielding of the cylinder can occur until the full overstrain pressure is attained. It is also notable that the maximum effective stress occurs at the overstrain radius. Therefore, in case of incremental collapse type of cyclic loading, any failure is likely to initiate at the overstrain radius. From a practical point of view, a crack starting at this overstrain radius would be more difficult to detect and could require careful use of non destructive testing techniques.

4.2.6 Economics of Autofrettage

This section presents the material economy that is achieved through the autofrettage process. For the various degrees of overstrain, the percentage economy in material is as shown in table 4.1. This table shows that as the overstrain is increased, the re-yield pressure also increases. This means that on re-loading, the cylinder can take up more pressure before any new signs of material flow, than would be the case for the cylinder which has not been autofrettaged. The corresponding curve for this behaviour is shown in figure 4.25. The best gain in re-yield pressure is seen to be for cases where the overstrain is small. For higher values of overstrain, the gain in re-yield pressure is less per unit overstrain increment.

There are two ways of evaluating the material economy. One approach is to consider a fixed inner bore radius (R_i) and evaluate the size of the outer surface radius (R_O) that would experience incipient yielding at an internal pressure given by the re-yield pressure for the given overstrain. This method yields the material savings shown in figure 4.26. This curve shows that as the degree of overstrain increases, the material savings are more,

with the curve having a fairly linear shape. The other approach is to have a fixed outer radius (R_O) of the cylinder and to seek an inner bore radius (R_i) that would lead to incipient yielding at the value of the re-yield pressure for the given overstrain. The results for this approach are shown in figure 4.27. The savings for this second method are clearly less than those obtained by considering the first method.

Real and advantageous savings are realised when we consider the case of an equivalent cylinder (in terms of materials) with an equal bore radius and an adjustable outer radius. The percentage savings increase linearly as the limit of the internal pressure of 260 N/mm^2 is approached. For the cylinder to carry any pressure beyond this point, the yield stress needs to be increased, no matter what value of outside radius is used. In the case of fixed outside radius, the savings increase less rapidly. The limit of internal pressure of 260 N/mm^2 also applies. Therefore, any discussion of the saving in material must be confined to the case where the internal pressure, P, is less than $Y_S/\sqrt{3}$. Considering the case of fixed inner radius, it is clear that a much larger outside radius would be required. This would be a problem where dimensional, weight and cost limitations must be observed. Autofrettage would also require special tools and their maintenance costs. Over a period of time, the advantages of autofrettage would outweigh these initial and running costs.

Whereas the advantages of autofrettage have been demonstrated in this work, certain practical requirements must be observed in order to make the process a success. These are: initial careful inspection of cylinder to ensure that there are no cracks at the bore; controlled and gradual overstraining to reduce the chances of gross deformation; careful selection of the overstrain level to ensure that no reverse yielding takes place due to residual stresses; controlled and gradual offloading to avoid collapse; continuous and skilled non destructive testing inspection in service to detect any cracks due to the relatively higher service stresses in the inside parts of the cylinder wall. Any crack like flaws would tend to open once the service hoop stresses become positive especially for low overstrains.

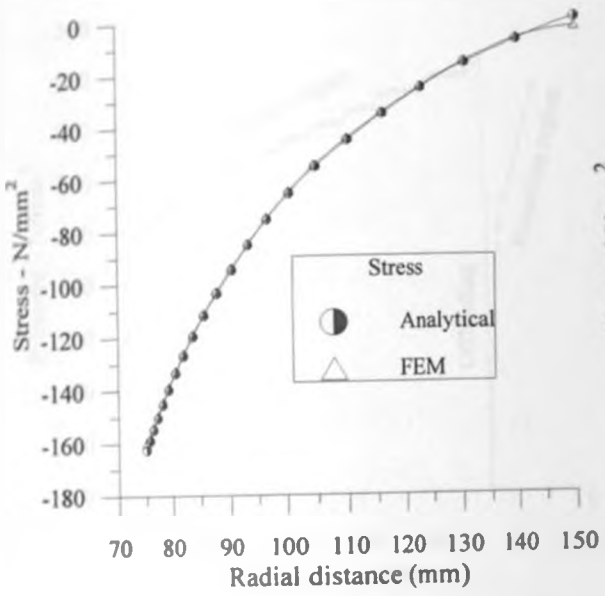

FIG. 4.1 Elastic radial stress for plain cylinder.

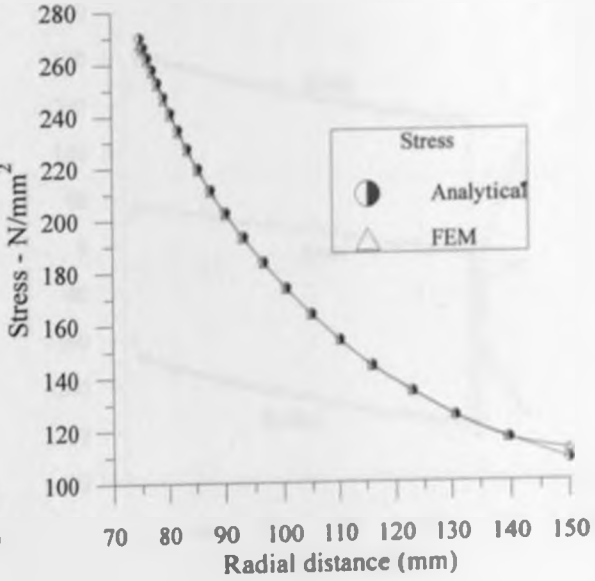

FIG. 4.2 Elastic hoop stress for plain cylinder

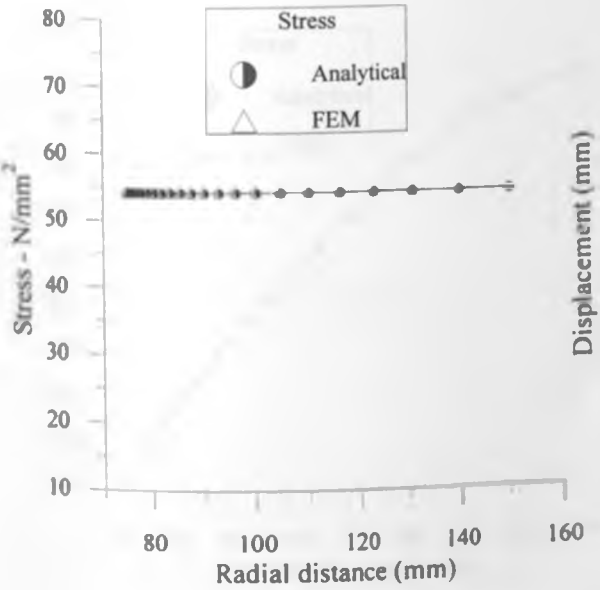

FIG. 4.3 Elastic axial stress for plain cylinder.

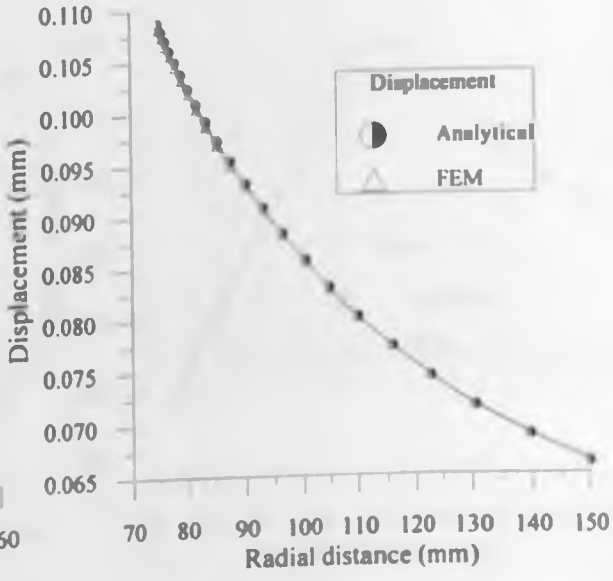

FIG. 4.4 Radial displacement for plain cylinder.

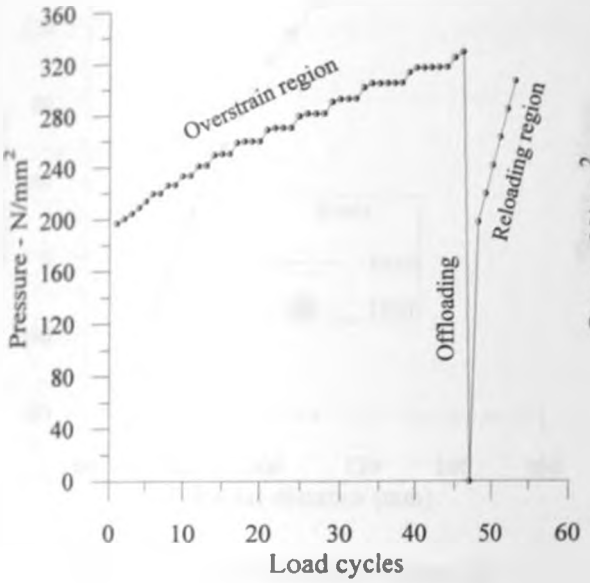

FIG. 4.5. Applied pressure vs. load cycles.

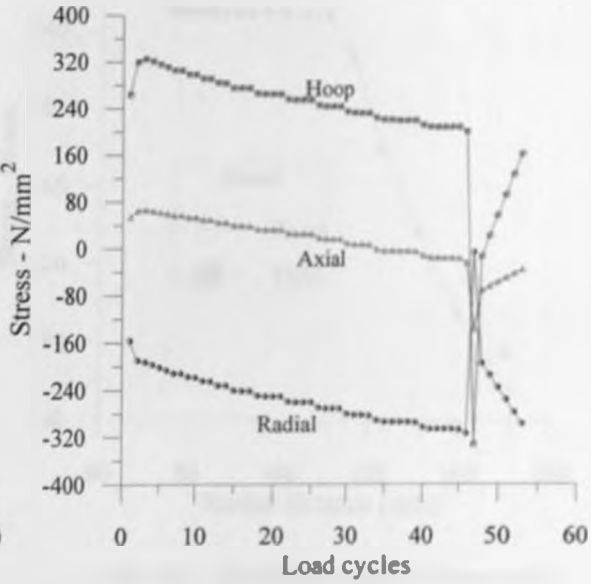

FIG. 4.6. Typical element overstrain stresses for 51% overstrain.

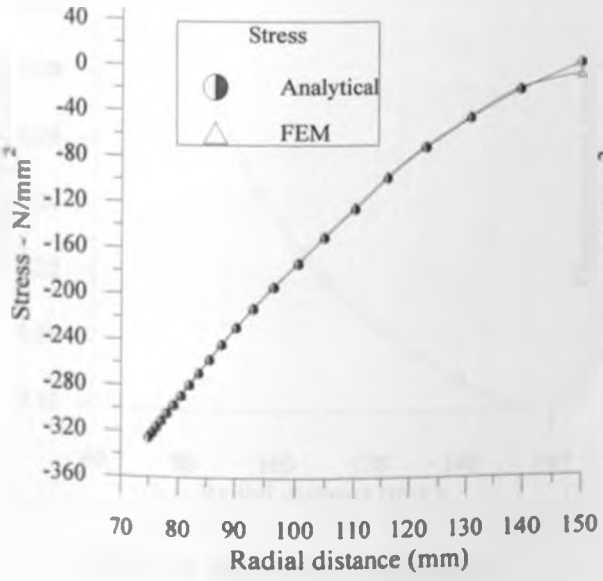

FIG. 4.7 Overstrain radial stresses for 51% overstrain.

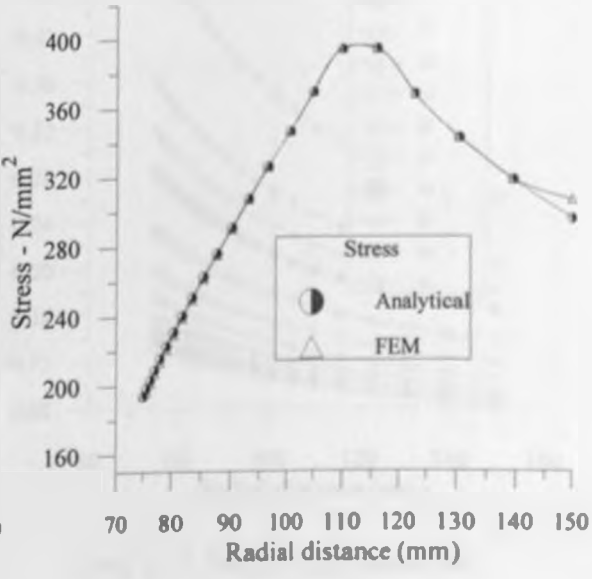

FIG. 4.8 Overstrain hoop stresses for 51% overstrain.

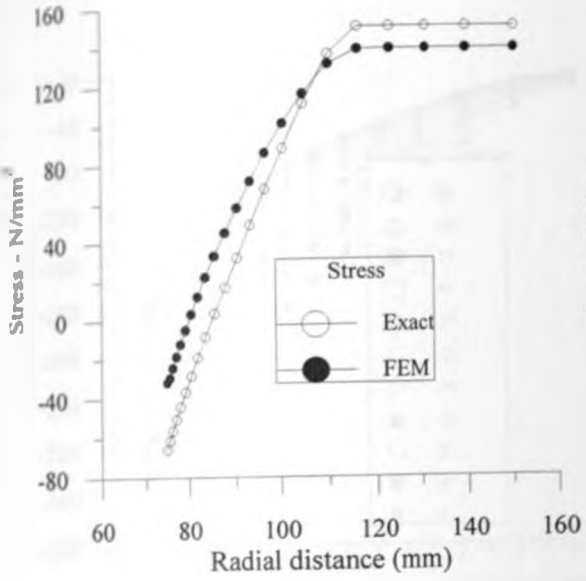

FIG. 4.9 Overstrain axial stresses for 51% overstrain.

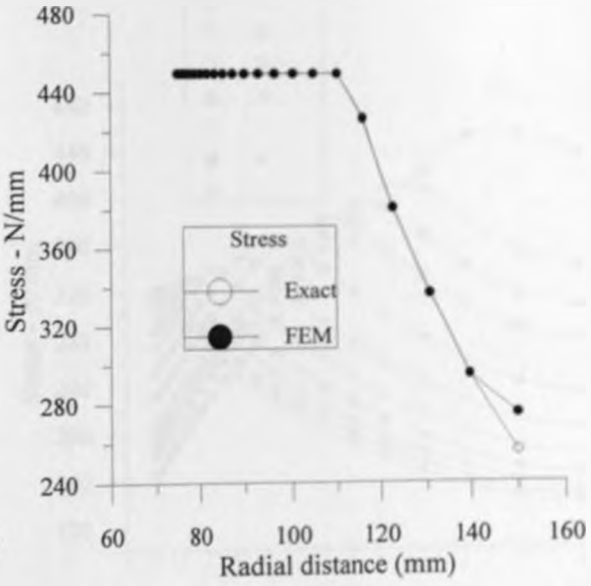

FIG. 4.10 Overstrain effective stresses for 51% overstrain.

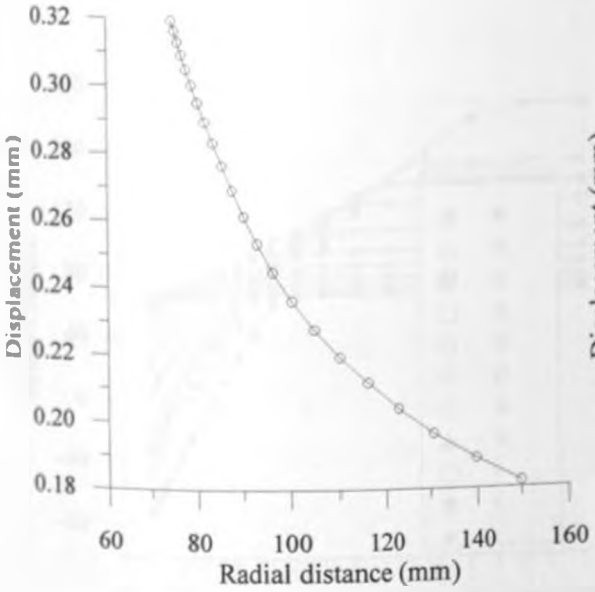

FIG. 4.11 Radial displacements for 51% overstrain.

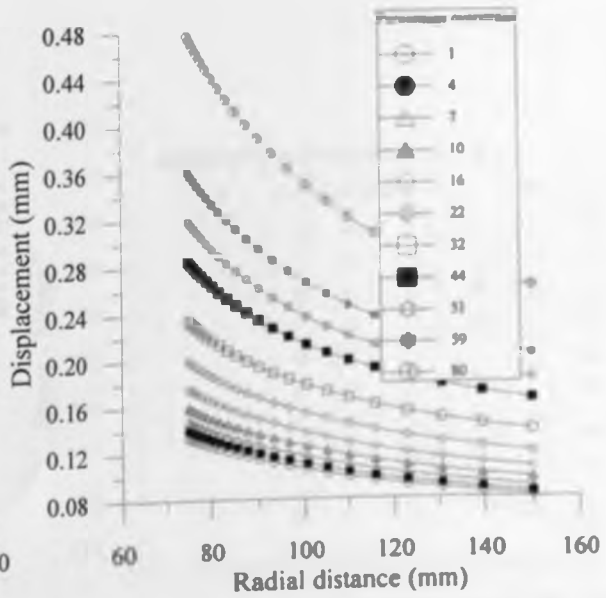

FIG. 4.12 Radial displacements for varying overstrains.

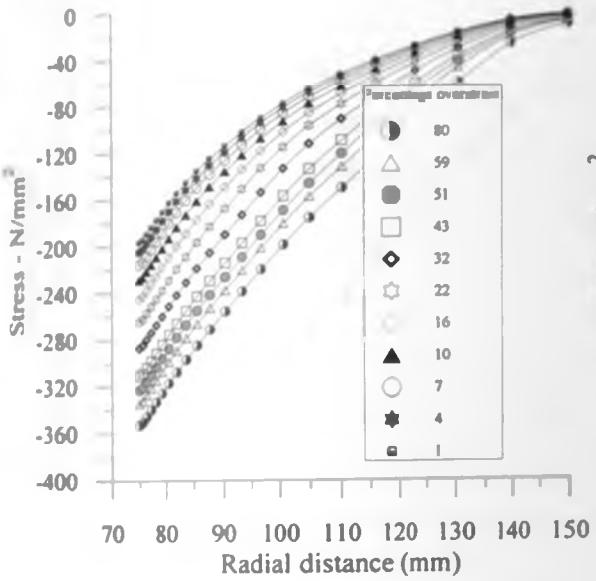

FIG. 4.13 Overstrain radial stresses for varying overstrains.

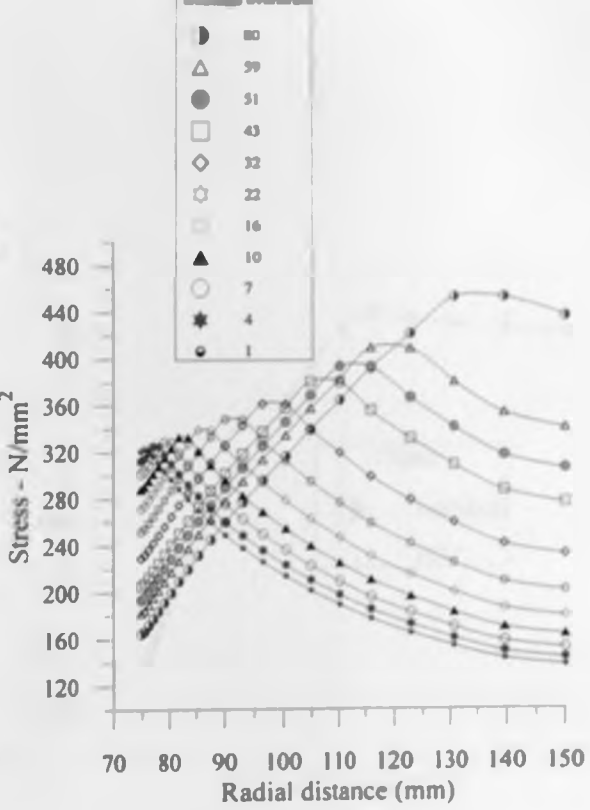

FIG. 4.14 Overstrain hoop stresses for varying overstrains.

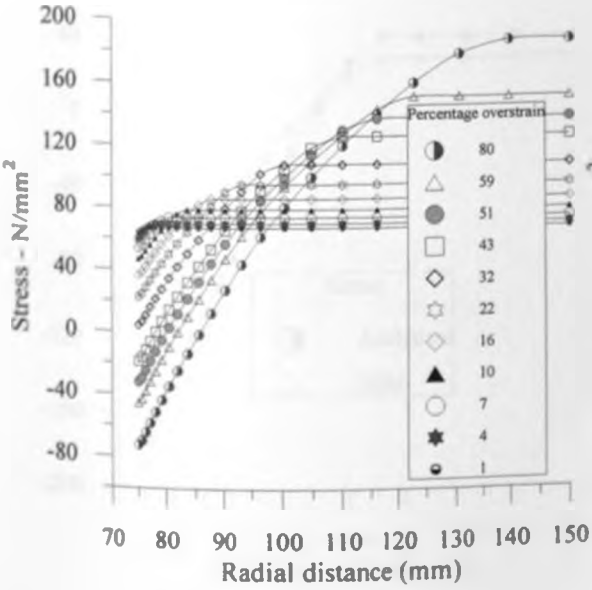

FIG. 4.15 Overstrain axial stresses for varying overstrains.

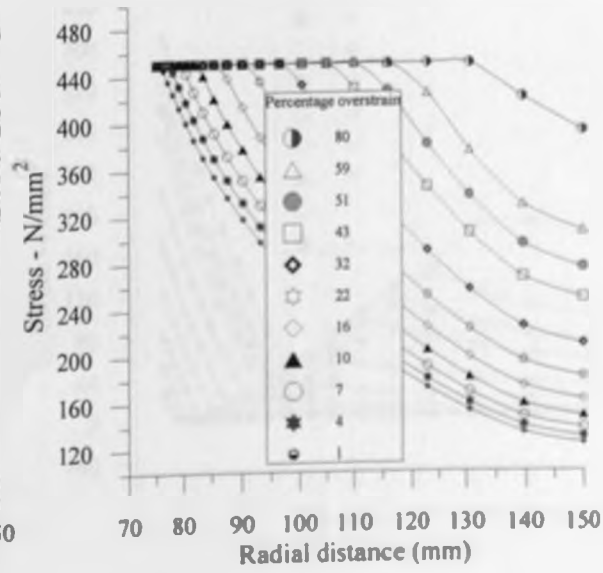

FIG. 4.16 Overstrain effective stresses for varying overstrains.

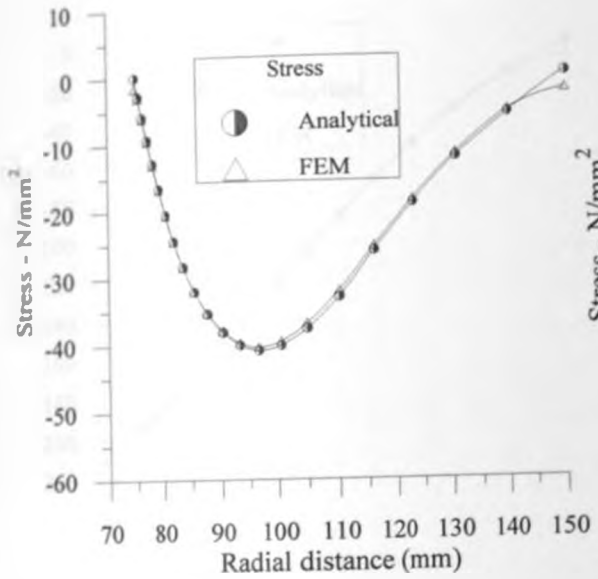

FIG. 4.17 Residual radial stress for 51% overstrain.

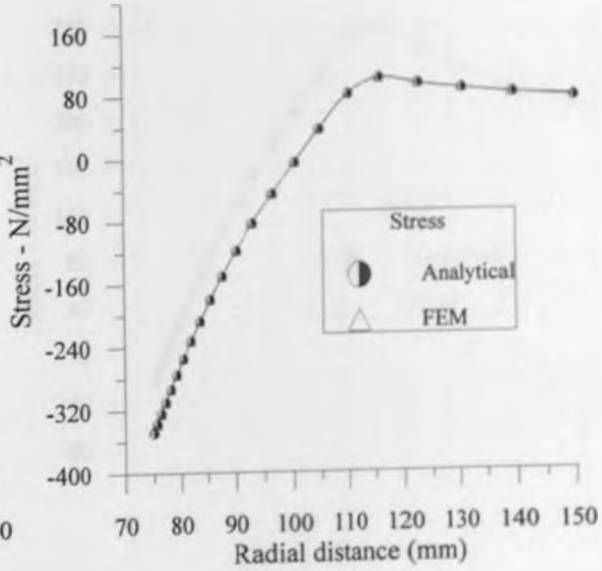

FIG. 4.18 Residual hoop stress for 51% overstrain.

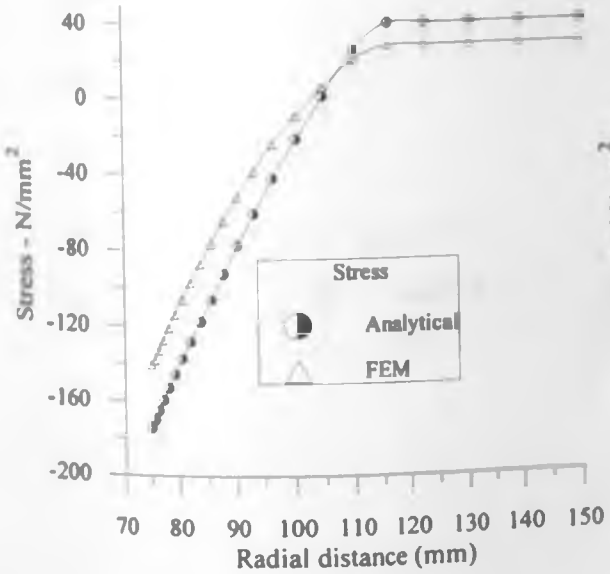

FIG. 4.19 Residual axial stress for 51% overstrains.

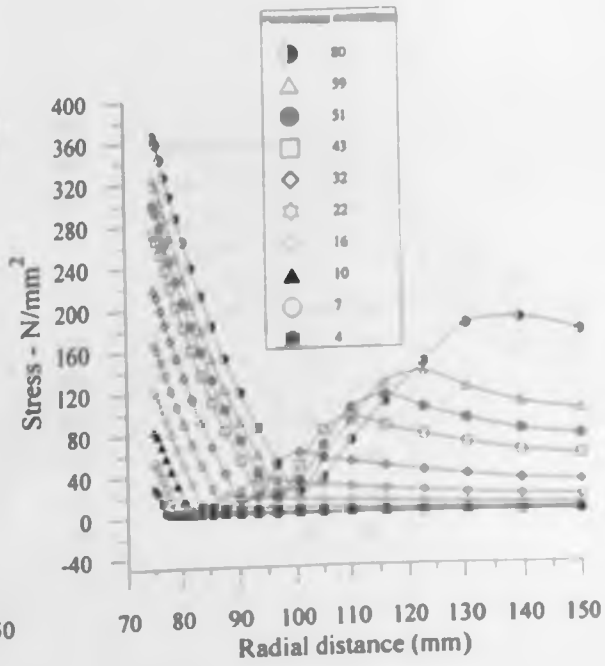

FIG. 4.20 Effective residual stresses for varying overstrains.

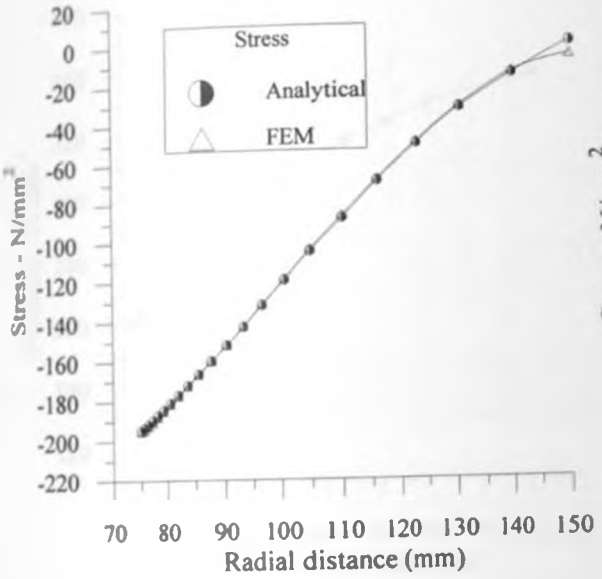

FIG. 4.21 Service radial stress for 51% overstrain.

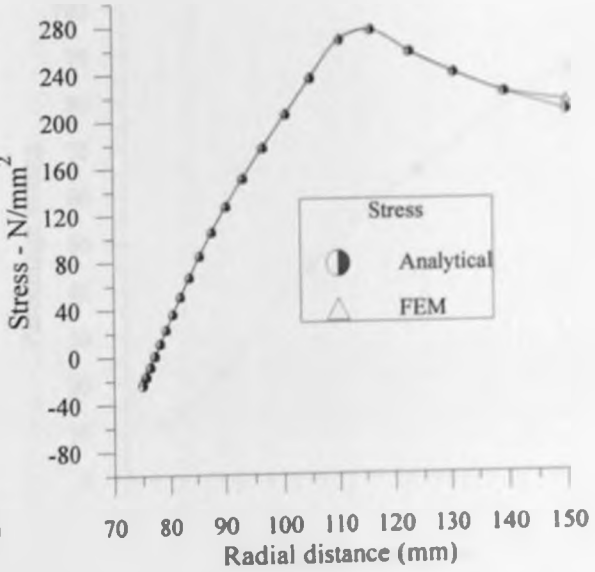

FIG. 4.22 Service hoop stress for 51% overstrain.

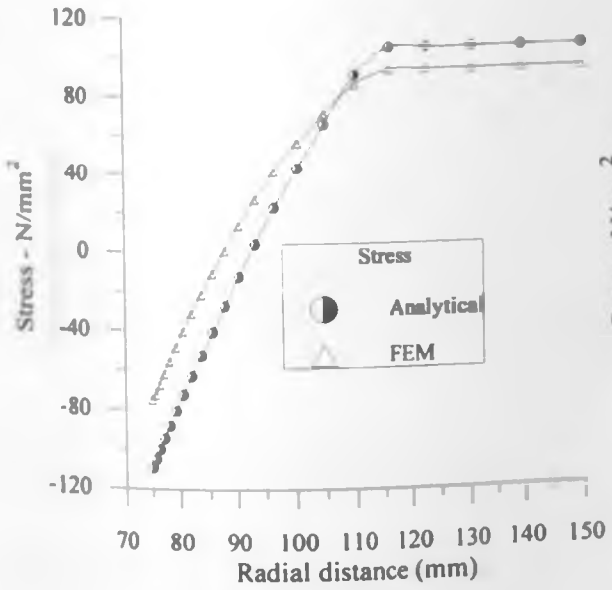

FIG. 4.23 Service axial stress for 51% overstrain.

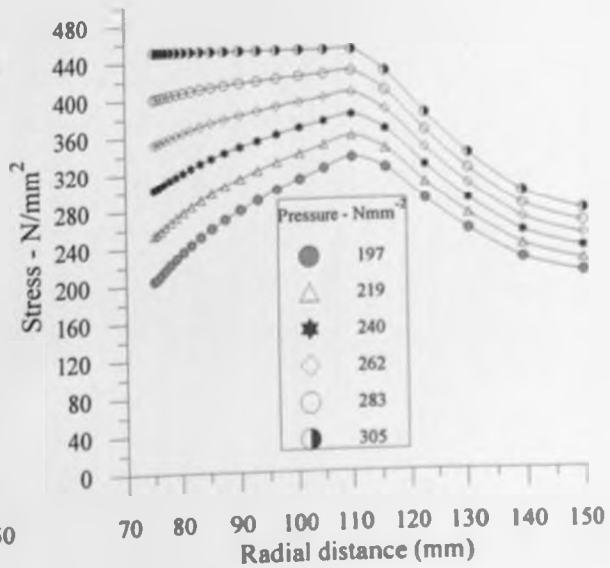

FIG. 4.24 Service effective stresses for varying service pressures.

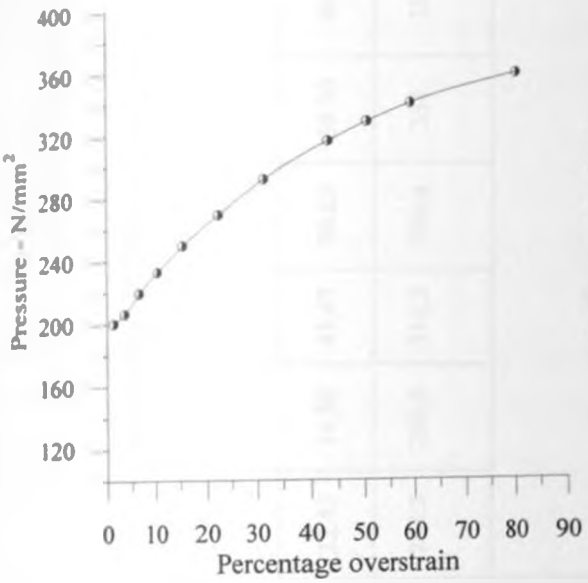

FIG. 4.25 Re-yield pressure for varying overstrain.

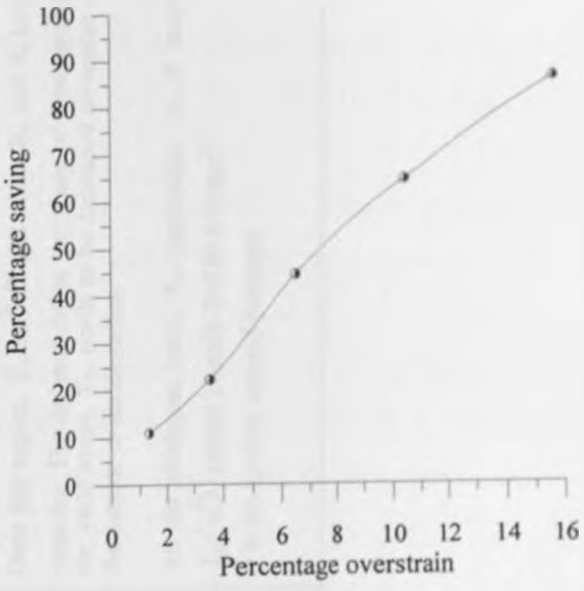

FIG. 4.26 Percentage saving vs. overstrain for fixed inner radius.

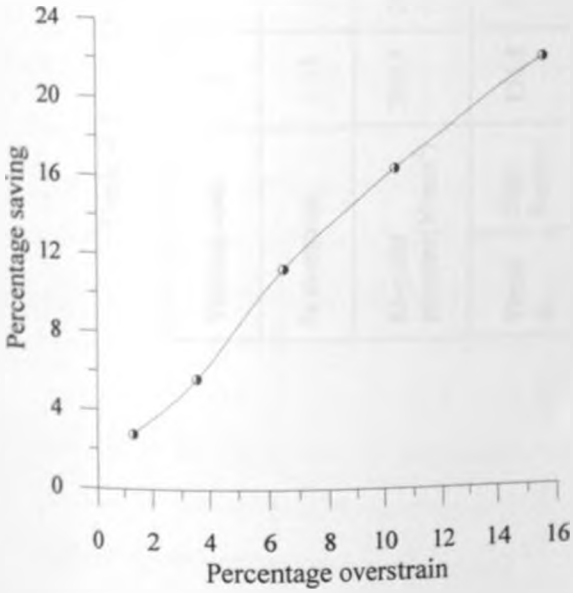

FIG. 4.27 Percentage saving vs. overstrain for fixed outer radius.

Table 4.1. Overstrain, re-yield pressure and material percentage savings

Yielding node		3	5	7	9	11	13	15	17	18	19	21
% overstrain		1.33	3.56	6.52	10.43	15.61	22.45	31.50	43.47	50.83	59.30	80.24
Re-yield pressure(N/mm^2)		200.4	206.4	219.4	232.7	249	268.3	290.5	314.5	326.6	338	356.6
Fixed R_i	New R_o(mm)	156.8	165.4	190.2	232.2	367.7						
	% Saving	11.07	22.37	44.75	65.05	86.98						
Fixed R_o	New R_i(mm)	71.7	68.0	59.2	48.5	30.6						
	% Saving	2.77	5.59	11.19	16.26	21.74						

Over this region, $Y_S \leq \sqrt{3}P$ and hence R_o and R_i have no meaning. For the material to carry any of these pressures, the yield stress, Y_S, needs to be increased no matter what the outside or inside radius.

As the thickness ratio, K, approaches ∞, P tends to $Y_S/\sqrt{3}$ (upper bound). $P \leq 259.8$ N/mm^2.

P is the applied internal pressure.

4.3 Plain Cross-Bored Cylinder

4.3.1 Elastic Stress Response

4.3.1.1 Introduction

In this elastic analysis, the structural configuration of the cylinder is as shown in figure 3.2. A thick walled cylinder having a thickness ratio of 2.25 and a cross bore to main bore radius ratio of 0.1 will be specifically considered for the stress profiles. Other thickness ratios and cross bore to main bore radius ratios will be analyzed for stress concentration factors. The applied internal pressure will be dependent of the thickness ratio being considered. The radial, hoop and axial stress profiles and values will be shown. In thick walled cylinder studies, emphasis is normally laid on the behaviour of the hoop stress since it is normally the highest and involves separation of material leading to failure of the structure. There will therefore be a tendency to emphasize on this stress in the discussion.

4.3.1.2 Elastic stresses

Figure 4.28 shows the resulting transverse plane stress profiles. In this case the hoop stress is positive and highest at point A, having a value of 60 N/mm^2. As the cross bore is approached, the hoop stress reduces sharply and reaches a value of about –40 N/mm^2 at the cross bore-main bore intersection. It settles to this value of –40 N/mm^2 for the rest of the points along the cross bore edge CD. The general profile of this curve is expected since in this plane, the normal force on the cross bore elements surface is such as to compress the material in the negative hoop stress direction.

The axial stress starts at 10 N/mm^2 and is quite steady in value till the intersection point C is approached. It then increases very sharply to about 40 N/mm^2. After this maximum value at the intersection, the axial stress falls very sharply to about 25 N/mm^2. There is further increase of the axial stress which is quite rapid but not sharp. The axial stress is a maximum on the outer surface at point D with a value of about 45 N/mm^2. It is easy to understand this behaviour of the axial stress by noting that in the main bore, axial stress is the true global axial stress. In the cross bore, the axial stress is the true local hoop stress about the transverse plane. The cross bore may then be considered to be a cylindrical

opening in a non-prismatic structure having a large thickness in one direction and a rather small and non-uniform thickness in the second direction. This bahaviour of the axial stress is similar to the hoop stress results obtained from an analysis of internal pressure loading in a thick walled cylinder with a uniform outer diameter and two different uniform bore diameters having a venturi transition piece. The cross bore to main bore configuration in the transverse plane may be viewed as such.

The radial stress starts at point A with a value of -40 N/mm^2 and rises slowly. It then drops to a value of about -43 N/mm^2 at the intersection point C. Along the vertical line CD, it drops sharply to about -50 N/mm^2. It then rapidly rises to a value of -10 N/mm^2 at the outer edge of the cross bore point D. It is worth noting that the global radial stress along the cross bore edge CD is related to but is not the true local radial stress of the cross bore. This local radial stress is now a function of the global hoop stress. This is the reason that the value of radial stress at the top edge D does not vanish.

The meridional plane stresses for a cylinder with a thickness ratio of 2.25 and a cross bore to main bore radius ratio of 0.1 are shown in figure 4.29. Due to the relatively large axial dimension of the cylinder, only the nodes in this direction and close to the crotch corner are shown. The hoop stress rises very rapidly to a value of 175 N/mm^2 and then falls off in a manner characteristic of a plain cylinder under internal pressure. However, it is important to note that the maximum hoop stress does not occur at the crotch corner node but rather at a node placed at 2.1 mm from the crotch corner node or at 2.3% of the cylinder wall thickness. This phenomenon is peculiar and is indeed noted by other previous researchers [17,45]. However, so far, no explanation has been put forward since the previous studies were not exhaustive.

The axial stress falls off to a value of -37 N/mm^2 at the crotch corner and remains at the same value along the cross bore edge IJ up to the top point J. Similarly, the radial stress has a constant value of -40 N/mm^2 up to the crotch corner. It then gradually rises to zero in a manner similar to that of a plain cylinder under internal pressure. It is then important

to understand and appreciate this difference in response between the hoop stress on one hand and the axial and radial stresses on the other.

The phenomenon of the location of maximum hoop stress, point p, being away from the crotch corner in the radial direction is observed for all cases of cylinder thickness ratios for the configurations where the cross bore to main bore radius ratio is 0.2 and below. For the cylinder thickness ratio of 1.25, this occurs for the configurations where the cross bore to main bore radius ratio is 0.1 and below. In all cases, the location of the maximum hoop stress approaches the crotch corner as the radius ratio increases. Once the radius ratio reaches the critical value, depending on the cylinder thickness ratio, the location of the maximum hoop stress is always at the crotch corner.

Figure 4.30 shows how the location of the maximum hoop stress is influenced by the cross bore to main bore radius ratios. For a thickness ratio of 2.25, the maximum location of 2.11 mm (2.25% of wall thickness) away from the crotch corner occurs when this ratio is between 0.05 and 0.15. A more accurate determination of the exact location can be done if much smaller elements are used. A polynomial curve is used to estimate this relationship in a case where infinitely small elements are employed.

This phenomenon may be explained by considering the relative dimensions of the two intersecting holes. One is the main bore with a uniform thickness. The other is the cross bore which is rather like a hole in an irregular and non-prismatic structural block. Each one may be considered to have a local coordinate system. Consider the case where the cross bore surface elements are not loaded. The meridional hoop stress profile would be as shown in figure 4.31, showing a maximum hoop stress located away from the crotch corner. When the cross bore surface elements alone are loaded the stress profiles are also shown in figure 4.31. In this latter case, the local hoop stress in the meridional plane is also the global hoop stress and may be added to the initial hoop stress directly without any stress tensor transformation procedure being carried out. The cross bore local radial stress along the meridional vertical edge IJ now acts as a global compressive axial stress tending to increase the cylinder thickness and hence increase the hoop stress. The global

radial stress also acts as a compressive axial stress in the cross bore local coordinate system and tends to increase the cross bore radius, thereby increasing the local hoop stress. Due to the crotch corner edge effects in both the main bore and the cross bore only loaded cases, the stress response at the crotch corner does not exactly mirror the stress response in the cross bore along the vertical edge IJ or along the horizontal edge HI in the main bore. Hence, though the crotch corner may be considered the geometrically most singular point in the structure, it may not necessarily be the point of the maximum global hoop stress. This is due to the interactions of the complex stress systems in the cross bore and the main bore. The location of the maximum global hoop stress is then solely determined by the relative dimensions and dispositions of the cross bore and the main bore. These are the cross bore radius, main bore radius and the cylinder thickness ratio.

Figure 4.31 shows the meridional stress profiles when either the main bore and the cylinder end are loaded or the cross bore alone is loaded. The resultant stresses in figure 4.29 are a direct superposition of the stresses arising from the two stress systems. When the cross bore alone is loaded, the location of the maximum hoop stress is at the crotch corner. Adjacent to the crotch corner, the hoop stress falls slightly but immediately stabilizes to a constant value for the rest of the section. Therefore the edge effect has little influence on the location of maximum hoop stress for a cross bore of this size. We may then conclude that the phenomenon where the location of the maximum hoop stress is not at the crotch corner is largely contributed by the loading in the main bore for this cross bore to main bore configuration.

For this structural configuration, it was found important to establish the accuracy of the finite element method stress and displacement profiles in the far field, where the effect of cross bore geometry and loading have insignificant influence, with those of a plain cylinder. The results are shown in figures 4.32 and 4.33. The importance of this verification is that it can confirm that the source computer program code is properly written and that the input parameters such as the material properties and geometrical dimensions are error free. All that remains is to properly discretize the elements around

the cross bore to achieve results that are accurate enough. The finite element results were found to be very accurate, reliable and dependable.

Figure 4.34 shows the hoop stress profiles along one quadrant of the cross bore in arcs parallel to CI and DJ as shown in the discretization figure 3.2. Different radial positions are shown. The results agree quite well with what is discussed above, especially concerning figure 4.29. Furthermore, from this figure it is then possible to draw a curve on the cross bore surface connecting all the points and indicating the angles in the x-z plane where the hoop stress vanishes. The area to the left of this curve has negative hoop stresses and that to the right has positive hoop stresses.

Figure 4.35 shows the general state of hoop stresses in one quadrant on the face of the cross bore (parallel to the lines CD and IJ) and immediately adjacent on the main bore. The nodes on the transverse section are shown by the lower curve while meridional section nodes are shown by the top curve. Other intermediate section nodes are shown by the enclosed curves. The curves show a tendency to converge on the main bore side since the stress gradients are higher in this region. From the main part of the cross bore, it can also be deduced that all nodes enclosed within 30^0 in the x-z plane have a negative hoop stress.

Figure 4.36 shows the effective stresses for nodes in one quadrant of the cross bore. The general profiles are similar to those of the hoop stresses. However, at the points of maximum effective stress (which corresponds to the points of maximum hoop stresses), the curves are sharper and the stress gradients are steeper.

4.3.1.3 Stress concentration factors

For all the combinations of cylinder thickness ratio and cross bore to main bore radius ratios considered, the corresponding stress concentration factors are shown in figure 4.37. The stress concentration factor is the most important parameter in the pressure vessel analysis studies and is the one used for design purposes. For thickness ratios between 1.75 and 3.0, the stress concentration factor profiles are very similar in behaviour. The

stress concentration factor rises sharply as the cross bore to main bore radius ratio is increased. For the higher values of thickness ratio, this falls off gradually and is followed by a slow fall then a slow rise in the stress concentration factor. For this range of thickness ratio, there exists a critical value of cross bore to main bore radius ratio, equal to 0.2, where the stress concentration factor is the same for all cases. Beyond this critical value, the stress concentration factor is greater for the smaller thickness ratios, with a general trend for the stress concentration factors to increase as the radius ratio approaches 0.4. Before this critical value, the stress concentration factor is higher for the higher thickness ratios. To the left of the point 0.2, the curves have a local maximum value of stress concentration factor with the thicker cylinders having higher maximum stress concentration factor values than the thinner cylinders. The maximum stress concentration factor points are found at cross bore to main bore radius ratio of 0.05.

The 1.25 and 1.5 thickness ratio cylinders behave like the thicker cylinders only for cross bore to main bore radius ratios less than 0.15. Beyond this value of cross bore to main bore radius ratio, the stress concentration factors rise very rapidly, with the thinner cylinder having higher stress concentration factors. For these thickness ratios the stress concentration factor curves have inflexion points rather than stationary points as exhibited by the thicker cylinders.

This critical value is also the value equal to or below which the location of the maximum meridional hoop stresses are displaced from the crotch corner. Since it is common for all thickness ratios between 1.75 and 3.0, then it must be considered to be a geometrical universal constant for plain cross-bored cylinders within this range. It is a constant that may be easily used to predict, as a rule and without the need for a rigorous analysis, the elastic stress response of the thick walled cylinders within the thickness ratio range of 1.75 and 3.0.

To establish the constancy of the universal geometrical constant, the stress concentration factors were evaluated at the cross bore to main bore radius ratio of 0.2 for a wide range of thickness ratios between 1.75 and 5.0 as shown in figure 4.38. For the full range, the

average stress concentration factor was found to be 2.734, with a standard deviation of 2.163e-2 and a range of 7.04e-2. For the smaller cylinder thickness ratio range of 1.75 to 3.0, the average stress concentration factor was found to be 2.753, with a standard deviation of 5.416e-3 and a range of 1.432e-2. For normal pressure vessel designs, this is the more practical range of thickness ratios. This procedure then confirmed that the cross bore to main bore radius ratio of 0.2 is indeed a geometrical constant.

Looking at figure 4.37 in more detail, consider the stress concentration factor curve for a thickness ratio of 2.25. As the cross bore radius increases, the stress concentration factor increases very sharply. This response could be well understood by considering the following facts. An increase in the radius of the cross bore results in more cross bore surface area being loaded, leading to higher forces and stresses in a non-uniform outer dimensional structure. Also, the volume of the material removed in placing the cross bore increases, leading to the overall stiffness of the structure being reduced particularly around this cross bore region. Consequently the resistance of the structure to deformation is undermined particularly in the transverse plane whose thickness becomes narrower and the included angle between curves BC and CD becomes more oblique away from 90^0. Finally, the ratio of the cross bore loaded area to main bore loaded area increases. In all the cases, the evaluation of the stress concentration factor is based on the hoop stress in the far field, for example, point G in figure 3.2, which is greatly influenced by the loading in the main bore. The stress response of the thick walled cylinder is governed by any or a combination of any of the above factors each having its own weighting factor.

As the cross bore to main bore radius ratio increases, the overall structural stiffness rapidly declines leading to higher hoop stresses around the cross bore. Therefore, the stress concentration factor increases and reaches a maximum value of 2.87 at a radius ratio of 0.05. The stress concentration factor then reduces very gradually, reaching a minimum of 2.75 at a radius ratio of 0.2. This reduction in stress concentration factor may be attributed to existing favourable geometrical conditions. One of these conditions is the increase of the included angle between lines CD and BC on the cross bore surface and the main bore respectively. An increase of this angle reduces the overall geometrical

singularity of the intersection curve CI and hence will result in a reduced stress concentration factor. Beyond this region, the volume of the material removed overrides all the other factors to weaken the structure. Higher displacements result from loading and this results in higher hoop stresses and stress concentration factors.

Consider a cross bore to main bore radius ratio of 0.05 to the left of the critical point of 0.2 for a cylinder with a fixed outer radius. As the thickness ratio increases, the stress concentration factor is seen to rise also. As thickness ratio increases, the included angle remains constant. The main bore loaded area decreases while the cross bore area increases. The cross bore volume increases while the overall cylinder volume increases more rapidly. The combination of these factors lead to increased stress concentration factor. The maximum stress concentration factor curves for different thickness ratios are shown in figure 4.39. For cross bore radius ratios greater than 0.2, the influence of the above factors is reversed and the stress concentration factor increases with a reduction of the thickness ratio.

The behaviour of the 1.25 and 1.50 thickness ratio curves is very similar to that of the curves discussed in the foregoing section. The difference being that at the cross bore radius ratio of 0.2, the stress concentration factors are higher, increasing with the reduction of the thickness ratio. This deviation may lead to further classification of thick walled cylinders. The conventional classifications are: thin shells (thickness ratio of 1.1 or less) and thick walled cylinders (thickness ratio greater than 1.1). This work now proposes to have the following categories: thin shells (thickness ratio of 1.1 and below), thick shells (thickness ratio greater than 1.1 and less than 1.75) and thick walled cylinders (thickness ratio greater than 1.75). The stress concentration factor curves for these two thickness ratios also do not exhibit stationary points but instead have inflexion points. It is also notable that the stress concentration factor curves for these two thickness ratios intersect at a point where the cross bore to main bore radius ratio is 0.11. This is close to the point 0.1 which may be considered a critical value for the thickness ratio of 1.25.

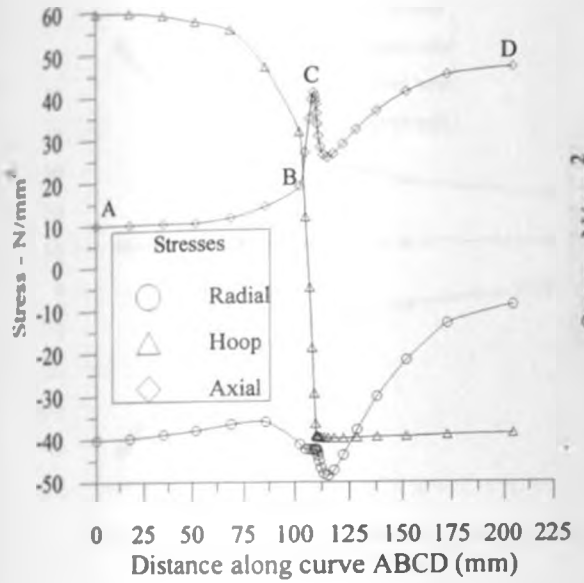

FIG. 4.28 Transverse stresses (k=2.25, d=0.1).

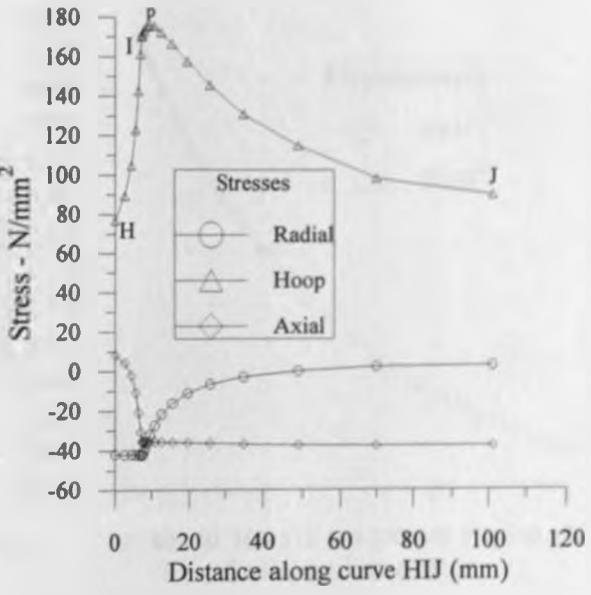

FIG. 4.29 Meridional stresses (k=2.25, d=0.1).

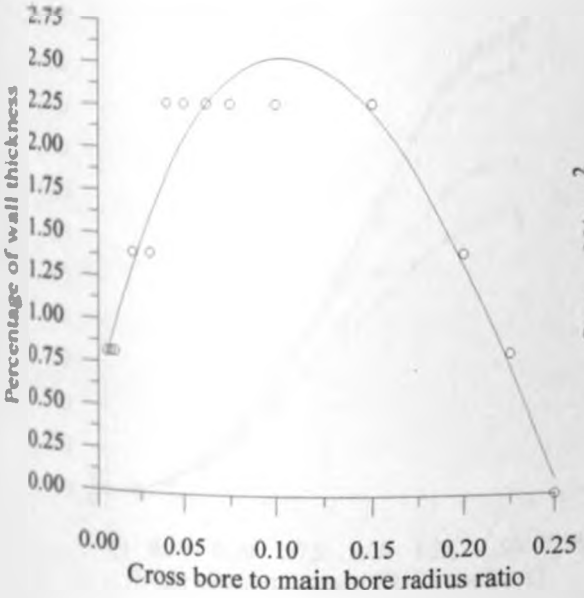

FIG. 4.30 Location of maximum hoop stress (k=2.25).

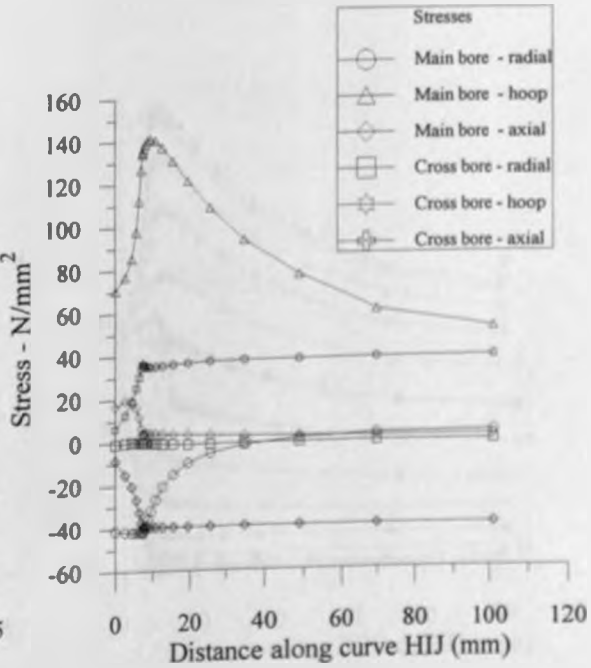

FIG. 4.31 Stresses on cross bore surface when main bore and cross bore loaded separately (k=2.25, d=0.1).

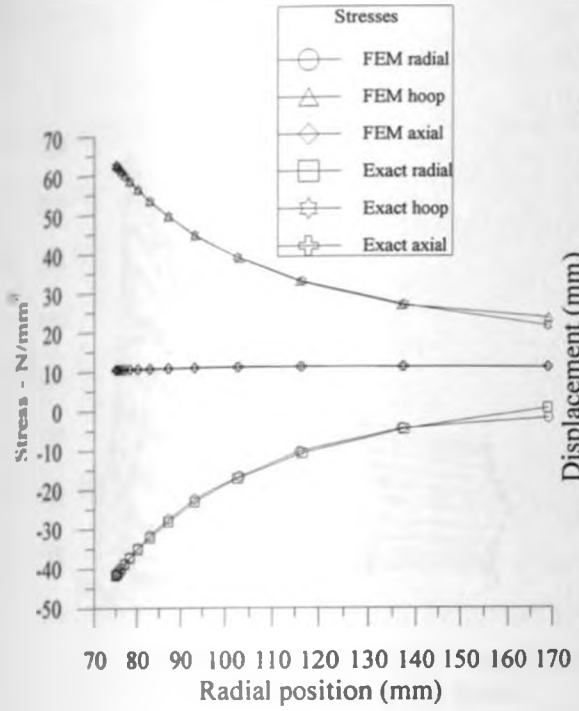

FIG. 4.32 Far field stresses (k=2.25, d=0.1).

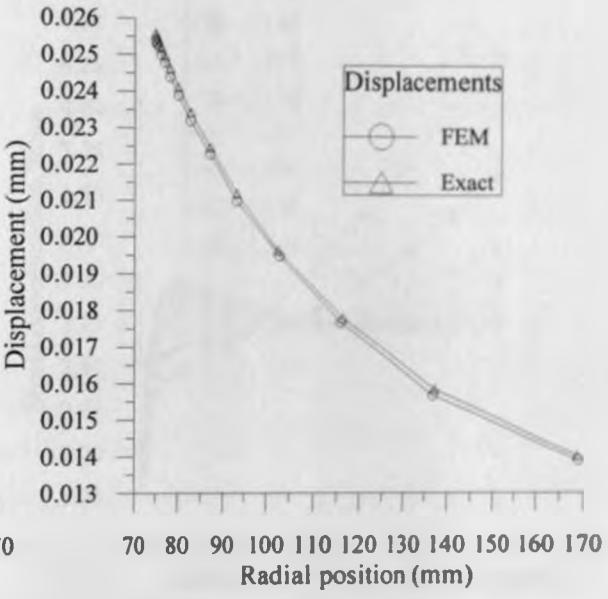

FIG. 4.33 Far field radial displacements (k=2.25, d=0.1).

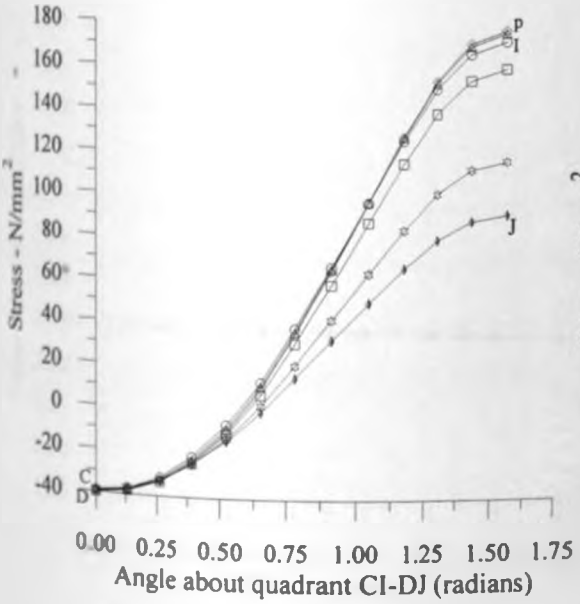

FIG. 4.34 Hoop stresses in one quadrant of cross bore surface at various radial positions.

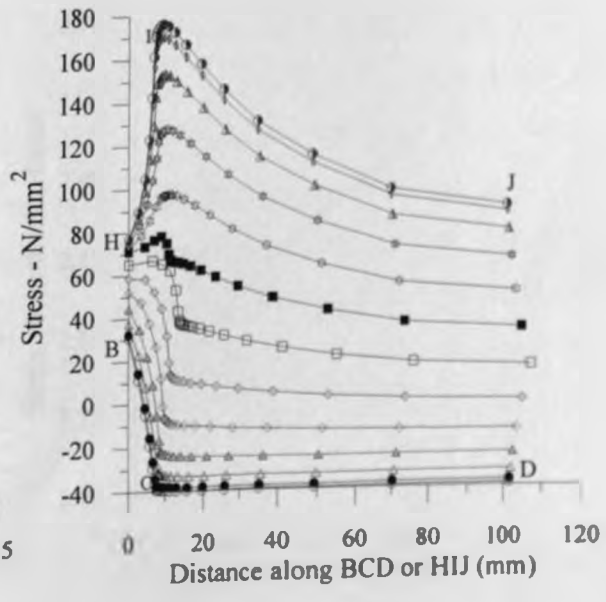

FIG. 4.35 Hoop stresses on cross bore surface (K=2.25, d=0.1).

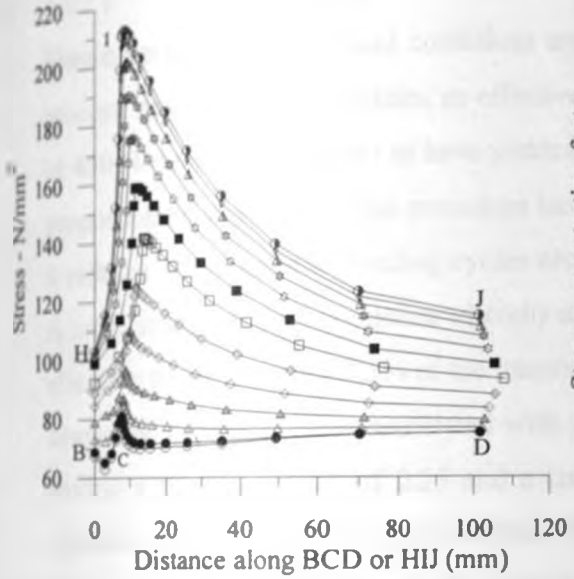

FIG. 4.36 Effective stresses on cross bore surface (k=2.25, d=0.1).

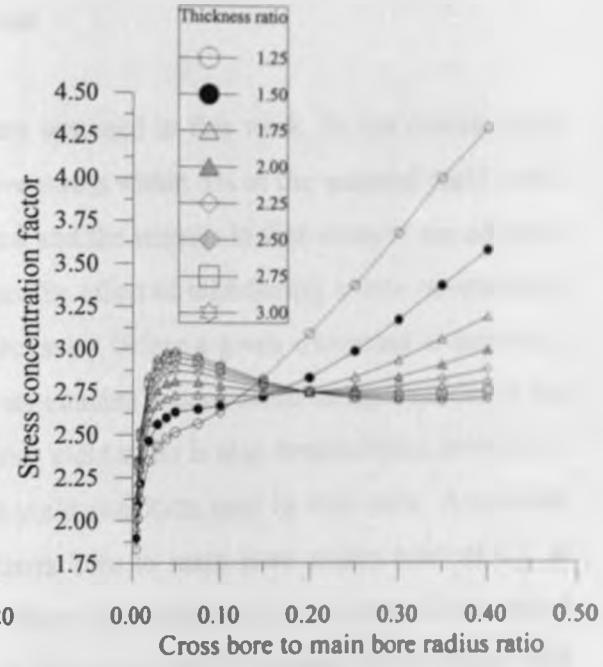

FIG. 4.37 SCF vs. cross bore to main bore radius ratio for various thickness ratios.

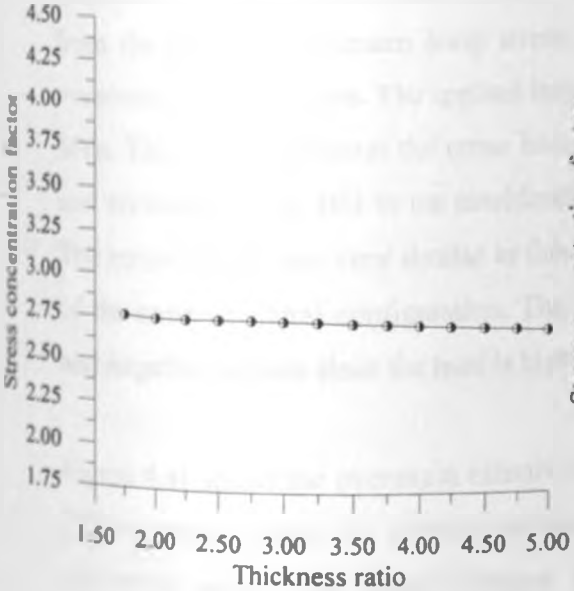

FIG. 4.38 SCF vs. thickness ratio (d=0.2).

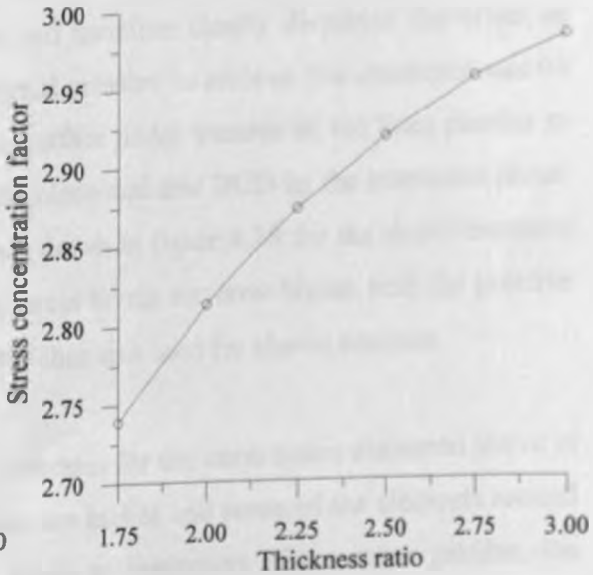

FIG. 4.39 Variation of maximum SCF vs. thickness ratio (d<0.2).

4.3.2 Elastic-Plastic Stress Response

4.3.2.1 Introduction

Elastic perfectly plastic yield conditions are assumed in this work. In the overstraining process, any element that attains an effective stress within 5% of the material yield stress of 450 N/mm^2 is considered to have yielded and the stresses in that element are adjusted proportionately. Whereas this procedure has the effect of introducing errors, nevertheless it reduces the number of loading cycles necessary before a given overstrain is achieved. A more stringent yield condition whereby an element is considered to have yielded if the effective stress is within 0.5% of the material yield stress is also demonstrated in order to assess the degree of error associated with yield condition used in this work. A cylinder having a thickness ratio of 2.25 and a cross bore to main bore radius ratio of 0.1 is considered for the general stress profiles. Other combinations of cylinder thickness ratios and cross bore to main bore radius ratios are considered for overstrain pressures and minimum residual stresses. The stress curves presented represent the cylinder configuration as shown in figure 3.2.

4.3.2.2 Overstrain stresses

The overstrain hoop stresses around the cross bore are shown in figure 4.40 for an overstrain of 7%. For this geometry, an overstrain of 7% coincided with a position away from the point of maximum hoop stress and therefore clearly displayed the effect of overstrain on the stresses. The applied internal pressure to achieve this overstrain was 94 MPa. The curves represent the cross bore surface nodal stresses of the lines parallel to and enclosed by line HIJ in the meridional plane and line BCD in the transverse plane. The stress patterns are very similar to those shown in figure 4.35 for the elastic response of the same structural configuration. The stress levels are now higher both for positive and negative stresses since the load is higher than that used for elastic analysis.

Figure 4.41 shows the overstrain effective stresses for the same nodes discussed above at 7% overstrain. Again, the effective stresses are higher and some of the elements around the crotch corner have already yielded. From an inspection of the stress profiles, the nodes within 15^0 of the crotch corner in the x-z plane have already yielded. By observing

how close these stress curves are at around point I, then it is clear that the elastic-plastic front is rather narrow in the x-z plane and does not spread out much along the IC direction.

A clear display of the overstrain stress response along the meridional curve HIJ is shown in figure 4.42 for 7% overstrain. For the overstrain pressure of 94 N/mm^2 applied, the overstrain radial stress has a value of about −100 N/mm^2 at the point H. At the crotch corner, the overstrain radial stress reduces asymptotically approaching zero along line IJ. This behaviour is normal since radial stresses are expected to vanish at point J. The overstrain axial stress has a value of about 22 N/mm^2 at point H and drops to about −75 N/mm^2 at point I. It remains at this level along line IJ. The overstrain hoop stress has a value of 175 N/mm^2 at point H and rises sharply to reach a value of 380 N/mm^2 at a point between points I and J. This is followed by a gradual drop. It is notable that the location of the maximum overstrain hoop stress has now moved deeper inside the wall thickness. The location of this point corresponds to the elastic-plastic interface. Due to overstrain, the elements already yielded tend to have lower overstrain hoop stress. This behaviour normally occurs in plain cylinders where the outer elastic shell tends to restrain the inner plastic core from moving out in the radial direction, thus reducing the hoop stress. The overstrain effective stress curve shows that at 7% overstrain, the crotch corner plus the adjacent elements along IJ have reached the yield limit while the rest on either side of point I are still elastic. The elastic-plastic behaviour around the cross bore is not quite like that of the plain cylinder. In this case, the elastic shell is not perfect since some elements are on the free cross bore surface and are not restricted to the same boundary conditions as those in the plain cylinder case. The yielding of an element on the cross bore surface weakens this particular point causing a redistribution in the local structural stiffness. The resultant local displacements and stresses are therefore not as predictable as those in a plain cylinder.

The overstrain pressure to achieve the 0.3% overstrain for various combinations of cylinder thickness ratio and cross bore to main bore radius ratio are shown in figure 4.43. In general, and for all cases considered, the higher cylinder thickness ratios have higher

overstrain pressures. For each thickness ratio, the maximum overstrain pressure is observed for the lowest cross bore to main bore radius ratios. As the cross bore to main bore radius ratio is increased from 0.005, the overstrain pressure drops with a sharp gradient, with the higher thickness ratio of 3 having the highest overstrain pressure gradient. This is followed by a gradual drop in the case of low thickness ratio or a slight increase followed by a gradual drop in the case of higher thickness ratios. The curves in this figure may be expected to be a function of the inverse of the stress concentration factor curves in figure 4.37 of the elastic analysis. The configuration with the highest stress concentration factor would be expected to have the lowest overstrain pressure. The local maximum and minimum observed in figure 4.37 are not reflected in figure 4.43 since the curves do not intersect. The curves in this figure tend to follow this expectation only for the cases where the cross bore to main bore radius ratio is greater than or equal to 0.2.

This behaviour could be attributed to the fact that whereas in the elastic analysis, the attention is only on the highest loaded element with all the elements having the same material properties, in the elastic-plastic case, the material properties are constantly changing as each element attains the yield conditions.

It is important to appreciate that for the higher thickness ratio cylinders, the stress gradients are different from those of a lower thickness ratio cylinder. Also, the 0.3% overstrain means a higher absolute dimension in the higher thickness ratio cylinders than in the lower thickness ratio cylinders.

The variation of the incipient yield pressure with respect to the cross bore to main bore radius ratio is shown in figure 4.44. Thickness ratios between 1.25 and 3 were considered. The incipient pressure patterns are very much like those of the figure 4.43 discussed above. However, the curves are smooth since only one element is loaded to the yield point during the incipient yield process and the structural stiffness adjustments associated with overstrain have not taken place.

To understand how the cylinder configuration responds to increasing overstrain pressure, the cylinder was subjected to varying overstrains between 7% and 83%. This was for a cross bore to main bore radius ratio of 0.1 and a cylinder thickness ratio of 2.25. The meridional overstrain hoop stresses are shown in figure 4.45. It is observed that for each overstrain, the maximum overstrain hoop stress occurs at the elastic-plastic interface and progressively decreases in magnitude and shifts away from the crotch corner in the radial direction as the overstrain is increased. The overstrain hoop stresses increase very rapidly along line HI. At the crotch corner, the overstrain hoop stress drops sharply and then rises along line IJ. The extent of this rise is governed by the elastic-plastic interface location. The observed reduction in the overstrain hoop stress is greatest for the highest overstrain of 83%. This reduction in overstrain hoop stress is due to the stress redistribution which arises from yielded elements having a lowered stiffness. Each of the curves shows a plateau once the maximum hoop stress is achieved and before the interface.

Figure 4.46 shows the meridional overstrain effective stress for a cylinder thickness ratio of 2.25 and a cross bore to main bore radius ratio of 0.1 for various overstrains. It is now clear from the curves how the elastic-plastic interface location shifts with increase of overstrain. For the case of 83% overstrain, all the nodes on the meridional line IJ have yielded. This through thickness yielding should always be avoided since then there is no elastic shell containment in the global coordinate system to hold the material from deforming to limits outside the cylinder outer shell. This situation could lead to gross deformation and rupture of the cylinder at the cylinder edge around point J. However, in the cross bore local coordinate system, the elastic containment may be considered to exist though it is not uniformly distributed about the full arc of the cross bore. This non-uniformity introduces further complexity in the overstrain stress system around the cross bore.

The variation of overstrain with overstrain pressure is shown in figure 4.47 for a cylinder thickness ratio of 2.25 and a cross bore to main bore radius ratio of 0.1. It is observed that for the 7%, 11% and 16% overstrains, the overstrain pressure is the same. This is due to the yield condition used, that elements with effective stress within 5% of the material

yield stress are considered to have yielded and the fact that around the crotch corner, the effective stress curves are very close. A more stringent yield condition would show a straight curve around these values of overstrain as shown when the yield condition is 0.5% instead of the 5% used in this work.

4.3.2.3 Residual stresses

The meridional residual hoop stresses are shown in figure 4.48 for varying overstrains. For nodes along line HI, the meridional residual hoop stress drops sharply, reaches a minimum value, and then rises asymptotically approaching zero along line IJ away from the crotch corner. The nominal minimum value increases with increase of overstrain. The 83% overstrain curve shows a minimum residual hoop stress of about -360 N/mm^2. After the drop in the meridional residual hoop stress, the point at which the curves attain a zero value is dependent on the overstrain, this point progressively moving away from the crotch corner as the overstrain is increased. Figure 4.49 shows the corresponding curves for the meridional effective residual stresses for varying overstrains. These curves are almost like a mirror image of the meridional residual hoop stresses about the line $y = 0$. The curves show a maximum meridional residual effective stress at a point away from and around the crotch corner. This maximum increases with an increase of ovestrain. The 83% overstrain curve has a maximum value of about 360 N/mm^2.

The higher the value of the meridional residual hoop stress, the better the cylinder is predisposed to accommodate further positive pressure loading in service. However, the residual stress system should not be such that reverse yielding of the elements takes place. This would induce cycling in service which can lead to early fatigue failure.

An interesting observation is the relationship between the minimum residual hoop stress and the cross bore to main bore radius ratio as shown in figure 4.50. For all cases of thickness ratio considered, the curve has no gradual variation but tends to have scattered and unpredictable points. However, as a group of curves, the general behaviour is predictable and the general variation may be approximated using a polynomial curve (of fifth order) as shown. It would be easy to imagine the superposition of the hoop stress

curve (in the negative sense) in figure 4.29 of the elastic analysis results when pressure equal to the overstrain pressure is applied to the elastic-plastic curve shown in figure 4.42. It is important to note that the maximum hoop stress for the elastic and elastic-plastic curves do not lie at the same point as the radius ratio is changed. The elastic-plastic interface shape and extent varies from one cross bore to main bore radius ratio to the other. This has the effect of changing the resultant superposed residual stress system in a rather unpredictable manner. The stress behaviour could be further confirmed by adopting a more stringent yield condition.

The variation of the minimum residual hoop stress for the varying overstrains is shown in figure 4.51. The curve shows an increase in the nominal value of the minimum meridional residual hoop stress with increasing overstrain. Different yield conditions are considered.

The method of overstrain carried out in this work is such that a cylinder with a plain cross bore is overstrained to the desired level. It is then offloaded with a negative pressure equal to the overstrain pressure. This means that the full effects of autofrettage are only felt by the elements around the cross bore. This process does not achieve the true benefits of autofrettage and is limited in order to avoid through thickness yielding of elements around the meridional curve IJ. For the whole cylinder to experience autofrettage, it would be necessary that a plain cylinder is first autofrettaged to the required overstrain. The cross bore should then be introduced. The resultant residual stress system around the cross bore would then be interesting to determine when compared to the results in this work.

4.3.2.4 Service stresses

In evaluating the autofrettage process, it is important to quantify and demonstrate the service stress levels and their distributions around the cross bore. For a plain cross-bored cylinder with a thickness ratio of 2.25 and a cross bore to main bore radius ratio of 0.1, the in-service meridional hoop stresses are shown in figure 4.52. The curves only represent a selected number of overstrains. For the 0% overstrain, the maximum hoop

stress occurs at point p away from the crotch corner as earlier discussed. It is observed that increasing the overstrain results in lower minimum service hoop stresses accompanied by a decreasing maximum hoop stress. As the overstrain is increased, point p does not become the point of minimum hoop stress. The point having a minimum hoop stress is located between point p and the crotch corner. Towards points J and H, the hoop stresses have the same value for all the overstrains. Between points I and p, the hoop stress has very high gradients. This is in contrast to the 0% overstrain case. The 37% overstrain case results in the minimum hoop stress and this has a negative value. Negative service hoop stresses have the advantage of stopping any crack like flaws especially near the crotch corner from propagating. It can be deduced from these curves that the cylinder can now accommodate much higher pressures before re-yielding can take place. This can be useful in preventing accidental over-pressure damage in case of short term over-pressure control failure and increases the safety factor. It should be noted that for the overstrain values which result in negative hoop stresses, this may lead to stress reversals in situations where the pressure rises above the required level. This results in accelerated fatigue failure. In terms of hoop stress, the new distribution is not as smooth as that of 0% overstrain.

Figure 4.53 shows the corresponding effective service stresses. It is observed that the point of minimum effective stress coincides with the point of minimum hoop stress. For overstrains greater than 16% the maximum effective stress occurs between points H and I. This also applies to the hoop stresses.

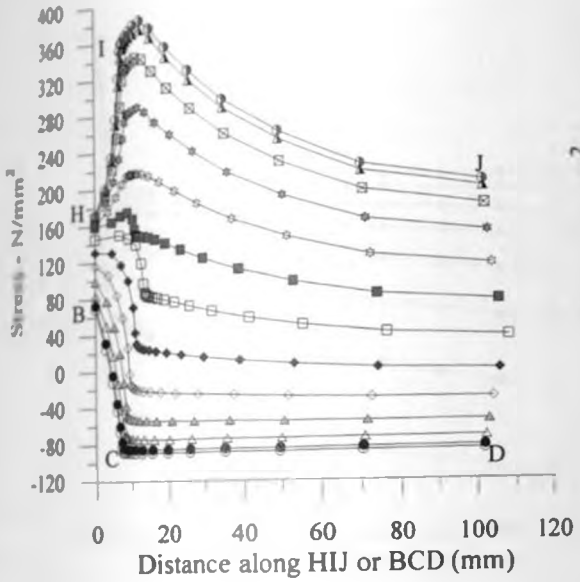

FIG. 4.40 Overstrain hoop stresses for 7% overstrain (k=2.25, d=0.1).

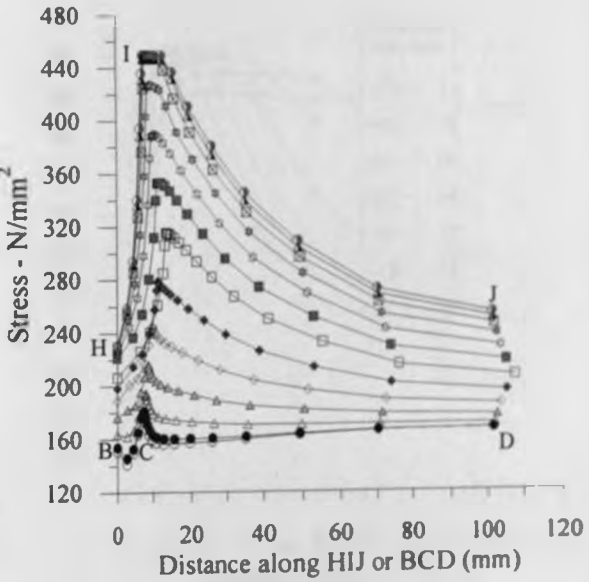

FIG. 4.41 Overstrain effective stresses for 7% overstrain (k=2.25, d=0.1).

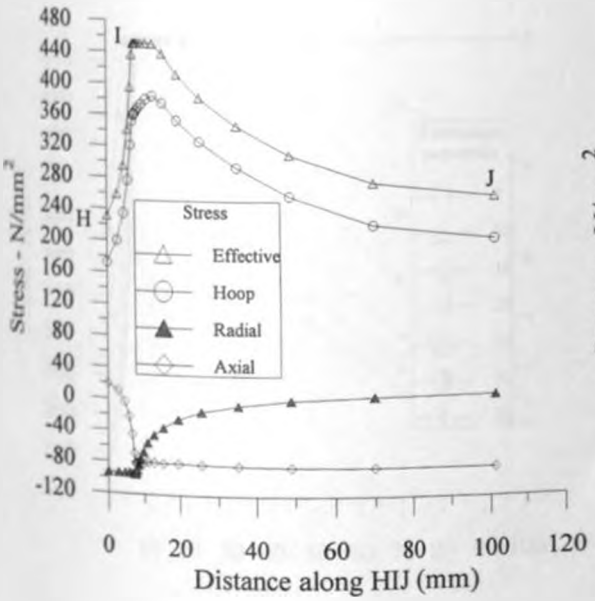

FIG. 4.42 Meridional overstrain stresses for 7% overstrain (k=2.25, d=0.1).

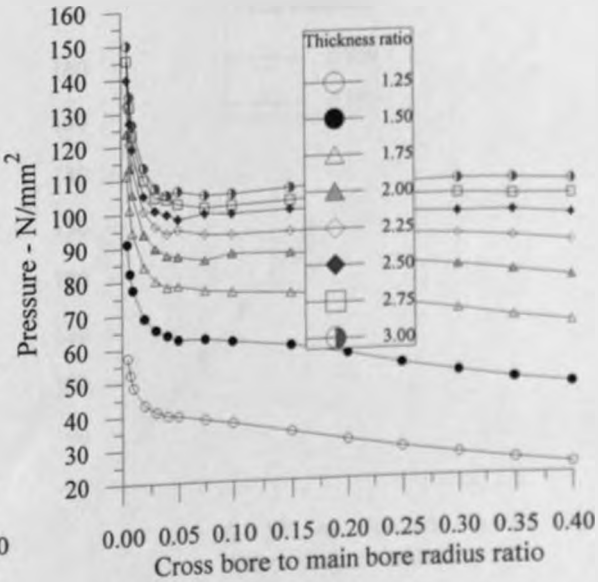

FIG. 4.43 Overstrain pressure vs. radius ratio for 0.3% overstrain.

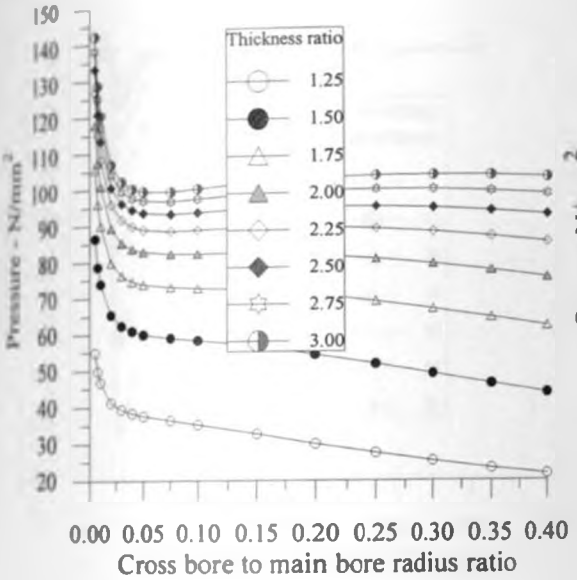

FIG. 4.44 Incipient pressure vs. d.

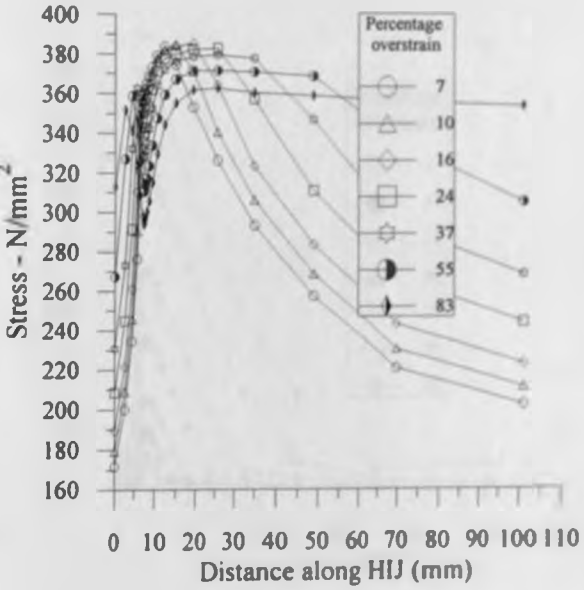

FIG. 4.45 Meridional overstrain hoop stresses for varying overstrains (k=2.25, d=0.1).

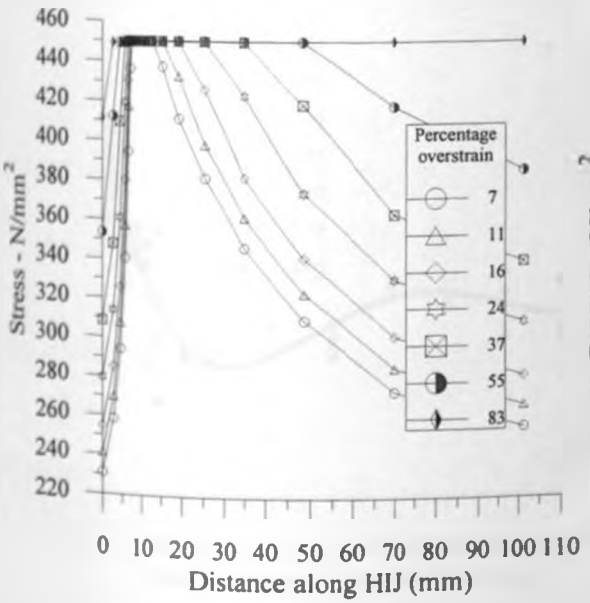

FIG. 4.46 Meridional effective overstrain stresses for varying overstrains (k=2.25, d=0.1).

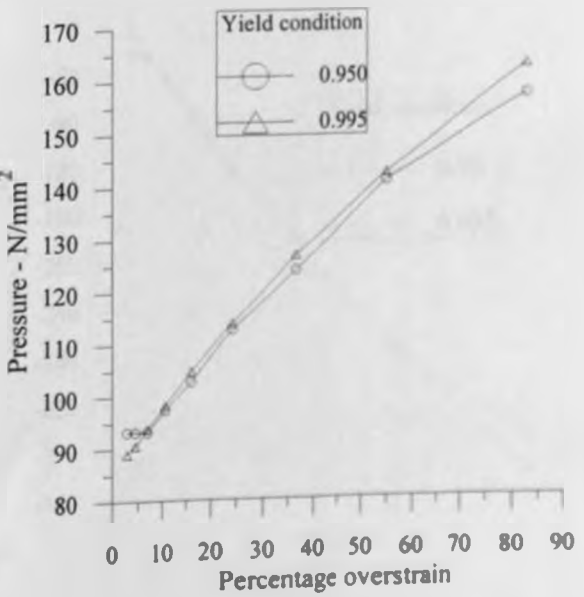

FIG. 4.47 Overstrain pressure vs. overstrain for two yield conditions.

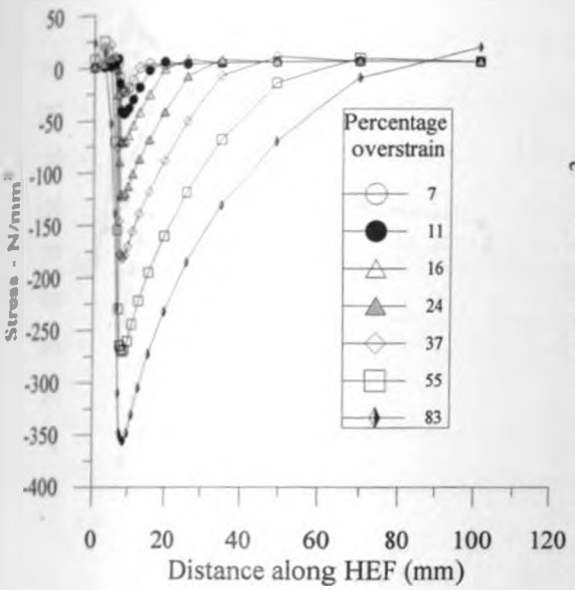

FIG. 4.48 Meridional residual hoop stress for varying overstrain (k=2.25, d=0.1).

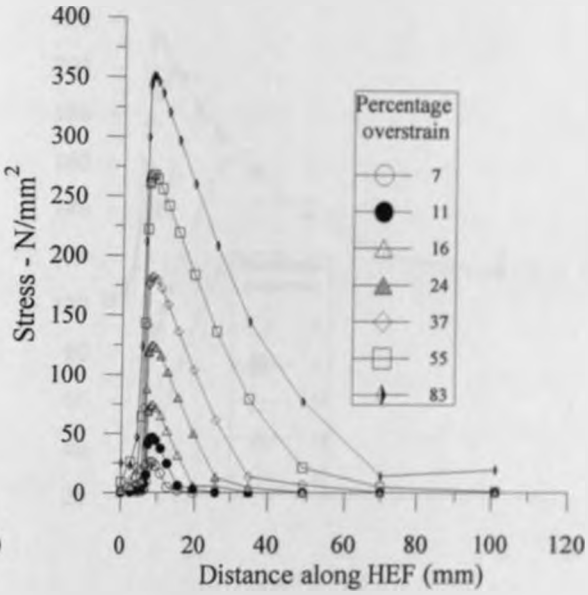

FIG. 4.49 Meridional residual effective stress for varying overstrain (k=2.25, d=0.1).

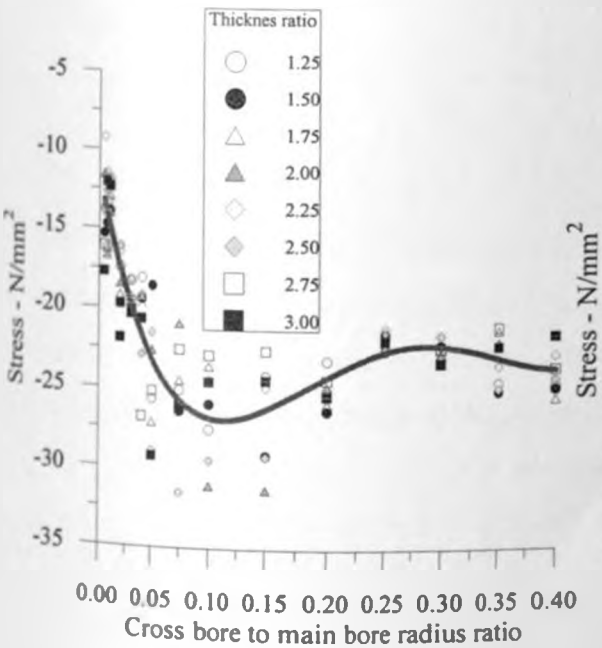

FIG. 4.50 Minimum residual hoop stresses for 7% overstrain.

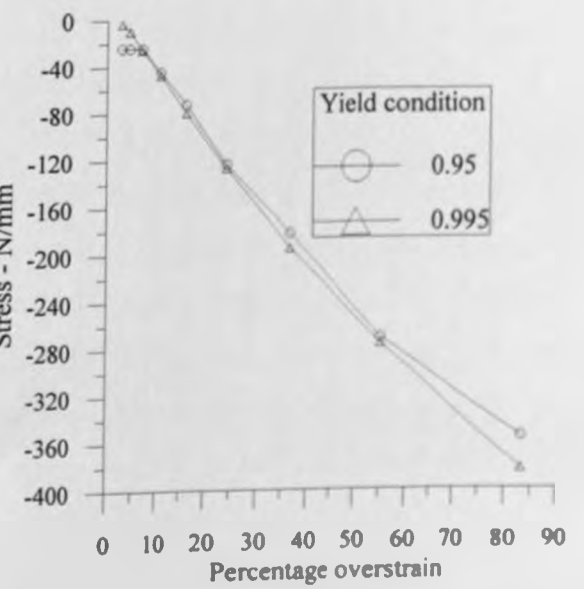

FIG. 4.51 Minimum residual hoop stress for two yield conditions.

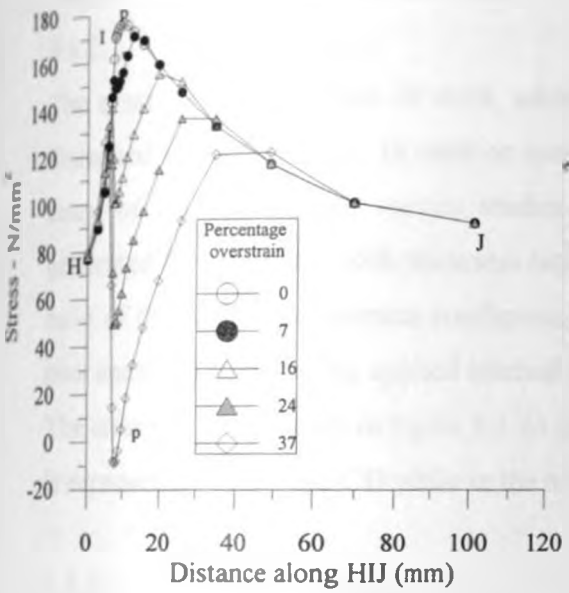

FIG. 4.52 Service hoop stresses for varying overstrain in plain cross bore (k=2.25, d=0.1).

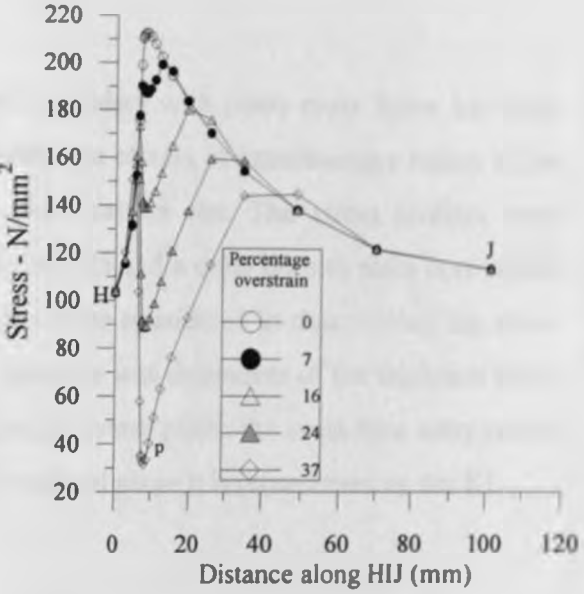

FIG. 4.53 Service effective stresses for varying overstrain in plain cross bore (k=2.25, d=0.1).

4.4 Radiused Entry Cross-Bored Cylinder

4.4.1 Elastic Stress Response

4.4.1.1 Introduction

The elastic stress response of thick walled cylinders with plain cross bores has been discussed in section 4.3.1. In order to quantify the effects of introducing a radius at the entry of the cross bore, various studies were carried out. The stress profiles were generated for a cylinder with thickness ratio of 2.25 and a cross bore to main bore radius ratio of 0.1. Other geometrical configurations were considered in determining the stress concentration factors. The applied internal pressure was dependent of the thickness ratio. The structure is as shown in figure 3.3. In the transverse plane, the cross bore entry radius is represented by the arc CD while in the meridional plane it is represented by arc KL.

4.4.1.2 Elastic stresses

Figure 4.54 shows the transverse plane elastic stresses when the cross bore entry radius ratio is 0.2 (20% of the main bore radius). In the far field at point A, the radial stress has a value of –40 N/mm^2. This steady value is maintained up to point B when the radial stress rises sharply to a value of –20 N/mm^2 at point C. Along the radius curve, the radial stress continues rising, reaches a value of about 10 N/mm^2 just before point D. Beyond point D, the radial stress quickly drops to negative values before approaching a positive value of about 5 N/mm^2 at point E. The behaviour of this stress curve is only similar to the radial stress curve for plain cross bore elastic analysis between points A and B.

The axial stress starts at point A having a value of about 10 N/mm^2. There is a small but gradual rise towards point B. The axial stress then sharply rises, reaching a maximum value of about 60 N/mm^2 just before point D. There is a further drop followed by a gradual rise, reaching a value of 45 N/mm^2 at point E. The hoop stress starts at point A having a value of about 56 N/mm^2. Towards point B there is a drop. Between points B and C, the hoop stress drops further, rises slightly and then drops again to reach a value of 8 N/mm^2 at point D. Between points D and E, the hoop stress is steady at about 5 N/mm^2.

These stress curves show that around the cross bore, the stress system has changed between the plain cross bore configuration and the radiused entry cross bore configuration. However, in the far field the stress response has not changed significantly.

Figure 4.55 shows the stress profiles along curve JKLM in the meridional plane. The hoop stress rises steadily, reaching a maximum value of 142 N/mm^2 at point s, just before point L. This is followed by an asymptotic drop to a value of 47 N/mm^2 at point M. The maximum hoop stress does not occur at points L or K. The axial stress rises to a maximum value just after point J and falls off very gradually approaching a stable value of zero towards point M. The maximum does not occur at points L or K. The radial stress rises from a negative value to a maximum of about 27 N/mm^2 at point L. This is followed by a gradual drop, approaching zero at point M.

From the above curves, it is clear that the sharp stress gradients which were evident in the case of the plain cross bore are now more smooth and the overall stress levels around the cross bore are lower. The stress patterns are also more complex, indicating that there are now additional factors which influence the stress response.

For a better understanding of the stress response around the cross bore, the hoop stresses for nodes parallel to and enclosed by the lines BCDE and JKLM are shown in figure 4.56. These curves are quite comparable to those of figure 4.35 in the elastic analysis of plain cross-bored cylinder. It may be noted that on the transverse plane and at this entry radius ratio of 0.2, the hoop stress is always positive, the hoop stress levels are lower and the range of stresses is smaller. Without extreme end stresses, it is easier to design and service a structure. It is also noted that the maximum hoop stress occurs adjacent to and below point L and not near point K.

Even though the introduction of a radius at the cross bore entry is seen to reduce the general stress levels, nevertheless, the geometry of the structure is more complex. A true and accurate entry radius is also not easy to accomplish. In most cases and for large pressure vessels, the entry radius is effected by means of grinding away material to

achieve a radius that can not be said to be true, accurate or even. The rough surface finish produced by the grinding operation acts as a source of minute stress concentrations. Experimental and numerical analysis results would then be at variance. By inspecting figure 3.3, there now exists three different local coordinate systems. One of these is the cross bore system defined by the edges DE and LM. The second one is the main bore system. The third one is the system defined by the edges CD and KL. The latter system is seen to be quite variable, more like a curvilinear system. The interaction of the stresses arising from the cross bore radiused entry with the other local coordinate system stresses is a complex one. Consider the arc LK in the meridional plane. Adjacent to point L, the local radial stress is the equivalent of radial stress in the main cross bore system and an axial stress in the global system. Adjacent to point K, the radial stress corresponds to the radial stress of the main bore. The effect of the presence of LM is to ensure smooth stress transition between the main bore and the cross bore. The introduction of the entry radius reduces the loaded areas in both the main bore and cross bore.

Considering the transverse plane curve ABCDE, between points C and D the normal force in the x-direction that tends to act against the positive hoop stress is lowered and hence the drop in the hoop stress is not like that observed in the plain cross bore elastic case. Since the cross bore area is reduced, the level of hoop stress between DE is also much higher.

In the meridional plane curve JKLM, there is lack of a clear geometrically singular point and hence the edge effects between the cross bore and the main bore are minimized as the entry radius increases. For this kind of configuration, the material removed is much more and this could be expected to weaken the structure. It is apparent that this disadvantage is overridden by the lack of sharp corners and the overall configuration is better disposed to carry the load with a better distribution of the stresses.

Figure 4.57 shows the corresponding effective stresses for the nodes discussed in figure 4.56. The stress patterns are very much like those of figure 4.36 in the elastic analysis of plain cross-bored elastic cylinder. In the present case, the effective stress levels are lower

and have a smaller dispersion. One conspicuous difference is that the effective stress for nodes close to line DE (within 9^0 in the x-z plane) have values very close to the values at point M. This arises from the overall stress response for this configuration where the stress levels around the cross bore are more positive. This means that in the design of the structure, equal care must be given to point E just as point M. This is unlike in the plain cross bore case where the effective stress margin is quite large.

To understand and be able to quantify the effects of the cross bore entry radius, several entry radius ratio values were considered and the results are shown in figure 4.58. These values were between 0.01 and 0.4. The meridional hoop stresses for a cylinder with a thickness ratio of 2.25 and a cross bore to main bore radius ratio of 0.1 are shown. From the points of maximum hoop stress, it can be seen that for the small entry radius ratio of 0.01, the maximum hoop stress occurs adjacent to point L on the side of point M. Increasing this entry radius ratio has the effect of shifting this point towards point K. This is however very gradual. It is also notable that the maximum hoop stress for each entry radius ratio reduces with this radius ratio. At the point of maximum hoop stress, the stress gradient reduces with increasing entry radius ratio, being fairly smooth for the largest entry radius ratio of 0.4. The stress patterns show a situation where two adjacent curves cross twice. This is a necessity since the lower entry radius ratio curves have higher stress gradients between points J and K, have higher stress levels, have higher stress gradients in moving from points K to L and also have higher stress levels at point M. The only curve that deviates from this observation is the entry radius ratio of 0.01. This is due to the conditions of this structural configuration being close to those of the plain cross-bored cylinder with the onset of edge effects having a bigger influence on the stresses.

Using the cross bore entry radius ratio configuration of 0.2, several cross bore to main bore radius ratios were considered for a cylinder thickness ratio of 2.25. The resultant meridional hoop stresses are shown in figure 4.59. The range of values considered was between 0.005 and 0.4. In the cross bore away from point L, the hoop stress increases with increasing cross bore radius. The value and location of the maximum hoop stress also depends on the cross bore radius ratio.

In this analysis, the value of the cross bore entry radius ratio of 0.2 was chosen as an average or typical value. Using this value, only a reasonable amount of the cylinder material would be removed, thus minimizing the weakening effect on the overall structure. This value was also considered quite reasonable and producing average stresses as earlier discussed.

4.4.1.3 Stress concentration factors

The maximum hoop stresses in the study of the effects of entry radiused cross bores are best understood in terms of stress concentration factors. Figure 4.60 shows the variation of stress concentration factors with the entry radius ratio for various values of cross bore to main bore radius ratios. This is for a cylinder thickness ratio of 1.5. In general, the stress concentration factor decreases almost linearly as the entry radius ratio is increased. As the cross bore radius ratio is increased, the stress concentration factor increases. Figure 4.61 represents the same variation for a cylinder thickness ratio of 2.25. The curves in this case cross one another at an entry radius ratio of between 0.25 and 0.3. Beyond 0.3, the lower cross bore to main bore radius ratio curves have lower stress concentration factors. Before the 0.25 entry radius ratio, the lower cross bore to main bore radius ratio curves have a higher stress concentration factor.

The results from a similar analysis for a cylinder thickness ratio of 3 are shown in figure 4.62. The stress concentration factor again decreases with increasing cross bore entry radius ratio, with the lower cross bore radius ratio curves having a higher stress concentration factor gradient. The curves have a focal point beyond the entry radius ratio of 0.4 and therefore tend to converge. This convergence point could be extrapolated and has the following values: stress concentration factor of 1.75 at an entry radius ratio of 0.5.

Compare the cross bore to main bore radius ratios of 0.1 and 0.4 in figure 4.60. At all values of the entry radius ratio the stress concentration factor is lower for the case of 0.1. Since the thickness ratio is small, a large cross bore makes the cross bore area weaker and therefore higher stresses arise. A small cross bore results in lower stresses. This applies to all cases of entry radius ratio. In figure 4.62 where the thickness ratio is 3, a large cross

bore results in a more balanced and stiff structure than the smaller cross bore of ratio 0.1. The cylinder thickness ratio of 2.25 is then a transition configuration where the effect of the size of cross bore and entry radius changes rapidly and very sensitively.

For a cross bore entry radius ratio of 0.2, the stress concentration factors were obtained for various cylinder thickness ratios and cross bore to main bore radius ratios. The results are shown in figure 4.63. The lower thickness ratio curves show a higher stress concentration factor. The curves for thickness ratios of 2 to 3 have a maximum stress concentration factor of about 2.3 at the cross bore to main bore radius ratio of 0.075. This is followed by a gradual drop and a small rise for the lower thickness ratio cases. At the low values of cross bore to main bore radius ratio of 0.005, the curves tend to converge at a stress concentration factor value of 2.2. From the curves, it is seen that the small thickness ratio curve of 1.25 is very sensitive to changes in cross bore to main bore radius ratios and has a maximum stress concentration factor of 3.55. Comparing these results with those of figure 4.37 in the elastic response case, it is clear that in general the stress concentration factors have been reduced by the presence of the cross bore entry radius. However, in the case of the small cross bore to main bore radius ratio of 0.005, this reduction is not evident particularly for the small thickness ratios of 1.25 and 1.5. This could be attributed to the fact that in the already weak structure of low thickness ratios, introducing an entry radius further weakens the structure and results instead in higher stress concentration factors.

For the practical cases of cross bore to main bore radius ratios, the introduction of a cross bore entry radius is seen to reduce the stress concentration factor. For example, with a thickness ratio of 3 and a cross bore to main bore radius ratio of 0.1, the cross bore entry radius ratio of 0.2 reduces the stress concentration factor by 21%. Evaluation of other cross bore entry radius ratios could be studied for their advantages in distributing the stresses more evenly around the cross bore and reducing the stress concentration factors.

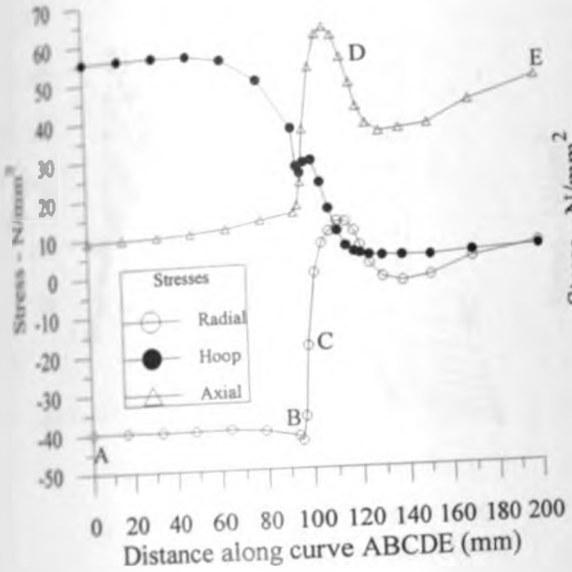

FIG. 4.54 Transverse stresses (k=2.25, d=0.1, rd=0.2).

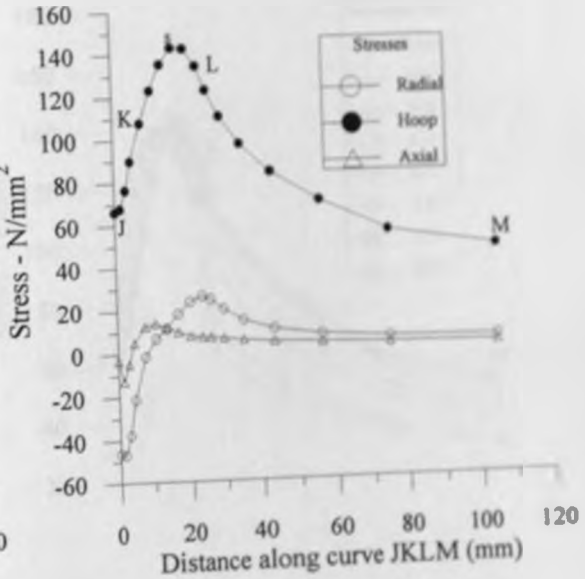

FIG. 4.55 Meridional stresses (k=2.25, d=0.1, rd=0.2).

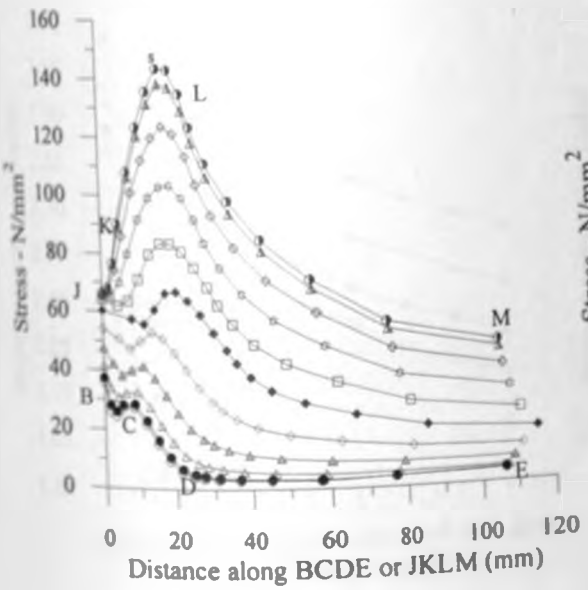

FIG. 4.56 Hoop stresses around cross bore (k=2.25, d=0.1, rd=0.2).

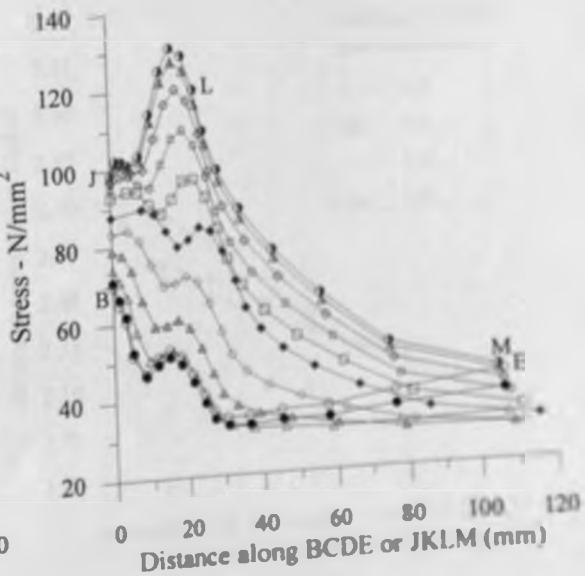

FIG. 4.57 Effective stresses around cross bore (k=2.25, d=0.1, rd=0.2).

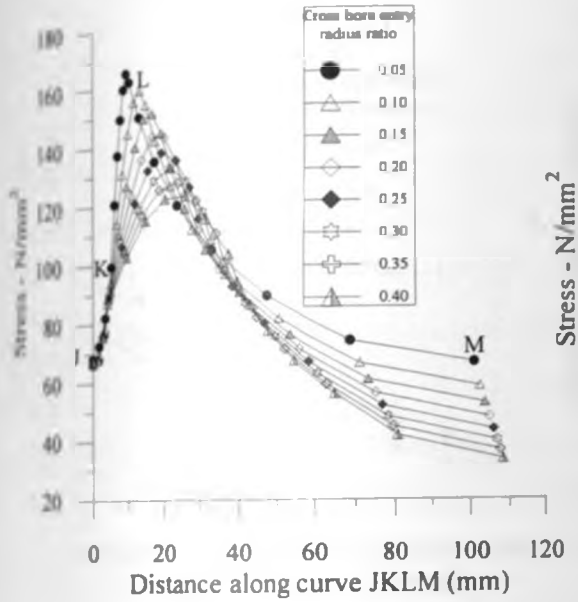

FIG. 4.58 Meridinal hoop stress for various cross bore entry radius ratios (k=2.25, d=0.1).

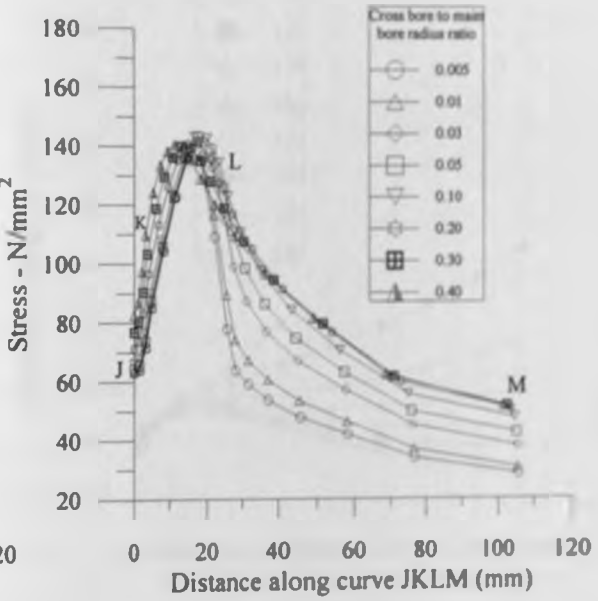

FIG. 4.59 Meridional hoop stress for various cross bore to main bore radius ratios (k=2.25, rd=0.2).

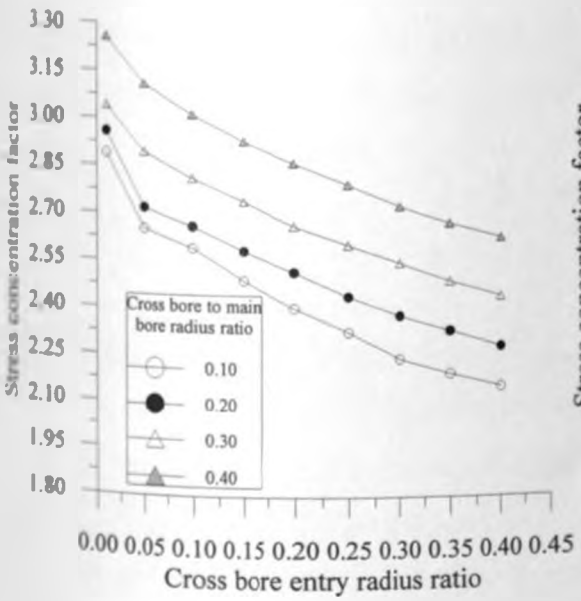

FIG. 4.60 SCF vs. cross bore entry radius ratio (k=1.50).

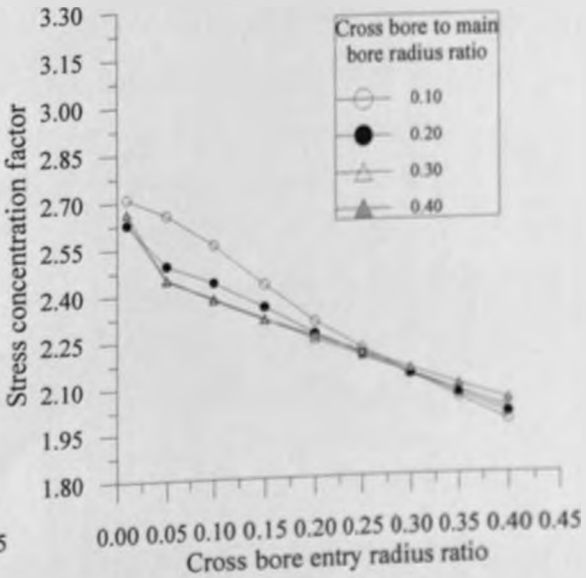

FIG. 4.61 SCF vs. cross bore entry radius ratio (k=2.25).

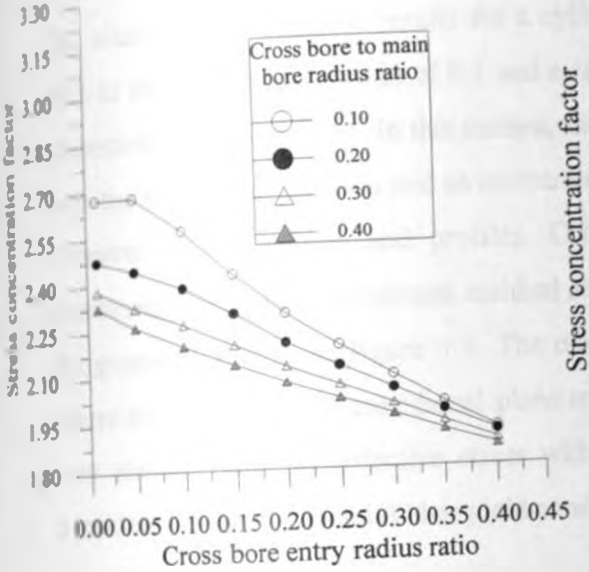

FIG. 4.62 SCF vs. cross bore entry radius ratio (k=3).

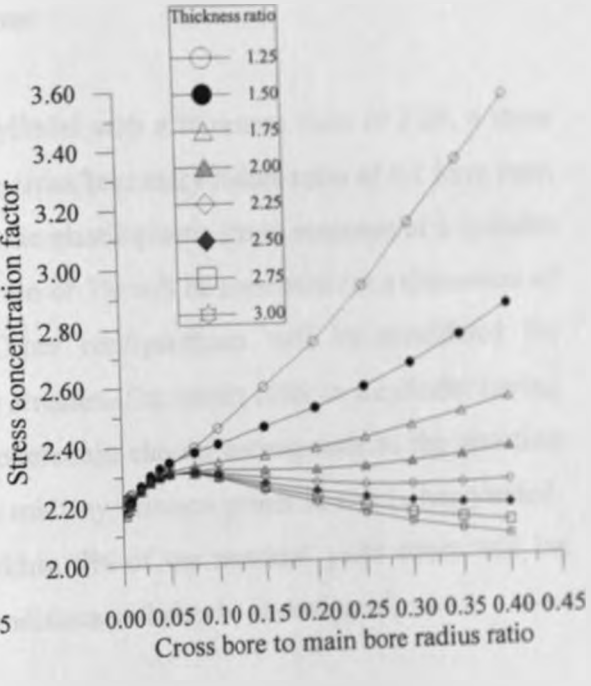

FIG. 4.63 SCF vs. cross bore to main bore radius ratio.

4.4.2 Elastic-Plastic Stress Response

4.4.2.1 Introduction

The elastic stress response results for a cylinder with a thickness ratio of 2.25, a cross bore to main bore radius ratio of 0.1 and a cross bore entry radius ratio of 0.2 have been presented in section 4.4.1. In this section, the elastic-plastic stress response of a cylinder with the same configuration and an overstrain of 3% will be presented for a discussion of overstrain stress values and profiles. Other configurations will be considered for overstrain pressure and minimum residual stresses. The results refer to a cylinder having the geometry shown in figure 3.3. The overstrain chosen corresponds to the situation where an element in the meridional plane midway between points K and L, has yielded. Any element with an effective stress within 5% of the material yield stress will be considered to have yielded. Other yield conditions will also be investigated.

4.4.2.2 Overstrain stresses

Figure 4.64 shows the meridional overstrain stresses for this structural configuration and an overstrain value of 3%. The 3% overstrain value was chosen since it coincided with a point away from the maximum hoop stress. The resulting overstrain stresses were therefore better displayed. The overstrain pressure was 118 N/mm^2 while the corresponding incipient yield pressure was 106 N/mm^2. The overstrain hoop stress has a value of 190 N/mm^2 at point J. This rises through point K to reach a maximum value of 380 N/mm^2 at point t. The overstrain hoop stress then drops asymptotically. Whereas the maximum overstrain hoop stress has now increased from the value of 142 N/mm^2 in the elastic analysis, the point of maximum hoop stress has shifted from point s to point t. The meridional overstrain radial stress starts at point J with a value of –125 N/mm^2 and smoothly increases in value to about –25 N/mm^2 at point L. After point L, a very small drop occurs and the values remain constant between point L and M. This point of maximum meridional overstrain radial stress coincides with that found in the elastic analysis but in this case the value is negative along line LM.

The meridional overstrain axial stress starts at point J with a value of 75 N/mm^2 and reduces to a value of about –90 N/mm^2 at point L. This value remains constant between

points L and M. In the elastic case, this stress is positive and only approaches zero towards point M. The meridional overstrain effective stress curve shows that around point L, a number of elements have already yielded, with more elements on the side of point s which showed a higher elastic hoop stress. At this overstrain value these same elements have a lower overstrain hoop stress, indicating that they yielded before the element at point L.

For the same overstrain and geometrical configuration, the overstrain hoop stresses for the nodes on the cross bore surface are shown in figure 4.65. These stresses correspond to the nodes parallel to and enclosed by the curves BCDE and JKLM. The hoop stress in this case along line DE is negative and has a value of about -85 N/mm^2. It is interesting to note from this figure that the curves are smoother than those found in the elastic analysis case and the range of stresses between points E and M or between points D and L is higher compared to the elastic case. The reduction of stress gradients is due to progressive reduction in hoop stress as overstrain is increased.

The corresponding overstrain effective stresses on the cross bore surface are shown in figure 4.66. From curve JKLM, only some of the elements between points K and I. have reached the yield stress level of 450 N/mm^2. However, other adjacent curves in the neighbourhood of line KL are very close to yielding at this overstrain. From this figure it is interesting to observe that towards points E and M, the effective stresses are higher for nodes closer to point E than those close to point M. Whereas this observation is unexpected, we may recall that the effective stress levels for the same nodes in the elastic analysis as shown in figure 4.57 are equally high. Progressive overstraining then results in point E becoming a critical point in the structure. It is then possible that with increased overstrain, the point E will yield before points K and C contrary to normal expectations. This observation is very new and needs verification. Classical designs never take note of this phenomenon. This observation led to further investigations of the overstrain effective stresses for different overstrains.

Figures 4.67 to 4.69 show meridional and transverse stress profile details for 15, 18 and 23% overstrains. As the overstrain is increased, the axial stress along line DE is seen to rise. This may be explained by the fact that the axial stress in the transverse plane is equivalent to hoop stress in the cross bore local coordinate system. At 15% overstrain, three nodes have already yielded along curve KL while the maximum effective stress along curve CD is about 400 N/mm^2. At 18% overstrain, five nodes have already yielded along curve KL while the level of the effective stress has increased along curve DE, having a value of 440 N/mm^2. At 23% overstrain, six nodes along curve KL have already yielded while all the nodes along curve DE have yielded. The results show that for higher overstrains, the entire transverse plane nodes yield before the meridional plane nodes. This observation was unexpected. To establish if this stress response is valid for or even forms a fair representaton of the entire range of entry radiused cross bores, other configurations were investigated. The results are shown in figures 4.70 and 4.71. The effective stress patterns are similar to those observed in figures 4.66 to 4.69 and they tend to confirm the weakness of the transverse plane under the configurations being discussed here. Further discussion about figures 4.70 and 4.71 is therefore not warranted.

Figure 4.72 shows the results of meridional overstrain hoop stresses for varying overstrain. The overstrains considered were between 2% and 42%. In the case of a radiused entry cross bore, a higher overstrain may not correspond to higher overstrain stresses. This is due to the position of the point of maximum hoop stress being located away from point K, which is the reference point for determining the overstrain. Away from the point of maximum stress which is around point L, the stresses decrease with increasing overstrain up to 6% overstrain. Further increase of overstrain results in higher stresses. The maximum hoop stress increases with increased overstrain up to 6% overstrain and then falls with further increase in overstrain. In the former case, an increase in overstrain means less overstrain pressure which leads to lower stresses. In the latter case, an increase of overstrain means more pressure which results in increased stresses.

Figure 4.73 shows the corresponding meridional effective stress for varying overstrains. The behaviour of the curves is very similar to that discussed in figure 4.72. The large plateau at effective stress of 450 N/mm^2 is as a result of the distribution of the highest stressed elements as the overstrain is increased progressively. The size of plateau decreases and then increases as the overstrain is increased up to 6% followed by a further increase to 42%.

Before the overstraining process was carried out, the incipient yield pressures were observed for various thickness ratios between 1.25 and 3 and also for various cross bore to main bore radius ratios between 0.005 and 0.4. The results are shown in figure 4.74. For thickness ratios between 1.25 and 2.25, the incipient yield pressure decreases with an increase of the cross bore to main bore radius ratio. The curves are very distinct and smooth. The increase in the incipient yield pressure with increase of thickness ratio is not linear and therefore the curves tend to be closer at the higher thickness ratio values. For these curves, the incipient yield pressure increases with an increase of the thickness ratio. For the thickness ratio curves of 2.5 and 3, the above relationship holds up to a cross bore to main bore radius ratio of 0.075. Beyond this point, the following is observed: The 2.5 thickness ratio curve intersects the 2.75 thickness ratio curve at a point with a cross bore to main bore radius ratio of 0.3; the 2.75 thickness ratio curve intersects the 2.5 thickness ratio curve at a point with a cross bore to main bore radius ratio of about 0.15 and also intersects the 2.0 thickness ratio curve at a point with a cross bore to main bore radius ratio of about 0.25; the 3.0 thickness ratio curve intersects the 2.75 thickness ratio curve at a point with a cross bore to main bore radius ratio of about 0.075, the 2.5 thickness ratio curve at a point with a cross bore to main bore radius ratio of about 0.1 and the 2.25 thickness ratio curve at a point with a cross bore to main bore radius ratio of about 0.2. This behaviour needs some explanation. To understand this behaviour, it is important to remember that the incipient yield pressure is the internal pressure required to bring the element with the highest effective stress to yield point. As the thickness ratio increases, the incipient yield pressure increases, showing that the structure is more resistant and therefore this corresponds to lower stress concentration factors. This may be confirmed from figure 4.63 of the elastic analysis.

Consider the curve representing a thickness ratio of 2.25 and a cross bore to main bore radius ratio of 0.3 in figure 4.63 of the elastic analysis. A careful observation shows that the stress concentration factor has started to increase, signifying a weakening of the structure.

Figure 4.75 shows the variation of the overstrain pressure with cross bore to main bore radius ratio for varying thickness ratios when the overstrain is 3% and the cross bore entry radius ratio is 0.2. For any thickness ratio, the tendency is for the overstrain pressure to decrease with increasing cross bore to main bore radius ratio. It is noted that the curves are not smooth. This could be attributed to the fact that at this overstrain, a number of elements have yielded and the structural response around the cross bore is not expected to be linear since there is a combination of elastic and plastic elements around this area.

For a thickness ratio of 2.25, cross bore to main bore radius ratio of 0.1 and a cross bore entry radius ratio of 0.2, the results of the variation of the overstrain pressure with overstrain are shown in figure 4.76. The results obtained by using the yield conditions of 0.95 and 0.995 are shown. The overstrain pressure is seen to drop as the overstrain is increased. This is followed by a point of minimum overstrain pressure at an overstrain of 8% and a further rise in the overstrain pressure. This behaviour is expected since an overstrain corresponding to elements about the point L would require the minimum overstrain pressure. By using the more stringent yield condition of 0.995, the maximum percentage error in the overstrain pressure is about 4.46% at the 8% overstrain. Even though giving more accurate results, this criterion is very expensive in that a lot more time is needed to achieve a given overstrain than when the 0.95 yield condition is used. At an overstrain of 3%, the time required for 0.95 yield condition is 29 minutes while that required for 0.995 yield condition is 124 minutes showing a time factor of 4.27. For greater overstrains beyond 18%, this factor increases exponentially and this method becomes very uneconomical compared to the gains in accuracy.

4.4.2.3 Residual stresses

After carrying out the overstrain analysis, the residual stress response of the structure was studied and the results for meridional stresses are shown in figure 4.77. The residual stresses are virtually zero except for the nodes between points K and L. The residual hoop stress curve has a maximum value of about -44 N/mm^2 at point s. Point s clearly does not coincide with the point L and also does not coincide with the point of maximum overstrain hoop stress, point t. This point is also the point of maximum residual effective stress.

The meridional residual hoop stresses for varying overstrains were also studied. The overstrains ranged from 2% to 42% and the results of the stresses are shown in figure 4.78. The nominal maximum residual hoop stress reduces with increasing overstrain up to 6% overstrain and then increases for increasing overstrain. The corresponding residual effective stress curves are shown in figure 4.79 and have patterns similar to those in figure 4.78. The behaviour of these curves is explained in the discussion for figure 4.76.

For various thickness ratios, cross bore to main bore radius ratios and a cross bore entry radius ratio of 0.2, figure 4.80 shows the minimum residual hoop stresses for 3% overstrain. This pattern indicates that for a particular thickness ratio, the curve is not smooth. Also, as discussed above for figure 4.77, the location of maximum overstrain hoop stress does not always coincide with the location of minimum residual hoop stress. Since these positions change from one cross bore to main bore radius ratio to another, then the value of the minimum residual hoop stress changes randomly.

However, as a group of curves, there is a general tendency which is represented by a polynomial curve (of fifth order). Figure 4.81 represents the variation of the minimum residual hoop stress with the increasing overstrain. The behaviour of this curve is as discussed above for figure 4.76.

In elastic-plastic cases, the hoop stress and effective stress are equally important. Whereas a point may not have yielded, a high hoop stress level may make this point just

as critical as another point which has yielded due to the possibility of material separation. The location of high hoop stress points on the outside of a thick walled cylinder for an elastic-plastic case is undesirable since the elastic shell containment is absent. Equally undesirable are high axial stress levels in the vicinity of the transverse plane. Other methods such as reinforcement may have to be used to keep the hoop stress levels below what may be considered unacceptable.

4.4.2.4 Service stresses

In order to quantify the advantages or effects of autofrettaging on the service structural response of a thick walled cylinder with a radiused entry cross bore, a selected set of overstrains was considered. Figure 4.82 shows the variation of service hoop stresses for varying overstrains. It is observed that apart from the nodes near point M, the service hoop stress levels are lower than the levels that would exist if autofrettage were not carried out. In the radiused entry region, the hoop stress levels are much lower except for the 6% overstrain whose pattern is easy to understand by referring to the residual hoop stress curves discussed earlier. It is observed that for the highest overstrain value of 42%, the hoop stress at point s has the lowest value and in fact this value is negative. As discussed elsewhere, negative service hoop stresses are advantageous especially in areas that may have small cracks. The propagation of such cracks tends to be arrested. From this figure and for this configuration, overstrains greater than 6% may be used to good advantage.

Figure 4.83 shows the corresponding effective stresses. It is observed that nodes near point M have much higher effective stresses in the case of autofrettage. However, this value tends to be constant for all overstrains and is well below the material yield stress. Around the radiused entry, overstrains greater than 23% show very favourable effective stress levels. It may be concluded that for this configuration, it is necessary to use high overstrains as long as gross deformation and reverse yielding do not take place. Gross deformation may lead to rupture of the cylinder wall. Reverse yielding results in plastic strain accumulation leading to incremental collapse.

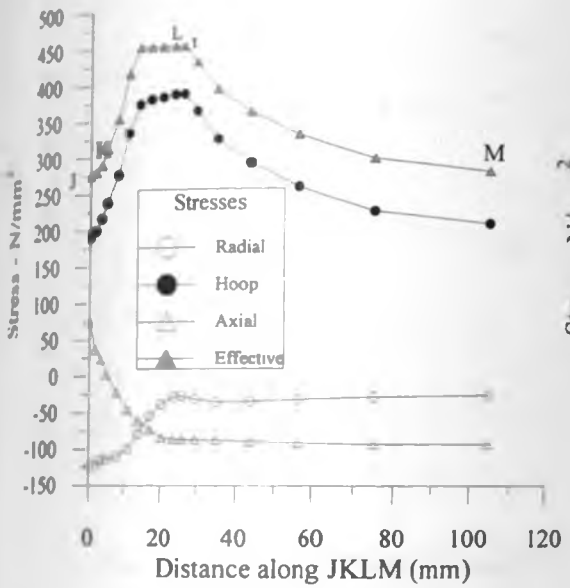

FIG. 4.64 Meridional overstrain hoop stresses at 3% overstrain (k=2.25, d=0.1, rd=0.2).

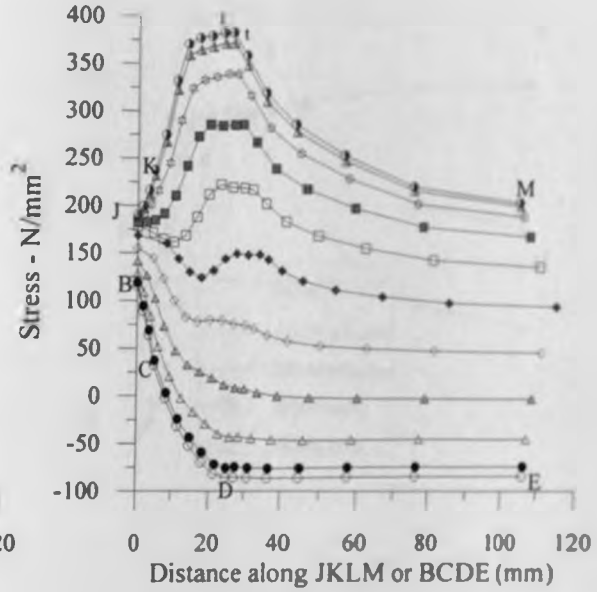

FIG. 4.65 Overstrain hoop stresses at 3% overstrain around cross bore (k=2.25, d=0.1, rd=0.2).

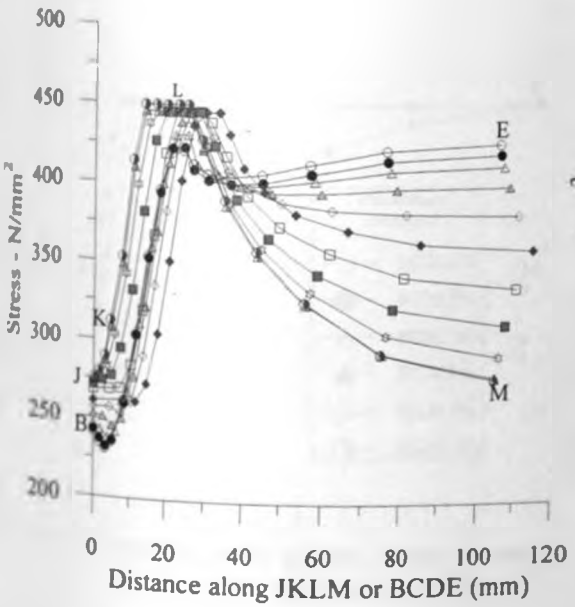

FIG. 4.66 Overstrain effective stresses aound cross bore for 3% overstrain (k=2.25, d=0.1, rd=0.2).

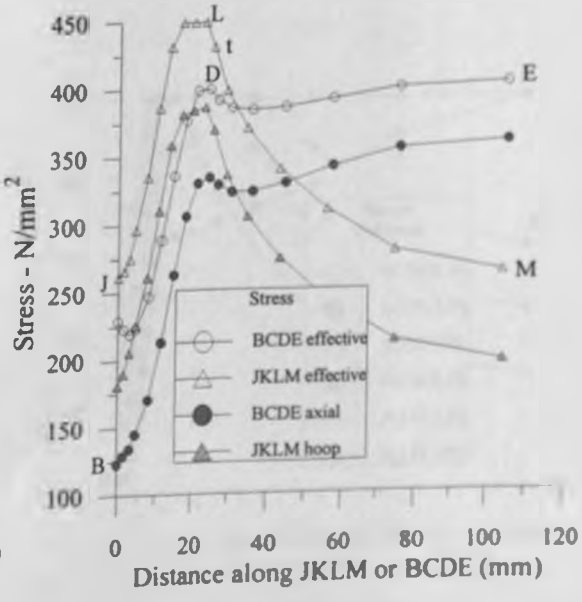

FIG. 4.67 Overstrain stresses around cross bore for 15% overstrain (k=2.25, d=0.1, rd=0.2).

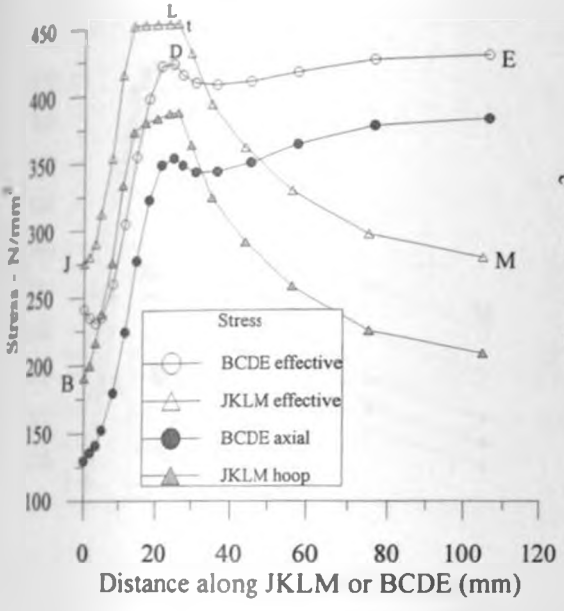

FIG. 4.68 Overstrain stresses around cross bore for 18% overstrain (k=2.25, d=0.1, rd=0.2).

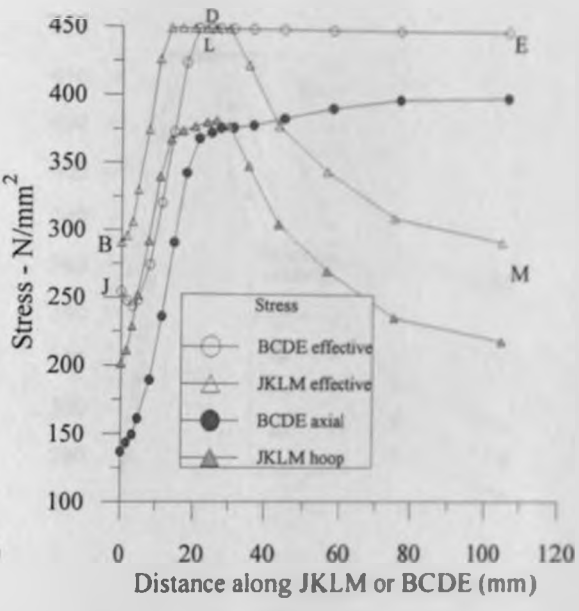

FIG. 4.69 Overstrain stresses around cross bore for 23% overstrain (k=2.25, d=0.1, rd=0.2).

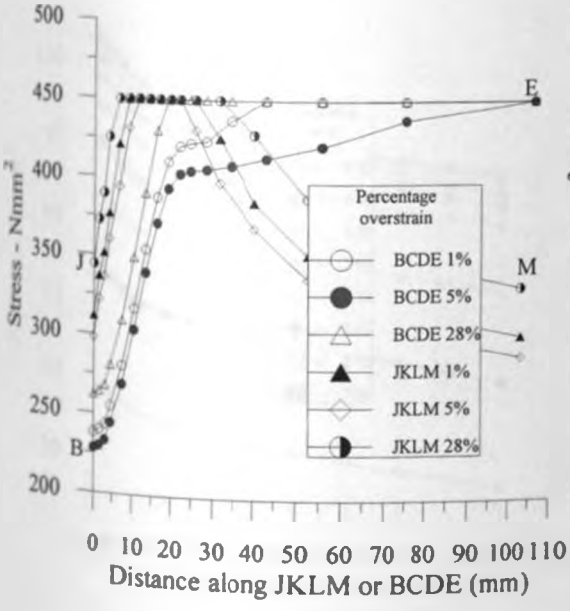

FIG. 4.70 Overstrain effective stresses around cross bore for varying overstrains (k=2.25, d=0.25, rd=0.2).

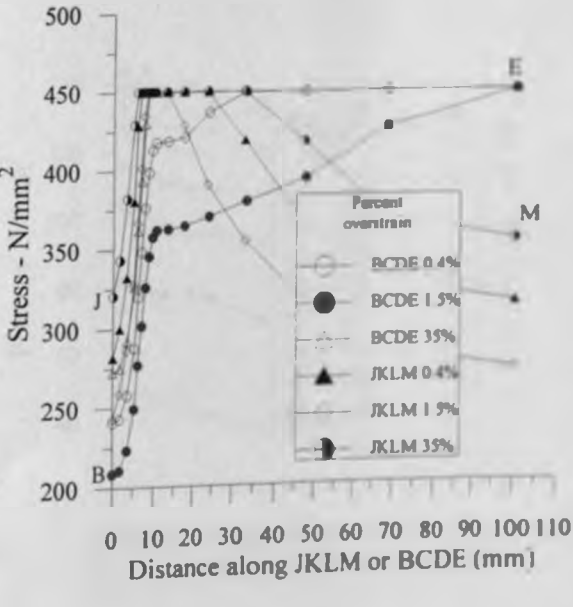

FIG. 4.71 Overstrain effective stresses around cross bore for varying overstrain (k=2.25, d=0.1, rd=0.05).

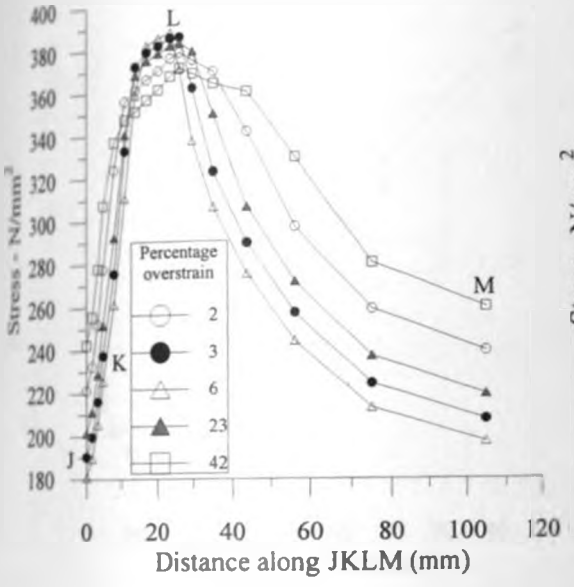

FIG. 4.72 Meridional overstrain hoop stresses for varying overstrains (k=2.25, d=0.1, rd=0.2).

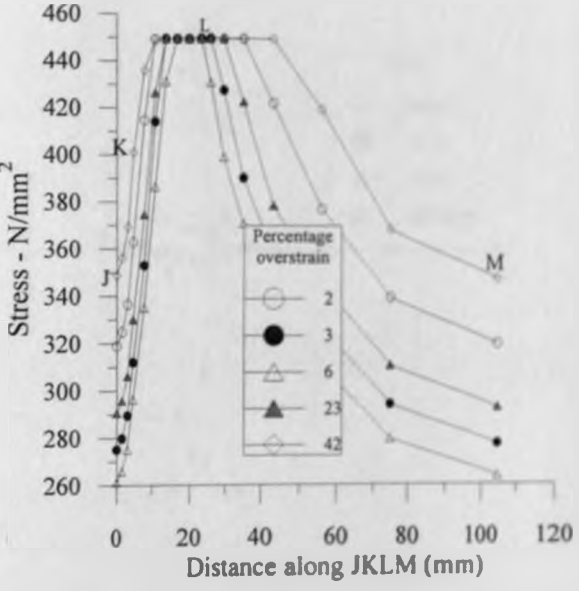

FIG. 4.73 Meridional overstrain effective stresses for varying overstrains (k=2.25, d=0.1, rd=0.2).

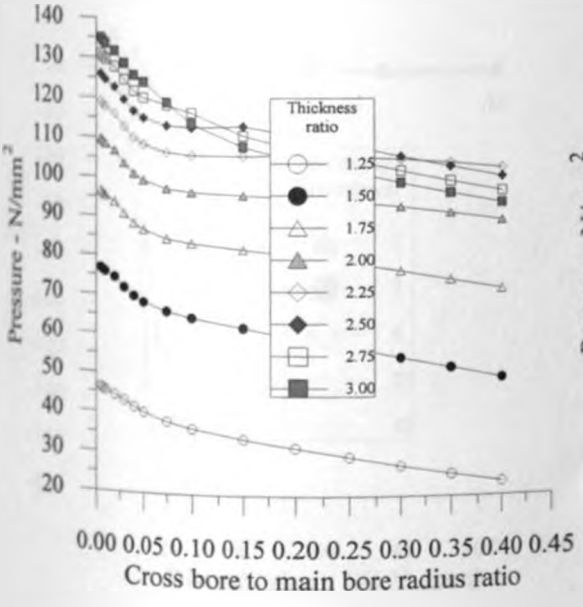

FIG. 4.74 Incipient yield pressure for 3% overstrain (rd=0.2).

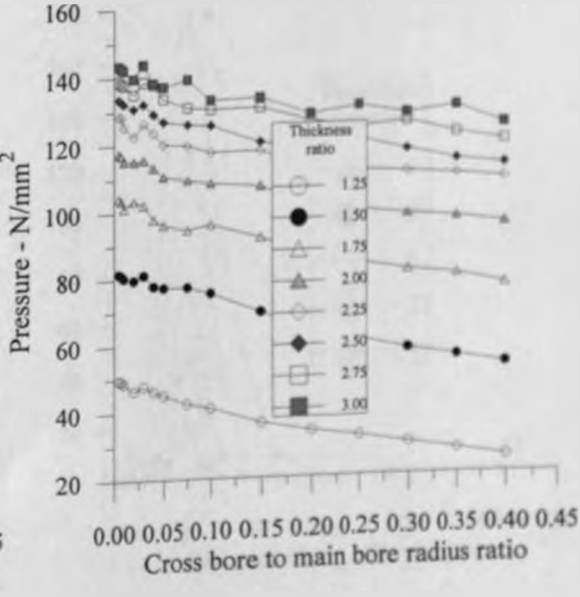

FIG. 4.75 Overstrain pressure for 3% overstrain (rd=0.2).

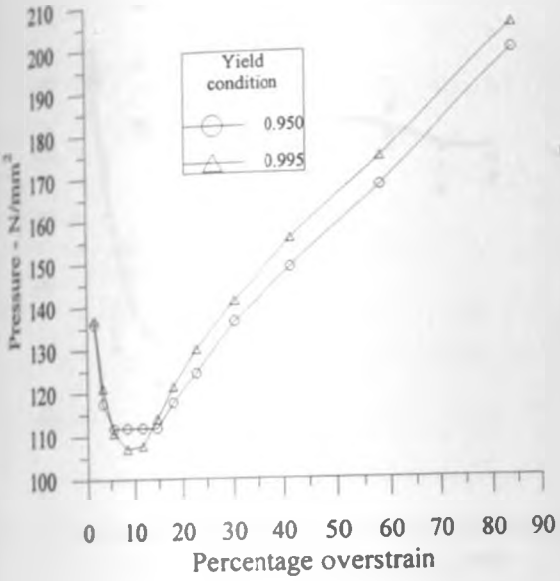

FIG. 4.76 Overstrain pressure vs. overstrain (k=2.25, d=0.1, rd=0.2).

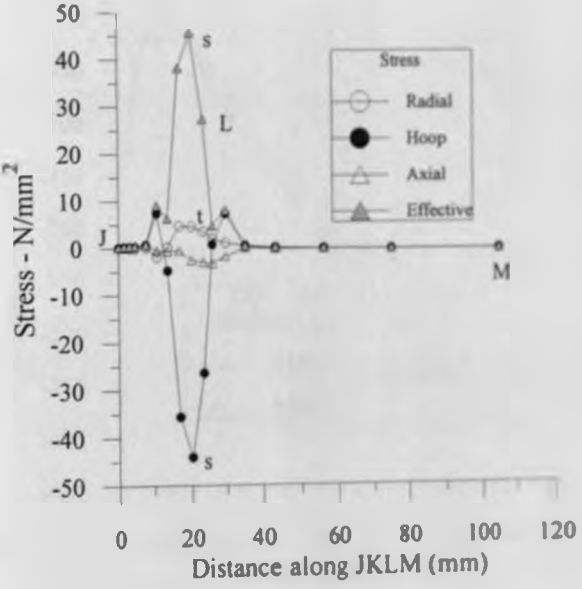

FIG. 4.77 Meridional residual stresses for 3% overstrain (k=2.25, d=0.1, rd=0.2).

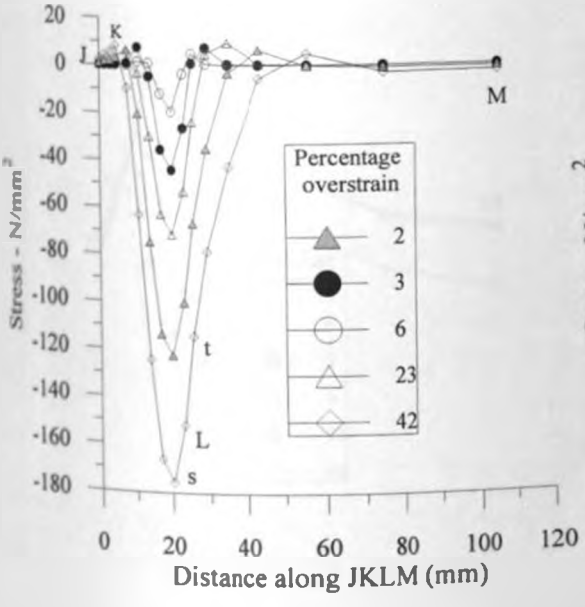

FIG. 4.78 Meridional residual hoop stress for varying overstrains (k=2.25, d=0.1, rd=0.2).

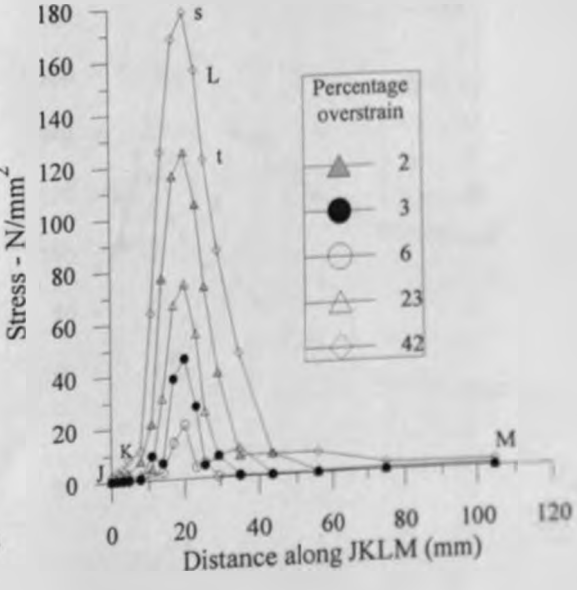

FIG. 4.79 Meridional residual effective stress for varying overstrain (k=2.25, d=0.1, rd=0.2).

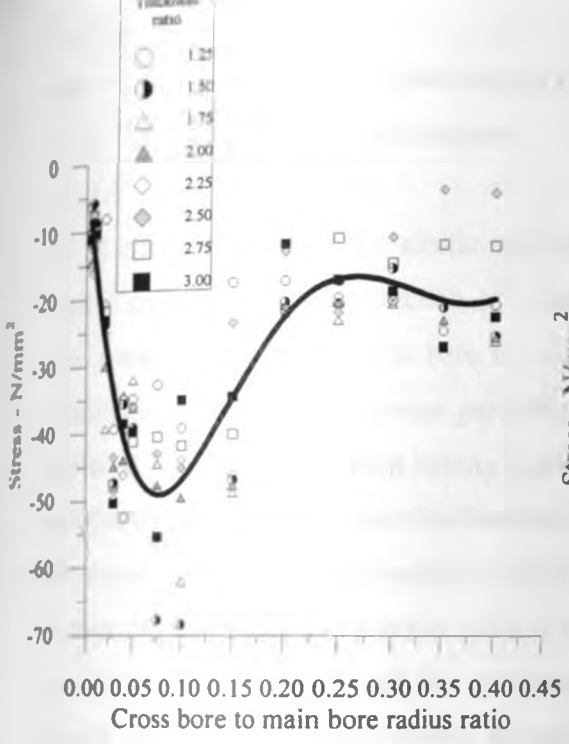

FIG. 4.80 Minimum residual hoop stress for 3% overstrain (rd=0.2).

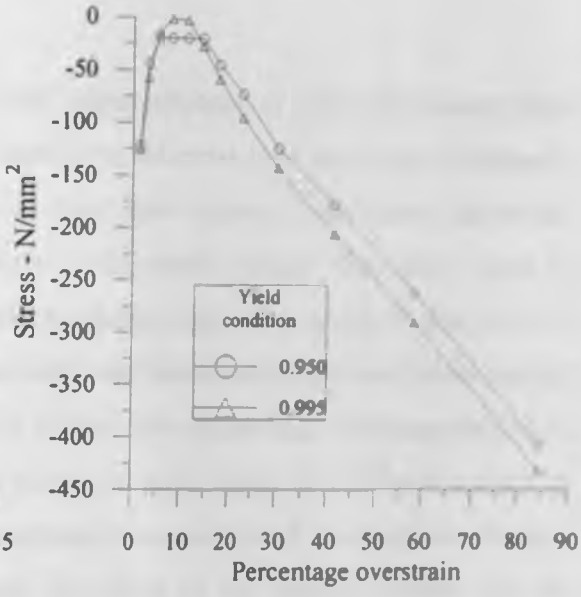

FIG. 4.81 Minimum residual hoop stress vs. overstrain (k=2.25, d=0.1, rd=0.2).

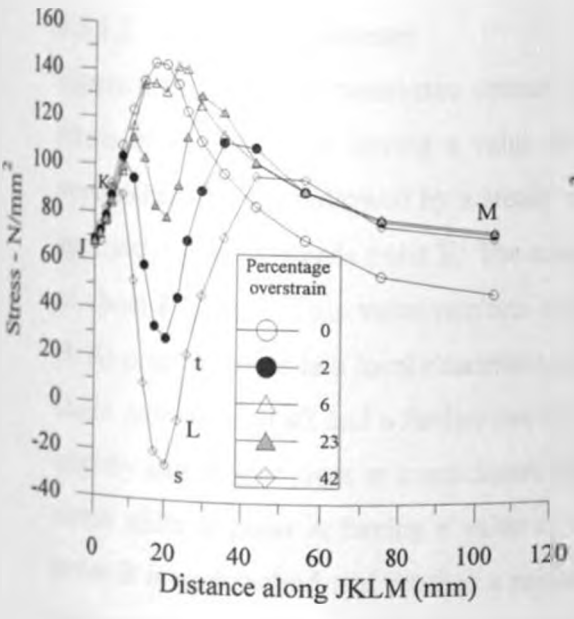

FIG. 4.82 Service hoop stresses for varying overstrain.

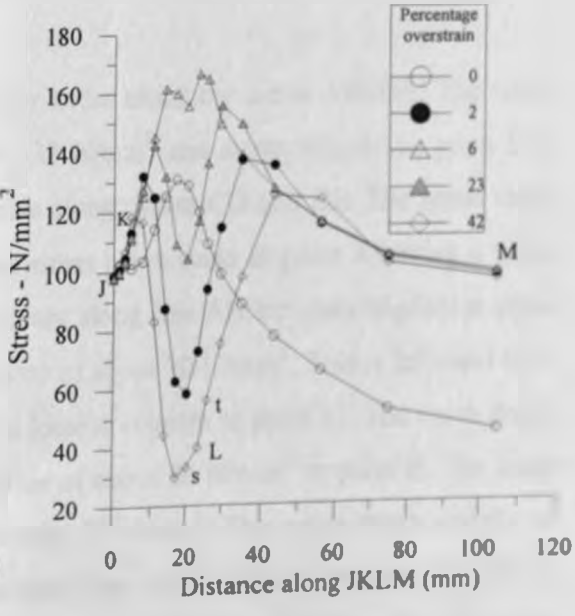

FIG. 4.83 Service effective stresses for varying overstrain.

4.5 Chamfered Cross-Bored Cylinder

4.5.1 Elastic Stress Response

4.5.1.1 Introduction

In an effort to improve the elastic structural stress response of plain cross-bored thick walled cylinders, the introduction of a chamfer at the cross bore entry was considered. The transition from the main bore to cross bore area improves smoothness due to the elimination of the sharp corner particularly at the crotch corner. The sharp corner is replaced by two corners each having greater included angles. It is expected that this will yield more favourable stress distributions and lower stress concentration factors around the cross bore area. In this analysis, a thick walled cylinder having a thickness ratio of 3, a cross bore to main bore radius ratio of 0.05, a chamfer angle of 11.5^0 and a chamfer length ratio of 0.25 (25% of the wall thickness) was considered. A moderate chamfer length ratio of 0.25 was chosen so that the effect of the chamfer length may be appreciated without removing too much cylinder material and thus weakening the structure particularly in the transverse plane. Other combinations of thickness ratio, cross bore to main bore radius ratio, chamfer length ratio and chamfer angle were also considered in the determination of stress concentration factors. The applied internal pressure was dependent of the thickness ratio. This structure is as shown in figure 3.4.

4.5.1.2 Elastic stresses

Figure 4.84 shows the transverse stresses for nodes along the curve ABCDE. The radial stress starts at point A having a value of –38 N/mm^2 and drops slightly as point B is approached. This is followed by a steady rise along curves CD and DE. The stress value approaches zero towards point E. The axial stress curve starts at point A having a value of about 8 N/mm^2. This value remains constant along line AB but rises slightly at point B. At point C, there is a local maximum value of about 30 N/mm^2. This is followed by a slight drop at point a2 and a further rise to a local maximum at point a1. The curve drops slightly and further rises to a maximum value of about 56 N/mm^2 at point E. The hoop stress starts at point A having a value of about 58 N/mm^2. The stress drops sharply as point B is approached and reaches a minimum value of –33 N/mm^2 at point a2. This is followed by a drop to an absolute minimum value of –27 N/mm^2 at point D. The stress

rises slightly and remains at a constant value of –33 N/mm^2 towards point E. For the hoop stress, D and a2 are singular points. For the axial stress, C and a1 are the critical points. It is also important to notice that along curve DE, the axial stress is of the same magnitude as the hoop stress along curve AB in the main bore.

To appreciate the importance of the interaction of the hoop, radial and axial stresses, it is important to discuss the corresponding effective stress profile along curve ABCDE. The effective stress has a maximum value of 87 N/mm^2 at point A. Points C and D are singular points showing stress discontinuities and having the same relative magnitude of effective stress. Point E is just as critical as point D in terms of yielding. The effective stress is lowest at a point located between points B and C. In terms of hoop stress, points A and E are the most critical considering material separation. Hence, in the transverse plane, point E needs special attention during both design and service.

Figure 4.85 shows the meridional plane stresses for nodes lying along curve JKLM. The radial stress starts at point J having a value of –43 N/mm^2, drops slightly and rises to reach a maximum value of 12 N/mm^2 at point v. There is a further slow drop with the value approaching zero at point M. The axial stress starts at point J having a value of zero. This curve drops to have minimum value of –37 N/mm^2 at point K. This is followed by a slight rise to a value of –18 N/mm^2. The curve then drops slightly, approaching a value of –28 N/mm^2 at point M. The hoop stress starts at point J having a value of 65 N/mm^2 and rises sharply to reach a maximum value of 143 N/mm^2 at point K. The stress then drops but rises again to have another maximum value of 143 N/mm^2 at point v. This is followed by a steady asymptotic decrease along line LM. For the chamfer angle of 11.5^0 chosen, the hoop stress curve has two points of maximum stress having equal values. These are points K and v.

Considering the effective stress along the same meridional curve, point K is seen to have the highest effective stress. Point v which also has a maximum hoop stress is a local maximum in terms of effective stress but the difference in the effective stress values for

the two points is very significant. Therefore point K at the crotch corner is a critical point in the meridional plane.

Figure 4.86 shows the elastic analysis results of hoop stress profiles for the cross bore surface nodes on moving from the curves BCDE to JKLM in the first quadrant. On moving from the transverse plane to meridional plane, the hoop stress levels are seen to increase for the successive layer of nodes. The locations of the local maxima and minima are also maintained for each successive layer. It is also important to note that a number of nodes parallel to and adjacent to line DE, within 30^0 in the x-z plane have negative hoop stress values. This observation may be compared to the radiused entry cross bore elastic analysis results where all the nodes have a positive hoop stress around the cross bore. However, the thickness ratio and cross bore to main bore radius ratio are different in the two cases. The reason for choosing the current configuration will be discussed elsewhere.

The cross bore surface nodes effective stresses are shown in figure 4.87. The effective stress patterns shown in figures 4.84 and 4.85 are also observed for the successive layers of nodes. Along the curve EM, the effective stress increases though the range of stress is not as large as that observed along curve DL or curve CK. This is quite in contrast to the behaviour of the stresses as discussed in figure 4.57 of the radiused entry cross bore where at points M and E, the effective stresses have almost the same value.

To determine the influence of the chamfer angle values on the elastic stress response of the structure, the chamfer angle for this cylinder configuration was varied between 0.5^0 and 60^0. The meridional hoop stresses starting from point s are shown in figures 4.88 to 4.91. Figure 4.88 shows the results for 0.5^0, 1^0, 5^0 and 10^0. While the maximum hoop stress at point K is seen to decrease with increasing chamfer angle, the shape of the hoop stress profiles changes dramatically, with the hoop stresses at points v and M rising. For this range of chamfer angle, point K remains a critical point while point v has a local maximum. Along line LM, the higher chamfer angle curves have higher hoop stress and the curves are fairly distinct. As the chamfer angle increases, the effect is that of a large

cross bore to main bore radius ratio at the entry thus giving a large stress concentration factor.

Figure 4.89 shows the hoop stress profiles for a chamfer angle varying between 11^0 and 20^0. The hoop stress at point K continues to decrease with increase of chamfer angle while the hoop stress at point v continues to increase. At the chamfer angle of 11.5^0, the hoop stresses at points K and v are equal. At a chamfer angle of 20^0, the hoop stress at point L is marginally higher than the hoop stress at point v. The hoop stresses along line LM are fairly uniform.

Figure 4.90 shows the hoop stress profiles when the chamfer angle varies between 25^0 and 40^0. From this figure, it is observed that the hoop stress at point L continues to rise while that at point K continues to decrease with increase of chamfer angle. Along curve LM, the stress curves have almost merged particularly close to point M. Figure 4.91 shows the hoop stress profiles when the chamfer angle varies between 45^0 and 60^0. The hoop stress at point L is the maximum with very high stress gradients on either side and the hoop stress value increases with increasing chamfer angle. Between points L and M, the stress curves are almost identical. The stress at point K continues to decrease with increase of chamfer angle and this point now seems to have little significance in terms of hoop stress. The hoop stress at point K and M have almost the same value and therefore K can not be said to be a critical stress point.

The observation that the maximum hoop stress has a minimum value for a certain chamfer angle, 11.5^0, from the above cylinder configuration analysis led to further investigations for selected cases of thickness ratios and cross bore to main bore radius ratios. The reason being to determine if this phenomenon is repeated for all cases. At chamfer angles greater than 11.5^0, the influence of the main bore hoop stress is larger at point L than the influence of the cross bore hoop stress is at point K. This analysis was done by determining the stress concentration factor variation with the chamfer angle for different chamfer length ratios.

4.5.1.3 Stress concentration factors

Figure 4.92 shows the variation of stress concentration factors with chamfer angle for chamfer length ratios varying from 0.2 to 0.9. Interesting observations are noted from these curves. All the curves cross at a point having a stress concentration factor of about 4.0 and a chamfer angle of 45^0. Beyond this chamfer angle, the stress concentration factor increases with increase of chamfer length ratio. When the chamfer angle is less than the 45^0, the stress concentration factor increases with a decrease of the chamfer length ratio.

Also to be observed is that all the curves have a maximum stress concentration factor value, the chamfer angle corresponding to which depends on the chamfer length ratio. This chamfer angle also increases with increase of the chamfer length ratio. None of the curves has a minimum value though the curves tend to approach a stress concentration value of 1.875 at the lowest chamfer angle of 1^0. This stress concentration factor value corresponds well to the stress concentration factor of 1.834 in the elastic analysis of a plain cross-bored cylinder. An important observation from the curves is that for all the chamfer length ratios considered, the stress concentration factor values are more than those obtained from the corresponding plain cross bore analysis. This shows that for the combination of the thickness ratio of 1.25 and a cross bore to main bore radius ratio of 0.005, the introduction of a chamfer does not reduce the stress concentration factor as would be expected. Extreme caution is therefore necessary in deciding whether to introduce chamfers as a means of establishing favourable stress distributions which should result in lower stress concentration factors.

As earlier discussed, the point of minimum meridional hoop stress corresponds to a shift in the position of maximum hoop stress. There is also a need to establish the mechanism behind the points showing a maximum stress concentration factor to determine if this also involves a shift in the location of maximum hoop stress. The results are shown in figures 4.93 to 4.95. Figure 4.93 shows the hoop stresses along line JKLM for the chamfer angles between 20^0 and 35^0 for a chamfer length ratio of 0.2. At the chamfer angle of 20^0, the maximum hoop stress occurs at point v. As the chamfer angle is increased, the maximum hoop stress value rises and this maximum value corresponds to point L at a chamfer angle

of 35^0 though the hoop stress value at point v is only slightly less. Figure 4.94 shows the same profiles for chamfer angles between 40^0 and 55^0. The maximum hoop stress values continues to increase with increase of chamfer angle. Point L is distinctly the point of maximum hoop stress. Figure 4.95 shows the hoop stresses when the chamfer angle varies between 60^0 and 80^0. The maximum hoop stress still occurs at point L for all the chamfer angles though this maximum decreases when the chamfer angle is more than 60^0. These figures show that the upper limits on the curves in figure 4.92 do not involve the shifting of the points of maximum hoop stress from K to L but rather as a realignment of the stresses as the cross bore geometry approaches that of a plain cross-bored cylinder.

The influence of the cross bore size and cylinder thickness ratio on the stress levels and stress concentration factors has been discussed in the elastic analysis of plain cross-bored cylinders. In the presence of a cross bore, we may consider that for this small thickness ratio (1.25) configuration, increasing the chamfer angle has the effect of increasing the cross bore loaded area and reducing the main bore loaded area. Since the chamfer length ratio is maintained constant, an increase in chamfer angle results in the resolved meridional forces producing an increased contribution towards the global hoop stress and contributing less to axial stress. This results in an increase of the maximum hoop stress. Further increase of the chamfer angle tends to make point L more singular, increase the cross bore area, reduce the main bore area and increase the contribution of the chamfered area hoop stress more to the global system. The combination of the above factors tends to increase the stress concentration factor to a maximum value at a certain point beyond which the net effect is to reduce the maximum hoop stress. Further increase of chamfer angle causes stress distributions with the point of maximum hoop stress shifting position. The above discussion holds for the chamfer length ratios shown in figure 4.92. For this configuration, the maximum chamfer angle that could be constructed was 75^0.

To establish if this detrimental effect of chamfers also applies for other cases of cylinder thickness ratios and cross bore to main bore radius ratios, other combinations were considered and the results are shown in figures 4.96 to 4.100. Figure 4.96 shows the stress concentration factor variation with chamfer angle profiles for a 1.25 thickness ratio

cylinder having a cross bore to main bore radius ratio of 0.1. Various chamfer length ratios were considered. The curves cross at a stress concentration factor of about 2.92 and a chamfer angle of 25^0. To the right of this common chamfer angle, the curves behave in a similar manner to those discussed in figure 4.92 except that the maximum stress concentration factor for all curves occurs at a chamfer angle of about 65^0. However, to the left of this angle, all the curves have an absolute minimum of stress concentration factor. These points of minimum stress concentration factor may be taken to be when the hoop stresses at points K and v are equal and occur at different chamfer angles for different chamfer length ratios. For the longest chamfer length with a chamfer length ratio of 0.9, this occurs at a chamfer angle of 10^0 while for the shortest chamfer with a chamfer length ratio of 0.2, it occurs at a chamfer angle of 5^0. From these curves, it is possible to place a horizontal line at a stress concentration factor value of that prevailing in the equivalent plain cross-bored cylinder. Above this line, the introduction of a chamfer is actually harmful to the structural integrity of the cylinder. Below this line, it is possible to select a combination of chamfer angle and chamfer length ratio which gives the lowest stress concentration factor and hence a favourable stress distribution, better than that prevailing in a plain cross-bored cylinder. In this case, a chamfer length ratio of 0.9 at a chamfer angle of 10^0 gives the best results of a stress concentration factor of about 2.52. The foregoing discussion applies to the curves shown in figures 4.97 to 4.100. For a thickness ratio of 2 and a cross bore to main bore radius ratio of 0.005, a chamfer length ratio of 0.9 and a chamfer angle of 20^0 gives a minimum stress concentration factor of about 2.1. For a thickness ratio of 2 and a cross bore to main bore radius ratio of 0.1, a chamfer length ratio of 0.9 and a chamfer angle of 15^0 gives a minimum stress concentration factor of about 2.36. For a thickness ratio of 3 and a cross bore to main bore radius ratio of 0.005, a chamfer length ratio of 0.7 and a chamfer angle of 20^0 gives a minimum stress concentration factor of about 1.8. For a thickness ratio of 3 and a cross bore to main bore radius ratio of 0.1, a chamfer length ratio of 0.7 and a chamfer angle of 15^0 gives a minimum stress concentration factor of about 2.1.

An overview of figure 4.92 and figures 4.96 to 4.100 shows that for a fixed thickness ratio cylinder, an increase in the cross bore to main bore radius ratio leads to chamfer

length ratio and chamfer angle combinations which offer better and wider options for selecting minimum stress concentration factors. Also, for a fixed cross bore to main bore radius ratio, an increase in the thickness ratio leads to more of the chamfer length ratio and chamfer angle combinations providing better selection options for minimum stress concentration factors, lower than that in a plain cross-bored cylinder.

For various cylinder thickness ratios and cross bore to main bore radius ratios, and using a chamfer length ratio of 0.25, various chamfer angles were iteratively tested to the nearest 0.5^{0} to determine which one resulted in a minimum stress concentration factor value. The results are shown in figure 4.101. As explained in the discussion on figure 4.92, not all combinations can yield a minimum stress concentration factor. The corresponding minimum stress concentration factors are shown in figure 4.102. For thickness ratios between 2.25 and 3.0, the curves do not cross and the minimum stress concentration factor increases with decrease in thickness ratio. This behaviour is similar to the one of plain cross bore to the right of the critical cross bore to main bore radius ratio of 0.2 and also to that of the radiused entry cross bore. However, for the thickness ratios of 1.25 to 2.0, the curves cross at a common point where the minimum stress concentration factor is 2.65 and the cross bore to main bore radius ratio is 0.075. This observation suggests that the cross bore to main bore radius ratio of 0.075 is a critical constant value for these thickness ratio curves. The behaviour of the curves to the left and right of this point is as discussed for the 1.75 to 3.0 thickness ratio plain cross-bored cylinders.

For chamfer length ratio and chamfer angle combinations where a minimum stress concentration factor could be obtained, then it is clear that this value is lower than that found in an equivalent plain cross-bored cylinder. For a 2.25 thickness ratio cylinder and varying cross bore to main bore radius ratio, figure 4.103 shows a stress concentration factor comparison between a plain cross-bored cylinder, a radiused entry cylinder with an entry radius ratio of 0.2 and a chamfered cross-bored cylinder with a chamfer length ratio of 0.25 and a chamfer angle giving the minimum stress concentration factor.

The radiused entry cross bore is seen to result in lower and better stress concentration factors than the plain cross bore except at the cross bore to main bore radius ratio of 0.005 as earlier discussed. Also, the radiused entry cross bore results in lower stress concentration factors than the chamfered cross bore for all cases of the cross bore to main bore radius ratio. The chamfered cross bore cylinder yields lower stress concentration factors than the plain cross bore where the cross bore to main bore radius ratio is 0.02 or larger. Below this value and for the chamfer angle and chamfer length ratio chosen, there is no absolute minimum of stress concentration factor. The foregoing discussions and comparisons of the various cross bore geometry are useful when designing and fabricating a cross-bored thick walled cylinder.

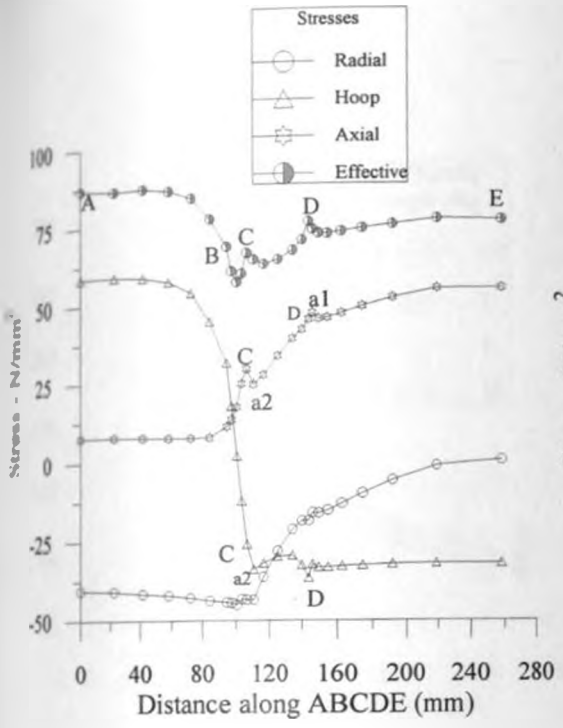

FIG. 4.84 Tranverse stresses (k=3.0, d=0.05, clr=0.25, ca=11.5^0).

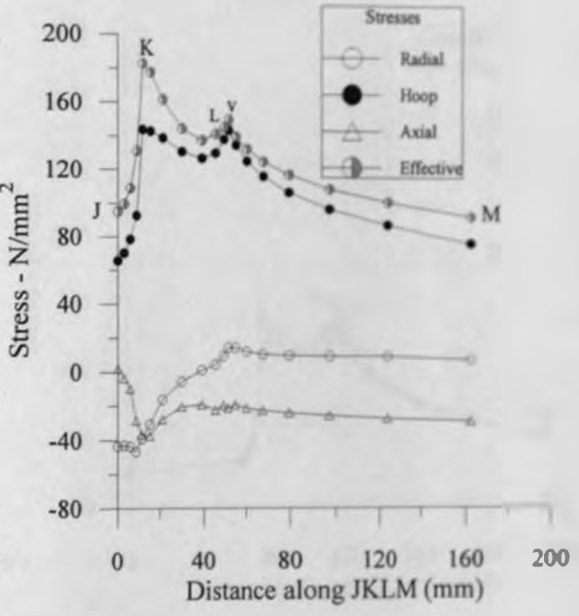

FIG. 4.85 Meridional stresses (k=3.0, d=0.05, clr=0.25, ca=11.5^0)

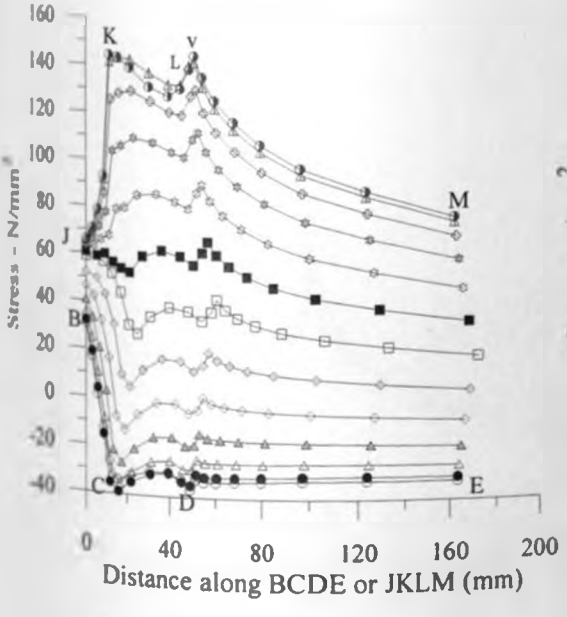

FIG. 4.86 Hoop stresses around cross bore (k=3, d=0.05, clr=0.25, ca=11.5^0)

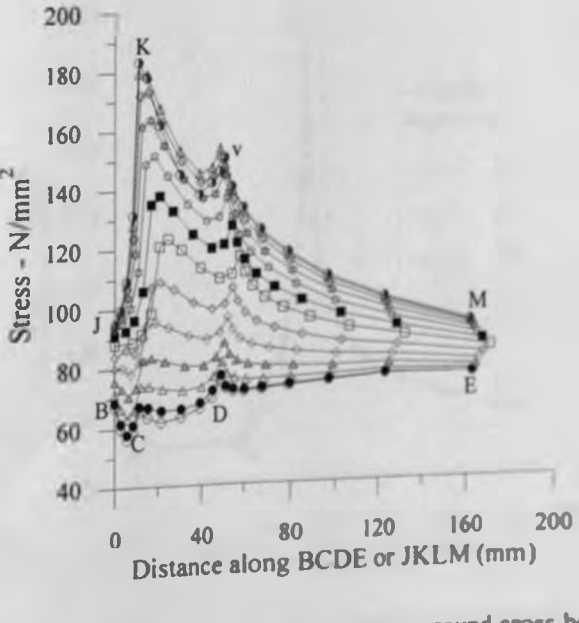

FIG. 4.87 Effective stresses around cross bore (k=3, d=0.05, clr=0.25, ca=11.5^0)

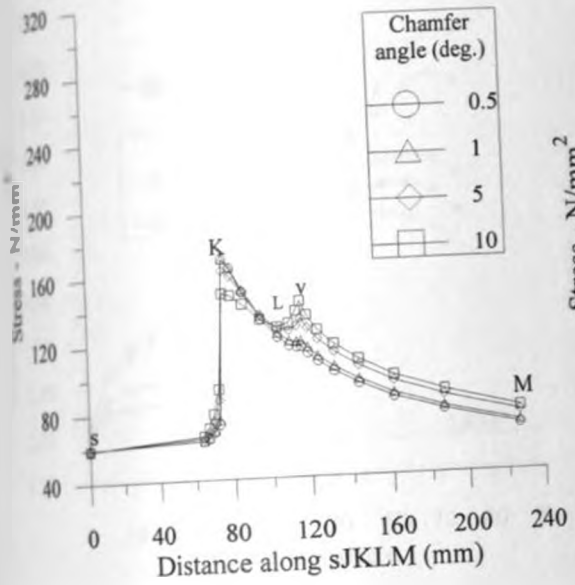

FIG. 4.88 Meridional hoop stresses (k=3, d=0.05, clr=0.25).

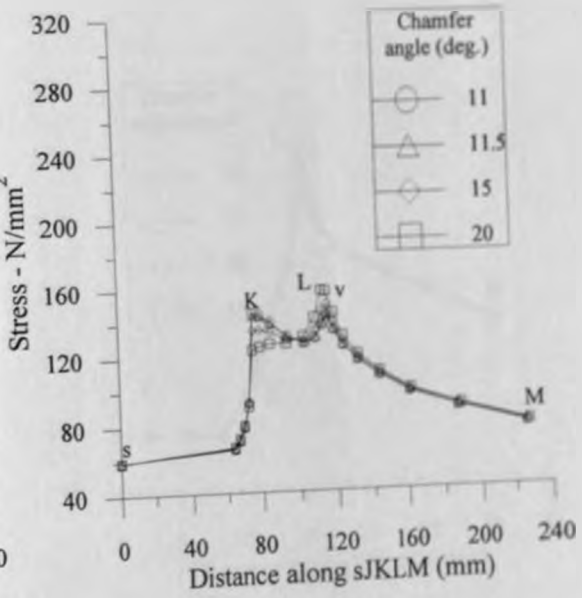

FIG. 4.89 Meridional hoop stresses (k=3, d=0.05, clr=0.25).

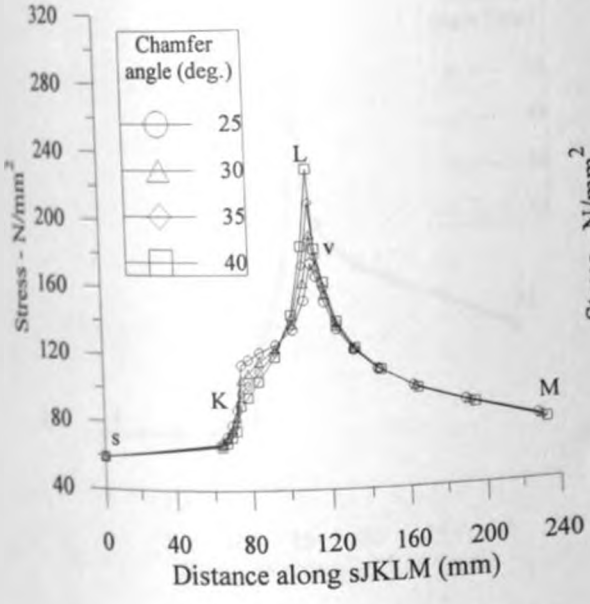

FIG. 4.90 Meridional hoop stresses (k=3, d=0.05, clr=0.25).

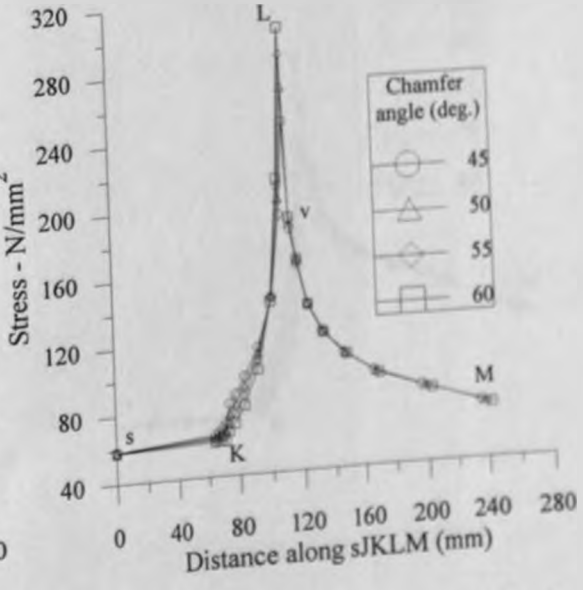

FIG. 4.91 Meridional hoop stresses (k=3, d=0.05, clr=0.25).

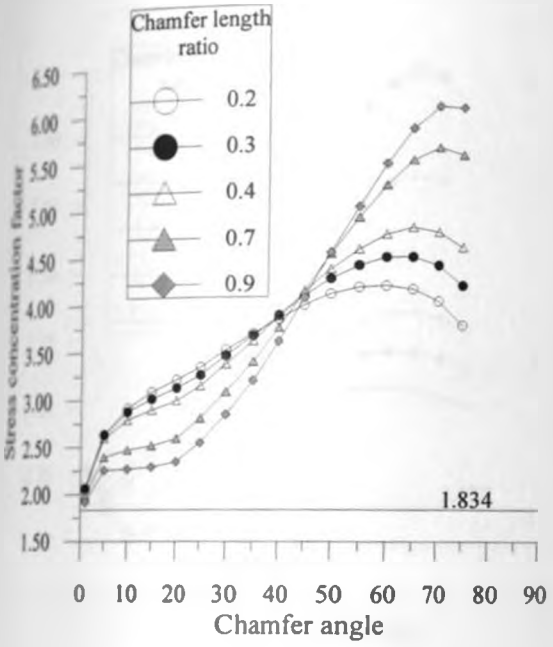

FIG. 4.92 SCF vs. chamfer angle (k=1.25, d=0.005).

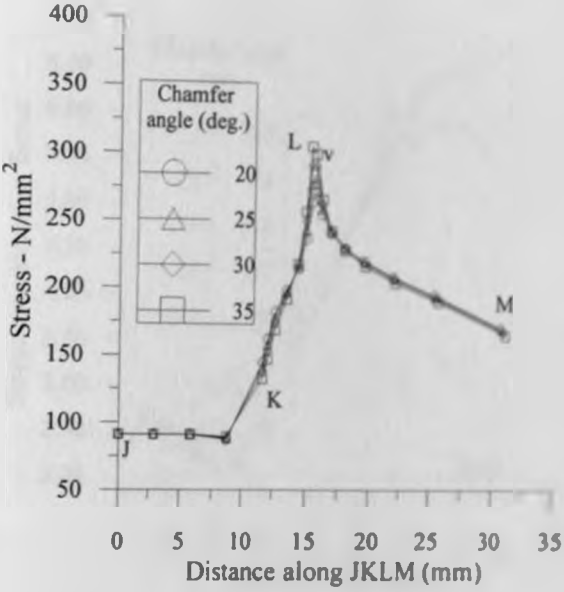

FIG. 4.93 Meridional hoop stresses (k=1.25, d=0.005, clr=0.2).

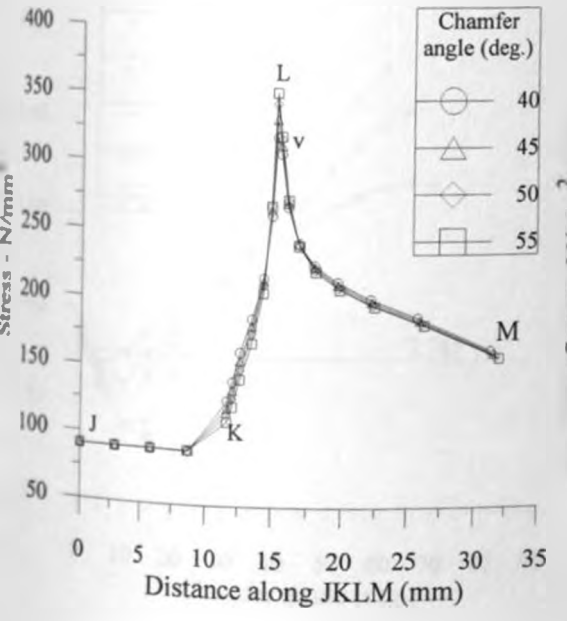

FIG. 4.94 Meridional hoop stresses (k=1.25, d=0.005, chr=0.2).

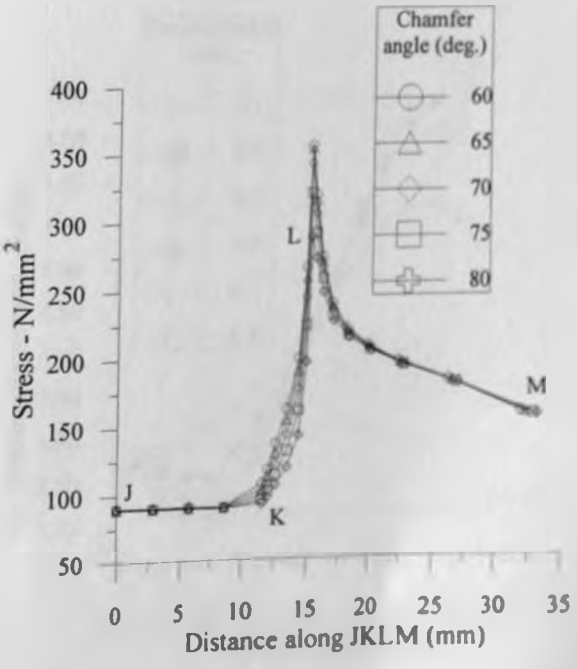

FIG. 4.95 Meridional hoop stresses (k=1.25, d=0.005, clr=0.2).

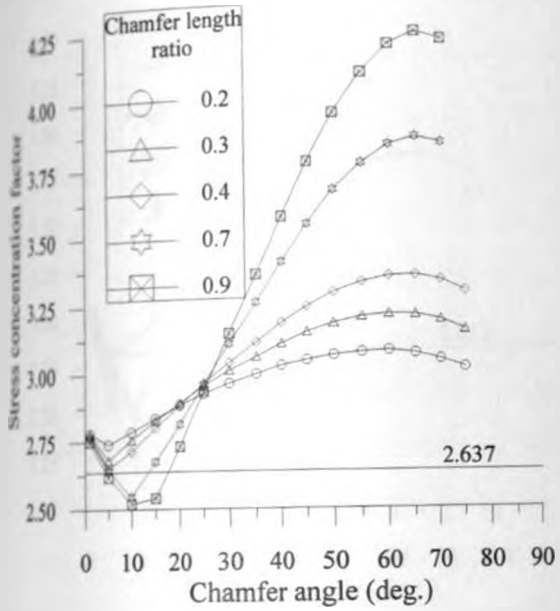

FIG. 4.96 SCF vs. chamfer angle (k=1.25, d=0.1).

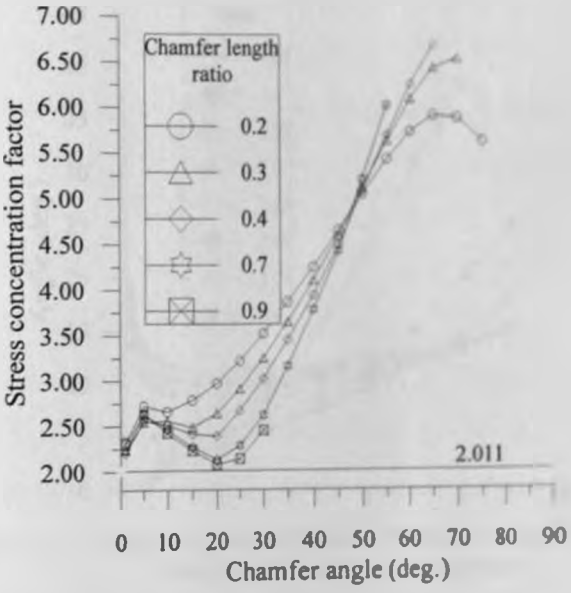

FIG. 4.97 SCF vs. chamfer angle (k=2, d=0.005).

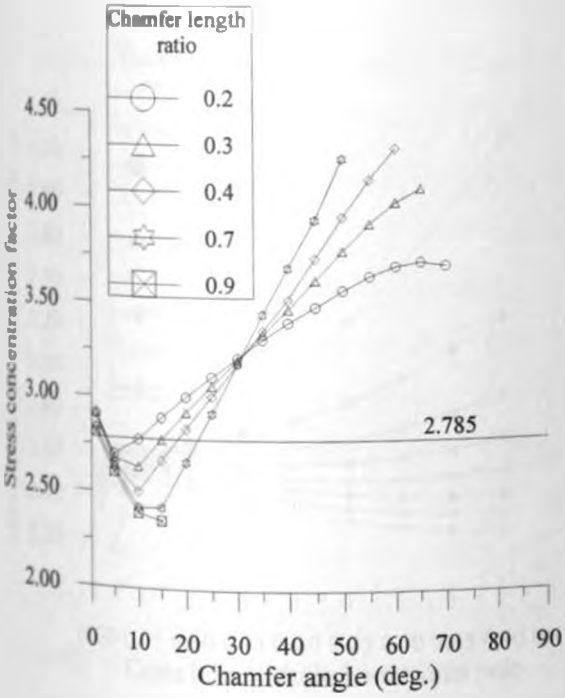

FIG. 4.98 SCF vs. chamfer angle (k=2, d=0.1).

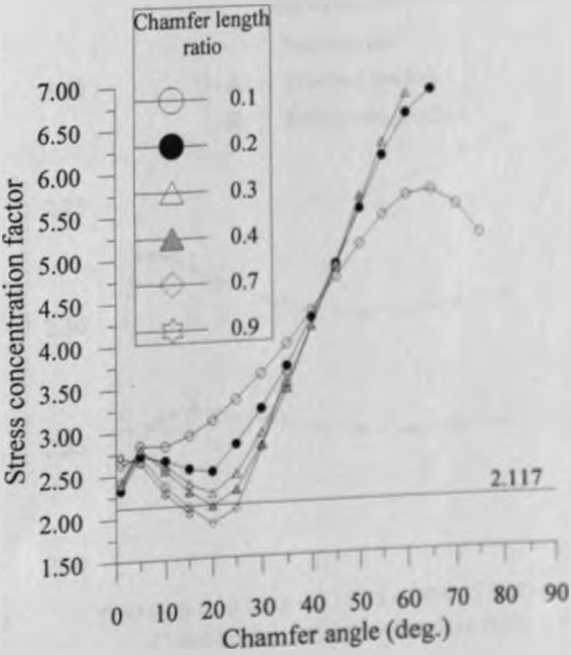

FIG. 4.99 SCF vs. chamfer angle (k=3, d=0.005).

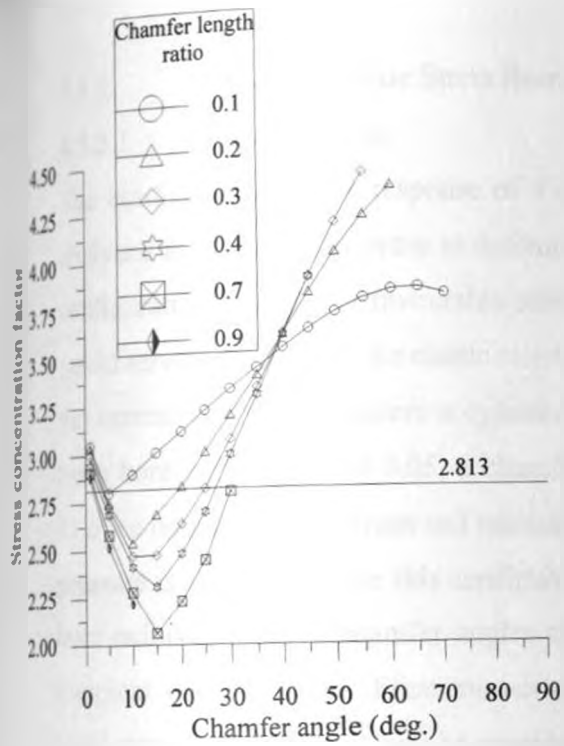

FIG. 4.100 SCF vs. chamfer angle (k=3, d=0.1).

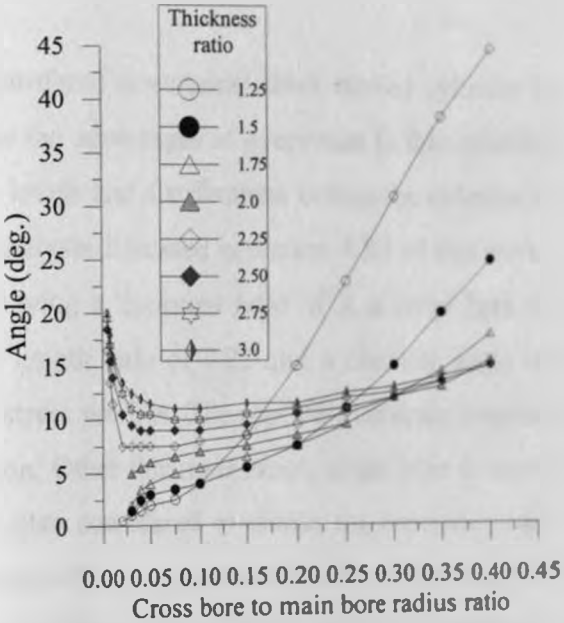

FIG. 4.101 Angles for minimum SCFs.

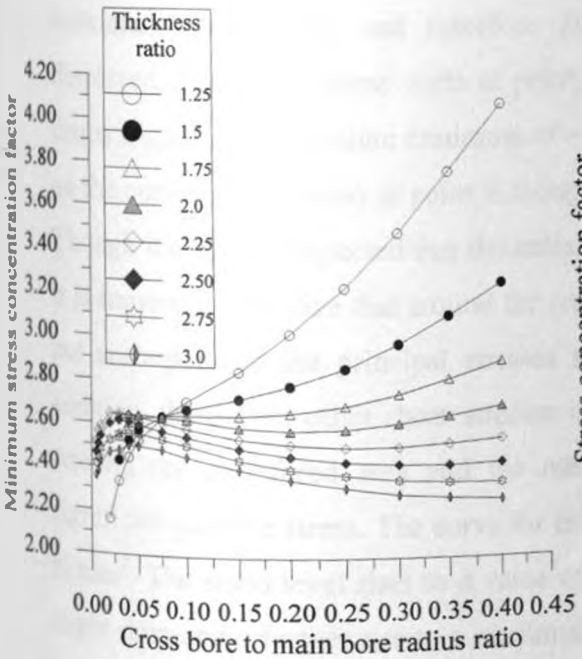

FIG. 4.102 Minimum SCF vs. cross bore to main bore radius ratio.

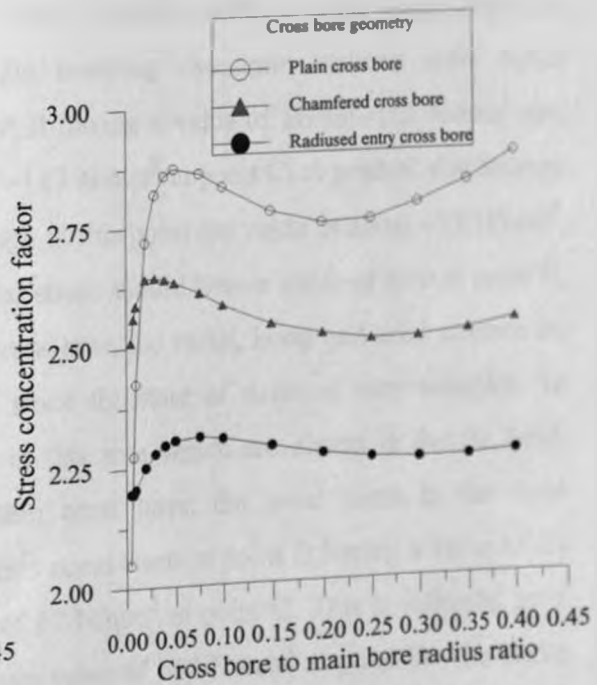

FIG. 4.103 SCF vs. cross bore to main bore radius ratio for various cross bore geometries (k=2.25).

4.5.2 Elastic-Plastic Stress Response

4.5.2.1 Introduction

The elastic-plastic stress response of a chamfered cross-bored thick walled cylinder is analyzed in this work in order to determine the advantages of overstrain in this cylinder configuration in terms of favourable stress levels and distributions before the cylinder is put in service. Following the elastic stress analysis discussed in section 4.5.1 of this work, the current analysis considers a cylinder having a thickness ratio of 3, a cross bore to main bore radius ratio of 0.05, a chamfer length ratio of 0.25 and a chamfer angle of 11.5^0 to obtain the overstrain and residual stress profiles. The applied overstrain internal pressure is 117 N/mm^2 for this configuration. Other thickness ratios, cross bore to main bore radius ratios and chamfer angles are also considered to obtain the overstrain and incipient yield pressures. Elements having an effective stress within 5% of the material yield stress of 450 N/mm^2 will be considered to have yielded. Other yield conditions will be investigated. The results presented refer to the cylinder discretization in figure 3.4.

4.5.2.2 Overstrain stresses

Figure 4.104 shows the overstrain transverse plane stresses along curve BCDE for an overstrain of 5%. The 5% overstrain value coincided with a point away from the maximum hoop stress and therefore the resulting overstrain stresses were better displayed. The radial stress starts at point B having a value of about -112 N/mm^2 and drops slightly to an absolute minimum of -117 N/mm^2 at point C. A gradual rise follows as the curve tends to zero at point E though at this point the value is about -12 N/mm^2. Though it might be expected that the radial stress should have a value of zero at point E, it is important to realize that around the cross bore, the radial, hoop and axial stresses do not correspond to the principal stresses since the state of stress is very complex. In addition, there exist other shear stresses in this area which are absent in the far field. Around the chamfered area and the main cross bore, the axial stress is the most significant positive stress. The curve for this stress starts at point B having a value of 25 N/mm^2. The stress level rises to a value of 67 N/mm^2 at point C. This is followed by a slight drop and a further rise to a maximum value of 108 N/mm^2 at point D. The curve then drops slightly before rising very gradually to have a value of 108 N/mm^2 at point E.

Therefore points D and E have the same value of axial stress. The hoop stress starts at point B having a value of 25 N/mm^2 and drops sharply to a value of –84 N/mm^2 at point a2. On moving from points a2 to D, the curve rises and then drops to a value of –84 N/mm^2 at point D. This value remains constant up to point E. Hence, the hoop stress values at points a2, D and E are equal. From the effective stress curve, point D is the most critical with a maximum stress of 182 N/mm^2. However, between points a1 and E, the effective stress is 175 N/mm^2 and therefore points D and E should receive the same attention for this value of overstrain.

Figure 4.105 shows the overstrain stress profiles along the meridional curve JKLM for 5% overstrain. It is observed that the radial and axial stresses are negative at all points of the curve. Between points L and M, the radial stress has a zero value and has a minimum value of –112 N/mm^2 at point J. The axial stress has a minimum value of –82 N/mm^2 at point K and is also the value that prevails for most of the nodes between points L and M. On moving from points K to L, there is a rise and then a drop in the axial stress. The hoop stress has a maximum value at point t and a local maximum at point L. Since the distance between the points of maximum hoop stress has decreased, it might be expected that as the overstrain is increased this distance will keep reducing with the point of maximum hoop stress around point K approaching point L until all the nodes have yielded. Contrary to observations from the elastic analysis where points K and v have equal hoop stresses, the stresses now have different values with the values at point K having risen more rapidly. From the observations of the effective stress curve, point K which is in an element which has yielded has a maximum value of 428 N/mm^2 though the material yield stress is 450 N/mm^2. This is due to the structural discretization whereby other elements sharing the same node as point K have not yielded. Stress projection techniques as employed in this work thereby result in an effective nodal stress lower than the material yield stress.

It is observed from figure 4.105 that point v has a lower effective stress value than point L. To appreciate the overstrain stress patterns on the cross bore surface nodes, the overstrain hoop stress profiles are shown in figure 4.106. These profile patterns are very

similar to the elastic hoop stress profile patterns particularly for planes around the transverse plane. The stress levels are now higher in both the positive and negative sense. For the meridional plane, the only difference is as explained for figure 4.103. Figure 4.105 shows the effective stress profile patterns for the cross bore surface nodes. Again the profiles are similar to those discussed in the elastic analysis of the same configuration with the range of effective stress along curve EM being much lower than that along curve KC.

From figures 4.106 and 4.107 it is observed that between points t and w, the set of nodes lying within 7.5^0 from the meridional plane have higher hoop stresses than those along the meridional plane. This was also noted in the case of elastic analysis. It is then possible to construct an ellipsoidol envelope enclosing points vLwtK, in the meridional plane, which prescribes the highest hoop stress points. Similar stress behaviour is observed in the transverse plane between points Ca2Da1. In this case, between points C and D, the minimum hoop stress occurs in the nodes lying 7.5^0 from the transverse plane. This phenomenon is still not well understood and requires further and proper explanation. Further analysis to better understand and explain this observation was carried out and the results are shown in figures 4.108 to 4.111. The analysis involved observing the effective stress profiles of lines of nodes lying within 22.5^0 from the meridional plane as the overstrain was increased. It is observed that between points L and K, the nodes with angles lying within 15^0 of the meridional plane have higher effective stresses though the maximum effective stress remains at point K. The point w which is within 7.5^0 remains a point of local maximum effective stress as the overstrain is increased up to 22.5^0. The nodes between points K and L show a relatively decreasing effective stress as the overstrain increases. For this configuration and range of overstrain, the transverse plane effective stress remains relatively low with the point D always having the highest effective stress. This shows that the geometrical singular point edge effects discussed in the case of elastic analysis have influence on the local stress distributions even in the case of elastic-plastic loading.

Figure 4.112 shows the overstrain hoop stresses along the meridional plane as the overstrain is increased. The stress at point K increases very rapidly as the hoop stress at point L increases only marginally. This is from the fact that point K is already yielded while point L is still elastic. Further increase in overstrain causes the hoop stress at point K to reduce progressively. Once point L has yielded, the hoop stress stops increasing and starts to decrease with further overstrain. At the highest overstrain of 65%, it is therefore observed that the midsection of curve KM has the highest hoop stresses. Figure 4.113 shows the corresponding effective stress curves. It is observed that at the overstrain value of 41%, all the nodes on line KL have yielded.

For cylinders of varying thickness ratios and cross bore to main bore radius ratios, the overstraining process was carried out to achieve yielding of the element around point t along line KL. The chamfer length ratio was 0.25 and the chamfer angle chosen was that which resulted in a minimum stress concentration factor from the elastic analysis of the same configuration. The variations of the incipient yield pressure with the cross bore to main bore radius ratio are shown in figure 4.114 for different thickness ratios. It is observed that the lower thickness ratio cylinders have lower incipient yield pressure. These curves serve as a good guide when intending to carry out overstrain in thick walled cylinders and they indicate the pressure below which initial yielding of the structure may not be expected. They can also be used in service to guard against over-pressure even when the structure is designed for elastic service only.

The overstrain pressure curves are shown in figure 4.115. The curves have similar patterns to those in figure 4.114 though the pressure levels are higher. While the incipient pressure curves are smooth, these curves are not. This may be attributed to the yield condition used in this work whereby any element having an effective stress within 5% of the material yield stress of 450 N/mm^2 is considered to have yielded. A more stringent yield condition would result in smooth curves. However, the time taken by using a stringent condition does not warrant the gain in accuracy. For example, by assuming that elements yield within 0.5% of the material yield stress, the overstrain process time factor is 2.5 even for this low value of overstrain.

Figure 4.116 shows the variation of the overstrain pressure with overstrains for this configuration. While the overstrain pressure increases with increase of overstrain, there is a drop in the pressure as the overstrain increases from 17% to 24%. This overstrain value corresponds to the elements around point L yielding whereby it was earlier discussed that point L has a local maximum effective stress.

4.5.2.3 Residual stresses

For the overstrain of 5%, figure 4.117 shows the meridional plane residual stresses. It is observed that most of the stress values are zero except around point K. The radial and axial stresses have maximum values of about 3 N/mm^2 while the hoop stress has a maximum value of –9 N/mm^2. The effective residual stress has a maximum value of 12.5 N/mm^2 at point K. It is therefore noticeable that though point K is not the point of maximum overstrain hoop stress, it is the point of maximum residual hoop, radial, axial and effective stresses.

Figure 4.118 shows the residual meridional hoop stress for varying overstrains. The maximum value occurs at point K and this maximum value increases with increase of overstrains. Figure 4.119 shows the corresponding effective residual stresses. Though a high value of residual hoop stress is desirable, the accompanying high value of residual effective stress is to be avoided since reverse yielding is likely to take place, resulting in cycling during normal service.

Figure 4.120 shows the minimum residual hoop stress relationship with cross bore to main bore radius ratio for various thickness ratios. The curves for each value of thickness ratio are not smooth variations. This phenomenon has been observed for plain and radiused entry cross-bored cylinders. As a group of curves, it is still possible to observe a general relationship which is shown by the continuous polynomial curve (of fifth order). Figure 4.121 represents the variations of minimum residual hoop stress with increase of overstrain.

4.5.2.4 Service stresses

Figure 4.122 shows the in-service meridional hoop stress levels after autofrettage compared to the elastic stress levels. A selected number of overstrain values are considered with the internal pressure applied being the same for all cases. It is clear from the figure that the higher overstrain curves give more favourable hoop stress levels. For overstrains greater than 5%, point K has the lowest hoop stress, with this value decreasing with increase in overstrain. It is also observed that the stress gradients on both sides of point K are very high. High stress gradients are not desirable. Therefore even though low values of hoop stress now exist in service, the hoop stress distribution can not be said to be more uniform than in the case of elastic loading. With increase of overstrain beyond 5%, point v becomes the point of maximum hoop stress. With increased overstrain beyond 27%, the hoop stress at point K may be expected to have a negative value. This could be a desirable outcome particularly if any suspected cracks exist around this point since the negative hoop stress tends to close the cracks and arrest any propagation.

As earlier discussed, a high overstrain is desirable though care should be taken to ensure that it does not result in gross deformation and the reverse yielding of elements. For high overstrain levels, the process of offloading must also proceed with strict safety precautionary procedures due to the high pressures involved.

Figure 4.123 shows the in-service meridional effective stress levels after autofrettage compared to the elastic stress levels. The effective stresses around point K decrease with increase of overstrain. The effective stress gradients around point K are also very high. For overstrains greater than 17%, point v has the highest effective stress.

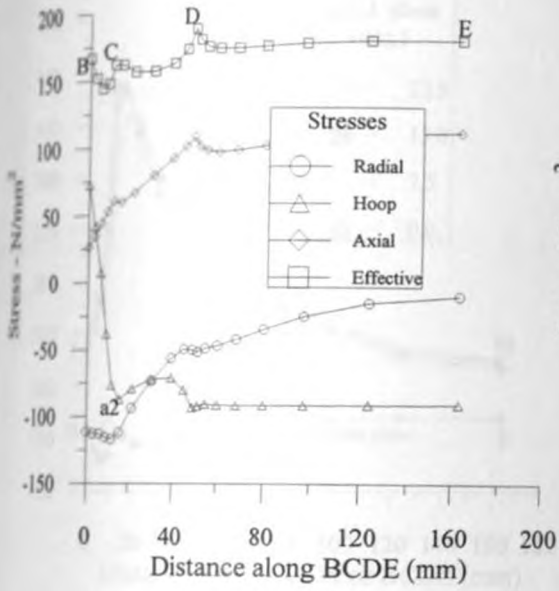

FIG. 4.104 Overstrain transverse stresses at 5% overstrain (k=3, d=0.05, clr=0.25, ca=11.5^0).

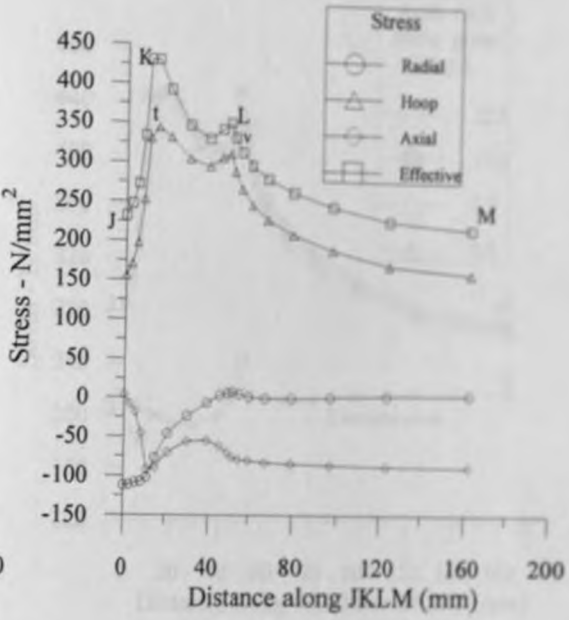

FIG. 4.105 Overstrain meridional stresses at 5% overstrain (k=3, d=0.05, clr=0.25, ca=11.5^0).

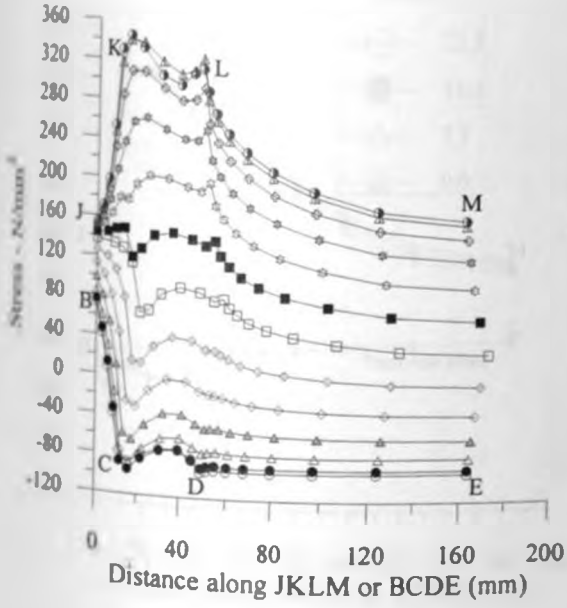

FIG. 4.106 Cross bore surface overstrain hoop stresses at 5% overstrain (k=3, d=0.05, clr=0.25, ca=11.5^0)

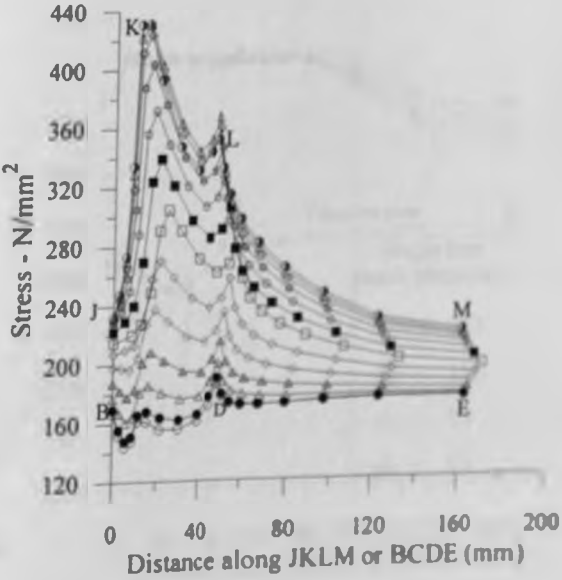

FIG. 4.107 Cross bore surface overstrain effecti stresses at 5% overstrain (k=3, d=0.05, clr=0.25, ca=11.5^0)

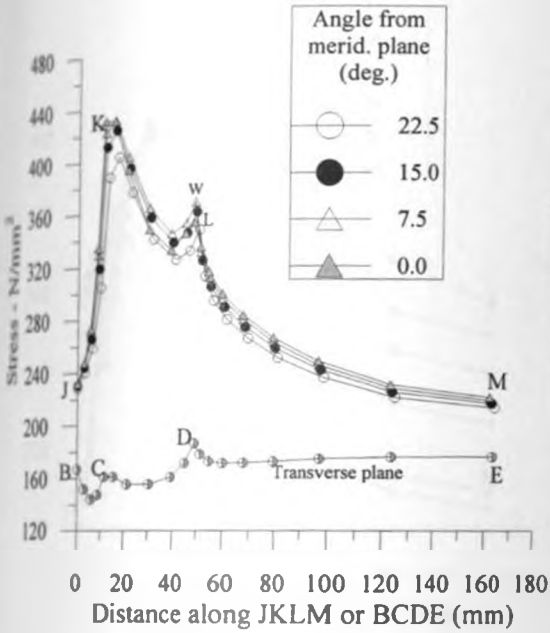

FIG. 4.108 Meridional effective stresses for 5% overstrain (k=3, d=0.05, clr=0.25, ca=11.5^0).

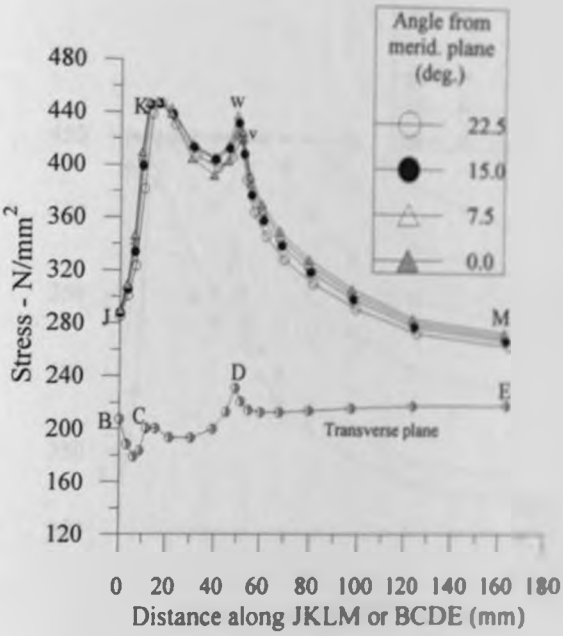

FIG. 4.109 Meridional effective stresses for 25% overstrain (k=3, d=0.05, clr=0.25, ca=11.5^0)

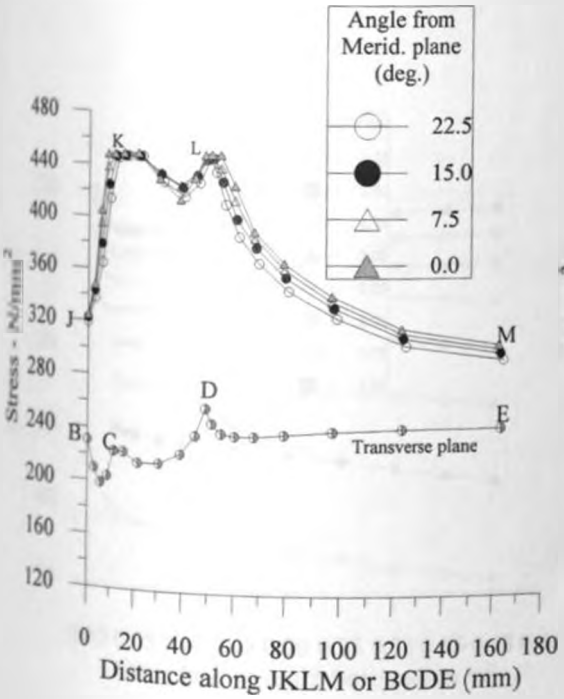

FIG. 4.110 Meridional effective stresses for 30% overstrain (k=3, d=0.05, clr=0.25, ca=11.5^0)

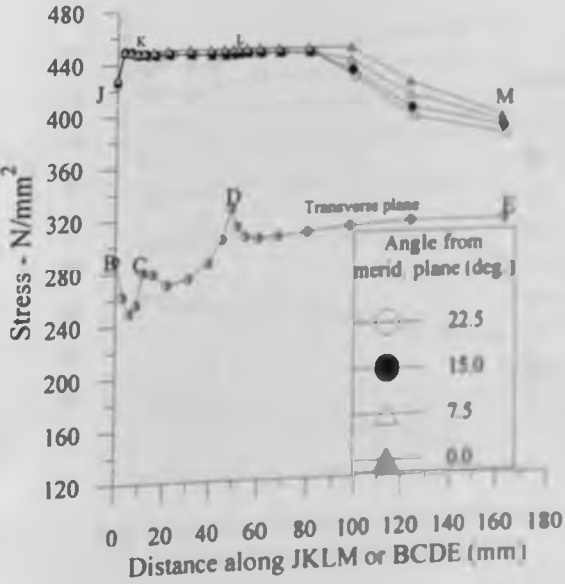

FIG. 4.111 Meridional effective stresses for 65% overstrain (k=3, d=0.05, clr=0.25, ca=11.5^0)

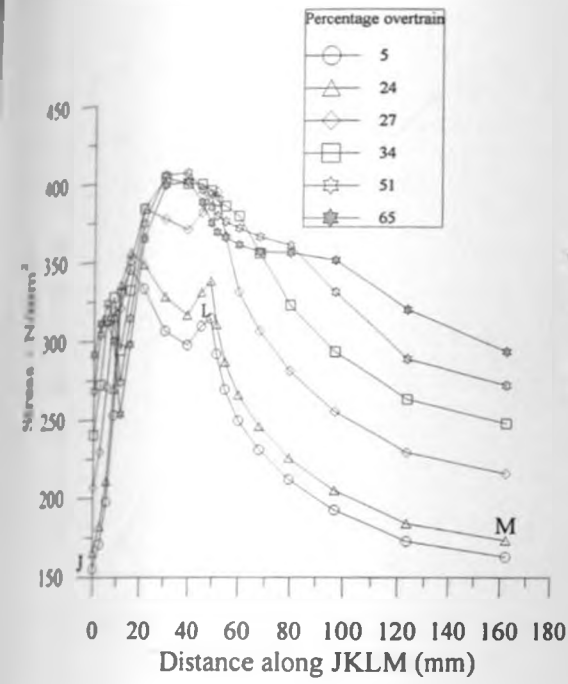

FIG. 4.112 Meridional overstrain hoop streses for varying overstrains (k=3, d=0.05, clr=0.25)

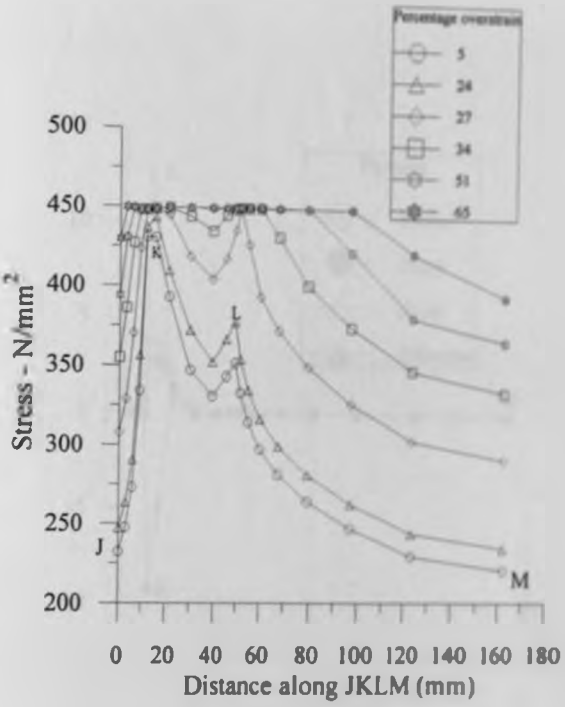

FIG. 4.113 Meridional overstrain effective stresses for varying overstrains (k=3, d=0.05, clr=0.25).

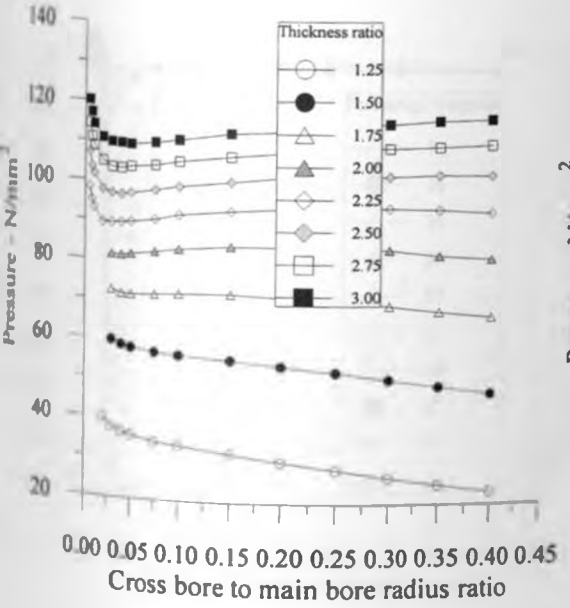

FIG. 4.114 Incipient yield pressure vs. cross bore to main bore radius ratio for chamfered cross bore.

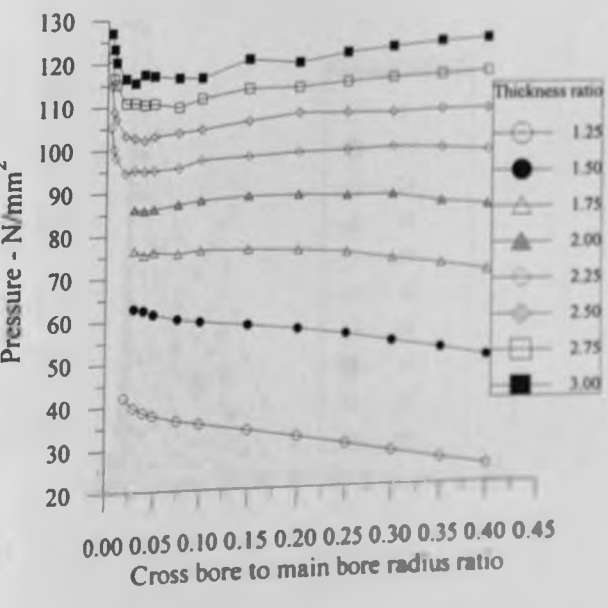

FIG. 4.115 Overstrain pressure vs. cross bore to main bore radius ratio for chamfered cross bore.

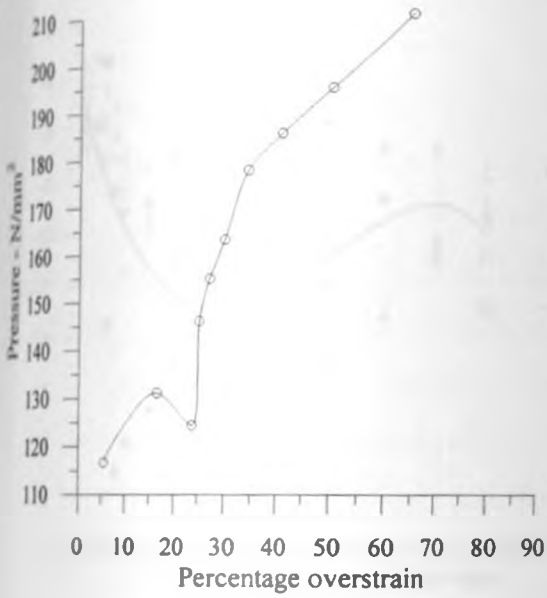

FIG. 4.116 Overstrain pressure vs. overstrain for chamfered cross bore (k=3, d=0.05,clr=0.25, ca=11.5^0)

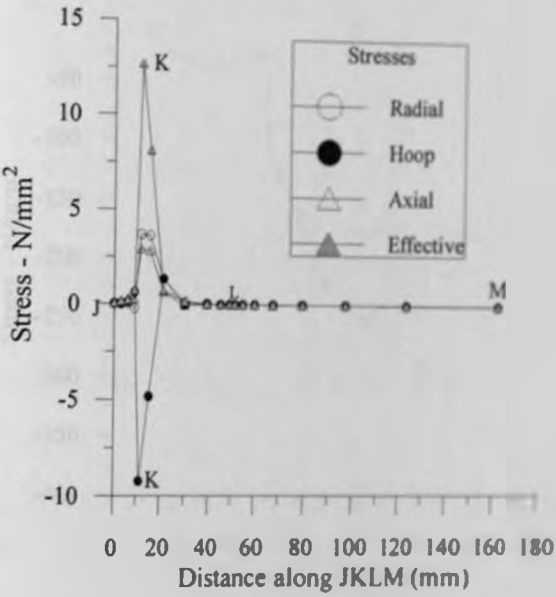

FIG. 4.117 Meridional residual stresses at 5% overstrain (k=3, d=0.05, clr=0.25, ca=11.5^0)

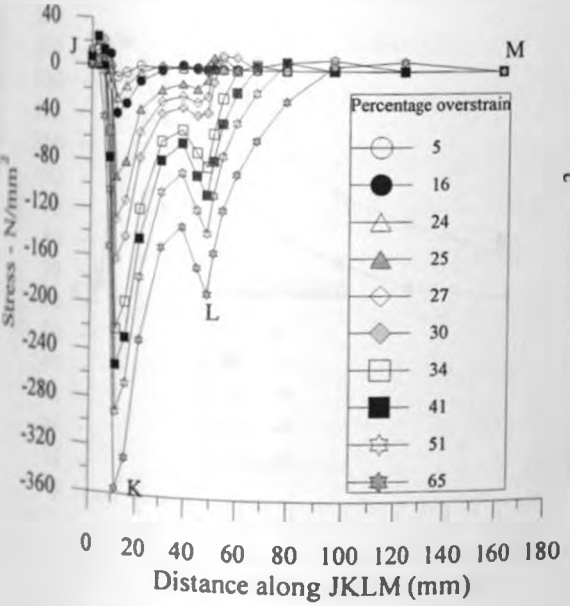

FIG. 4.118 Meridional residual hoop stresses for varying overstrains (k=3, d=0.05, clr=0.25, ca=11.5^0)

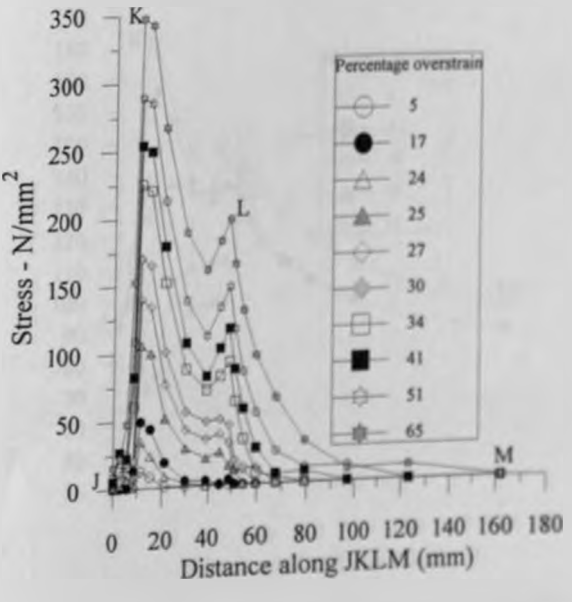

FIG. 4.119 Meridional residual effective stress for varying overstrains (k=3, d=0.0 clr=0.25, ca=11.5^0)

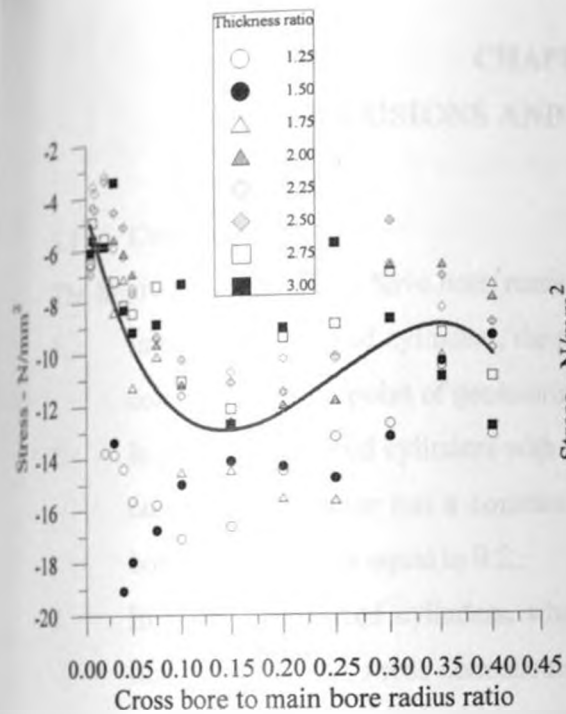

FIG. 4.120 Minimum residual hoop stresses vs. cross bore to main bore radius ratio for chamfered cross bore.

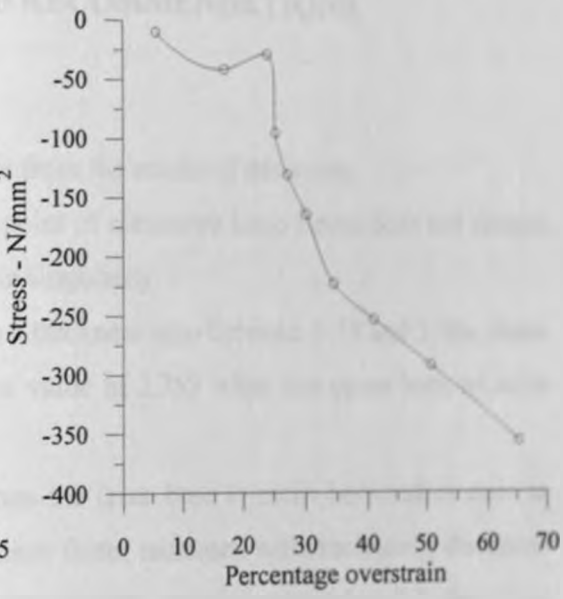

FIG. 4.121 Minimum residual hoop stress vs. overstrain for chamfered cross bore (k=3, d=0.05, clr=0.25, ca=11.5^0)

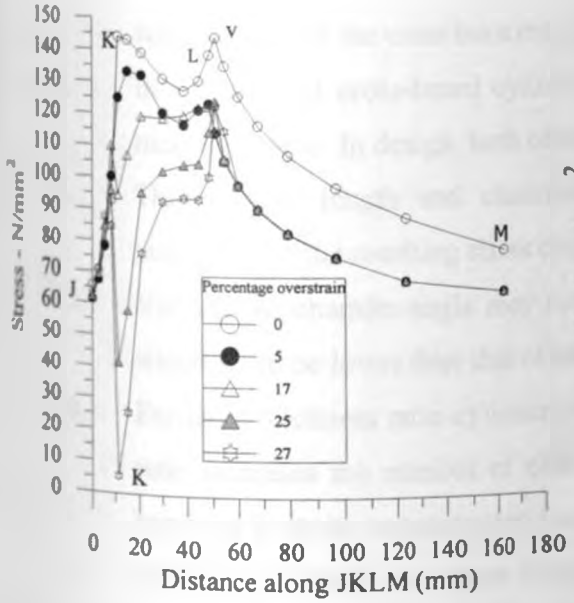

FIG. 4.122 Service hoop stresses after autofrettage for various overstrains.

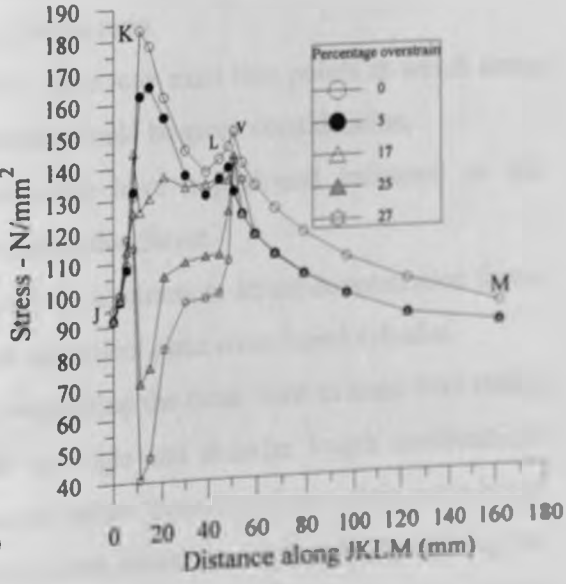

FIG. 4.123 Service effective stresses after autofrettage for various overstrains.

CHAPTER FIVE
CONCLUSIONS AND RECOMMENDATIONS

5.1 Conclusions

The following conclusions have been made from the results of this work:

1. In plain cross-bored cylinders, the point of maximum hoop stress does not always coincide with the point of geometric singularity.
2. In plain cross-bored cylinders with a thickness ratio between 1.75 and 3, the stress concentration factor has a constant value of 2.753 when the cross bore to main bore radius ratio is equal to 0.2.
3. In plain cross-bored cylinders, when the cross bore to main bore radius ratio is less than 0.2, the stress concentration factor increases with increasing thickness ratio. When the cross bore to main bore radius ratio is greater than 0.2, the stress concentration factor increases with decreasing thickness ratio.
4. The stress concentration factors and stress gradients in a radiused entry cross-bored cylinder are lower than those of an equivalent plain cross-bored cylinder.
5. In a radiused entry cross-bored cylinder, the maximum hoop stress is located near the upper end of the entry radius in the meridional plane.
6. In a radiused entry cross-bored cylinder, the stress concentration factors decrease with increase of the cross bore entry radius ratio.
7. In a chamfered cross-bored cylinder, there may exist two points at which stress maxima appear. In design, both of these should be given consideration.
8. The chamfer length and chamfer angle have a profound influence on the magnitude of the resulting stress concentration factor.
9. Varying the chamfer angle may result in a minimum stress concentration factor which could be lower than that of an equivalent plain cross bored cylinder.
10. For fixed thickness ratio cylinders, increasing the cross bore to main bore radius ratio increases the number of chamfer angle and chamfer length combinations resulting in stress concentration factors below those found in a plain cross-bored cylinder. For fixed cross bore to main bore radius ratio cylinders, increasing the thickness ratio increases the number of chamfer angle and chamfer length

combinations resulting in stress concentration factors below those found in a plain cross-bored cylinder.

11. In chamfered cross-bored cylinders, the stress concentration factors are higher than those found in equivalent radiused entry cross-bored cylinders.
12. The presence of residual stresses lowers the service stresses very considerably.
13. High overstrains provide high latitude in the selection of operating pressures without stress reversals at the cylinder bore.
14. In radiused entry cross-bored cylinders, yielding may start at the outer surface before it starts at the inside surface.

5.2 Recommendations

The initial objectives of this work have been successfully met and the data obtained, presented and discussed in this thesis could be very useful in the design, fabrication, operation and in-service inspections of thick walled cylinders.

While the results of this simulation work are satisfactory, it is recommended that practical experimental work using the three dimensional photoelasticity or strain gauge methods be used to verify the results of some of the cases of elastic and elastic-plastic analyses. In addition to the computer simulation method used in this work, the experimental methods should be used in the recommended work below.

In this work it was assumed that the cylinder operated in an ambient environment where temperature gradients had no influence on the structural response. In practice, thick walled cylinders may operate in cryogenic conditions or in high temperature conditions such as the hot extrusion processes where temperature gradients are high. The high or low temperatures may affect the cylinder bore, the cylinder outer surface or the cross bore differently depending on the temperature combinations. It is therefore recommended that the influence of low and/or high temperatures be investigated.

It was also assumed that the cross bore was isolated from any other cross bores. In some instances it may be inevitable to place cross bores near each other where conditions in

one cross bore may influence the conditions in the other. Future research is necessary to establish these interactions in the presence of varying entry geometry of the cross bores.

The finite element method used in this work gives displacements and stress results for all the nodes in the structure while the severest conditions have been shown to occur on the cross bore surface. The results for the nodes inside the material are then not useful unless discontinuities such as inclusions are to be modeled. The computer resources are therefore not optimised. It is recommended that in future work, the boundary element method, which only gives results for the surface nodes, be used. Though the algorithm for this method is more complex, it is cheaper in terms of processing time, computer memory requirements and the more closely spaced nodes should give more accurate results.

In this work, autofrettage was performed in the presence of cross bores. Residual stresses are then present only in the elements around the cross bore while the main body of the cylinder is stress free. It would be important to perform autofrettage before introducing the cross bores and the residual stresses compared to those obtained in this work.

The assumption of elastic perfectly plastic pressure vessel steel has been used to obtain the elastic-plastic analysis results presented in this work. In addition to the extra research work recommended above, strain hardening real material behaviour should be investigated.

REFERENCES

1. Zapfec C. A., 'Boiler Embrittlement', *Transactions of ASME*, Vol. 66, No. 2, pp81-126, 1942.

2. Ford, H., Watson, E. H. and Crossland, B., 'Thoughts on a Code of Practice for Forged High Pressure Vessels of Monobloc Design', *Transactions of ASME*, Vol. 103, 1981.

3. Fryer D. M. and Harvey J. F., 'High Pressure Vessels', Chapman and Hall, 1997.

4. Blake A. (EDITOR), 'Handbook of Mechanics, Materials and Structures', John Willey and Sons, 1985.

5. Langer B. F., 'Design Stress Basis for Pressure Vessels', Pressure Vessels and Piping: Design and Analysis; Vol. 1 - Analysis, 1972.

6. Townsend C. A., 'The Safe Venting of Chemical Reactors', *Journal of the Institution of Chemical Engineers*, Vol. 64, 1975.

7. Marshall V. C. and Cockran D., 'Safe Venting of Chemical Reactors'. *Journal of the Institution of Chemical Engineers*, Vol. 63, No.1, 1979.

8. O'Neil R. O., 'The Integrity of Pressure Vessels', Nuclear reactor safety proceedings. 1977.

9. Langer B. F., 'PRVC Interpretative Report of the Pressure Vessel Research Section. Section 1 - Design Considerations', Pressure Vessels and Piping: Design and Analysis; Vol. 1 - Analysis', 1972.

10. Daniels F. H., 'An Interesting Boiler Explosion', *Transactions of ASME*, New York Meeting, Vol. 15, pp118-146, 1892.

11. Harvey J. F., 'Theory and Design of Pressure Vessels', Chapman Hall, 1991

12. Bush S. H., 'Statistics of Pressure Vessel and Piping Failures', *Journal of Pressure Vessel Technology*, Vol. 110, pp225-233, August 1988.

13. Lihou D. A., 'Failures of Liquefied Gas Storage Vessels', *Journal Process Mechanical Engineering*, Vol. 205, pp27-31, 1991.

14. Labbens, R., 'Linear Elastic Fracture Mechanics Calculations in Pressure Vessel Analysis', *Journal of Pressure Vessel and Piping Technology*, Vol. 18, 1985.

15. Pemberton, H. W., 'Inspection of Primary Circuits and Reactor Pressure Vessels of Nuclear Power Plant', *Journal of the Institution of Mechanical Engineers*, vol. 75, 1961.

16. Iwadate T., Chiba K., Watanabe J., Mima S., Tokai K., Takedo H., 'Safety Analysis at a Cross Bore Corner of High Pressure Polyethylene Reactors', International Conference of Pressure Vessels and Piping: Materials, Nuclear Engineering and Solar Energy, *Transactions of ASME*, Vol. 103, 1981.

17. Masu, L. M., 'The Effect of Cross Bore Geometry on the Strength of Pressure Vessels', Ph.D. Thesis, University of Leeds, 1989.

18. Masu L. M. and Craggs G., 'Fatigue Strength of Thick Walled Cylinders Containing Cross bores with Blending Features', *Journal of Mech. Eng. Sci.*, Vol. 206, pp299-309, 1992.

19. Mahinfalah M and Harms M., 'Stress Concentration Associated with Circular Holes in Cylinders and Bone in Torsion', *Experimental Mechanics*, Vol. 34, No. 3, pp224-229, 1994.

20. Faupel, J.H. and Harris, B., 'Stress Concentrations in Heavy Walled Cylindrical Pressure Vessels', *Journal of Industrial and Engineering chemistry*, vol. 49, 1957.

21. Faupel J. H., 'Yield and Bursting Characteristics of Heavy-Wall Cylinders'. *Transactions of ASME*, Vol. 78, No. 5, July 1956.

22. Purcell T. E. and Whirl S. F., 'Embrittlement of Boiler Steel- Experiences with the Schroeder Detector', *Transactions of ASME*, Vol. 64, No. 5, pp397-402, July 1942.

23. Nelson G. A., 'Metals for High Pressure Hydrogenation Plants'. *Transactions of ASME*, pp205-213, February 1951.

24. Cottrell A. H., 'An Introduction to Metallurgy', Edward Arnolds Ltd., pp466-468. 1971.

25. Nichols R. W. (EDITOR), 'Developments in Pressure Vessel Technology- 2. Inspection and Testing', Applied science publishers, 1979.

26. Spence, J. and Tooth, A. S. (Editors), 'Pressure Vessel Design- Concepts and Principles', E & FN Spon, 1994.

27. Davies L. M., Garne L. and Collier J. G., 'Second Marshall Study Group on PWR Pressure Vessel Integrity', *Journal of Pressure Vessel Technology*, Vol. 105, pp53-57, February 1983.

28. S. Singh, 'Theory of Plasticity', Khanna Publishers, p170, 1981.

29 Ford, H., 'Advanced Mechanics of Materials', Ellis Horwood, 2nd Ed., p460, 1997.

30. McBride W. L. and Jacobs W. S., 'Design of Radial nozzles in Cylindrical Shells for Internal Pressure', *Journal of Pressure Vessel Technology*, Vol. 102, pp71-78, February 1980.

31. Mountain D. S. and Cooper G. P., 'TERSA- A New Technique for Assessing Residual Stresses', *Strain*, Vol. 25, No. 1, pp15-19, 1989.

32. Lee C., Chao Y. J., Sutton M. A., Peters W. H. and Ranson W. F., 'Determination of Plastic Strains at Notches by Image Processing Methods', *Experimental Mechanics*, Vol. 29, No. 2, pp214-220, June 1989.

33. Han G., Sutton M. A. and Chao Y. J., 'A Study of Stationary Crack-tip Deformation Fields in Thin Sheets by Computer Vision', *Experimental Mechanics*, Vol. 34, No. 2, pp125-147, June 1994.

34. Timoshenko S. and Dietz W., 'Stress Concentration Produced by Holes and Fillets', *Transactions of ASME*, Spring Meeting, Milwaukee, Wisconsin, USA, May 18-21, pp199-237, 1925.

35. Wahl A. M. and Beeuwkes R., 'Stress Concentration Produced by Holes and Notches', *Applied Mechanics, APM-56.11, Transactions of ASME*, Vol. 56, No. 8, pp617-625, 1933.

36. Taylor J. H. and Waters E. O., 'The Effect of Openings in Pressure Vessels', *Transactions of ASME, Applied Mechanics*, Vol. 56, No. 3, pp119-140, 1933.

37. Kooistra L. F. and Blaser R. V., 'Experimental Technique in Pressure Vessel Testing', *Transactions of ASME*, July 1950.

38. Gerdeen, J. C. and Smith, R. E., 'Experimental Determination of Stress Concentration Factors in Thick Walled Cylinders with Cross Holes'. *Journal of Experimental Mechanics*, Vol. 12, 1972.

39. Fessler, and Lewin, 'Stresses in Branched Pipes Under Internal Pressure'. *Journal of the Institution of Mechanical Engineers*, Vol. 176, 1962.

40. Giraltney R.C., Corum J. M., Bolt S. E. and Bryson J. W., 'Experimental Stress Analysis of Cylinder to Cylinder Shell Models and Comparisons with Theoretical Predictions', *Journal of Pressure Vessel Technology*, pp283-290, November 1976.

41. Cole B. N., Craggs G. and Finecec I., 'Strength of Cylinders Containing Radial or Offset Cross-Bores', *Journal of Mechanical Engineering Science*, Vol. 18, No. 6, pp279-285, 1976.

42. Bickell, M. B. and Dance, S.H., 'Stress Concentration Factors in Cylindrical Vessels Subjected to Internal Pressure', Third international conference on pressure vessel technology, *Transactions of the ASME*, 1977.

43. Friedman, E. and Jones, P., 'The Effect of Flaw Shape on the Fracture Propensity of Nozzle Corner Flaws', *Journal of Pressure Vessel Technology*. Vol. 110, 1988.

44. Palmer A. C., 'A Direct Design Technique for Pressure Vessels Intersections'. *Transactions of ASME*, 1st Int. Conf. on Pressure Vessel Technology. Part I. 1969.

45. Masu L. M., 'Stress and Fatigue Behaviour Model for a Pressure Vessel Containing a Cross Bore', *East African Journal of Engineering*, Vol. 1, No. 2. pp7-21. September 1994.

46. Soh A. K., 'An Improved Method for Determining Free Boundary Stresses'. *Journal of Strain Analysis*, Vol. 27, No. 2, pp93-99. 1992.

47. Richards T. H. and Daniels M. J., 'Enhancing Finite Element Surface Stress Predictions: A Semi-Analytic Technique for Axisymmetric Solids', *Journal of Strain Analysis*, Vol. 22, No. 3, pp75-86, 1987.

48. Richards T. H. and Daniels M. J., 'Enhancing Finite Element Boundary Stress Predictions for Plane and Axisymmetric Situations', *Journal of Strain Analysis*, Vol. 21, No. 1, pp33-44, 1986.

49. Koves W. J. and Nair S., 'A Finite Element for the Analysis of Shell Interactions', *Journal of Pressure Vessel Technology*, Vol. 118, pp399-406, November 1996.

50. Chen H., Jin J. and Yu J., 'Study on the Stress Concentration at the Round Corners of Flat Heads in Pressure Vessels Subjected to Internal Pressure', *Journal of Pressure Vessel Technology*, Vol. 118, pp429-433, November 1996.

51. Fenner, R. T. and Nadiri, F. 'On the Use of Elliptical Side Branches to Thick Walled Cylinders', *International Journal of Pressure Vessel and Piping*, Vol. 20, 1985.

52. Simos N. and Chassapis C, 'A Boundary Integral Approach to Attachment/Spherical Shell Interaction', *Journal of Pressure Vessel Technology*, Vol. 119, pp407-413, November 1997.

53. Xie, D. S. and Lu, Y. G., 'Prediction of Stress Concentration Factors for Cylindrical Pressure Vessels with Nozzles', *International Journal of Pressure Vessel and Piping*, Vol. 21, 1985.

54. Adams N. J. I., 'Stress Concentration in a Cylindrical Shell Containing a Circular Hole', *Journal of Engineering for Industry*, pp953-961, November 1971.

55. Redekop D and Schroeder J., 'Approximate Prediction of Hoop Stresses at Major Sections of Tee Intersections of Cylindrical Shells Subjected to Internal Pressure', *Journal of Pressure Vessel Technology*, Vol. 101, pp187-193, August 1979.

56. Updike D. P. and Kalnins A., 'Approximate Analysis of Intersecting Equal Diameter Cylindrical Shells Under Internal Pressure', *Journal of Pressure Vessel Technology*, Vol. 101, pp195-199, August 1979.

57. Pan K. C. and Beckett R. E., 'Stress and Displacement Analysis of a Shell Intersection', *Journal of Engineering for Industry*, pp303-308, May 1970.

58. Lomacky O. and Hyman B., 'Stress Analysis of Thin Elasto-Plastic Shells', *Journal of Engineering for Industry*, pp851-860, August 1971.

59. Steele C. R., Steele M. L. and Khathlan A., 'An Efficient Computational Approach for a Large Opening in a Cylindrical Vessel', *Journal of Pressure Vessel Technology*, Vol. 108, pp436-442, November 1986.

60. Jorgensen S. M., 'Overstrain Tests on Thick Walled Cylinders', *Journal of Engineering for Industry*, pp103-121, 1960.

61 Masu, L. M., 'Plasticity Analysis and Cross Bore Size Effects on the Fatigue Strength of Thick Walled Cylinders', *East African Journal of Engineering*, Vol. 1, no. 2, pp22-23, 1994.

62 Tomita Y., Shindo A., Kim Y. S. and Michiura K., 'Deformation Behaviour of Elastic Plastic Tubes Under External Pressure and Axial Load', *Int. J. of Mech. Sci.*, Vol. 28, No. 5, pp263-274, 1986.

63 Yamada, Y. and Koide, M., 'Analysis of the Bore Expanding Test by the Incremental Theory of Plasticity', *Int. J. Mech. Sci.*, Vol. 10, p1-14, 1968.

64. Tomita Y. Shindo A. and Nagai M., 'Axisymmetric Deformation of Circular Elastic Plastic Tubes Under Axial Tension and Internal Pressure', *Int. J. Mech. Sci.*, Vol. 26, No. 6-8, pp437-444, 1984.

65. Pillinger I., Hartley P., Sturgess C. E. N. and Rowe G. W., 'Use of Mean Normal Technique for Efficient and Numerically Stable Large Strain Elastic Plastic Finite Element Solutions', *Int. J. Mech. Sci.*, Vol. 28, No. 1, p23-29, 1986.

66. Yamada Y., Yashimura N. and Sakurai T., 'Plastic Stress Strain Matrix and its Application for the Solution of Elastic Plastic Problems by the Finite Element Method', *Int. J. Mech. Sci.*, Vol. 10, pp343-354, 1968.

67. Owen, D.R.J. and Salonen, E.M., 'Three Dimensional Elastic Plastic Finite Element Analysis', *Int. J. Num. Methods in Eng.*, Vol. 9, pp209-218, 1975.

68. Larsen P. K. and Popov E. P., 'Elastic-Plastic Analysis of Thick Walled Pressure Vessels with Sharp Discontinuities', *Journal of Engineering for Industry*, pp1017-1020, November 1971.

69. Tan, C. L., 'Stress Distributions in Thick Walled Cylinders due to the Introduction of Bore After Autofrettage', *Journal of Strain Analysis*, Vol. 21, 1986.

70. Dudans Z., 'Finite Element Incremental Elastic-Plastic Analysis in Pressure Vessels', *Journal of Engineering for Industry*, pp293-302, May 1970.

71. Marcal, P. V., 'A Stiffness Method for Elastic Plastic Problems', *Int. J. Mech. Sci.*, Vol. 7, p220-238, 1965.

72. Yen S. W., 'Theory of Stress Coining Techniques', *Engineering Fracture Mechanics*, Vol. 14, pp477-492, 1981.

73. Steele M. C., 'Partially Plastic Thick-Walled Cylinder Theory', *Journal of Applied Mechanics*, Vol. 19, pp133-140, June 1952.

74. Gerdeen J. C., 'Limit Analysis and Plasticity', Pressure Vessels and Piping: Design and Analysis; Vol. 1 - Analysis', 1972.

75. Hsu L. C., 'Analysis for Design - Part 1; Introduction', Pressure Vessels and Piping: Design and Analysis; Vol. 1 - Analysis', 1972.

76. Pu S. L. and Hussain M. A., 'Residual Stress Redistribution Caused by Notches and Cracks in a Partially Autofrettaged Tube', *Journal of Pressure Vessel Technology*, Vol. 103, pp303-306, November 1981.

77. Hussain M. A., Pu S. L., Vasilakis J. D. and O'Hara P., 'Simulation of Partial Autofrettage by Thermal Loads', *Journal of Pressure Vessel Technology*, Vol. 102, pp314-318, August 1980.

78. Zhou H. and Rao M. D., 'On the Error Analysis of Residual Stress Measurements by the Hole Drilling Method', *Journal of Strain Analysis*, Vol. 28, No. 4, pp273-276, 1993.

79. Schajer G. S. and Yang L., 'Residual-Stress Measurement in Orthotropic Materials Using the Hole-Drilling Method', *Experimental Mechanics*, Vol. 34, No. 4, pp324-334, 1994.

80. Makino A. and Nelson D., 'Residual Stress Determination by Single-Axis Holographic Interferometry and Hole-Drilling- Part I: Theory', *Experimental Mechanics*, Vol. 34, No. 1, pp66-88, 1994.

81. Joh D, Byun K. Y. and Ha J., 'Thermal Residual Stresses in Thick Graphite/Epoxy Composite Laminates- Uniaxial Approach', *Experimental Mechanics*, Vol. 33, No. 1, pp70-90, 1993.

82. Sharman D. J., Stark H. L. and Kelly D. W., 'Bench Marking of a Destructive Technique to Determine Residual Stresses in Thick Walled Axisymmetric Components', *Journal of Strain Analysis*, Vol. 32, No. 2, pp87-96, 1997.

83. Sharman D. J., Stark H. L. and Kelly D. W., 'A Comparison of Potential Methods for the Alleviation of Residual Stresses in the Necks of Aluminium Alloy Thick-Walled Gas Cylinders', *Journal of Strain Analysis*, Vol. 32, No. 5, pp315-323, April 1997.

84. Faupel J. H. and Furbeck A. R., 'Influence of Residual Stresses on Behaviour of Thick Walled Closed-End Cylinders', 7th National Instruments Conference, Cleveland, Ohio, Sept. 9-10, 1952.

85. Le' N. V., 'Method and Mechanism of Beneficial Residual Stresses in Tubes', *Journal of Pressure Vessel Technology*, Vol. 116, pp175-178, May 1994.

86. Perl M. and Arone' R., 'An Axisymmetric Stress Release Method for Measuring the Autofrettage Level in Thick-Walled Cylinders- Part I: Basic Concept and Numerical Simulation', *Journal of Pressure Vessel Technology*, Vol. 116, pp384-388, November 1994.

87. Perl M. and Arone' R., 'An Axisymmetric Stress Release Method for Measuring the Autofrettage Level in Thick-Walled Cylinders- Part II: Experimental Validation', *Journal of Pressure Vessel Technology*, Vol. 116, pp389-395, November 1994.

88. Sorem (Jr) J. R., Shadley J. R. and Rybicki E. F., 'Experimental Method for Determining Through Thickness Residual Hoop Stresses in Thin Walled Pipes and Tubes Without Inside Access', *Strain*, pp7-14, February 1990.

89. Roach D. P. and Priddy T. G., 'Effect of Material Properties on the Strain to Failure of Thick-Walled Cylinders Subjected to Internal Pressure', *Journal of Pressure Vessel Technology*, Vol. 116, pp96-104, May 1994.

90. Crossland B., Jorgensen S. M. and Bones J. A., 'The Strength of Thick-Walled Cylinders', *Journal of Engineering for Industry*, pp95-114, May 1959.

91. Loghman A. and Wahab M. A., 'Loading and Unloading of Thick Walled Cylindrical Pressure Vessels of Strain Hardening Material', *Journal of Pressure Vessel Technology*, Vol. 116, pp105-109, 1994.

92. Mendelson A., 'Plasticity Theory and Application', McMillan Co. New York, 1968.

93. Jorgensen S. M., 'Overstrain and Bursting Strength of Thick-Walled Cylinders', *Transactions of ASME*, Vol. 80, No. 3, pp561-570, April 1958.

94. Liu Y. and Shen N. J., 'The Residual Stress and Strain Solutions of Autofrettaged Pressure Vessels with a Cone and Cylinder Connection', *Journal of Strain Analysis*, Vol. 27, No.1, 1992.

95. Stark H. L., Bau J. and Kelly D. W., 'A destructive Procedure to Determine the Residual Stresses in Thick-Walled Cylindrical Pressure Vessels', *Journal of Strain Analysis*, Vol. 29, No. 1, pp57-63, 1994.

96. Kapp J. A. and Pflegl G. A., 'Stress Analysis of O.D. Notched Thick-Walled Cylinders Subjected to Internal Pressure or Thermal Loads', *Journal of Pressure Vessel Technology*, Vol. 103, pp76-84, February 1981.

105. Seshadri R., 'Residual Stress Estimation and Shakedown Evaluation Using GLOSS Analysis', *Journal of Pressure Vessel Technology*, Vol. 116, pp290-294. August 1994.

106. Jiang W., 'The Elastic-Plastic Analysis of Tubes- IV: Thermal Ratcheting', *Journal of Pressure Vessel Technology*, Vol. 114, pp236-245, May 1992.

107. Mershon J. L., 'Significance of Calculated Stresses in Pressure Vessels', Pressure Vessels and Piping: Design and Analysis; Vol. 1 - Analysis', 1972.

108. Pastor T. P. and Hechmer J., 'ASME Task Group Report on Primary Stress', *Journal of Pressure Vessel Technology*, Vol. 119, pp61-67, 1997.

109. Mackenzie D. and Boyle J. T., 'A Computational Procedure for Calculating Primary Stress for the ASME B&PV Code', *Journal of Pressure Vessel Technology*, Vol. 116, pp339-344, November 1994.

110. McKenzie D. and Boyle J. T., 'Computational Procedures for Calculating Primary Stress for the ASME Boiler and Pressure Vessel Code', *ASME Pressure Vessel and Piping*, Vol. 265, July 1993.

111. Seshadri R., 'Robust Stress Classification of Pressure Components Using the GLOSS Methods', *ASME Pressure Vessel and Piping*, Vol. 265, July 1993.

112. Popov E. P., Khojasten-Bakht M. and Sharifi P., 'Elastic-Plastic Analysis of Some Pressure Vessel Heads', *Journal of Engineering for Industry*, pp309-316, May 1970.

113. Cepluch R. J., 'ASME Boiler and Pressure Vessel Code Committee and Related Organizations', Pressure Vessels and Piping: Design and Analysis: Vol. 1 - Analysis', 1972.

114. Mraz G. J., 'Development of Design Criteria for a High Pressure Vessel Construction Code', *Journal of Pressure Vessel Technology*, Vol. 109, pp257-259, May 1987.

115. BS 5500: 'Unfired Fission Welded Pressure Vessels', 1982.

116. BS 5500, 'Unfired Fission Welded Pressure Vessels', Section 3, 1991.

117. Taylor D. A. W., 'Strain Gauge Proof Hydraulic Testing of Commercial Pressure Vessels', *Strain*, pp23-26, February 1996.

118. Crawley N. I., Moreton D. N., Moffat D. G. and Tolley A. F., 'The Effect of Proof Testing on the Shakedown Behaviour of Pressure Vessel Nozzles', *Journal of Strain Analysis*, Vol. 29, No. 2, pp81-92, 1994.

119. Mackenzie D., Boyle J. T. and Spence J., 'Some Recent Developments in Pressure Vessel Design by Analysis', *Proc. Instn. Mech. Engrs*, Vol. 208, pp23-29, 1994.

120. Hechnaer J. L. and Hollinger G. L., '3D Stress Criteria', *ASME Pressure Vessel and Piping*, Vol. 210, No. 2, pp181-191, San Diego, 1991.

121. Hollinger G. L., 'Summary of 3D Stress Classification', Proc. of Int. Conf. on Pressure Vessel Technology, Dusseldorf, 1992.

122. Nichols R. W. (EDITOR), 'Developments in Pressure Vessel Technology- 3, Design, Materials and Fabrication', Applied science publishers, 1980.

123. Quin S. and Widera G. E. O., 'Use of Stress-Strength Model in Determination of Safety Factor for Pressure Vessel Design', *Journal of Pressure Vessel Technology*, Vol. 118, pp27-32, February 1996.

124. Svensson N. L., 'The Bursting Pressure of Cylindrical and Spherical Vessels', *Journal of Applied Mechanics*, Vol. 25, No. 1, pp89-96, March 1958.

125. Witkin D. E. and Mraz G. J., 'Design Philosophy of Pressure Vessels for Service Above 10 ksi (70MPa)', *Journal of Pressure Vessel Technology*, pp266-276. November 1976.

126. Heinz S., 'Pressure Vessels- Material Problems, Testing and Inspection, Corrosion Protection and Operating Experience', Pressure Vessel Technology, 3rd International Conference on Pressure Vessel Technology, Japan, *Transactions of IME*, Vol. 3, 1980.

127. Latzko D., 'Reliable Economic Heavy Duty Pressure Components: The next twenty years', Pressure Vessel Technology, 3rd International Conference on Pressure Vessel Technology, Japan, *Transactions of IME*, Vol. 1, 1980.

128. Pascoe K. J., 'The Properties of Engineering Materials', Van Nostrand Reinhold Co., 1980.

129. Tahara T., 'A Feasibility Study of Manufacturing Ultra-Large Pressure Vessels for Coal Conversion Application', Pressure Vessel Technology, 3rd International Conference on Pressure Vessel Technology, Japan, *Transactions of IME*, 1980.

130. Mraz G. J. and Nisbett E. G., 'Design, Manufacture and Safety Aspects of Forged Vessels for High Pressure Service', *Journal of Pressure Vessel Technology*, Vol. 102, pp99-106, 1980.

131. Long S. S., 'High Temperature Properties and Constitutive Equations for 1Cr-1/2Mo Steel', *Journal of Pressure Vessel Technology*, Vol. 100, pp246-255, August 1978.

132. Barsom J. M. and Rolfe S. T., 'Fatigue and Burst Analysis of H_y–140 (T) Steel for Pressure Vessels', *Journal of Engineering for Industry*, pp11-16, February 1970

133. Morrison J. L. M., Crossland B. and Parry J. S. C., 'The Strength of Thick Cylinders Subjected to Repeated Internal Pressure', *Journal of Engineering for Industry*, pp143-153, May 1960.

134. Barton D. C., Amos A. R., Soden P. D. and Gill S. S., 'The Design of Ends of Cylindrical Pressure Vessels in Glass Reinforced Plastic', *Int. J. Mech. Sci.*, Vol. 26, No. 3, pp177-199, 1984.

135. Charles J. A. and Crane F. A. A., 'Selection and Use of Engineering Materials', 2nd Edition, Butterworths, pp59-62, 1989.

136. BS 4994 – 1987: Specifications for Vessels and Tanks in Reinforced Plastics. British Standards Institution, London.

137. Leach J., Soden P. D. W. and Kitching R., 'Strain Distributions in Hemispherical GRP Vessels with Radial Branch Connections Subjected to Internal Pressure and Radial Loading', *Proc. Instn. Mech. Engrs.*, Vol. 208, pp45-58. 1994.

138. Murphy P. V., 'A Lightweight Hydrocarbon Sample Vessel', *Journal Process Mechanical Engineering*, Vol. 205, pp21-25,1991.

139. Becker S. J. and Mollick L., 'The Theory of Ideal Design of a Compound Vessel', *Journal of Engineering for Industry*, pp136-142. May 1960.

140. Witherell M. D. and Scavullo M. A., 'Stress Analysis and Weight Savings of Iternally Pressurized Composite-Jacketed Isotropic Cylinders', *Journal of Pressure Vessel Technology*, Vol. 112, pp397-403. November 1990.

141. Widera G. E. O. and Logan D. L., 'Layered Cylindrical Pressure Vessels', *Journal of Pressure Vessel Technology*, Vol. 101, pp80-86, February 1979.

142. Cameron S. and Kennedy F., 'Influence of defect assessment on the design of structures', Pressure vessel technology, 3rd International Conference on Pressure Vessel Technology, JAPAN, *Transactions of the IME*, Vol. 1, 1980.

143. Mangalaramanan S. P. and Seshadri R., 'Minimum Weight Design of Pressure Components Using R-Nodes', *Journal of Pressure Vessel Technology*, Vol. 119, pp225-231, May 1997.

144. Manning C. H., 'A Method of Manufacture of Large Steam Pipes', *Transactions of ASME*, Vol. 15, pp571-576, 1894.

145. Harris D. O., 'A Means of Assessing the Effects of Periodic Proof Testing and NDE on the Reliability of Cyclically Loaded Structures', *Journal of Pressure Vessel Technology*, Vol. 100, pp151-157, May 1978.

146. Palusamy S and Lend W. C., 'Influence of External Loads on Pressure Carrying Capacity of Outlet Connections', *Journal of Engineering for Industry*, pp113-120, February 1973.

147. Irons B. M., 'A Frontal Solution Program', *Int. J. Num. Meth. Engng*, Vol. 2, pp5-32, 1970.

148. Thompson E. and Shimazaki Y., 'A Frontal Procedure Using Skyline Storage', *Int. J. Num. Meth. Engng*, Vol. 15, pp889-910, 1980.

149. Abbas S. F., 'Some Novel Applications of the Frontal Concept', *Int. J. Num. Meth. Engng*, Vol. 15, pp519-536, 1980.

150. Krishnamoothy C. S., 'Finite Element Analysis', Tata McGraw-Hill, 1987.

151. Kardestuncer, H. (EDITOR),' Finite Element Handbook', McGraw-Hill Book Company, 1st Edition, 1987.

152. Rheinboldt W. C., 'Adaptive Mesh Refinement Processes for Finite Element Solutions', *Int. J. Num. Meth. Engng*, Vol. 17, pp649-662, 1981.

153. Carey G. and Humphrey D. L., 'Mesh Refinement and Iterative Solution Methods for Finite Element Computations', *Int. J. Num. Meth. Engng*, Vol. 17, pp1717-1734, 1981.

154. Malvern L. E., 'Introduction to The Mechanics of Continuous Media', Prentice-Hill, Inc., 1969.

155. Marcal P. V. and King I. P., 'Elastic-Plastic Analysis of Two-Dimensional Stress Systems by the Finite Element Method', *Int. J. Mech. Sci.*, Vol. 9, pp143-155, 1967.

156. Kim H. O., 'A Finite Element Formulation Based on Nadai's Deformation Theory for Elasto-Plastic Analysis', *Int. J. Num. Meth. Engng*, Vol. 17, pp1861-1876, 1981.

157. Powell G. and Simons J., 'Improved Iteration Strategy for Nonlinear Structures', *Int J. Num. Meth. Engng*, Vol. 17,pp1455-1467, 1981.

158. Boyle E. F. and Jennings A., 'Accelerating the Convergence of Elastic-Plastic Stress Analysis', *Int. J. Num. Meth. Engng*, Vol. 7, No. 3, pp232-235, 1973.

159. Zienkiewicz O. C., Valliapan S. and King I. P., 'Elasto-Plastic Solutions of Engineering Problems 'Initial Stress', Finite Element Approach', *Int. J. Num. Meth. Engng*, Vol. 1, pp75-100, 1969.

160. Nayak G. C., 'Elasto Plastic Stress Analysis: A Generalization for Various Constitutive Relations Including Strain Softening', *Int. J. Num. Meth. Engng.* Vol. 5, pp123, 1972.

161. Cheng S. Y., Hsu T. R. and Too J. J. M., 'An Integrated Load Increment for Finite Elastic-Plastic Stress Analysis', *Int. J. Num. Meth. Engng.* Vol. 15, pp883-842, 1980.

APPENDIX I

THE FINITE ELEMENT METHOD

A1 Introduction

This is a numerical procedure for solving physical problems governed by a differential equation or an energy theorem. It has two characteristics that distinguish it from other numerical procedures:

(a) The method utilizes an integral formulation to generate a system of algebraic equations.

(b) The method uses continuous piecewise smooth functions for approximating the unknown quantity or quantities.

The method involves finding an approximate solution to a boundary value or initial value problem by assuming that the domain is divided into well defined subdomains and that the unknown function of the state variable is defined approximately within each element. With these individually defined functions matching each other at the element nodes or at certain points at the interfaces, the unknown function is approximated over the entire domain. Instead of finding an admissible function satisfying the boundary conditions for the entire domain, which is difficult for irregular domains, the admissible functions are defined over element domains with simple geometry, paying no attention to complications at the boundaries. Thus, the finite element method is a particular class of discretization procedure by which the original governing equations having infinite degrees of freedom are transformed into approximation equations with finite degrees of freedom. Three categories of finite element method exist:

(a) Nodal methods: element parameters are the values of the dependent variables of the true solution and their derivatives at the nodes.

(b) Coefficient methods: element parameters are the representative values of the functional representation over the element.

(c) Cell methods: element parameters represent the values of the dependent variables and their derivatives.

The most important and widely used of them all is the nodal method. The nodal finite

element method can be further subdivided according to the procedure by which the equations in the nodal values are formulated. The methods are:

(a) Variational finite element methods: an extremal principle is used with the finite element approximation to derive a set of equations in terms of the nodal values. Often, a functional or functionals obtained from the extremal principle is the starting point.

(b) Residual finite element methods: a function is chosen and the difference in value this function has between the true solution and the approximate solution is defined as the residual or error. This error is then minimized.

(c) Direct finite element method: the finite element representation of the solution in terms of the nodal values and prescribed functions within the element is substituted directly into the governing equations to obtain the nodal value equations.

(d) The energy balance method: this relies on the balance of the thermal and/or mechanical energy of the system.

The mathematical interpretation of the finite element method views the element as a part of the solution domain where the phenomena of interest are occurring. In solid and structural mechanics problems, the elements are viewed as locations in space where a displacement field exists. The finite element method has the following features as an effective computational technique:

(a) A sound mathematical as well as physical basis.

(b) No limitations with regard to the geometry and the physical composition of the domain as well as the nature of the loading.

(c) Independence of the shape of the domain and the boundary conditions.

(d) Flexibility in choosing a desired degree of approximation without reformulating the entire problem.

(e) Involves a systematic procedure that can be automated for use on digital computers.

Equilibrium and compatibility considered at each node in a finite element method problem formulation lead to a set of algebraic equations, in which the unknowns may be nodal displacements, internal nodal forces or both, depending upon the specific method used. In

the displacement formulation method, the set of algebraic equations involves the nodal displacements. In the force method, the equations are expressed in terms of unknown nodal forces. In the finite element method, the solid continuum is discretized by a finite number of elements, connected not only at their nodes, but also along the hypothetical interelement boundaries as well. In addition to the nodal compatibility and equilibrium, compatibilty must also be satisfied along the boundaries between elements.

A2 Finite Element Method Procedure

The following steps are involved in the finite element analysis of a typical engineering problem:

A2.1 Discretization of the Domain.

This is the subdivision of the domain into a collection of preselected finite elements (this step can be postponed until after the finite element formulation of the equation is completed). The subdivision process is essentially an exercise of engineering judgement. The number, shape, size and configuration of the elements is done in such a way that the original body is simulated as closely as possible. The nodes and elements are numbered. The node numbering is done in such a way as to minimize the bandwidth of the assembled stiffness matrix. The resulting mesh may be uniform or graded according to the nature of the problem. The intersection points of the elements and possibly some intermediate points are called the global nodes. The geometric properties, i.e., the coordinate points of the nodes, cross-sectional areas, volumes of elements are then generated. The most obvious locations of nodes are places where abrupt changes in geometry, loading and material properties occur.

A2.2 Derivation of Element Equations for all Elements in the Mesh

The variational formulation of the given differential equation over the typical element is constructed. A typical dependent variable, u, is assumed to be of the form,

$$u = \sum_{i=1}^{n} U_i \Psi_i \qquad \text{(A1.1)}$$

where, n is the number of nodes in the element,

U_i is the value of the variable at node i,

Ψ_i is the shape function of node i.

The shape functions Ψ_i are derived or selected from available literature and the value of u is now used to obtain the element stiffness matrix and the element force vector.

A2.3 Static Condensation

The nodes in the element which are wholly within the element and are not shared by the neighbouring element are eliminated from the equations. This has the effect of reducing the number of element equations and hence simplifies the computational procedure.

A2.4 Transformation of Element Matrices from Local to Global Coordinate System

If the formulation in step (A2.2) was carried out in the local coordinate system of the element, then the resulting stiffness matrix and force vector are transformed back to the global coordinate system through the appropriate Jacobian of transformation for each element.

A2.5 Assembly of Element Equations

The connectivity matrix is constructed and the inter-element continuity conditions among the primary variables are identified. The equations are then assembled on the global stiffness matrix and force vector equations by the use of the connectivity matrix.

A2.6 Imposition of the Boundary Conditions of the Problem

The specified global primary degrees of freedom and the specified global secondary degrees of freedom are identified. These are eliminated from the assembled equations and this has the effect of reducing the equations. Before imposition of the boundary conditions, the stiffness matrix is singular and the equations can not be solved. Imposition of the boundary conditions makes the equations solvable.

A2.7 Solution of the Assembled Equations

Using the available matrix reduction, elimination and inversion techniques, the primary

degrees of freedom are obtained.

A2.8 Postprocessing of the Results

Any other desired quantities are computed from the primary degrees of freedom results obtained in step (A2.7). These quantities include stresses.

A3 Shape Functions

In stress analysis problems, the field variables of interest are the displacements. From the knowledge of the displacements, the element resultants such as the stresses and strains may be computed through the use of constitutive equations.

The functions which are used to represent the displacement on an element basis are referred to as parameter functions or shape functions. These must meet two primary requirements: compatibility and completeness. The primary reason is to ensure convergence as the element size is reduced or as the mesh is refined in a regular fashion.

A3.1 Convergence

Since the finite element method provides a numerical solution, it is expected that the solution must converge to the exact solution under certain circumstances. It can be shown that the displacement formulation of the method leads to an upper bound solution of the actual stiffness of the structure. Hence, as the mesh is made finer, the solution should converge to the correct result. This is achieved if:

(a) The shape functions are continuous within the element. This is satisfied by choosing polynomials for the displacement model.

(b) The shape functions are capable of representing rigid body displacements of the element. This is met by use of the constant terms in the polynomials.

(c) The shape functions are capable of representing constant strain states within the element. For one, two and three dimensional elasticity problems, the linear terms present in the polynomial satisfy this requirement.

A3.2 Compatibility

The displacements must be compatible between adjacent elements. When the elements deform, there must not be any discontinuity between elements. Elements must not overlap or separate. In the case of beam or shell elements, there should be no sudden changes in slope across the inter-element boundaries.

A3.3 Geometric Invariance

Besides the requirements stated above, the shape functions are so chosen that the element has no preferred direction. That is, that the shape functions will not change with a change in the local coordinate system. This is geometric invariance. Geometric invariance is met if the polynomial includes all the terms. However, if all the terms can not be included in the shape functions, invariance can be achieved by balancing the polynomial. Considering the variables u = u (x,y,z) below, the choice of the polynomial given by;

$$u = b_1 + b_2 x + b_3 y + b_4 z \qquad \text{(A1.2)}$$

meets the three requirements if we consider only one degree of freedom at a node.

A4 Coordinate Systems

All finite element solutions require the evaluation of integrals. Many of these are difficult to evaluate analytically so that numerical techniques are employed. The evaluation can be simplified by changing the limits of integration, i.e., expressing the integral in a local natural coordinate system. A local coordinate system is only defined for the element and not for the whole domain. A natural coordinate system is a local system in which a point within an element is expressed by dimensionless sets of numbers whose magnitude never exceed unity. This system is so defined that the nodal points have unit magnitude or zero. This is to facilitate the integration.

For plane linear triangular elements, the relationship between the natural and global coordinates is given by;

$$\begin{bmatrix} 1 \\ x \\ y \end{bmatrix} = \begin{bmatrix} 1 & 1 & 1 \\ x_1 & x_2 & x_3 \\ y_1 & y_2 & y_3 \end{bmatrix} \begin{bmatrix} L_1 \\ L_2 \\ L_3 \end{bmatrix} \quad \text{(A1.3)}$$

L_i (i=1, 3) are area coordinates and X_i, Y_i are the global positions. For three dimensional tetrahedral element, the relationship is given by;

$$\begin{bmatrix} 1 \\ x \\ y \\ z \end{bmatrix} = \begin{bmatrix} 1 & 1 & 1 & 1 \\ x_1 & x_2 & x_3 & x_4 \\ y_1 & y_2 & y_3 & y_4 \\ z_1 & z_2 & z_3 & z_4 \end{bmatrix} \begin{bmatrix} L_1 \\ L_2 \\ L_3 \\ L_4 \end{bmatrix} \quad \text{(A1.4)}$$

where L_i (i=1,4) are volume coordinates and x_i , y_i , z_i are global positions.

For plane rectangular elements, the natural coordinates are ξ and η. The shape functions for a linear element expressed in this natural coordinate system are:

$$\Psi_i = (1+\xi_i \xi)(1+\eta_i \eta)/4 \quad i = 1, 4 \quad \text{(A1.5)}$$

where, ξ_i is the value of ξ at i,

η_i is the value of η at i.

Similarly, for three dimensional cuboid linear element, the coordinates are ξ, η and ζ. The shape functions are:

$$\Psi_i = (1+\xi_i \xi)(1+\eta_i \eta)(1+\zeta_i \zeta)/8 \quad i = 1, 8 \quad \text{(A1.6)}$$

A5 Element Shapes and Types

In three dimensional elasticity, the elements used are grouped in three families:

A5.1 Tetrahedron

These may be four node (linear), ten node (quadratic) or twenty node (cubic). The terms

linear, quadratic and cubic indicate the degree of the polynomial used to approximate the shape functions. The main disadvantage of the tetrahedral family is that:

(a) It requires small and costly subdivision.

(b) The division of a space volume into individual tetrahedron sometimes presents difficulties in visualization and could lead to errors in nodal numbering and element connectivity in data preparation.

A5.2 Triangular Prism

These may be six noded (linear), fifteen noded (quadratic) or twenty-four noded (cubic). For the six node prism, the polynomial function in natural curvilinear coordinates ξ, η, ζ describing the geometry and the variation of displacement over the element is:

$$[\Psi] = [1, \xi, \eta, \zeta, \zeta\eta, \eta\xi] \qquad \text{(A1.7)}$$

For the fifteen node prism, the polynomial function is;

$$[\Psi] = \{1, \xi, \eta, \zeta, \xi\eta, \zeta\xi, \zeta\eta, \xi\eta^2, \xi^2\eta, \zeta\xi^2, \zeta^2\xi, \eta\xi^3, \xi\eta\eta^3, \xi^3\zeta, \zeta^3\xi\} \qquad \text{(A1.8)}$$

A5.3 Hexahedral Elements

These may be eight node (linear) or twenty node (quadratic). The polynomial for the eight node linear element is:

$$[\Psi] = [1, \xi, \eta, \zeta, \xi\eta, \zeta\xi, \zeta\eta, \zeta\eta\zeta] \qquad \text{(A1.9)}$$

and for the twenty node element is:

$$[\Psi] = [1, \xi, \eta, \zeta, \xi\eta, \zeta\xi, \zeta\eta, \zeta\eta\xi, \xi^2, \eta^2, \zeta^2, \xi^2\eta, \eta^2\zeta, \zeta^2\xi, \eta^2\xi, \xi\eta^3, \xi^3\zeta, \xi^2\eta, \eta^2\zeta, \zeta^2\xi, \eta^2\zeta, \xi^2\zeta, \eta^2\zeta^2, \zeta\xi\eta^2, \xi\eta\zeta^2, \zeta\eta\xi\} \qquad \text{(A1.10)}$$

The polynomial selected depends on the accuracy required. Elements with polynomials of degree greater than one and with curved boundaries are called higher order elements. The higher the degree, the more accurate the approximation but the more costly it is due to

computation time.

A6 Isoparametric Elements

The isoparametric elements may have curved edges and faces in the two and three dimensional cases. The dependent variable, u, is approximated by the expression:

$$u = \sum_{i=1}^{n} U_i \Psi_i \qquad \text{(A1.11)}$$

Thus u is approximated by shape functions of degree (n-1). In general, the degree of approximation used to describe the coordinate transformation, i.e.,

$$x = \sum_{i=1}^{r} X_i \Psi_i(\xi) \qquad \text{(A1.12)}$$

is equal to the degree of approximation for the dependent variable. This means that two independent sets of nodes can exist for a region. One set of nodes for the coordinate transformation, which describes the shape of the element and the second set of nodes for the interpolation of the dependent variable. The elements may then be grouped as:

(a) Subparametric: $r < n$.

(b) Isoparametric: $r = n$.

(c) Superparametric: $r > n$.

The isoparametric elements are most commonly used due to ease and efficiency of calculation in the finite element implementation. The geometry of the isoparametric element is described by:

$$\begin{bmatrix} x \\ y \\ z \end{bmatrix} = \sum_{i=1}^{n} [\Psi_i] \begin{bmatrix} x_i \\ y_i \\ z_i \end{bmatrix} \qquad \text{(A1.13)}$$

where x_i , y_i and z_i are the global coordinates of node i. The variation of the displacement

inside the element can be expressed by using the same shape functions as:

$$\begin{bmatrix} u \\ v \\ w \end{bmatrix} = \sum_{i=1}^{n} [\Psi_i] \begin{bmatrix} u_i \\ v_i \\ w_i \end{bmatrix} \qquad \text{(A1.14)}$$

The shape functions Ψi are called Lagrangian family of interpolation functions because they satisfy the requirements that:

$$\Psi_i(\xi_i) = \begin{cases} 1 & \text{if } i = j \\ 0 & \text{if } i \neq j \end{cases} \qquad \text{(A1.15)}$$

The associated elements are said to belong to the Lagrangian family of finite elements.

The isoparametric concept is very useful because it facilitates an accurate representation of irregular domains. However, the use of curvilinear isoparametric elements makes it difficult to compute the element coefficient matrices and column vectors directly in terms of the global coordinates x, y and z. This is overcome by introducing an invertible transformation between a curvilinear element Ω^*, and a master element $\Omega^{\sim}$, of simple shape that facilitates numerical integration of element equations. The coordinate of the master element are chosen to be the natural coordinates (ξ, η, ζ), such that $-1 \leq (\xi, \eta, \zeta) \leq 1$. By using isoparametric elements, we are able to discretize the irregular domain using few curved elements instead of many straight sided elements. This of course reduces computational effort. The transformation between the elements Ω^* and $\Omega^{\sim}$ is given by the expressions below:

$$\begin{bmatrix} dx \\ dy \\ dz \end{bmatrix} = \begin{bmatrix} \frac{\partial x}{\partial \xi} & \frac{\partial x}{\partial \eta} & \frac{\partial x}{\partial \zeta} \\ \frac{\partial y}{\partial \xi} & \frac{\partial y}{\partial \eta} & \frac{\partial y}{\partial \zeta} \\ \frac{\partial z}{\partial \xi} & \frac{\partial z}{\partial \eta} & \frac{\partial z}{\partial \zeta} \end{bmatrix} \begin{bmatrix} d\xi \\ d\eta \\ d\zeta \end{bmatrix} \qquad \text{(A1.16)}$$

$$\begin{bmatrix} dx \\ dy \\ dz \end{bmatrix} = [J]^T \begin{bmatrix} d\xi \\ d\eta \\ d\zeta \end{bmatrix} \qquad \text{(A1.17)}$$

Where J is the Jacobian of the transformation,

$$x = x(\xi, \eta, \zeta),\ y = y(\xi, \eta, \zeta),\ z = z(\xi, \eta, \zeta) \qquad \text{(A1.18)}$$

The Jacobian can be expressed in terms of the curvilinear coordinates as:

$$\begin{bmatrix} dx \\ dy \\ dz \end{bmatrix} = \begin{bmatrix} \sum x_i \frac{\partial \Psi_i}{\partial \xi} & \sum x_i \frac{\partial \Psi_i}{\partial \eta} & \sum x_i \frac{\partial \Psi_i}{\partial \zeta} \\ \sum y_i \frac{\partial \Psi_i}{\partial \xi} & \sum y_i \frac{\partial \Psi_i}{\partial \eta} & \sum y_i \frac{\partial \Psi_i}{\partial \zeta} \\ \sum z_i \frac{\partial \Psi_i}{\partial \xi} & \sum z_i \frac{\partial \Psi_i}{\partial \eta} & \sum z_i \frac{\partial \Psi_i}{\partial \zeta} \end{bmatrix} \begin{bmatrix} d\xi \\ d\eta \\ d\zeta \end{bmatrix} \qquad \text{(A1.19)}$$

The coefficient matrix is the Jacobian whose elements vary from point to point.

$$[J] = \begin{bmatrix} \frac{\partial \Psi_1}{\partial \xi} & \frac{\partial \Psi_2}{\partial \xi} & \cdots \\ \frac{\partial \Psi_1}{\partial \eta} & \frac{\partial \Psi_2}{\partial \eta} & \cdots \\ \frac{\partial \Psi_1}{\partial \zeta} & \frac{\partial \Psi_2}{\partial \zeta} & \cdots \end{bmatrix} \begin{bmatrix} x_1 & y_1 & z_1 \\ x_2 & y_2 & z_2 \\ \cdot & \cdot & \cdot \\ \cdot & \cdot & \cdot \\ \cdot & \cdot & \cdot \end{bmatrix} \qquad \text{(A1.20)}$$

Equation (A1.16) represents a linear transformation of line elements $d\xi$, $d\eta$ and $d\zeta$ in the master element Ω^- into line elements dx, dy and dz in the curvilinear element, Ω^*. Hence any curved or distorted element with known global nodal coordinates may be transformed into the master element. The element equations are then evaluated and later transformed back to the global coordinates. There are several conditions to be observed in the use of isoparametric elements:

(a) The coordinate change and its derivatives must be easily compatible.

(b) The change must not distort the elements excessively as excessive distortion

destroys the accuracy built into the polynomial element or the Jacobian determinant may vanish in the region of integration.

(c) The coordinate changes should be uniformly smooth so as to preserve the approximation theory. This should be so because the polynomials in the new variables do not correspond to those in the old system.

(d) In order to preserve global continuity, the conformal mapping must be one to one.

A7 Elasticity Problems

The state of stress at a point is defined by six components expressed as:

$$\{\sigma\}^T = \{ \sigma_{xx} \ \sigma_{yy} \ \sigma_{zz} \ \tau_{xy} \ \tau_{yz} \ \tau_{zx}\} \qquad \text{(A1.21)}$$

These stress components are produced by internal forces that counteract the externally applied forces. The application of forces to a solid body causes the body to deform and each point in the body moves to a new location. The resultant displacement has three components u, v and w parallel to the x, y and z-axes respectively. From the displacements, the resulting state of strain is expressed as:

$$\{ \varepsilon \}^T = \{ \varepsilon_{xx} \ \varepsilon_{yy} \ \varepsilon_{zz} \ \gamma_{xy} \ \gamma_{yz} \ \gamma_{zx}\} \qquad \text{(A1.22)}$$

The stress and strain components are related by a set of coefficients known as the generalized Hooke's law.

$$\{ \sigma \} = [D] \{ \varepsilon \} \qquad \text{(A1.23)}$$

The coefficients of [D] are given by:

$$[D] = \frac{E}{1+\nu}\begin{bmatrix} f & b & b & 0 & 0 & 0 \\ b & f & b & 0 & 0 & 0 \\ b & b & f & 0 & 0 & 0 \\ 0 & 0 & 0 & c & 0 & 0 \\ 0 & 0 & 0 & 0 & c & 0 \\ 0 & 0 & 0 & 0 & 0 & c \end{bmatrix} \qquad \text{(A1.24)}$$

where, $f = (1-\nu)/(1-2\nu)$; $b = \nu/(1-2\nu)$; and $c = 1/2$.

Each displacement component of each point is a function of three coordinate directions, that is,

$$u = f(x,y,z),\ v = g(x,y,z) \text{ and } w = h(x,y,z) \qquad \text{(A1.25)}$$

The objective of the finite element analysis is to determine the equations above. The finite element approximations for these functions are continuous, piecewise smooth equations defined over the individual elements. The displacement equations are then expressed as:

$$\begin{bmatrix} u \\ v \\ w \end{bmatrix} = [\Psi]\{U^e\} \qquad \text{(A1.26)}$$

Where $\{ U^e \}$ is a column vector containing the element nodal displacements and the matrix given by $[\Psi]$ contains the element shape functions. $[\Psi]$ has three rows and as many columns as there are components in $\{ U^e \}$, i.e., the number of nodes in the element. The strain components in $\{ \varepsilon \}$ and the displacements are related through the strain-displacement equations below:

$$\left.\begin{aligned} \varepsilon_{xx} &= \frac{\partial u}{\partial x}, \quad \varepsilon_{yy} = \frac{\partial v}{\partial y}, \quad \varepsilon_{zz} = \frac{\partial w}{\partial z} \\ \gamma_{xy} &= \frac{\partial u}{\partial y} + \frac{\partial v}{\partial x}, \quad \gamma_{xz} = \frac{\partial u}{\partial z} + \frac{\partial w}{\partial x}, \quad \gamma_{yz} = \frac{\partial v}{\partial z} + \frac{\partial w}{\partial y} \end{aligned}\right\} \qquad \text{(A1.27)}$$

and in a matrix form;

$$\begin{bmatrix} \varepsilon_{xx} \\ \varepsilon_{yy} \\ \varepsilon_{zz} \\ \gamma_{xy} \\ \gamma_{yz} \\ \gamma_{xz} \end{bmatrix} = \begin{bmatrix} \frac{\partial}{\partial x} & 0 & 0 \\ 0 & \frac{\partial}{\partial y} & 0 \\ 0 & 0 & \frac{\partial}{\partial z} \\ \frac{\partial}{\partial y} & \frac{\partial}{\partial x} & 0 \\ 0 & \frac{\partial}{\partial z} & \frac{\partial}{\partial y} \\ \frac{\partial}{\partial z} & 0 & \frac{\partial}{\partial x} \end{bmatrix} \begin{bmatrix} u \\ v \\ w \end{bmatrix} \qquad \text{(A1.28)}$$

$$\{ \varepsilon \} = [B] \{ U^e \} \qquad \text{(A1.29)}$$

The matrix [B] has six rows and as many columns as there are rows in $\{ U^e \}$.

The element stiffness matrix and the element force vector are the elements contribution to the system of equations that result when the potential energy is minimized. The potential energy consists of the strain energy in the system minus the work done by the forces acting on the system. The strain energy in a three dimensional body is given by:

$$\Lambda^E = 0.5 \iiint_V [\sigma_{xx}\varepsilon_{xx} + \sigma_{yy}\varepsilon_{yy} + \sigma_{zz}\varepsilon_{zz} + \sigma_{xy}\gamma_{xy} + \sigma_{xz}\gamma_{xz} + \sigma_{yz}\gamma_{yz}] dv \qquad \text{(A1.30)}$$

$$\Lambda^E = 0.5 \iiint_V [\sigma]^T [\varepsilon] \, dv \qquad \text{(A1.31)}$$

$$\Lambda^E = 0.5 \iiint_V [\varepsilon]^T [D] [\varepsilon] \, dv \qquad \text{(A1.32)}$$

expressing the above equations in terms of displacements,

$$\Lambda^E = 0.5 \int_V [U^e]^T [B][D][B][U^e]\, dv \qquad \text{(A1.33)}$$

Ignoring body forces and concentrated forces, the work done by distributed loads that act on the surface is:

$$W^E = \int_\Gamma (u P_x + v P_y + w P_z)\, d\Gamma \qquad \text{(A1.34)}$$

Where P_x, P_y and P_z are the force components parallel to the x, y and z coordinate directions. $d\Gamma$ is the surface element.

$$W^E = \int_\Gamma [U^e]^T [\Psi]^T \begin{bmatrix} P_x \\ P_y \\ P_z \end{bmatrix} d\Gamma \qquad \text{(A1.35)}$$

From the above equations, it can be shown that the element stiffness matrix is given by [86].

$$[K^e] = \int_v [B][D][B]\, dv \qquad \text{(A1.36)}$$

And the element force vector is given by:

$$\{f^e\} = \int_\Gamma [N]^T \begin{bmatrix} P_x \\ P_y \\ P_z \end{bmatrix} d\Gamma \qquad \text{(A1.37)}$$

The surface element $d\Gamma$ will generally lie on a surface where one of the coordinates is constant, say, ζ. $d\Gamma$ may conveniently be assigned as a vector oriented in the direction normal to the surface. For three dimensional problems,

$$d\Gamma = \begin{bmatrix} \frac{\partial x}{\partial \xi} \\ \frac{\partial y}{\partial \xi} \\ \frac{\partial z}{\partial \xi} \end{bmatrix} X \begin{bmatrix} \frac{\partial x}{\partial \eta} \\ \frac{\partial y}{\partial \eta} \\ \frac{\partial z}{\partial \eta} \end{bmatrix} d\xi\, d\eta \qquad \text{(A1.38)}$$

$$d\Gamma = \begin{bmatrix} \frac{\partial x}{\partial \xi} \\ \frac{\partial y}{\partial \xi} \end{bmatrix} X \begin{bmatrix} \frac{\partial x}{\partial \eta} \\ \frac{\partial y}{\partial \eta} \end{bmatrix} d\xi\, d\eta \qquad \text{(A1.39)}$$

The stiffness matrix is evaluated in the natural coordinate system as;

$$[K^e] = \int_{-1}^{1}\int_{-1}^{1}\int_{-1}^{1} [B]^T [D][B]\, d\xi\, d\eta\, d\zeta \qquad \text{(A1.40)}$$

The numerical integration is done using the Gauss-Legendre quadrature rules.

A8 Finite Element Method in Elastoplastic Problems

Different kinds of materials exhibit different elastoplastic characteristics. The Tresca's and von Mises laws closely approximate metal plasticity behaviour while Mohr-Coulomb and Drucker-Prager criteria are applicable to concrete, rocks and soils. The mathematical theory of plasticity provides a theoretical description of the relationship between stress and strain for a material which exhibits an elastoplastic response. Plastic behaviour is characterised by an irreversible straining which is not time dependent and which can only be sustained once a certain level of stress has been reached. To formulate a theory which models elastoplastic material deformation, we need:

(a) An explicit relationship between stress and strain to describe material behaviour under elastic conditions.

(b) A yield criterion indicating the stress level at which plastic flow commences.

(c) A relationship between stress and strain for the post yield behaviour when the

deformation is made up of both elastic and plastic components.

For most metals, von Mises law fits the experimental data more closely than Tresca's law, though the Tresca's law is simpler to use in theoretical application.

All the steps observed in the elastic analysis are also observed in the elastoplastic analysis. The elastoplastic structural situations are included in the solution of non-linear finite element problems. The two main types of non-linear problems are those where the magnitude of the stresses, displacements velocities, etc., are sufficient to alter the nature of the constitutive relationship or to make non-linear terms in the governing strain displacement relationship or differential equation significant. In mechanics of solids, these are the non-linear material (constitutive) and large displacement problems.

With the non-linear materials, Hooke's law is no longer valid but it is possible to obtain a relationship between small increments of stress and strain:

$$d(\sigma)=D_T\, d(\varepsilon) \tag{A1.41}$$

Where large geometry changes occur, strains become non-linear relationships of displacement or displacement gradients, given by:

$$\varepsilon_x=\frac{\partial u}{\partial x}+\frac{1}{2}\left[\left(\frac{\partial u}{\partial x}\right)^2+\left(\frac{\partial v}{\partial x}\right)^2+\left(\frac{\partial w}{\partial x}\right)^2\right] \tag{A1.42}$$

$$\varepsilon_y=\frac{\partial v}{\partial y}+\frac{1}{2}\left[\left(\frac{\partial u}{\partial y}\right)^2+\left(\frac{\partial v}{\partial y}\right)^2+\left(\frac{\partial w}{\partial y}\right)^2\right] \tag{A1.43}$$

$$\varepsilon_z=\frac{\partial w}{\partial z}+\frac{1}{2}\left[\left(\frac{\partial u}{\partial z}\right)^2+\left(\frac{\partial v}{\partial z}\right)^2+\left(\frac{\partial w}{\partial z}\right)^2\right] \tag{A1.44}$$

$$\varepsilon_{xy}=\frac{\partial u}{\partial y}+\frac{\partial v}{\partial x}+\frac{1}{2}\left[\frac{\partial u}{\partial x}\frac{\partial u}{\partial y}+\frac{\partial v}{\partial x}\frac{\partial v}{\partial y}+\frac{\partial w}{\partial x}\frac{\partial w}{\partial y}\right] \tag{A1.45}$$

$$\varepsilon_{yz}=\frac{\partial v}{\partial z}+\frac{\partial w}{\partial y}+\frac{1}{2}\left[\frac{\partial u}{\partial y}\frac{\partial u}{\partial z}+\frac{\partial v}{\partial y}\frac{\partial v}{\partial z}+\frac{\partial w}{\partial y}\frac{\partial w}{\partial z}\right] \quad \text{(A1.46)}$$

$$\varepsilon_{zx}=\frac{\partial u}{\partial z}+\frac{\partial w}{\partial x}+\frac{1}{2}\left[\frac{\partial u}{\partial z}\frac{\partial u}{\partial x}+\frac{\partial v}{\partial z}\frac{\partial v}{\partial x}+\frac{\partial w}{\partial z}\frac{\partial w}{\partial x}\right] \quad \text{(A1.47)}$$

The existence of non-linear terms causes a non-linear relationship between loads and displacements in the displacement finite element method even when the material obeys Hooke's law. Formulation of problems involving the non-linear effects may be approached by the theorem of virtual work:

$$\int(\delta\varepsilon')(\sigma)dV-\int(\delta\bar{u})(T)d\Gamma=0 \quad \text{(A1.48)}$$

Introducing the finite element approximations:

$$\sum\int B'\{\sigma\}dV=\int F\{T\}d\Gamma\sum\{q_i\} \quad \text{(A1.49)}$$

If the system is not in equilibrium,

$$\sum\int B'\{\sigma\}\,dV=\sum\{q_i\}=\{R\} \quad \text{(A1.50)}$$

where $\{\sigma\}=\{\sigma(\{\varepsilon\})\}$ are the non-linear functions of strain.

The non-linear finite element problems can be exactly solved by calculating the left hand integral of equation A1.50, the element reactions at each step of an iterative procedure until the residual loads vanish. This method is called the equilibrium iteration. Another useful method is the load stepping or Euler's method. While the equilibrium iteration involves application of the total load in one step and iterating till convergence of the residual loads, the load stepping method involves application of small loads such that;

$$\{Q_n\} = \sum_{i=1}^{n} \{\delta q_i\} \qquad \text{(A1.51)}$$

A9 Non Linear Materials

The behaviour of non-linear materials under three dimensional stress is described by calculating some stress, strain or energy quantity and equating this to a limiting yield or fracture value of this, observed at a stress level Y_s (yield), F_t (tensile cracking) or F_c (compressive crushing).

One of the most widely used is the von Mises criterion, limiting the distortion energy, which is obtained by subtracting the strain energy of the isotropic component from the total strain energy;

$$\sigma_1^2 + \sigma_2^2 + \sigma_3^2 - \sigma_1\sigma_2 - \sigma_2\sigma_3 - \sigma_3\sigma_1 = F_y^2 \qquad \text{(A1.52)}$$

To derive the plastic stress-strain matrix, some fundamental assumptions are made:

(1) In uniaxial stress states, the material obeys Hooke's law. In an elastic perfectly plastic material, the Tangent Modulus (H') after yielding is zero.

(2) Prior to yield, the material is elastic, frequently being assumed to obey Hooke's law both on loading and unloading as shown in figure A1.1.

(3) Under multiaxial stress states, it is useful to take the view that there exists an equivalent uniaxial stress $\sigma^* = f(\{\sigma\})$ such that yielding occurs when; $\sigma^* = Y_S$, the yield stress in uniaxial tension.

(4) In a strain hardening material, the stress level is regarded as a function of the plastic work, $W_p = \{\sigma\}^t \{\varepsilon^p\}$ and the strain hardening takes place whenever plastic work is done on the material.

(5) In the post-yield range, the plastic strains are usually regarded as not recoverable so that stress-strain laws in the plastic range are of necessity incremental in nature.

(6) Plastic strains are usually assumed to be unaffected by the hydrostatic stress components, that is, they are related only to the deviatoric components of the

direct stresses and to the shear stresses.

(7) When the stress state moves from point P to P_2, as in figure A1.2, it can do so via P_1, by elastic unloading and re-loading followed by plastic strain under constant stress conditions at P_2. Thus in general strain increments are given by; $\{d\varepsilon\} = \{d\varepsilon_e\} + \{d\varepsilon_p\}$, where $\{d\varepsilon_e\}$ and $\{d\varepsilon_p\}$ are the elastic and plastic increments respectively. This is the partition hypothesis.

(8) As plastic strain increments involve less strain energy than partially elastic increments, it is postulated that plastic increments occur normal to the yield surface. This follows from the method of steepest descent where in unconstrained minimization problems, $-\{\partial f/\partial x_i\}$, that is normal to the contours $f(x) = \text{constant}$.

(9) It follows from (8) that the progression past the yield surface $d\sigma_p^*$ is given by;

$$d\sigma_p^* = \{\partial f/\partial \sigma\}^t \{d\sigma\} = F^t \{d\sigma\} \qquad \text{(A1.53)}$$

where $f(\{\sigma\})$ defines the equivalent uniaxial stress σ^* and, as it is obtained from yield criteria, also defines the shape of the yield surface. $\{\partial f/\partial \sigma\}$ denotes the vector formed by differentiating this function with respect to each stress component in turn.

(10) The plastic strain increments are often assumed to be given by;

$$\{d\varepsilon_p\} = F\, d\varepsilon_p^* \qquad \text{(A1.54)}$$

where $d\varepsilon_p^*$ corresponds to $d\sigma_p^*$ and this is called the associated flow rule.

(11) If the material strain hardens, as in figure A1.3, it is usual to assume that the size of the yield surface increases but it does not change in shape and this is referred to as isotropic hardening.

The derived plastic constitutive stress-strain matrix can be simplified as;

$$[D^p]=\frac{2G}{\frac{2}{3}(\bar{\sigma})^2\left(1+\frac{H'}{3G}\right)}\begin{bmatrix} \sigma_{Dx}^2 & \sigma_{Dx}\sigma_{Dy} & \sigma_{Dx}\sigma_{Dz} & \sigma_{Dx}\tau_{xy} & \sigma_{Dx}\tau_{yz} & \sigma_{Dx}\tau_{xz} \\ \sigma_{Dx}\sigma_{Dy} & \sigma_{Dy}^2 & \sigma_{Dy}\sigma_{Dz} & \sigma_{Dy}\tau_{xy} & \sigma_{Dy}\tau_{yz} & \sigma_{Dy}\tau_{xz} \\ \sigma_{Dx}\sigma_{Dz} & \sigma_{Dy}\sigma_{Dz} & \sigma_{Dz}^2 & \sigma_{Dz}\tau_{xy} & \sigma_{Dz}\tau_{yz} & \sigma_{Dz}\tau_{xz} \\ \sigma_{Dx}\tau_{xy} & \sigma_{Dy}\tau_{xy} & \sigma_{Dz}\tau_{xy} & \tau_{xy}^2 & \tau_{xy}\tau_{yz} & \tau_{xy}\tau_{xz} \\ \sigma_{Dx}\tau_{yz} & \sigma_{Dy}\tau_{yz} & \sigma_{Dz}\tau_{yz} & \tau_{xy}\tau_{yz} & \tau_{yz}^2 & \tau_{yz}\tau_{xz} \\ \sigma_{Dx}\tau_{xz} & \sigma_{Dy}\tau_{xz} & \sigma_{Dz}\tau_{xz} & \tau_{xy}\tau_{xz} & \tau_{yz}\tau_{xz} & \tau_{xz}^2 \end{bmatrix}$$

.....(A1.55)

where; $H' = \dfrac{d\,\bar{\sigma}}{d\,\bar{\varepsilon}^{\,p}}$ is the slope of the curve relating effective stress $\bar{\sigma}$ and the effective plastic strain given as; $\int d\bar{\varepsilon}^{p}$

Using the von Mises law,

$$\bar{\sigma}=\frac{1}{\sqrt{2}}\left[(\sigma_1-\sigma_2)^2+(\sigma_2-\sigma_3)^2+(\sigma_3-\sigma_1)^2\right]^{\frac{1}{2}} \qquad \text{(A1.56)}$$

$$\bar{\varepsilon}=\frac{\sqrt{2}}{2}\left[(\varepsilon_1-\varepsilon_2)^2+(\varepsilon_2-\varepsilon_3)^2+(\varepsilon_3-\varepsilon_1)^2\right]^{\frac{1}{2}} \qquad \text{(A1.57)}$$

and $\{\sigma_D\}=\{\sigma_x-J_1/3,\ \sigma_y-J_1/3,\ \sigma_z-J_1/3,\ \tau_{xy},\tau_{yz},\tau_{xz}\}$ (A1.58)

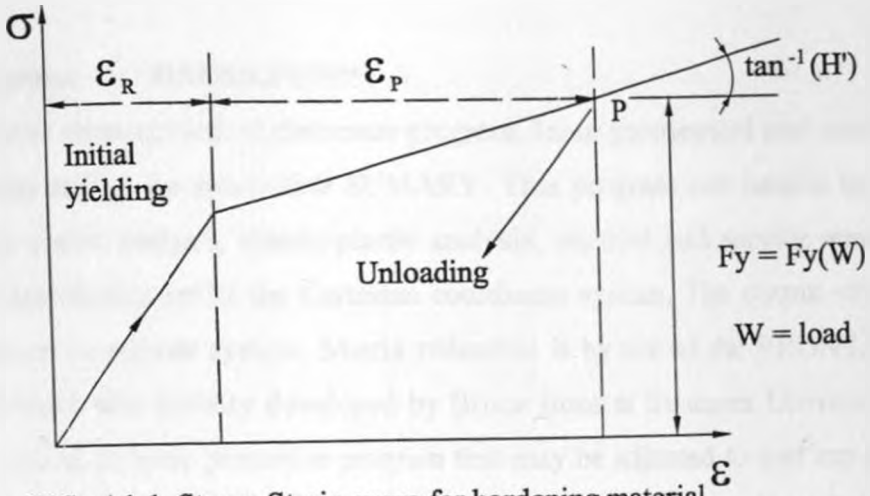

FIG. A1.1 Stress-Strain curve for hardening material.

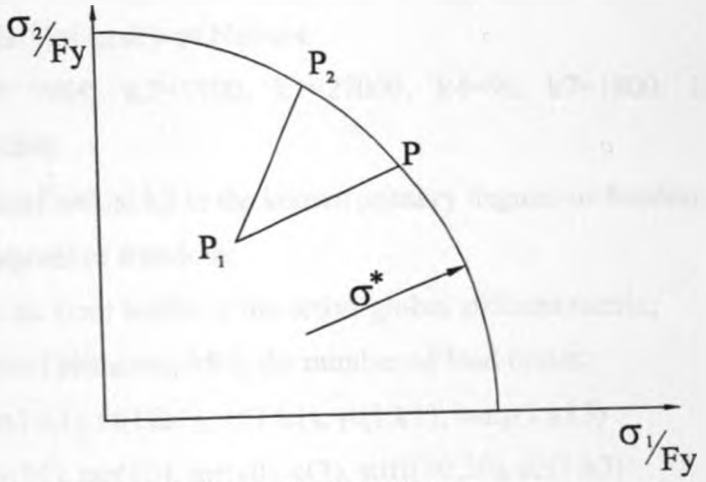

FIG. A1.2 Perfectly plastic behaviour.

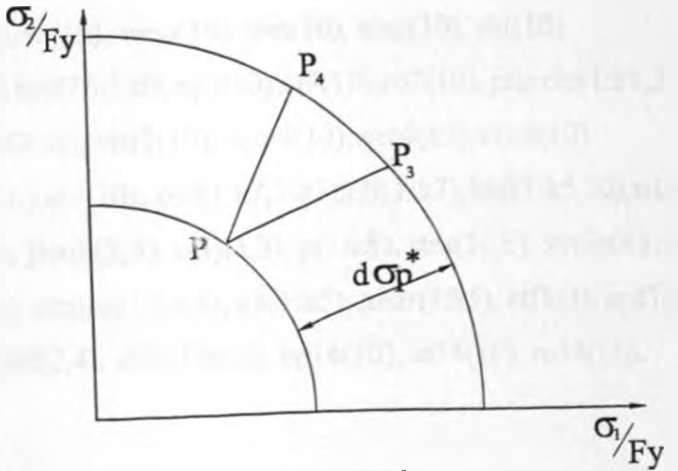

FIG. A1.3 Strain hardening behaviour.

APPENDIX II

PROGRAM LISTING

Main Program: GAUSS.FOR™

This is a finite element method processor program. Input geometrical and material data is read through calling the subroutine SUMARY. This program can handle the following cases: pure elastic analysis, elastic-plastic analysis, residual and service stress analysis. The input coordinates are in the Cartesian coordinate system. The output stresses are in the cylindrical coordinate system. Matrix reduction is by use of the FRONTAL solution technique which was initially developed by Bruce Irons at Swansea University in 1970. This is a general-purpose processor program that may be adjusted to suit any geometrical problem with very minor additions. This program was developed by ***Eng. John M. Kihiu*** while carrying out stress analysis research leading to Ph.D. degree in mechanical engineering at the University of Nairobi.

Parameter (k1= 9000, k2=1700, k3=27000, k4=90, k7=1800, k5=8500, k8=200, K12=350, k15=200)

k1 is the number of nodes; k2 is the known primary degrees of freedom;

k3 is the total degrees of freedom;

k7 is the maximum front width of the active global stiffness matrix;

k5 is the number of elements; k8 is the number of load cycles;

real rt(1:k1), tht(1:k1), zt(1:k1), xt(1:k1), yt(1:k1), bang(1:k15)

real mx(10), my(10), mz(10), mr(10), c(3), stiff(30,30), u2(1:k3)

real x1(10,3), dsf(3,10), bb(6,30), cyl(1:k1,6), d(6,6), a(3),b(3), s(1:k7)

real u10(30), sigma(10,6), stress(1:k1,6), str(1:k5,6), mu

real ep(10), et(10), ro(10), wep(10), wet(10), wro(10), det(10)

real dispinc(1:k3),epz(1:k1,6), ep3(10),et3(10),ro3(10), princip(1:k1,3)

real wep3(10),wet3(10),wro3(10), wep4(10),wet4(10),wro4(10)

real ep4(10),et4(10),ro4(10), ovf(1:k7,1:k7),elf(1:k7),forf(1:k5,30),u1(1:k7)

real strain(1:k5,6), jacob(3,3), invj(3,3), p(1:k8), stra(10,6), strain0(1:k5,6)

real strenc(1:k5,6), strainc(1:k5,6), y3(1:k5), hbar(1:k5), etf1(4), epf1(4)

real shape1(4), dsff(2,4), str0(1:k5,6), ep14(10), et14(10), ro14(10).

```
real wep14(10),wro14(10), xy(4,2), volu(1:k5),el14(10),wel14(10),wet14(10)
integer con(1:k5,10),dk(1:k1,60),lenn(1:k1),itype(1:k5),lnon(4)
integer nload(1:k15,1:k15), nhoriz(1:k15), bcircle(1:k15), bxd, ivert(1:k5)
integer nmerid(1:k15), xmerid(1:k15), ncircle(1:k15), kpdof(1:k2),nyield(1:k5)
integer beh, ber, ile(1:k5), Nend(1:k5), nvert(1:k9), lastY(1:k15), brd, ibrd(30,30)
integer eldest(1:k5,10), ndest(1:k1), nface2f(4), npr(1:k9), npre(1:k9), ltr22(4)
integer Ltr2(2,3), ltr3n(2,3),ltr3nB(6), mt3(1,3), lend(2,3),lend1(4), mark(1:k5),ely
data (ep14(i),i=1,6)/.5,0,.5,.5,0,.5/
data (et14(i),i=1,6)/.5,.5,0,.5,.5,0/
data (el14(i),i=1,6)/0,.5,.5,0,.5,.5/
data (ro14(i),i=1,6)/3*-.57735,3*.57735/
data (wep14(i),i=1,6)/6*.3333/
data (wet14(i),i=1,6)/6*.3333/
data (wel14(i),i=1,6)/6*.3333/
data (wro14(i),i=1,6)/6*1/
data (epf1(i),i=1,4)/-.57735,2*.57735,-.57735/
data (etf1(i),i=1,4)/2*-.57735,2*.57735/
data (ep(i),i=1,8)/-.57735,2*.57735,2*-.57735, 2*.57735,-.57735/
data (et(i),i=1,8)/2*-.57735,2*.57735, 2*-.57735,2*.57735/
data (ro(i),i=1,8)/4*-.57735,4*.57735/
data (wep(i),i=1,8)/1,1,1,1,1,1,1,1/
data (wet(i),i=1,8)/1,1,1,1,1,1,1,1/
data (wro(i),i=1,8)/1,1,1,1,1,1,1,1/
data (ep3(i),i=1,10)/-.57735,2*.57735,-.57735, .57735,-.57735,2*.57735,-.57735,.57735/
data (et3(i),i=1,10)/2*-.57735,3*.57735, 2*-.57735,3*.57735/
data (ro3(i),i=1,10)/5*-.57735,5*.57735/
data (wep3(i),i=1,10)/10*1/
data (wet3(i),i=1,10)/10*1/
data (wro3(i),i=1,10)/10*1/
data (ep4(i),i=1,10)/-.57735,2*.57735,3*-.57735, 2*.57735,2*-.57735/
data (et4(i),i=1,10)/2*-.57735,3*.57735, 2*-.57735,3*.57735/
```

```
data (ro4(i),i=1,10)/5*-.57735,5*.57735/
data (wep4(i),i=1,10)/10*1/
data (wet4(i),i=1,10)/10*1/
data (wro4(i),i=1,10)/10*1/
data (nface2f(i),i=1,4)/5,6,7,8/
data ((ltr2(i,j),j=1,3),i=1,2)/4,5,1,4,8,5/
data (ltr22(i),i=1,4)/1,4,8,5/
data ((ltr3n(i,j),j=1,3),i=1,2)/4,3,7,4,7,8/
data (ltr3nb(i),i=1,4)/4,3,7,8/
data ((mt3(i,j),j=1,3),i=1,1)/1,2,3/
data ((lend(i,j),j=1,3),i=1,2)/5,6,7,5,7,8/
data (lend1(i),i=1,4)/5,6,7,8/
```

Program Starts Here

```
t1=secnds(0.0)
suma=0
This subroutinc reads data from the preprocessor
Call    Sumary(itnon,noe,ber,beh,nez,neh,lmerid,lxmerid,
.lload,xt,yt,zt,rt,tht,roc,ric,stv,zs,pi,itype,k5,k1,lnon,con,,nload,nhoriz,nmerid,xmerid,k9,
mark,ile,Nend,,ndof,ni,npipe,kpdof,lastY,nyi,npr,npre,nvert,ncircle,bang,bcircle,bxd,k15,
k2,,brd,nupper,ner,ls1,ibrd,ivert)
This subroutine changes the six noded prism into a tetrahedron if necessary.
call change3(noe,itype,con,k5,k1,zt,rt, lnon,mark,nel,yt,xt,ile,nend,ner,brd,nvert,k9, ivert)
Poissons ratio, mu.3
Young's Modulus, ym=210e3
Yield stress, ys=450
Safety factor, sf=5
Thickness ratio, thr=roc/ric
Yield criterion = von Mises
Internal pressure, press=(ys/sf)*((thr**2-1)/thr**2)*(1/3**.5)
itdof=ndof*itnon
```

```
c      ncase=0!=elastic analysis only|ncase=1!=elasto-plastic analysis
c      nresi=1! Residual stress obtained after ncase=1
c      nresi=0! No Residual stress obtained after ncase=1
c      nreload=1! Reload stress obtained after ncase=1 and nresi=1
c      nreload=0! No reload stress obtained after ncase=1 and nresi=1
c      npipe=1! open pipe! npipe=0! closed cylinder
c      nreel=0! only elastic stress after offloading!=1 reloading fully
       npipe=0
       ncase=1
       nresi=1
       nreload=1
       nreel=0
       ndiv=2
       ElY=nyi-1
c ElY is the yielding element position along the radius
lcount=1 ! counts load cycles
loop=1 ! Counts loop cycles
Lcon=0
c array dk[] has the elements around a node
do 237 i=1,itnon
n3=0
do 238 nel=1,noe
do 239 j=1,lnon(itype(nel))
if(con(nel,j).ne.i)goto 239
n3=n3+1
dk(i,n3)=nel
239 continue
238 continue
lenn(i)=n3
237 continue
call watch(suma,t1,t2)
```

```
Modify connectivity matrix con[  ] to give element and nodal destination vectors.
call prere(itnon,noe,itype,lnon,con,ndest,eldest,maxfw, ovf,elf,k1,k5,k7,ndof)
call watch(suma,t1,t2)
negdis=0
nneg=0
nzrelo=700
nxa=700
nxb=0
nvert=0
513    do 400 nel=1,noe
 400   nyield(nel)=0
 998   do 551 i=1,noe
       do 551 j=1,ndof*lnon(itype(i))
 551   forf(i,j)=0
       do 17 i=1,maxfw
       elf(i)=0
       do 18 j=1,maxfw
       ovf(i,j)=0
  18   continue
  17   continue
Force vector starts here.
       do 126 nel=1,noe
       n3=itype(nel)
       do 26 j=1,ndof*lnon(itype(nel))
       forf(nel,j)=0
  26   continue
       do 22 j=1,lnon(itype(nel))
       n5=abs(con(nel,j))
       mx(j)=xt(n5)
       my(j)=yt(n5)
       mz(j)=zt(n5)
```

```
      mr(j)=rt(n5)
      x1(j,1)=xt(n5)
      x1(j,2)=yt(n5)
      x1(j,3)=zt(n5)
22    continue
      if(ile(nel).eq.1)then
      area1=0
      do 80 na=1,2
      call face2(a,b,mx,my,mz,ltr2,na)
      call norm(c,a,b,area,nel)
      area1=area1+area
80    continue
      for=area1*press/4
      do 63 l=1,4
      n6=ltr22(l)
      call post (k5,nel,c,n6,for,forf)
63    continue
      endif
      if(mark(nel).eq.1)then
      area1=0
      do 205 na=1,2
      call face3N(a,b,mx,my,mz,ltr3N,na)
      call norm(c,a,b,area,nel)
      area1=area1+area
205   continue
      for=area1*press/4
      do 206 l=1,4
      n6=ltr3NB(l)
      call post(k5,nel,c,n6,for,forf)
206   continue
      endif
```

```
      if(npipe.eq.0)then
      if(Nend(nel).eq.1)then
      area1=0
      do 654 na=1,2
      call Enda(a,b,mx,my,mz,lend,na)
      call norm(c,a,b,area,nel)
      area1=area1+area
  654 continue
      for=area1*press/4
      do 655 l=1,4
      n6=lend1(l)
      call post(k5,nel,c,n6,for,forf)
  655 continue
      endif
      endif
  126 continue
  738 format(1x,i4,2x,4(e12.3,2x))
      kfss=0
      nf=0
  992 do 10 nel=1,noe
      n8=itype(nel)
      do 5 i=1,lnon(itype(nel))*ndof
      do 5 j=1,lnon(itype(nel))*ndof
    5 stiff(i,j)=0
      do 13 j=1,lnon(itype(nel))
      n4=abs(con(nel,j))
      x1(j,1)=xt(n4)
      x1(j,2)=yt(n4)
      x1(j,3)=zt(n4)
      mx(j)=xt(n4)
      my(j)=yt(n4)
```

```
      mz(j)=zt(n4)
13    continue

conselast is the elastic constitutive matrix
consplast is the plastic constitutive matrix
      if(nyield(nel).eq.0.or.loop.eq.2) call conselast(d,ym,mu)
      if(nyield(nel).eq.1) call consplast(d,str,nel,k5,mu,ym,y3,hbar)
      if(itype(nel).eq.2) ngt=8
      if(itype(nel).eq.1) ngt=6
      if(itype(nel).eq.3) ngt=1
Obtain the stress-strain matrix and the Jacobian of the transformation
      do 250 m=1,ngt
      if(itype(nel).eq.2) call type2(dsf,m,ep,et,ro)
      if(itype(nel).eq.1) call type14(dsf,ro14,ep14,et14,m,el14)
      if(itype(nel).eq.3)call Shape3(lnon,itype,k5,ndof,bb,volu,nel,mx,my,mz)
      if(itype(nel).ne.3) call jacobi(dsf,x1,bb,nel,det,m,lnon,itype,k5,jacob,invj)
      call stif(d,bb,stiff,det,m,wep,wet,wro,lnon,itype,k5,wep14,wep3,wet3,wro3,
      +wep4,wet4,wro4,wel14,wet14)
      sumd=sumd+det(m)
250   continue
      do 700 nj=1,lnon(itype(nel))
      if(eldest(nel,nj).gt.kfss)then
      kfss=eldest(nel,nj)
      endif
700   continue
      kfs=kfss*ndof
      call assembf(itype,lnon,eldest,nel,ndof,elf,forf,ovf,stiff,k5, k7)
      call elimini(itype,lnon,con,nel,ndest,ndof,ni,kpdof,kfs,ovf,elf,s,k1,k2,k5,k7,nf)
      if(nf.eq.1) then
      call warn2(nel,p,povr,lcount,k8)
      goto 999
```

```
      endif
      call watch(suma,t1,t2)
 10   continue
do the back substitution
      call backsub(itype,lnon,con,noe,eldest,ndof,ni,kpdof, s,maxfw,u1,u2,k2,k3,k5,k7
     +,dispinc,lcount,negdis,loop,itnon)
      if(lcount.gt.1)Rmin=2e7
      if(lcount.eq.1) sigmax=0
      nely=0
      y1sum=0
      do 230 nel=1,noe
      n8=itype(nel)
      do 231 nx=1,lnon(itype(nel))
      ig=abs(con(nel,nx))
      do 553 kl=1,ndof
      ih=ig*ndof-(ndof-kl)
      if(lcount.eq.1) u10(nx*ndof-(ndof-kl))=u2(ih)
      if(lcount.gt.1) u10(nx*ndof-(ndof-kl))=dispinc(ih)
 553  continue
 231  continue
      do 232 j=1,lnon(itype(nel))
      n7=abs(con(nel,j))
      x1(j,1)=xt(n7)
      x1(j,2)=yt(n7)
      x1(j,3)=zt(n7)
      mx(j)=xt(n7)
      my(j)=yt(n7)
      mz(j)=zt(n7)
 232  continue
      if(nyield(nel).eq.0.or.loop.eq.2) call conselast(d,ym,mu)
      if(nyield(nel).eq.1) call consplast(d,str,nel,k5,mu,ym,y3,hbar)
```

```
      if(itype(nel).eq.2) ngt=8
      if(itype(nel).eq.1) ngt=6
      if(itype(nel).eq.3) ngt=1
      do 260 m=1,ngt
      if(itype(nel).eq.2) call type2(dsf,m,ep,et,ro)
      if(itype(nel).eq.1) call type14(dsf,ro14,ep14,et14,m,el14)
      if(itype(nel).eq.3)call Shape3(lnon,itype,k5,ndof,bb,volu,nel,mx,my,mz)
      if(itype(nel).ne.3) call jacobi(dsf,x1,bb,nel,det,m,lnon,itype,k5,jacob,invj)
      call strss(sigma,u10,bb,d,m,stra,k5,nel,lnon,itype)
  260 continue
      do 234 nn=1,6
      bh=0
      bj=0
      do 235 j=1,ngt
      bh=bh+sigma(j,nn)
      bj=bj+stra(j,nn)
  235 continue
      if(lcount.eq.1) str(nel,nn)=bh/ngt
      if(lcount.eq.1) strain(nel,nn)=bj/ngt
      if(lcount.gt.1.and.loop.ne.2) strenc(nel,nn)=bh/ngt
      if(lcount.gt.1.and.loop.ne.2) strainc(nel,nn)=bj/ngt
      if(loop.eq.2) str(nel,nn)=str(nel,nn)+bh/ngt
      if(loop.eq.2) strain(nel,nn)=strain(nel,nn)+bj/ngt
      if(loop.eq.3.and.nreel.eq.0) then
      strenc(nel,nn)=bh/ngt
      strainc(nel,nn)=bj/ngt
      str(nel,nn)=str0(nel,nn)+strenc(nel,nn)
      strain(nel,nn)=strain0(nel,nn)+strainc(nel,nn)
      endif
  234 continue
      if(loop.eq.3.and.nreel.eq.0) then
```

```
call sigbar(str,nel,y3,k5)
goto 230
endif
if(lcount.eq.1.and.loop.ne.2)then
call sigbar(str,nel,y3,k5)
if(Y3(nel).gt.sigmax) then
sigmax=Y3(nel)
Mmax=nel
Re=ys/sigmax
endif
endif
if(lcount.gt.1.and.nyield(nel).eq.0.and.loop.ne.2)then
stinv1=strenc(nel,1)+strenc(nel,2)+strenc(nel,3)
Txx=strenc(nel,1)-stinv1/3
Tyy=strenc(nel,2)-stinv1/3
Tzz=strenc(nel,3)-stinv1/3
Txy=strenc(nel,4)
Tyz=strenc(nel,5)
Txz=strenc(nel,6)
YA=(3*(Txx**2+Tyy**2+Tzz**2+2*(Txy**2+Tyz**2+Txz**2))/2)**.5
stinv2=str(nel,1)+str(nel,2)+str(nel,3)+strenc(nel,1)+strenc(nel,2)+strenc(nel,3)
Txx=str(nel,1)+strenc(nel,1)-stinv2/3
Tyy=str(nel,2)+strenc(nel,2)-stinv2/3
Tzz=str(nel,3)+strenc(nel,3)-stinv2/3
Txy=str(nel,4)+strenc(nel,4)
Tyz=str(nel,5)+strenc(nel,5)
Txz=str(nel,6)+strenc(nel,6)
YB=(3*(Txx**2+Tyy**2+Tzz**2+2*(Txy**2+Tyz**2+Txz**2))/2)**.5
dx=YB-Y3(nel)
gama=YA**2-2*dx*Y3(nel)-dx**2
R1=gama+(gama**2+4*YA**2*(ys**2-Y3(nel)**2))**.5
```

```
      R2=2*YA**2
      R=R1/R2
      if(R.lt.Rmin) then
      Rmin=R
      Mmin=nel
      endif
      endif
230   continue
      if(ncase.eq.1.and.loop.ne.2) then
      if(loop.eq.1.or.loop.eq.3.and.nreel.eq.1) then
      call chkyield(nyiel,md1,nyield,npr,k5,k9,nyire,npre,md2,nvert, mvert,ely,ber
     +,ner,brd,nyi)
      if(loop.eq.1.and.nyiel.ne.md1.or.loop.eq.3.and.nyire.ne.md2)then
      if(lcount.eq.1)then
      nyield(Mmax)=1
      Hbar(Mmax)=0
      do 175 i=1,itnon*ndof
      u2(i)=u2(i)*Re
175   continue
      do 176 nel=1,noe
      do 177 k=1,6
      str(nel,k)=str(nel,k)*Re
      strain(nel,k)=strain(nel,k)*Re
177   continue
      call sigbar(str,nel,y3,k5)
176   continue
      press=press*Re
      pintip=press
      p(lcount)=press
      call updat1(nel,noe,nyield,y3,ys,Hbar,str,strain,k5,Lcon)
      call loader(lcount,p,k8)
```

```
      press=.1
      lcount=lcount+1
      goto 998
      endif
      if(lcount.gt.1) then
      nyield(Mmin)=1
      Hbar(Mmin)=0
      press=press*Rmin
      p(lcount)=p(lcount-1)+press
      press=.1
      do 178 i=1,itnon*ndof
      dispinc(i)=dispinc(i)*Rmin
      u2(i)=u2(i)+dispinc(i)
178   continue
      do 179 nel=1,noe
      do 180 k=1,6
      strenc(nel,k)=strenc(nel,k)*Rmin
      strainc(nel,k)=strainc(nel,k)*Rmin
      if(lcount.eq.nzrelo+1)then
      str(nel,k)=str0(nel,k)+strenc(nel,k)
      strain(nel,k)=strain0(nel,k)+strainc(nel,k)
      else
      str(nel,k)=str(nel,k)+strenc(nel,k)
      strain(nel,k)=strain(nel,k)+strainc(nel,k)
      endif
180   continue
      call sigbar(str,nel,y3,k5)
      if(nyield(nel).eq.1)then
      call epbar(nel,y3,hbar,strainc,str,k5,ym,mu,nneg,eplas)
      endif
      if(Nneg.gt.0) then
```

```
      print*,' STRUCTURAL FAILURE WILL OCCUR DUE TO GROSS'//
     +'DEFORMATION. LOADING MUST STOP'
      print*,' COLLAPSED LOAD WAS....',' ',p(lcount)
      call warn1(nel,p,povr,lcount,k8,eplas)
      endif
  179 continue
      call updat1(nel,noe,nyield,y3,ys,Hbar,str,strain,k5,Lcon)
      call loader(lcount,p,k8)
      call chkyield(nyiel,md1,nyield,npr,k5,k9,nyire,npre,md2,nvert,
     +mvert,ely,ber,ner,brd,nyi)
      if(mvert.eq.1.and.loop.eq.1.and.ncase.eq.1)then
      call warn4(povr,p,lcount,k8)
      goto 511
      endif
      if(loop.eq.3.and.p(lcount).ge.pintip) goto 511
      if(loop.eq.1.and.nyiel.eq.md1) goto 511
      lcount=lcount+1
      goto 998
      endif
      endif
      endif
      endif
  511 do 240 i=1,itnon
      do 241  n=1,6
      sm=0
      sn=0
      do 242 j=1,lenn(i)
      ja=dk(i,j)
      sm=sm+str(ja,n)
      sn=sn+strain(ja,n)
  242 continue
```

```
      stress(i,n)=sm/lenn(i)
      epz(i,n)=sn/lenn(i)
241   continue
      call principal(i,stress,princip,k1)
240   continue
30    format(6(i3,2x))
      call transf(k1,itnon,stress,rt,tht,cyl)
      call display(rt,cyl,u2,ndof,k1,k3,t3N,np,epz, oop,h0case,h0resi,h0relo,ncase
     +l,h0elast,pfin,press,pintip,roc,ric,thr,sf,ys,nxb,p,lcount,k8,lload,
     +nload,yt,beh,lmerid,nmerid,zt,xt,nhoriz,princip,k15,ber,nez,lxmerid,xmerid,
     +lastY,bxd,brd,ner,ibrd)
      if(ncase.eq.0) call elsana(rt,k1,hexalast,ys,mu,press,thr,ric,
     +sf,ym,npipe,k15,ber,brd,lastY,ner)
      if(ncase.eq.1.or.nresi.eq.1.or.nreload.eq.1) then
      if(nxb.eq.0) then
      call exact(thr,ric,rt,k1,ys,roc, loop,hexacase,hexaresi,prec
     + pincip,hexarelo,npipe,ber,lastY,k15,nyi,brd,ner)
      endif
      endif
      if(nresi.eq.1.and.loop.eq.1) then
      nzresi=lcount
      loop=2
      lcount=lcount+1
      press=-p(nzresi)
      pfin=p(nzresi)
      p(lcount)=-press
      call loader(lcount,p,k8)
      call transf(k1,itnon,stress,rt,tht,cyl)
      call hscf(itnon,cyl,k1,hmax,mhmax)
      goto 513
      endif
```

```
      if(loop.eq.2) call effe(noe,nel,y3,k5,str)
      if(loop.eq.2) call strains(noe,strain0,strain,k5,str0,str,itnon,ndof,u2,dispinc,k3)
      if(nreload.eq.1.and.loop.eq.2)then
      loop=3
      call checkYIEL(noe,y3,ys,nyield,Hbar,Lcon,str,strain,k5,nxa,nel)
      nzrelo=lcount
      if(nxa.eq.0)then
      press=pintip
      press=repress
      lcount=lcount+1
      p(lcount)=press
      goto 998
      elseif(nxa.gt.0)then
      call warn3(povr,thr,pfin)
      goto 999
      endif
      endif
      if(loop.eq.3) call effe(noe,nel,y3,k5,str)
      if(loop.eq.3) call loader(lcount,p,k8)
      if(nxb.eq.0.and.loop.eq.3)then
      Pinter=(pfin-pintip)/ndiv
      Pmax=p(lcount)
      do 154 i=1,ndiv
      xc=pintip+(i-1)*pinter
      open(157,file='c:\proj2\reload.dat',access='direct',form='formatted',
      +status='unknown',recl=13)
      write(157,fmt=155,rec=i) xc
154   continue
155   format(1x,f12.3)
      close(157)
      endif
```

```
      call scfact(scf,itnon,cyl,k1,hexalast,
     +rlast,lastY,k15,nupper)
      if(loop.eq.2) then
      call RESCF(cyl,k1,itnon,resscf,mhmin)
      pscf=abs(resscf/p(lcount))
      endif
512   call watch(suma,t1,t2)
      call Maxeff(cyl,k1,itnon,xt,yt,zt,ys)
      if(ncase.eq.0) call mloader(beh,cyl,k1,k15,bang,ncircle,bcircle)
999   stop
      end
```

End of Main Program

Returns the stress-strain matrix

```
      subroutine jacobi(dsf,x1,bb,nel,det,m,lnon,itype,k5,
     +jacob,invj)
      real jacob(3,3),dsf(3,10),invj(3,3),bb(6,30),dph(3,10),x1(10,3)
      real det(10)
      integer lnon(4),itype(1:k5)
      ns=lnon(itype(nel))
      do 1 i=1,3
      do 2 j=1,3
      sum=0
      do 3 k=1,ns
      sum=sum+dsf(i,k)*x1(k,j)
3     continue
      jacob(i,j)=sum
2     continue
1     continue
      e11=jacob(2,2)*jacob(3,3)-jacob(2,3)*jacob(3,2)
      e12=jacob(2,1)*jacob(3,3)-jacob(2,3)*jacob(3,1)
      e13=jacob(2,1)*jacob(3,2)-jacob(2,2)*jacob(3,1)
```

```
      e21=jacob(1,2)*jacob(3,3)-jacob(1,3)*jacob(3,2)
      e22=jacob(1,1)*jacob(3,3)-jacob(1,3)*jacob(3,1)
      e23=jacob(1,1)*jacob(3,2)-jacob(1,2)*jacob(3,1)
      e31=jacob(1,2)*jacob(2,3)-jacob(1,3)*jacob(2,2)
      e32=jacob(1,1)*jacob(2,3)-jacob(1,3)*jacob(2,1)
      e33=jacob(1,1)*jacob(2,2)-jacob(1,2)*jacob(2,1)
      det(m)=e11*jacob(1,1)-e12*jacob(1,2)+e13*jacob(1,3)
      invj(1,1)=e11/det(m)
      invj(1,2)=-e21/det(m)
      invj(1,3)=e31/det(m)
      invj(2,1)=-e12/det(m)
      invj(2,2)=e22/det(m)
      invj(2,3)=-e32/det(m)
      invj(3,1)=e13/det(m)
      invj(3,2)=-e23/det(m)
      invj(3,3)=e33/det(m)
      do 6 i=1,3
      do 7 j=1,ns
      sum=0
      do 8 k=1,3
      sum=sum+invj(i,k)*dsf(k,j)
8     continue
      dph(i,j)=sum
7     continue
6     continue
      do 9 i=1,6
      do 10 j=1,ns*3
      bb(i,j)=0
10    continue
9     continue
      do 11 j=1,ns
```

```
      bb(1,(j-1)*3+1)=dph(1,j)
      bb(2,(j-1)*3+2)=dph(2,j)
      bb(3,(j-1)*3+3)=dph(3,j)
      bb(4,(j-1)*3+1)=dph(2,j)
      bb(4,(j-1)*3+2)=dph(1,j)
      bb(5,(j-1)*3+2)=dph(3,j)
      bb(5,(j-1)*3+3)=dph(2,j)
      bb(6,(j-1)*3+1)=dph(3,j)
      bb(6,(j-1)*3+3)=dph(1,j)
11    continue
      return
      end
```

Returns gauss point stiffness matrix

```
      subroutine stif(d,bb,stiff,det,m,wep,wet,wro,lnon,itype,k5, wep14,wro14,nel,volu
     +ndof,wep3,wet3,wro3,wep4,wet4,wro4,wel14,wet14)
      real d(6,6),bb(6,30),bc(6,30),bd(24,6),stiff(30,30),det(10)
      real wep(10),wet(10),wro(10),wep3(10),wet3(10),wro3(10)
      real wep4(10),wet4(10),wro4(10),wel14(10)
      real wep14(10),wro14(10),volu(1:k5),wet14(10)
      integer lnon(4),itype(1:k5)
      ns=lnon(itype(nel))
      do 1 i=1,6
      do 2 j=1,ndof*ns
      sum=0
      do 3 k=1,6
      sum=sum+d(i,k)*bb(k,j)
3     continue
      bc(i,j)=sum
2     continue
1     continue
      do 4 j=1,ndof*ns
```

```
      do 5 i=1,6
      bd(j,i)=bb(i,j)
5     continue
4     continue
      do 6 i=1,ndof*ns
      do 7 j=1,ndof*ns
      sum=0
      do 8 k=1,6
      sum=sum+bd(i,k)*bc(k,j)
8     continue
      if(ns.eq.8) then
      stiff(i,j)=stiff(i,j)+sum*det(m)*wep(m)*wet(m)*wro(m)
      elseif(ns.eq.6) then
      stiff(i,j)=stiff(i,j)+sum*det(m)*wep14(m)*wet14(m)*wro14(m)/2
      elseif(ns.eq.4) then
      stiff(i,j)=stiff(i,j)+sum*volu(nel)
      elseif(ns.eq.10.and.itype(nel).eq.3)then
      stiff(i,j)=stiff(i,j)+sum*det(m)*wep3(m)*wet3(m)*wro3(m)
      elseif(ns.eq.10.and.itype(nel).eq.4)then
      stiff(i,j)=stiff(i,j)+sum*det(m)*wep4(m)*wet4(m)*wro4(m)
      endif
7     continue
6     continue
      return
      end
```

Returns the stress

```
      subroutine strss(sigma,u10,bb,d,m,stra,k5,nel,lnon,
      +itype)
      real sigma(10,6),u10(30),bb(6,30),d(6,6),stra(10,6)
      integer lnon(4),itype(1:k5)
      ns=lnon(itype(nel))
```

```
      do 1 i=1,6
      sum=0
      sumgp=0
      do 2 j=1,3*ns
      sum=sum+bb(i,j)*u10(j)
2     continue
      stra(m,i)=sum
1     continue
      do 3 i=1,6
      sum=0
      sumgp=0
      do 4 j=1,6
      sum=sum+d(i,j)*stra(m,j)
4     continue
      sigma(m,i)=sum
3     continue
      return
      end
      subroutine type2(dsf,m,ep,et,ro)
      real dsf(3,10),ep(10),et(10),ro(10)
      dsf(1,1)=-(1-et(m))*(1-ro(m))/8
      dsf(2,1)=-(1-ep(m))*(1-ro(m))/8
      dsf(3,1)=-(1-ep(m))*(1-et(m))/8
      dsf(1,2)=(1-et(m))*(1-ro(m))/8
      dsf(2,2)=-(1+ep(m))*(1-ro(m))/8
      dsf(3,2)=-(1+ep(m))*(1-et(m))/8
      dsf(1,3)=(1+et(m))*(1-ro(m))/8
      dsf(2,3)=(1+ep(m))*(1-ro(m))/8
      dsf(3,3)=-(1+ep(m))*(1+et(m))/8
      dsf(1,4)=-(1+et(m))*(1-ro(m))/8
      dsf(2,4)=(1-ep(m))*(1-ro(m))/8
```

```
dsf(3,4)=-(1-ep(m))*(1+et(m))/8
dsf(1,5)=-(1-et(m))*(1+ro(m))/8
dsf(2,5)=-(1-ep(m))*(1+ro(m))/8
dsf(3,5)=(1-ep(m))*(1-et(m))/8
dsf(1,6)=(1-et(m))*(1+ro(m))/8
dsf(2,6)=-(1+ep(m))*(1+ro(m))/8
dsf(3,6)=(1+ep(m))*(1-et(m))/8
dsf(1,7)=(1+et(m))*(1+ro(m))/8
dsf(2,7)=(1+ep(m))*(1+ro(m))/8
dsf(3,7)=(1+ep(m))*(1+et(m))/8
dsf(1,8)=-(1+et(m))*(1+ro(m))/8
dsf(2,8)=(1-ep(m))*(1+ro(m))/8
dsf(3,8)=(1-ep(m))*(1+et(m))/8
return
end
subroutine transf(k1,itnon,stress,rt,tht,cyl)
real stress(1:k1,6),rt(1:k1),tht(1:k1),cyl(1:k1,6), trt(3,3),Q(3,3),qt(3,3),temp(3,3)
real,temp1(3,3)
do 1 i=1,itnon
trt(1,1)=stress(i,1)
trt(2,2)=stress(i,2)
trt(3,3)=stress(i,3)
trt(1,2)=stress(i,4)
trt(1,3)=stress(i,5)
trt(2,3)=stress(i,6)
trt(2,1)=trt(1,2)
trt(3,1)=trt(1,3)
trt(3,2)=trt(2,3)
Q(1,1)=cos(tht(i))
Q(1,2)=-sin(tht(i))/rt(i)
Q(1,3)=0
```

```
      Q(2,1)=sin(tht(i))
      Q(2,2)=cos(tht(i))/rt(i)
      Q(2,3)=0
      Q(3,1)=0
      Q(3,2)=0
      Q(3,3)=1
      do 20 k=1,3
      do 21 j=1,3
      Qt(k,j)=Q(j,k)
   21 continue
   20 continue
      do 2 l=1,3
      do 3 j=1,3
      sum=0
      do 4 k=1,3
      sum=sum+trt(l,k)*Q(k,j)
    4 continue
      temp(l,j)=sum
    3 continue
    2 continue
      do 5 l=1,3
      do 6 j=1,3
      sum=0
      do 7 k=1,3
      sum=sum+qt(l,k)*temp(k,j)
    7 continue
      temp1(l,j)=sum
    6 continue
    5 continue
      cyl(i,1)=temp1(1,1)
      cyl(i,2)=temp1(2,2)*rt(i)**2
```

```
      cyl(i,3)=temp1(3,3)
      cyl(i,4)=temp1(1,2)*rt(i)
      cyl(i,5)=temp1(1,3)
      cyl(i,6)=temp1(2,3)*rt(i)
1     continue
      return
      end
      subroutine prere(itnon,noe,itype,lnon,con,ndest,eldest,maxfw, ovf,elf,k1,k5,k7
      ndof)
      real ovf(1:k7,1:k7),elf(1:k7)
      integer con(1:k5,10),eldest(1:k5,10),ndest(1:k1),itype(1:k5),lnon(4)
      do 1 i=1,itnon
      do 2 nel=1,noe
      do 3 j=1,lnon(itype(nel))
      ns=con(nel,j)
      if(ns.ne.i) goto 3
      nu=j
      nv=nel
3     continue
2     continue
      con(nv,nu)=-(con(nv,nu))
1     continue
      do 4 i=1,itnon
      ndest(i)=0
4     continue
      nh=lnon(itype(1))
      do 5 nel=1,noe
      if(nel.eq.1)then
      do 6 j=1,lnon(itype(nel))
      eldest(nel,j)=j
      ns=abs(con(nel,j))
```

```
      ndest(ns)=j
    6 continue
      else
      do 7 j=1,lnon(itype(nel))
      ny=0
      ns=abs(con(nel,j))
      if(ndest(ns).ne.0) goto 7
      do 8 nal=1,nel-1
      do 9 ji=1,lnon(itype(nal))
      nl=con(nal,ji)
      if(nl.lt.0)then
      nu=nal
      nv=ji
      goto 10
      else
      ny=ny+1
      goto 9
      endif
    9 continue
    8 continue
      if(ny.ne.0)then
      nh=nh+1
      ndest(ns)=nh
      goto 7
      endif
   10 ndest(ns)=ndest(abs(nl))
      con(nu,nv)=abs(con(nu,nv))
    7 continue
      endif
    5 continue
      do 11 i=1,noe
```

```
      do 12 j=1,lnon(itype(i))
      ns=abs(con(i,j))
      eldest(i,j)=ndest(ns)
   12 continue
   11 continue
      do 13 i=1,itnon
      do 14 nel=1,noe
      do 15 j=1,lnon(itype(nel))
      ns=abs(con(nel,j))
      if(ns.ne.i) goto 15
      nu=j
      nv=nel
   15 continue
   14 continue
      con(nv,nu)=-abs(con(nv,nu))
   13 continue
      max=0
      do 16 i=1,itnon
      if(ndest(i).gt.max) max=ndest(i)
   16 continue
      maxfw=max*ndof
      do 17 i=1,maxfw
      elf(i)=0
      do 18 j=1,maxfw
      ovf(i,j)=0
   18 continue
   17 continue
      return
      end
      subroutine assembf(itype,lnon,eldest,nel,ndof,elf,forf,ovf,stiff,k5,k7)
      real elf(1:k7),forf(1:k5,30),ovf(1:k7,1:k7),stiff(30,30)
```

```
      integer eldest(1:k5,10),itype(1:k5),lnon(4)
      do 1 i=1,lnon(itype(nel))
      ns=eldest(nel,i)
      do 3 l=1,ndof
      kl=ndof-l
      nss=ns*ndof-kl
      elf(nss)=elf(nss)+forf(nel,i*ndof-kl)
      do 4 j=1,lnon(itype(nel))
      nt=eldest(nel,j)
      do 5 n=1,ndof
      nl=ndof-n
      ntt=nt*ndof-nl
      ovf(nss,ntt)=ovf(nss,ntt)+stiff(i*ndof-kl,j*ndof-nl)
5     continue
4     continue
3     continue
1     continue
      return
      end
      subroutine elimini(itype,lnon,con,nel,ndest,ndof,ni,kpdof,kfs,
      +ovf,elf,s,k1,k2,k5,k7,nf)
      real ovf(1:k7,1:k7),elf(1:k7),s(1:k7)
      integer con(1:k5,10),ndest(1:k1),kpdof(1:k2),itype(1:k5),lnon(4)
      do 1 nl=1,lnon(itype(nel))
      naq=0
      nz=con(nel,nl)
      ny=abs(nz)
      if(nz.lt.0)then
      naq=naq+1
      if(naq.gt.1) goto 40
      do 2 i=1,lnon(itype(nel))
```

```
      ns=con(nel,i)
      nx=abs(ns)
      nd=ndest(nx)
      do 3 j=1,ni
      do 4 l=1,ndof
      if(nx*ndof-(ndof-l).eq.kpdof(j))then
   52 do 5 k=1,kfs
      ovf(k,nd*ndof-(ndof-l))=0
      ovf(nd*ndof-(ndof-l),k)=0
    5 continue
      ovf(nd*ndof-(ndof-l),nd*ndof-(ndof-l))=1
      elf(nd*ndof-(ndof-l))=0
      endif
    4 continue
    3 continue
    2 continue
   40 nd=ndest(ny)
      do 7 l=1,ndof
      mg=nd*ndof-(ndof-l)
      mi=ny*ndof-(ndof-l)
      do 8 i=1,kfs
      if(i.eq.mg) goto 8
      if(ovf(i,i).eq.0)goto 8
      p1=ovf(mg,mg)
      p2=ovf(i,mg)
      elf(i)=elf(i)-p2*elf(mg)/p1
      do 9 j=1,kfs
      ovf(i,j)=ovf(i,j)-p2*ovf(mg,j)/p1
    9 continue
    8 continue
      do 10 i=1,kfs
```

```
      s(i)=ovf(mg,i)
10    continue
      force=elf(mg)
      do 13 ki=1,kfs
      if(s(ki).ne.0)then
      kfirst=ki
      goto 14
      endif
13    continue
14    do 15 ki=kfs,1,-1
      if(s(ki).ne.0)then
      klast=ki
      goto 16
      endif
15    continue
16    open(1,file='c:\proj2\jmk1',access='direct',form='formatted',
      +status='unknown',recl=70)
      write(1,fmt=30,rec=mi) kfirst,klast,kfs,mi,force,s(mg)
30    format(4(i7,1x),2x,e16.8,4x,e16.8)
      open(2,file='c:\proj2\jmk2',access='direct',form='formatted',
      +status='unknown',recl=30600)
      write(2,fmt=17,rec=mi) (s(nw),nw=1,kfs)
17    format(1800(e16.8,1x))
7     continue
      endif
1     continue
      do 18 ml=1,lnon(itype(nel))
      nj=con(nel,ml)
      nk=abs(nj)
      nm=ndest(nk)
      if(nj.gt.0) goto 18
```

```
      do 19 l=1,ndof
      ms=nm*ndof-(ndof-l)
      elf(ms)=0
      do 20 il=1,kfs
      ovf(il,ms)=0
      ovf(ms,il)=0
 20   continue
 19   continue
 18   continue
100   return
      end
      subroutine backsub(itype,lnon,con,noe,eldest,ndof,ni,kpdof,s,
     +maxfw,u1,u2,k2,k3,k5,k7,dispinc,lcount,negdis,loop,itnon)
      real s(1:k7),u1(1:k7),u2(1:k3), dispinc(1:k3)
      integer con(1:k5,10),eldest(1:k5,10),kpdof(1:k2),itype(1:k5), lnon(4)
      do 1 i=1,maxfw
 1    u1(i)=0
      do 2 nel=noe,1,-1
      do 3 j=lnon(itype(nel)),1,-1
      ns=con(nel,j)
      ny=abs(ns)
      nd=eldest(nel,j)
      if(ns.gt.0) goto 3
      do 4 l=ndof,1,-1
      mg=nd*ndof-(ndof-l)
      mi=ny*ndof-(ndof-l)
      open(1,file='c:\proj2\jmk1',access='direct',form='formatted',
     +status='unknown',recl=70)
      read(1,fmt=17,rec=mi)  kfirst,klast,kfs,mi,force,s(mg)
 17   format(4(i7,1x),2x,e16.8,4x,e16.8)
      open(2,file='c:\proj2\jmk2',access='direct',form='formatted',
```

```
     +status='unknown',recl=30600)
     read(2,fmt=37,rec=mi) (s(nw),nw=1,kfs)
37   format(1800(e16.8,1x))
     pivot=s(mg)
     s(mg)=0
     sum=0
     do 6 i=kfirst,klast
     sum=sum+s(i)*u1(i)
6    continue
     nc=0
     do 7 kj=1,ni
     if(mi.eq.kpdof(kj)) nc=nc+1
7    continue
     if(lcount.eq.1) then
     if(nc.ne.1) u2(mi)=0
     if(nc.eq.0) u2(mi)=(force-sum)/pivot
     u1(mg)=u2(mi)
     endif
     if(nc.ne.1) dispinc(mi)=0
     if(nc.eq.0) dispinc(mi)=(force-sum)/pivot
     u1(mg)=dispinc(mi)
     endif
     endif
4    continue
3    continue
2    continue
100  return
     end
     subroutine conselast(d,ym,mu)
     real d(6,6),mu
     do 1 i=1,6
```

```
      do 1 j=1,6
    1 d(i,j)=0
      a1=ym/((1+mu)*(1-2*mu))
      d(1,1)=a1*(1-mu)
      d(2,2)=a1*(1-mu)
      d(3,3)=a1*(1-mu)
      d(1,2)=a1*mu
      d(1,3)=a1*mu
      d(2,1)=a1*mu
      d(2,3)=a1*mu
      d(3,1)=a1*mu
      d(3,2)=a1*mu
      d(4,4)=a1*(1-2*mu)/2
      d(5,5)=a1*(1-2*mu)/2
      d(6,6)=a1*(1-2*mu)/2
      return
      end
      subroutine consplast(d,str,nel,k5,mu,ym,y3,hbar)
      real str(1:k5,6),d(6,6),mu,y3(1:k5),hbar(1:k5)
      stinv1=str(nel,1)+str(nel,2)+str(nel,3)
      Txx=str(nel,1)-stinv1/3
      Tyy=str(nel,2)-stinv1/3
      Tzz=str(nel,3)-stinv1/3
      Txy=str(nel,4)
      Tyz=str(nel,5)
      Txz=str(nel,6)
      G=ym/(2*(1+mu))
      sd=Hbar(nel)/(3*G)+1
      S=(2*Y3(nel)**2/3)*sd
      xs=ym/(1+mu)
      d(1,1)=xs*((1-mu)/(1-2*mu)-Txx**2/S)
```

```
d(2,2)=xs*((1-mu)/(1-2*mu)-Tyy**2/S)
d(3,3)=xs*((1-mu)/(1-2*mu)-Tzz**2/S)
d(4,4)=xs*(0.5-Txy**2/S)
d(5,5)=xs*(0.5-Tyz**2/S)
d(6,6)=xs*(0.5-Txz**2/S)
d(1,2)=xs*(mu/(1-2*mu)-Txx*Tyy/S)
d(1,3)=xs*(mu/(1-2*mu)-Txx*Tzz/S)
d(1,4)=-xs*Txx*Txy/S
d(1,5)=-xs*Txx*Tyz/S
d(1,6)=-xs*Txx*Txz/S
d(2,3)=xs*(mu/(1-2*mu)-Tyy*Tzz/S)
d(2,4)=-xs*Tyy*Txy/S
d(2,5)=-xs*Tyy*Tyz/S
d(2,6)=-xs*Tyy*Txz/S
d(3,4)=-xs*Tzz*Txy/S
d(3,5)=-xs*Tzz*Tyz/S
d(3,6)=-xs*Tzz*Txz/S
d(4,5)=-xs*Txy*Tyz/S
d(4,6)=-xs*Txy*Txz/S
d(5,6)=-xs*Tyz*Txz/S
do 1 i=1,6
do 2 j=1,i
if(j.ne.i) d(i,j)=d(j,i)
2  continue
1  continue
return
end
subroutine sigbar(str,nel,y3,k5)
real str(1:k5,6),y3(1:k5)
stinv1=str(nel,1)+str(nel,2)+str(nel,3)
Txx=str(nel,1)-stinv1/3
```

```
      Tyy=str(nel,2)-stinv1/3
      Tzz=str(nel,3)-stinv1/3
      Txy=str(nel,4)
      Tyz=str(nel,5)
      Txz=str(nel,6)
      y3(nel)=(3*(Txx**2+Tyy**2+Tzz**2+2*(Txy**2+Tyz**2+Txz**2))/2)**.5
      return
      end
      subroutine loader(lcount,p,k8)
      real p(1:k8)
      open(53,file='c:\proj2\load.dat',access='direct',
     +form='formatted',status='unknown',recl=23)
      write(53,fmt=1,rec=lcount) lcount,p(lcount)
      close(53)
1     format(i5,2x,(e15.4,1x))
      return
      end
      subroutine updat1(nel,noe,nyield,y3,ys,Hbar,str,
     +strain,k5,Lcon)
      real y3(1:k5),Hbar(1:k5),str(1:k5,6),strain(1:k5,6)
      integer nyield(1:k5)
      do 1 nel=1,noe
      if(nyield(nel).eq.0)then
      r1=y3(nel)/ys
      r2=1/r1
      if(r1.ge.0.95)then
      Lcon=Lcon+1
      nyield(nel)=1
      Hbar(nel)=0
      do 3 k=1,6
      str(nel,k)=str(nel,k)*r2
```

```
      strain(nel,k)=strain(nel,k)*r2
3     continue
      endif
      endif
      call sigbar(str,nel,y3,k5)
1     continue
      return
      end
      subroutine epbar(nel,y3,hbar,strainc,str,k5,ym,mu,nneg,eplas)
      real y3(1:k5),hbar(1:k5),mu
      real strainc(1:k5,6),str(1:k5,6)
      stinv1=str(nel,1)+str(nel,2)+str(nel,3)
      Txx=str(nel,1)-stinv1/3
      Tyy=str(nel,2)-stinv1/3
      Tzz=str(nel,3)-stinv1/3
      Txy=str(nel,4)
      Tyz=str(nel,5)
      Txz=str(nel,5)
      b1=Txx*strainc(nel,1)
      b2=Tyy*strainc(nel,2)
      b3=Tzz*strainc(nel,3)
      b4=Txy*strainc(nel,4)
      b5=Tyz*strainc(nel,5)
      b6=Txz*strainc(nel,6)
      b7=b1+b2+b3+2*(b4+b5+b6)
      G=ym/(2*(1+mu))
      sb1=y3(nel)*(1+hbar(nel)/(3*G))
      eplas=b7/sb1
      return
      end
      subroutine watch(suma,t1,t2)
```

```
      t2=secnds(0.0)
      if(t2.gt.t1) delta=t2-t1
      if(t2.lt.t1) delta=86400-t1+t2
      t1=t2
      suma=suma+delta
      return
      end
      subroutine chkyield(nyiel,md1,nyield,npr,k5,k9,nyire,npre,
     +md2,nvert,mvert,ely,ber,ner,brd,nyi)
      integer npr(1:k9),nyield(1:k5),npre(1:k9),nvert(1:k9)
      integer ely,ber,brd
      nyiel=0
      do 1 i=1,md1
      if(nyield(npr(i)).eq.1) nyiel=nyiel+1
1     continue
      nyire=0
      do 2 i=1,md2
      if(nyield(npre(i)).eq.1) nyire=nyire+1
2     continue
      mvert=0
      if(nyield(nvert(nyi)).eq.1) mvert=mvert+1
      return
      end
      subroutine checkYIEL(noe,y3,ys,nyield,Hbar,Lcon,str,strain,k5,nxa,nel)
      real y3(1:k5),Hbar(1:k5),str(1:k5,6),strain(1:k5,6)
      integer nyield(1:k5)
      nxa=0
      do 1 nel=1,noe
      call sigbar(str,nel,y3,k5)
      if(y3(nel).ge.ys) then
      nyield(nel)=1
```

```
Hbar(nel)=0
nxa=nxa+1
endif
if(y3(nel).lt.ys) then
nyield(nel)=0
r1=y3(nel)/ys
r2=1/r1
if(r1.ge.0.95)then
Lcon=Lcon+1
nyield(nel)=1
Hbar(nel)=0
nxa=nxa+1
do 3 k=1,6
str(nel,k)=str(nel,k)*r2
strain(nel,k)=strain(nel,k)*r2
3     continue
call sigbar(str,nel,y3,k5)
endif
endif
1     continue
return
end
subroutine effe(noe,nel,y3,k5,str)
real y3(1:k5)
real str(1:k5,6)
do 1 nel=1,noe
call sigbar(str,nel,y3,k5)
1     continue
return
end
subroutine strains(noe,strain0,strain,k5,str0,str,itnon,ndof,u2,dispinc,k3)
```

```
      real strain0(1:k5,6),strain(1:k5,6),str0(1:k5,6),str(1:k5,6),u2(1:k3),dispinc(1:k3)
      do 1 nel=1,noe
      do 2 j=1,6
      strain0(nel,j)=strain(nel,j)
      str0(nel,j)=str(nel,j)
2     continue
1     continue
      do 3 i=1,itnon*ndof
3     u2(i)=u2(i)+dispinc(i)
      return
      end
      subroutine warn1(nel,p,povr,lcount,k8,eplas)
      real p(1:k8)
      character*(*) wer,war,wlc,wel,wlo,wepl
      parameter(wer='STOP ANY FURTHER LOADINDS. GROSS DEFORMATION
     +' HAS BEEN DETECTED')
      parameter(war='LIMIT OF OVERSTRAIN IS')
      parameter(wlc='LOAD CYCLE NUMBER AT COLLAPSE')
      parameter(wel='COLLAPSED ELEMENT WAS')
      parameter(wlo='COLLAPSE LOAD WAS Mpa')
      parameter(wepl='GROSS OVERSTRAIN WAS')
      open(160,file='c:\proj2\WARN10.dat',access='direct',
     +form='formatted',status='unknown',recl=61)
      write(160,fmt=1,rec=1) wer
1     format(1x,A60)
      open(161,file='c:\proj2\WARN11.dat',access='direct',
     +form='formatted',status='unknown',recl=38)
      write(161,fmt=2,rec=1) wlc,lcount
      write(161,fmt=2,rec=2) wel,nel
2     format(1x,A30,1x,i6)
      open(162,file='c:\proj2\WARN12.dat',access='direct',
```

```
     +form='formatted',status='unknown',recl=44)
     write(162,fmt=3,rec=1) war,povr
     write(162,fmt=3,rec=2) wlo,p(lcount)
     write(162,fmt=3,rec=3) wepl,eplas
3    format(1x,A30,1x,e12.4)
     return
     end
     subroutine warn3(povr,thr,pfin)
     character*(*) wco,war,wlc,wel,wlo
     parameter(wco='PROGRAM STOPPED DUE TO ELEMENTS YIELDING
     UNDER RESIDUAL STRESS')
     parameter(war='LIMIT OF OVERSTRAIN IS')
     parameter(wlc='LOAD CYCLE NUMBER AT ERROR')
     parameter(wel='THICKNESS RATIO')
     parameter(wlo='LOAD IN ERROR WAS Mpa')
     open(170,file='c:\proj2\WARN31.dat',access='direct',
     +form='formatted',status='unknown',recl=70)
     write(170,fmt=1,rec=1) wco
1    format(1x,A70)
     open(171,file='c:\proj2\WARN32.dat',access='direct',
     +form='formatted',status='unknown',recl=44)
     write(171,fmt=2,rec=1) war,povr
     write(171,fmt=2,rec=2) wel,thr
     write(171,fmt=2,rec=3) wlo,pfin
2    format(1x,A30,1x,F12.3)
     return
     end
     subroutine face2(a,b,mx,my,mz,ltr2,na)
     real a(3),b(3),mx(10),my(10),mz(10)
     integer ltr2(2,3)
     a(1)=mx(ltr2(na,2))-mx(ltr2(na,1))
```

```
a(2)=my(ltr2(na,2))-my(ltr2(na,1))
a(3)=mz(ltr2(na,2))-mz(ltr2(na,1))
b(1)=mx(ltr2(na,3))-mx(ltr2(na,1))
b(2)=my(ltr2(na,3))-my(ltr2(na,1))
b(3)=mz(ltr2(na,3))-mz(ltr2(na,1))
return
end
subroutine norm(c,a,b,area,nel)
real c(3),a(3),b(3)
c(1)=a(2)*b(3)-a(3)*b(2)
c(2)=-(a(1)*b(3)-a(3)*b(1))
c(3)=a(1)*b(2)-a(2)*b(1)
if(c(3).lt.0) c(3)=0
if(c(2).lt.0) c(2)=0
if(c(1).lt.0) c(1)=0
area=((c(1)**2+c(2)**2+c(3)**2)**.5)/2
c(1)=c(1)/(2*area)
c(2)=c(2)/(2*area)
c(3)=c(3)/(2*area)
do 3 i=1,3
if(c(i).lt.0)then
3 continue
return
end
subroutine post(k5,nel,c,n6,for,forf)
real c(3),forf(1:k5,30)
do 1 k=1,3
ng=n6*3-(3-k)
forf(nel,ng)=forf(nel,ng)+for*c(k)
1 continue
return
```

```
end
subroutine type14(dsf,ro14,ep14,et14,m,el14)
real dsf(3,10),ep14(10),et14(10),ro14(10),el14(10)
dsf(1,1)=(1-ro14(m))/2
dsf(2,1)=0
dsf(3,1)=-ep14(m)/2
dsf(1,2)=0
dsf(2,2)=(1-ro14(m))/2
dsf(3,2)=-et14(m)/2
dsf(1,3)=-(1-ro14(m))/2
dsf(2,3)=-(1-ro14(m))/2
dsf(3,3)=-el14(m)/2
dsf(1,4)=(1+ro14(m))/2
dsf(2,4)=0
dsf(3,4)=ep14(m)/2
dsf(1,5)=0
dsf(2,5)=(1+ro14(m))/2
dsf(3,5)=et14(m)/2
dsf(1,6)=-(1+ro14(m))/2
dsf(2,6)=-(1+ro14(m))/2
dsf(3,6)=el14(m)/2
return
end
subroutine principal(i,stress,princip,k1)
real princip(1:k1,3),stress(1:k1,6)
stinv1=stress(i,1)+stress(i,2)+stress(i,3)
stinv2=(stress(i,1)*stress(i,2)-stress(i,4)**2)+
+(stress(i,2)*stress(i,3)-stress(i,6)**2)+
+(stress(i,1)*stress(i,3)-stress(i,5)**2)
+stinv3=stress(i,1)*(stress(i,2)*stress(i,3)-
+ stress(i,6)**2)-stress(i,4)*(stress(i,4)*stress(i,3)-
```

```
     +stress(i,5)*stress(i,6))+stress(i,5)*(stress(i,4)*stress(i,6)-
     + stress(i,2)*stress(i,5))
     pi=3.141592654
     H=stinv2-stinv1**2/3
     Gi=stinv3-stinv1*stinv2/3+2*stinv1**3/27
     ri=-1
     raz=-H/3
     Gam1=(Gi/2)/(-H/3)**1.5
     Gam=acos(Gam1)
     do 30 k=1,3
     princip(i,k)=stinv1/3+2*(-H/3)**0.5*cos((Gam+2*(k-1)*pi)/3)
30   continue
     return
     end
     subroutine change3(noe,itype,con,k5,k1,zt,rt,
     +lnon,mark,nel,yt,xt,ile,nend,ner,brd,nvert,k9,ivert)
     real zt(1:k1),rt(1:k1),yt(1:k1),xt(1:k1)
     integer itype(1:k5),con(1:k5,10),mt(10),lnon(4),mark(1:k5)
     integer ile(1:k5),nend(1:k5),brd,nvert(1:k9),ivert(1:k5)
     nas=0
     mas=0
     do 10 i=1,noe
     if(itype(i).eq.1) nas=nas+1
     if(itype(i).eq.2) mas=mas+1
10   continue
     ndak=noe
     do 1 nel=ndak,1,-1
     if(itype(nel).eq.1)then
     do 2 l=1,6
2    mt(l)=con(nel,l)
     noe=noe+2
```

```
mark(nel)=0
itype(nel)=3
ile(nel)=0
nend(nel)=0
ivert(nel)=0
if(nel.lt.ndak) call Puller3(noe,nel,itype,k5,lnon,
+con,mark,ile,nend,ivert)
mark(nel+1)=0
mark(nel+2)=0
itype(nel+1)=3
itype(nel+2)=3
ile(nel+1)=0
ile(nel+2)=0
nend(nel+1)=0
nend(nel+2)=0
ivert(nel+1)=0
ivert(nel+2)=0
con(nel,1)=mt(3)
con(nel,2)=mt(6)
con(nel,3)=mt(4)
con(nel,4)=mt(5)
con(nel+1,1)=mt(1)
con(nel+1,2)=mt(3)
con(nel+1,3)=mt(4)
con(nel+1,4)=mt(5)
con(nel+2,1)=mt(1)
con(nel+2,2)=mt(2)
con(nel+2,3)=mt(3)
con(nel+2,4)=mt(5)
endif
1     continue
```

```
      return
      end
      subroutine Puller3(noe,nel,itype,k5,lnon,con,mark,ile,nend,ivert)
      integer itype(1:k5),lnon(4),con(1:k5,10),mark(1:k5)
      integer ile(1:k5),Nend(1:k5),ivert(1:k5)
      nas=0
      do 1 ks=noe,nel+3,-1
      itype(ks)=itype(ks-2)
      mark(ks)=mark(ks-2)
      ile(ks)=ile(ks-2)
      Nend(ks)=Nend(ks-2)
      ivert(ks)=ivert(ks-2)
      do 2 j=1,lnon(itype(ks))
      con(ks,j)=con(ks-2,j)
2     continue
1     continue
      return
      end
      subroutine Shape3(lnon,itype,k5,ndof,bb,volu,
     +nel,mx,my,mz)
      integer lnon(4),itype(1:k5)
      real b(4),c(4),d(4),dph(3,10),mx(10),my(10),mz(10), bb(6,30),volu(1:k5)
      h1=mx(2)*(my(3)*mz(4)-my(4)*mz(3))
      h2=my(2)*(mz(4)*mx(3)-mz(3)*mx(4))
      h3=mz(2)*(mx(3)*my(4)-mx(4)*my(3))
      h4=mx(1)*(my(3)*mz(4)-my(4)*mz(3))
      h5=mx(1)*my(2)*(mz(4)-mz(3))
      h6=mx(1)*mz(2)*(my(4)-my(3))
      h7=my(1)*(mx(3)*mz(4)-mx(4)*mz(3))
      h8=my(1)*mx(2)*(mz(4)-mz(3))
      h9=my(1)*mz(2)*(mx(4)-mx(3))
```

```
h10=mz(1)*(mx(3)*my(4)-mx(4)*my(3))
h11=mz(1)*mx(2)*(my(4)-my(3))
h12=mz(1)*my(2)*(mx(4)-mx(3))
Volu(nel)=(h1-h2+h3-h4+h5-h6+h7-h8+h9-h10+h11-h12)/6
cVol=volu(nel)
b(1)=-(my(3)*mz(4)-my(4)*mz(3)-my(2)*(mz(4)-mz(3))+
+mz(2)*(my(4)-my(3)))
b(2)=my(3)*mz(4)-my(4)*mz(3)-my(1)*(mz(4)-mz(3))+
+mz(1)*(my(4)-my(3))
b(3)=-(my(2)*mz(4)-my(4)*mz(2)-my(1)*(mz(4)-mz(2))+
+mz(1)*(my(4)-my(2)))
b(4)=my(2)*mz(3)-my(3)*mz(2)-my(1)*(mz(3)-mz(2))+
+mz(1)*(my(3)-my(2))
c(1)=mx(3)*mz(4)-mx(4)*mz(3)-mx(2)*(mz(4)-mz(3))+
+mz(2)*(mx(4)-mx(3))
c(2)=-(mx(3)*mz(4)-mx(4)*mz(3)-mx(1)*(mz(4)-mz(3))+
+mz(1)*(mx(4)-mx(3)))
c(3)=mx(2)*mz(4)-mx(4)*mz(2)-mx(1)*(mz(4)-mz(2))+
+mz(1)*(mx(4)-mx(2))
c(4)=-(mx(2)*mz(3)-mx(3)*mz(2)-mx(1)*(mz(3)-mz(2))+
+mz(1)*(mx(3)-mx(2)))
d(1)=-(mx(3)*my(4)-mx(4)*my(3)-mx(2)*(my(4)-my(3))+
+my(2)*(mx(4)-mx(3)))
d(2)=mx(3)*my(4)-mx(4)*my(3)-mx(1)*(my(4)-my(3))+
+my(1)*(mx(4)-mx(3))
d(3)=-(mx(2)*my(4)-mx(4)*my(2)-mx(1)*(my(4)-my(2))+
+my(1)*(mx(4)-mx(2)))
d(4)=mx(2)*my(3)-mx(3)*my(2)-mx(1)*(my(3)-my(2))+
+my(1)*(mx(3)-mx(2))
dph(1,1)=b(1)/(6*cVol)
dph(1,2)=b(2)/(6*cVol)
```

```
dph(1,3)=b(3)/(6*cVol)
dph(1,4)=b(4)/(6*cVol)
dph(2,1)=c(1)/(6*cVol)
dph(2,2)=c(2)/(6*cVol)
dph(2,3)=c(3)/(6*cVol)
dph(2,4)=c(4)/(6*cVol)
dph(3,1)=d(1)/(6*cVol)
dph(3,2)=d(2)/(6*cVol)
dph(3,3)=d(3)/(6*cVol)
dph(3,4)=d(4)/(6*cVol)
do 11 j=1,lnon(itype(nel))
bb(1,(j-1)*ndof+1)=dph(1,j)
bb(2,(j-1)*ndof+2)=dph(2,j)
bb(3,(j-1)*ndof+3)=dph(3,j)
bb(4,(j-1)*ndof+1)=dph(2,j)
bb(4,(j-1)*ndof+2)=dph(1,j)
bb(5,(j-1)*ndof+2)=dph(3,j)
bb(5,(j-1)*ndof+3)=dph(2,j)
bb(6,(j-1)*ndof+1)=dph(3,j)
bb(6,(j-1)*ndof+3)=dph(1,j)
11  continue
    return
    end
    subroutine face3N(a,b,mx,my,mz,ltr3N,na)
    real a(3),b(3),mx(10),my(10),mz(10)
    integer ltr3N(2,3)
    a(1)=mx(ltr3N(na,2))-mx(ltr3N(na,1))
    a(2)=my(ltr3N(na,2))-my(ltr3N(na,1))
    a(3)=mz(ltr3N(na,2))-mz(ltr3N(na,1))
    b(1)=mx(ltr3N(na,3))-mx(ltr3N(na,1))
    b(2)=my(ltr3N(na,3))-my(ltr3N(na,1))
```

```
b(3)=mz(ltr3N(na,3))-mz(ltr3N(na,1))
return
end
subroutine Enda(a,b,mx,my,mz,lend,na)
real a(3),b(3),mx(10),my(10),mz(10)
integer lend(2,3)
a(1)=mx(lend(na,2))-mx(lend(na,1))
a(2)=my(lend(na,2))-my(lend(na,1))
a(3)=mz(lend(na,2))-mz(lend(na,1))
b(1)=mx(lend(na,3))-mx(lend(na,1))
b(2)=my(lend(na,3))-my(lend(na,1))
b(3)=mz(lend(na,3))-mz(lend(na,1))
return
end
subroutine f3n(a,b,mx,my,mz,mt3,na)
real a(3),b(3),mx(10),my(10),mz(10)
integer mt3(1,3)
a(1)=mx(mt3(na,2))-mx(mt3(na,1))
a(2)=my(mt3(na,2))-my(mt3(na,1))
a(3)=mz(mt3(na,2))-mz(mt3(na,1))
b(1)=mx(mt3(na,3))-mx(mt3(na,1))
b(2)=my(mt3(na,3))-my(mt3(na,1))
b(3)=mz(mt3(na,3))-mz(mt3(na,1))
return
end
```

VITAE

Eng. John Muniu Kihiu was born in the splush green and chilly tea growing highland areas of central Kenya in 1962. He attended Passenga primary school between 1968 and 1974. He latter attended Alliance High School between 1975 and 1980. In 1981, he worked with Pyrethrum Board of Kenya as a quality control assistant. Thereafter, he was awarded a scholarship by the Kenya Power and Lighting Company (KPLC) to study Mechanical Engineering at the University of Nairobi from where he graduate with a first class honours Bachelor of Science degree in 1985. While at the university, he also worked as an apprentice engineer at KPLC and was awarded the trophy of best mechanical trainee engineer at the end of the training period. He latter held various positions in KPLC between 1985 and 1989, while attached to various hydroelectric power stations. In 1990 he joined Total Kenya as a lubricants supply and planning officer.

In 1992 he was employed by Jomo Kenyatta University of Agriculture and Technology (JKUAT) as a teaching assistant and awarded a scholarship by Japanese International Cooperation Agency (JICA) to pursue a Master of Science degree (Applied Mechanics option) course at the University of Nairobi. He was awarded the Master of Science degree in 1995. In 1997, he undertook a nine-month JICA sponsored research training course at Tottori University in Japan. In 1999, he was awarded a scholarship by DAAD and admitted to the University of Nairobi to pursue a Ph.D. research program.

During his teaching career at JKUAT and the University of Nairobi, he has taught the following B.Sc. courses: *solid and structural mechanics, mechanics of machines, engineering design and materials testing*. He has also taught the following M.Sc. courses at the University of Nairobi: *finite element methods, continuum mechanics and quality control*. He has proposed and supervised several final year B.Sc. projects. In addition, he has been a co-supervisor of an M.Sc. research project.

He is a member of the following technical committees of the Kenya Bureau of Standards: Pressure Vessels and Boilers, Aluminium and Steel Structures and Mechanical Engineering Industry Standards. He is a registered engineer, a corporate member of the Institution of Engineers of Kenya (IEK) and a regular contributor to the bi-monthly journal of the IEK. He has also done several consultancy projects. With the support of JICA he has carried out and presented the reports of a number of research projects. He has also developed two commercial finite element method design software for use by civil and structural engineers.

Some of his publications and articles are:

- Kihiu J. M. and Masu L. M., 'The Effect of Chamfer size and Angle on the Stress Distributions in Thick Walled Cylinders with Cross Bores Under Internal Pressure', *Journal of Research and Development*, University of Stellenbosch, South Africa, Vol. 11, No. 3. 1995
- Kihiu J. M. and Mutuli S. M., 'Time and Space Management in Structural Analysis Problems', *International Journal of Mechanical Engineering Education*, University of Manchester, Vol. 26, No. 4, Oct. 1998.
- Kihiu J. M., Rading G. O. and Mutuli S. M., 'Autofrettage in Thick Walled Cylinders', *International Journal of Mechanical Engineering Education*, University of Manchester, 2002. (paper accepted).
- Kihiu J. M., Rading G. O. and Mutuli S. M., 'Geometric Constants in Plain Cross-Bored Cylinders', *Journal of Pressure Vessel Technology*, 2002 (paper accepted).
- Kihiu J. M. and Rading G. O., 'Stress Intensity and Stress Concentration Factors in Thick Walled Cylinders with Multiple Radial Cracks Under Internal Pressure', *Journal of Pressure Vessel Technology*, (paper under review).
- Kihiu J. M., 'Part I:-Introduction to Finite Element Method', *Kenya Engineer*, Oct/Nov. 1995.
- Kihiu J. M., 'Part II:-The Principles of the Finite Element Method', *Kenya Engineer*, Mar/April 1996.
- Kihiu J. M., 'The Role of the Engineer in the Industrialisation Process', *Kenya Engineer*, July/August 1996.

- Kihiu J. M., 'Practical Application of Steel Hardening in Punching Tools', *Training Document, Ministry of Research, Science and Technology/World Bank, 1996.*

Postgraduate research work supervised:

- Wekesa M. W., 'Modeling of Heat Flow, Precipitate Formation and Grain Growth in the Heat Affected Zone of Aluminium Alloy Weldments', MSc Thesis, University of Nairobi, 2002.